Journal of the Serbian Chemical Society

*e*Version
*e*lectronic

Society
115th
Anniversary
1897 - 2012

VOLUME 77

No 9

BELGRADE 2012

Available on line at

СХД
1897

www.shd.org.rs/JSCS/

CONTENTS

Available online at www.shd.org.rs/JSCS/

Journal of the Serbian Chemical Society

REVIEW

Transition metal complexes with Girard reagents and their hydrazones

LJILJANA S. VOJINOVIĆ-JEŠIĆ[1#], SLAĐANA B. NOVAKOVIĆ[2#],
VUKADIN M. LEOVAC[1#*] and VALERIJA I. ČEŠLJEVIĆ[1#]

[1]*Faculty of Sciences, University of Novi Sad, Trg Dositeja Obradovića 3, 21000 Novi Sad, Serbia and* [2]*Vinča Institute of Nuclear Sciences, Laboratory of Theoretical Physics and Condensed Matter Physics, University of Belgrade, P. O. Box 522, 11001 Belgrade, Serbia*

Abstract: This is the first review dealing with the coordination chemistry of metal complexes with Girard reagents and their hydrazones. The short introduction indicates the chemical properties and significance of these organic compounds. The next section briefly describes synthetic methods for preparing complexes with Girard reagents, as well as the modes of coordination of these ligands. The last two extensive sections review the preparation, stereochemistry and structural characteristics of metal complexes with Girard hydrazones, including also some newer non-hydrazonic derivatives of Girard reagents.

Keywords: Girard reagents; hydrazones; metal complexes; synthesis; physico-chemical characteristics; X-ray crystallography.

CONTENTS

---

1. INTRODUCTION

There are a large number of organic compounds that are used as reagents for the identification of some other compounds, *i.e.*, their corresponding functional groups.[1,2] Among them, Girard reagents form an important group (Fig. 1), which serve for the separation of carbonyl compounds from their complex mixtures, by forming water-soluble hydrazones.
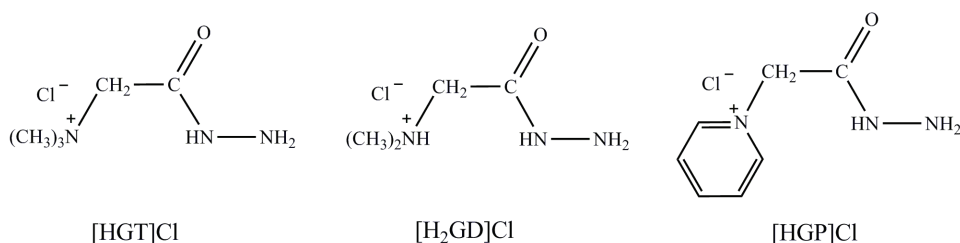
Fig.1. Structures of Girard reagents.

To these reagents, which may be considered as N-substituted glycine hydra-zides, belong:

Girard-T (trimethylacetylhydrazide ammonium chloride), [HGT]Cl,

Girard-D (*N,N*-dimethylglycine hydrazide hydrochloride), [H$_2$GD]Cl and

Girard-P (pyridinioacetohydrazide chloride), [HGP]Cl.

The Girard-T and Girard-P reagents were synthesized first by A. Girard and G. Sandulesco in 1936, by the reaction of ethyl chloroacetate with trimethyl-amine or pyridine, yielding quaternary ammonium esters, which in the reaction with hydrazine afforded the corresponding [HGT]Cl and [HGP]Cl Girard reagents.[3] These two reagents are soluble in water and biological studies showed that they inhibit certain enzymes (histidine decarboxylase,[4] acetylcholine esterase[5] and aryl sulfatase[6]). [H$_2$GD]Cl was synthesized much later by the reaction of *N,N*-dimethylglycine ethyl ester and hydrazine hydrate with addition of *cc.* hydrochloric acid.[7]

The Girard-T and Girard-P reagents have been widely used to facilitate various separations[1,2,8–10] and were recently utilized by Lehn *et al.*[11] as platforms for the slow release of fragrance aldehydes.

The Girard-T reagent is very soluble in water, less soluble in methanol, ethanol, 2-propanol, glycerol, 1,2-ethanediol and acetic acid, and insoluble in non-hydroxylic organic solvents.[3,12,13] It is very hygroscopic and it decomposes in the presence of moisture and air, liberating an unpleasant odor. The crystals can be cleaned by washing with ethanol.[14]

The Girard-P reagent is less soluble in polar solvents and, in contrast to the Girard-T reagent, it is not hygroscopic.[14]

Due to the high hygoscopicity of the Girard-T reagent, Viscontini and Maier[7] proposed the use of the neutral Girard-D reagent, which is formed by the neutralization of an aqueous solution of the hydrochloride salt of this reagent with Na_2CO_3, giving water-insoluble hydrazones.

Based on analytical data, it was concluded that the Girard-T reagent behaves as a monoprotic acid (Scheme 1, a) and the Girard-D reagent as a diprotic acid (Scheme 1,b and c).[15]

Scheme 1. Dissociation of the Girard-T (a) and Girard-D (b and c) reagents.

To the best of our knowledge, there are no literature data on dissociation of the Girard-P reagent; however, based on its structure, it may be expected that it behave as a monoprotic acid.

The possibility of condensation of the Girard-T reagent with ketones has found its application in the isolation of ketones from essential oils, which represent mixtures of different hydrocarbons, alcohols, esters and ketones, and this reagent appeared to be more efficient than semicarbazides.[16,17]

In addition to the mentioned application, Girard reagents are also used in steroid chemistry for the separation and preparation of ketonic and non-ketonic steroids.[2]

The charged species of the Girard-reagent hydrazones (except for the neutral form of the Girard-D reagent) are soluble in water, and thus can be utilized for the electrophoretic separation of, *e.g*., progesterone, testosterone and estrone.[18]

The Girard-T hydrazones are also used in paper chromatography.[19]

In addition to these applications, some Girard reagents hydrazones appeared to show biological activity.[1] Hence, they are also interesting from a pharmacological point of view.

More recently, it was found that some Girard-T or Girard-P derivatives are good inhibitors of C-steel corrosion in acidic medium.[20,21]

2. COMPLEXES OF GIRARD REAGENTS

As can be seen from their formulas (Fig. 1), Girard reagents have several atoms as potential donors, *viz*. two nitrogen of the hydrazine moiety and one oxygen atom, and in the case of neutral and monoanionic forms of the Girard-D reagent, also the amine nitrogen atom. As will be shown later, a common feature of all Girard reagents is that, in addition to the oxygen atom, the terminal hydrazine nitrogen atom participates in coordination, forming a five-membered metallocycle. To date, the largest number of complexes have been synthesized with the Girard-T reagent, whereas, to the best of our knowledge, no complexes with the Girard-P reagent have been reported.

Although these reagents are known since 1936, the first paper in the field of coordination chemistry dealing with Girard reagents, describing a copper(II) complex with the Girard-T reagent, was published in 1969.[15] Thus, the reaction of aqueous solutions of $CuSO_4$ and this reagent, in the presence of a small amount of methanol, gave the blue bis(ligand) complex of the formula $[Cu(HGT)_2](SO_4)_2·2H_2O$. The investigations showed that variation of the metal––ligand molar ratio from 1:2 to 1:4 always resulted in the bis(ligand) complex. Based on IR and UV spectral analyses, the authors[15] proposed a bidentate NO coordination.

More recently, some new complexes of copper(II) and copper(I) and Girard-T reagent of the formulas $[Cu(HGT)Cl_2(H_2O)_2]Cl·H_2O·EtOH$, $[Cu(GT)(EtOH)_{3/2}]Br_2$, $[Cu(HGT)I_2]·H_2O$ and $[Cu(HGT)I]I$ were reported by Mostafa and Abdel-Rhman.[22] The first was prepared by the reaction of ethanolic solutions of $CuCl_2·2H_2O$ and the Girard-T reagent in the molar ratio of 1:2, and the second one by the reaction of the first complex with KBr. It is interesting to note that this tribochemical reaction of preparation of the bromide salt is accompanied by the deprotonation of the organic ligand. For both complexes, a bidentate NO coordination of the Girard-T reagent was proposed. The iodido complexes were also prepared by the tribochemical reaction of the mentioned chlorido complex and CaI_2 or KI, and, due to the reducing properties of iodide, the product was a diamagnetic copper(I) complex. It is important to note that the newest evaluation of the biological activity of the above-mentioned chlorido complex showed that it is a promising antitumor agent.[23]

The reaction of an ethanolic solution of the neutral Girard-D reagent with an aqueous solution of $Cu(ClO_4)_2$ gave a copper(II) complex of the formula $Cu(GD)ClO_4·H_2O$. This reagent, with copper chloride or sulfate, also gave copper(II) complexes of analogous compositions.[15] In all cases where the metal:ligand ratio was changed from 1:1 to 1:4, only monoligand complexes were obtained.

In the same paper, the authors also considered the possibility of a bidentate coordination of the monoanion of this reagent (Fig. 2), and proposed the most probable NO coordination (Fig. 2a), analogous to copper(II) coordination in di-peptides.[24]
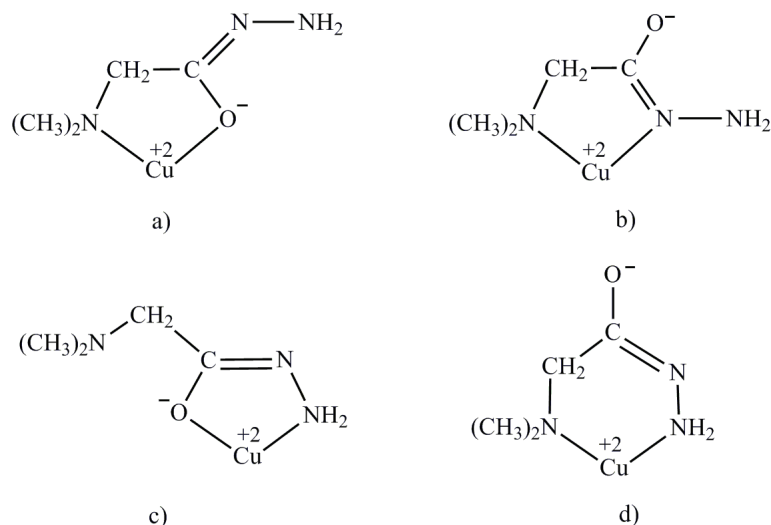
Fig. 2. Possible coordination modes of the Girard-D reagent monoanion.

3. HYDRAZONES OF GIRARD REAGENTS AND THEIR COMPLEXES

3.1. Preparation of Girard hydrazones

Girard reagents hydrazones are obtained in condensation usually of ethanolic or methanolic solutions of Girard reagents and carbonyl compounds in the presence of acetic acid (Scheme 2).

$(R = (CH_3)_3N^+, (CH_3)_2\overset{+}{N}H, C_5H_5N^+)$
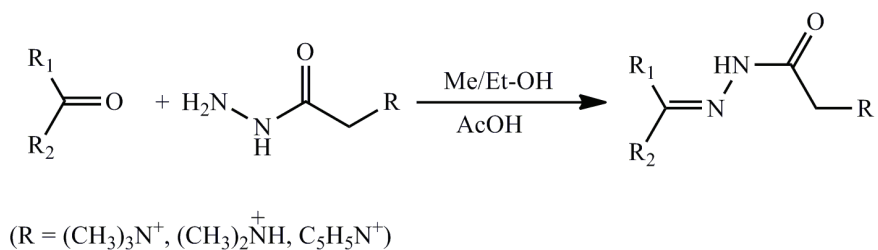
Scheme 2. Preparation of Girard hydrazones.

The mentioned mixtures were refluxed for 20–60 min in the case of alde-hydes,[3] and up to 12 h in the case of the less reactive ketones.[25]

Solutions of Girard reagent hydrazones are stable in approximately neutral media (pH 6.5–7.0), whereas they undergo hydrolysis in acidic media.[3]

Up to now, a number of Girard reagent hydrazones of different mono- and poly-functional carbonyl compounds are known.[15,21,26–38]

Apart from numerous hydrazonic derivatives of Girard reagents, there are also some non-hydrazonic Girard-T/P derivatives of the general formula R–CH$_2$––C(=O)–NH–NH–C(=S)–NHR' (R = –(CH$_3$)$_3$N$^+$Cl$^-$, –C$_5$H$_5$N$^+$Cl$^-$; R' = –C$_2$H$_5$, –CH$_2$CH=CH$_2$, –C$_6$H$_5$). These compounds were obtained by Mostafa[39] by boiling under reflux the corresponding R' isothiocyanates and Girard-T/P reagents in absolute ethanol.

3.2. Complexes of Girard hydrazones

Girard hydrazones may have three or more potential ligator atoms; hence, they are also of interest to coordination chemists.

Although Girard hydrazones have been known for a very long time, the number of their complexes with metals is relatively small. In all the complexes described to date, the Girard hydrazones behave as mono-, di-, tri- and penta-dentate Schiff bases.

3.2.1. Complexes with Girard-T hydrazones

Most of the synthesized complexes with Girard hydrazones are with Girard-T hydrazone of various denticities. Thus, Mostafa *et al.*[35] in the reaction of equimolar amounts of diacetylmonoxime Girard-T hydrazone, [(CH$_3$)$_3$N$^+$–CH$_2$––C(=O)NH–N=C(CH$_3$)–C(CH$_3$)= =NOH]Cl, [HDMGT]Cl, and CuCl$_2$ obtained complexes, which, in dependence of the nature of the solvent and pH, have different compositions, as well as different ligand denticity.[35] Namely, it was found that from an ethanolic solution, a square-planar mono(ligand) complex [Cu(HDMGT)Cl$_2$]Cl·H$_2$O crystallized, in which this, potentially tridentate, ligand is coordinated in a bidentate manner, involving the hydrazone and oxime nitrogen atoms (Fig. 3).
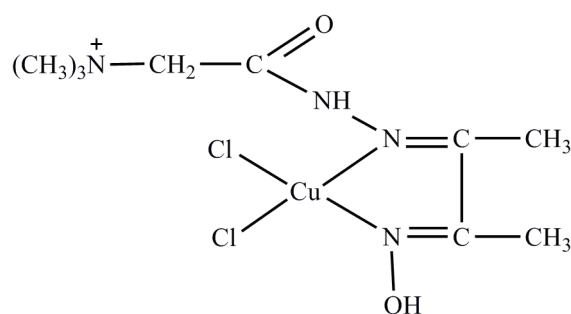

Fig. 3. Supposed square-planar structure of [Cu(HDMGT)Cl$_2$]$^+$.

If, however, the reaction is performed in an aqueous solution at pH 5, the result was an octahedral bis(ligand) complex [Cu(HDMGT)$_2$Cl$_2$]Cl$_2$, with the al-

ready mentioned NN coordination of the ligand. Finally, from an aqueous solution of pH 10, the octahedral mono(ligand) complex $[Cu(DMGT)Cl(H_2O)_2]Cl·H_2O$ crystallized. In this complex, the ligand is coordinated in a tridentate mono-deprotonated enol form, [DMGT], through the hydrazine and oxime nitrogen atoms, as well as through the deprotonated oxygen atom of the enolised carbonyl group.[35]

With anisaldehyde Girard-T hydrazone, $[(CH_3)_3N^+–CH_2–C(=O)NH–N=$ $=CH–C_6H_4–OCH_3)]Cl$, [HAGT]Cl, two complexes were reported, *viz.* the square-planar copper(II) complex $[Cu(HAGT)Cl_2]Cl$ and the square-pyramidal iron(III) complex $[Fe(HAGT)Cl_3]Cl$.[37] Moreover, in the same paper, octahedral bis(ligand) complexes of manganese(II) and cobalt(II) of the general formula $[M(HAGT)_2Cl_2]Cl_2$ were described. In these complexes, the ligand is coordinated bidentately, through the nitrogen atom of the azomethine group and the carbonyl oxygen atom.

With tridentate ONO salicylaldehyde Girard-T hydrazone, $[(CH_3)_3N^+–CH_2–$ $–C(=O)NH–N=CH–C_6H_4–OH)]Cl$, $[H_2SalGT]Cl$, the first synthesized complexes were those of dioxovanadium(V) and dioxomolybdenum(VI) of the formulas $[VO_2(SalGT)]$[28] and $[MoO_2(SalGT)(CH_3OH)]I$, respectively.[40] The complexes were obtained in the reactions of methanolic solutions of Et_4NVO_3, and $MoO_2(acac)_2$ (addition of I_2) with $[H_2SalGT]Cl$, respectively.

X-Ray analysis of these complexes showed that the ligand was coordinated as tridentate in the monoanionic form, *via* the oxygen atom of the deprotonated phenolic OH and the enolized carbonyl group, as well as *via* the azomethine nitrogen atom. It was found that the structure of the dioxovanadium(V) complex was a very deformed square pyramid (Fig. 4a).[28] On the other hand, the dioxomolybdenum(VI) complex had a deformed octahedral geometry in which, in addition to the two oxygen atoms of the dioxomolybdenum(VI) and the tridentate chelate ligand, the sixth coordination site was occupied by the methanol oxygen atom (Fig. 4b).[40]
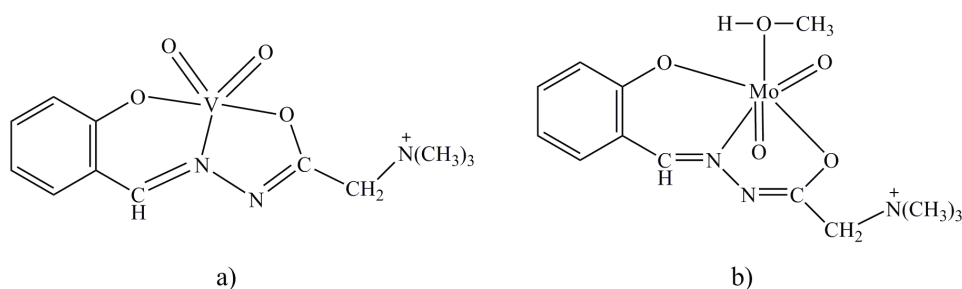

Fig. 4. Structures of the V(V) (a) and Mo(VI) (b) complexes with salicylaldehyde Girard-T hydrazone.
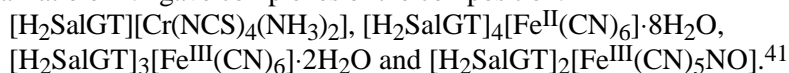
More recently, some new complexes of the same ligand were synthesized, and some of them, as well as the ligand itself, were characterized by X-ray structural analysis.[31,41,42]

In its crystalline state, the ligand consists of the $[H_2SalGT]^+$ cation and Cl^-, and the donor atoms – the hydrazine nitrogen N(1), carbonyl oxygen O(1) and phenolic oxygen O(2), are mutually in a *cis*-position, *i.e.*, in the position that is favorable for coordination[31] (*vide infra*). Otherwise, this is not the case with compounds of a similar class, such as the majority of semicarbazones,[43,44] in which the carbonyl oxygen in the free ligand is in the *trans* position with respect to the hydrazine nitrogen.

In the isostructural square-pyramidal complexes of copper(II) with the same ligand, of the formula $[Cu(HSalGT)X_2]\cdot H_2O$ (X = Cl, Br), the tridentate ONO ligand is coordinated in its neutral, *i.e.*, monodeprotonated form, through the carbonyl oxygen, hydrazine nitrogen and the oxygen of the deprotonated phenolic hydroxyl.[31]

Apart from the mentioned copper(II) complexes, a zinc(II) complex of the formula $Zn(SalGT)Cl\cdot 2H_2O$[42] was prepared. It involves the monodeprotonated form of the ligand, as in the previously described complexes of dioxovanadium(V)[28] and dioxomolybdenum(VI).[40]

Finally, there are also the complexes in which the ligand $[H_2SalGT]Cl$ plays the role of the cation, which is capable of precipitating some voluminous complex anions. Thus, the reaction of aqueous solutions of the ligand and $NH_4[Cr(NCS)_4(NH_3)_2]$, $K_4[Fe(CN)_6]$, $K_3[Fe(CN)_6]$, or $Na_2[Fe(CN)_5NO]$, in a molar ratio of 1:1 gave complexes of the composition:

$[H_2SalGT][Cr(NCS)_4(NH_3)_2]$, $[H_2SalGT]_4[Fe^{II}(CN)_6]\cdot 8H_2O$,
$[H_2SalGT]_3[Fe^{III}(CN)_6]\cdot 2H_2O$ and $[H_2SalGT]_2[Fe^{III}(CN)_5NO]$.[41]

Revenco *et al.*[33] synthesized and characterized the structure of a new ligand, a derivative of the Girard-T reagent and 5-bromosalicylaldehyde, $[(CH_3)_3N^+-$ $-CH_2-C(=O)NH-N=CH-C_6H_3(OH)(Br))]Cl$, $[5-BrH_2SalGT]Cl$, and its complexes with Fe(III) of the formulas:

$[Fe(5-BrSalGT)Cl_2]$ and $[Fe(5-BrSalGT)(NCS)_2(H_2O)]$.
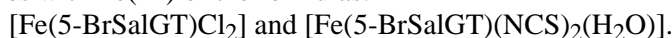
The chlorido complex was obtained in the reaction of an ethanolic solution of $FeCl_3$ and the ligand, while the thiocyanato one was formed in the reaction of an aqueous ethanolic solution of the chlorido complex and NH_4NCS.

It was found that the Fe(III) in the chloride complex was in a distorted square-pyramidal environment, which was realized by ONO coordination of the doubly deprotonated Schiff base ligand and two chloride ligands. In the second complex, the octahedral surroundings of Fe(III), in addition to the ONO donor atoms of the organic ligand, were realized with two nitrogen atoms of the NCS^- and the oxygen atom of a water molecule. Both complexes were high-spin and were ordinary paramagnets down to 2 K.

The condensation of 2-formylpyridine with the Girard-T reagent in MeOH yielded $[(CH_3)_3N^+–CH_2–C(=O)NH–N=CH–C_5H_4N)]Cl$, $[H(2-PyGT)]Cl$.[34] This compound (DMF solution) reacted with iron(III) or copper(II) chloride to give the deformed octahedral complex $[Fe(2-PyGT)Cl_3]$ (*vide infra*) and the deformed square-pyramidal complex $[Cu(2-PyGT)Cl_2]·H_2O$. In these complexes, the tridentate NNO organic ligand is formally a neutral species, but acts as a zwitterion, *i.e.*, the quaternary ammonium cationic group is compensated by a negative charge resulting from deprotonation of the enolic tautomer. As expected for mononuclear complexes, the small and negative Weiss constant of this compounds indicates that the spin carriers are only in very weak antiferromagnetic interactions in the crystal lattice.

The metal complexes with Schiff bases derived from pyridoxal (PL), *e.g.*, 3-hydroxy-5-(hydroxymethyl)-2-methylpyridine-4-carboxaldehyde (one of the forms of vitamin B6) and the Girard-T reagent was the subject of studies of Leovac *et al.*[30,41,42,45,46] The dichloride salt of the ligand, pyridoxal Girard-T hydrazone dihydrate, $[(CH_3)_3N^+–CH_2–C(=O)NH–N=CH–C_5HN^+H(CH_3)(OH)-(CH_2OH))]Cl_2$, $[H_3PLGT]Cl_2·2H_2O$, was obtained by reaction of an ethanolic solution of the Girard-T reagent and pyridoxal hydrochloride. In $[H_3PLGT]Cl_2·2H_2O$, the pyridine nitrogen of the pyridoxal is protonated. Its first deprotonation step was the loss of the most acidic proton (of the phenolic hydroxyl), whereas the neutral form resulted from an additional deprotonation of the enolized form of the carbonyl group. To obtain a monoanionic form, it is necessary to extract additionally the least acidic proton bound to the pyridine nitrogen of pyridoxal, for which the presence of a proton acceptor, *e.g.*, ammonia, acetate, *etc*. is required.[47]

The first structurally characterized complex with this ligand is the cobalt(III) complex $[Co(HPLGT)(NO_2)_3]·H_2O$,[30] which was obtained by the reaction of aqueous solutions of $Na_3[Co(NO_2)_6]$ and the ligand in a molar ratio of 1:1 (Scheme 3). In this complex, the central atom is in an octahedral environment, which is realized by the meridionally arranged ONO atoms of the tridentate Schiff base and three monodentate N-bonded NO_2 groups (*vide infra*). The pyridoxal fragment is in a zwitterionic form, which in the case of the coordinated ligand is formed by deprotonation of the coordinated oxygen atom of the phenolic OH group and protonation of the pyridine nitrogen.

The crystallization of the bis(HPLGT) cobalt(III) complex with common small anions appeared to be unsuccessful,[41] whereas the addition of more voluminous anions enabled the isolation of the complexes $[Co(HPLGT)_2](PF_6)_3$,[30] and $[Co(HPLGT)_2][Cr(NCS)_4(NH_3)_2]_3·8H_2O$.[41] These complexes were prepared by the reaction of aqueous solutions of $Na_3[Co(NO_2)_6]$ and the ligand in a molar ratio of 1:2, in the presence of ammonium salts of PF_6^-, or $[Cr(NCS)_4(NH_3)_2]^-$ (Scheme 3).

$$[Co(NO_2)_6]^{3-}$$

$[H_3PLGT]Cl_2 \cdot 2H_2O$ $2[H_3PLGT]Cl_2 \cdot 2H_2O$

H_2O H_2O, reflux

$[Co(HPLGT)(NO_2)_3] \cdot H_2O$ $[Co(HPLGT)_2]^{3+}$

(solution)

MeOH
NH_3

                                     PF_6^- $[Cr(NCS)_4(NH_3)_2]^-$

$[Co(PLGT)(NO_2)_2(NH_3)] \cdot 3H_2O$

$[Co(HPLGT)_2](PF_6)_3$ $[Co(HPLGT)_2][Cr(NCS)_4(NH_3)_2]_3 \cdot 8H_2O$
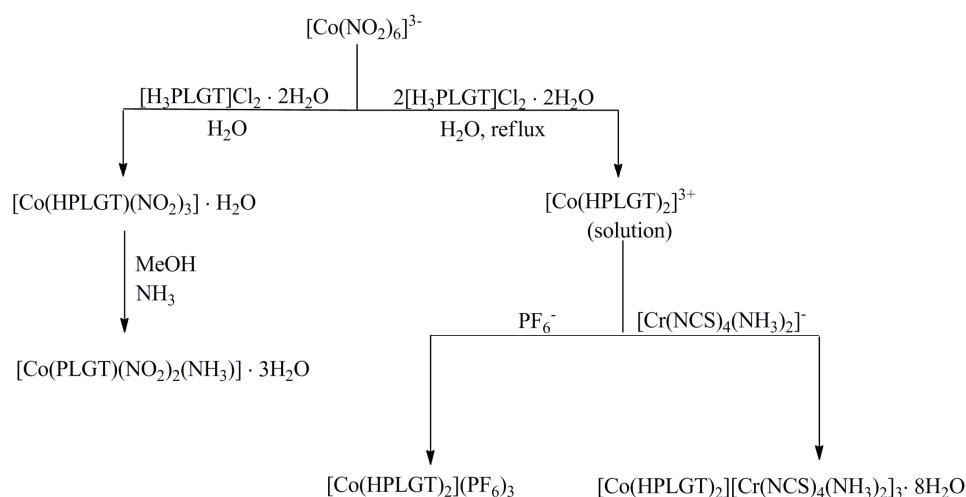
Scheme 3. Preparation of the Co(III) complexes with pyridoxal Girard-T hydrazone.

Finally, the reaction of the MeOH solution of the complex [Co(HPLGT)-$(NO_2)_3] \cdot H_2O$[30] with an excess of $NH_{3(aq)}$ gave the non-electrolyte complex: $[Co(PLGT)(NO_2)_2(NH_3)] \cdot 3H_2O$.[41,45]

As can be seen from the formula, the replacement of one nitro ligand with an NH_3 molecule occurred, with the simultaneous deprotonation of the Schiff base, *i.e.*, of the pyridoxal ring. This is the first example of a complex in which the ligand is coordinated in its triply deprotonated form.

Isostructural, most probably square-pyramidal, complexes of Cu(HPLGT)X_2 (X = Cl or Br) were obtained in the reaction of CuX_2 (X = Cl or Br) with $[H_3PLGT]Cl_2 \cdot 2H_2O$.[42] Starting from copper(II) nitrate, the authors obtained a complex Cu(HPLGT)Cl(NO_3).[41] In two other complexes of this metal,[45] the ligand is coordinated in its triply deprotonated (monoanionic) and doubly deprotonated (neutral) form, giving the $[Cu(PLGT)N_3]$ and the square-pyramidal $[Cu(HPLGT)(NCS)_2]$ complexes, respectively, the latter of which was characterized by X-ray structural analysis.

Here, it is important to stress that attempts to synthesize copper complexes that would, in addition to this ligand, contain also pyridine and its methyl derivatives, were unsuccessful, since the result was the mentioned complexes.[41] Such a behavior of pyridoxal Girard-T hydrazone is in contrast to the behavior of the similar tridentate Schiff bases.

To date, two zinc complexes with this ligand are known, one of them being the chloride complex of composition Zn(HPLGT)Cl$_2$,[42] which in reaction with NH_4NCS gave Zn(HPLGT)(NCS)$_2 \cdot H_2O$.[45]

In the reaction with ammonium metavanadate, pyridoxal Girard-T hydrazone gave gold-yellow crystals, the preliminary structural analysis of which showed

that the composition of the formed complex was $[VO_2(PLGT)]\cdot H_2O$ (Fig. 5).[48] As can be seen from the formula, the complex contains the ligand in its monoanionic form, formed by deprotonation of the pyridine nitrogen atom, which could be expected since the reaction was performed in an ammoniacal medium. The complex has a pentacoordinated structure (deformed square-pyramid) with two oxo-ligands in the *cis* position. As mentioned above, there is another analogous complex with the salicylaldehyde ligand, $[VO_2(SalGT)]$.[28]
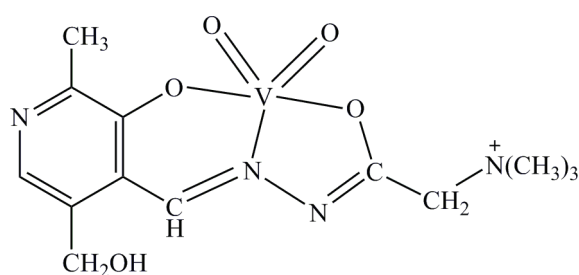
Fig. 5. Structure of $[VO_2(PLGT)]$.

Finally, the reaction of pyridoxal Girard-T hydrazone with some anionic complexes of Cr(III) and Fe(II and III) gave complexes in which the hydrazone ligand plays the role of the outer-sphere counter ion $[H_3PLGT]^{2+}$. Thus, the reaction of a methanolic solution of the ligand and Reinecke salt, $NH_4[Cr(NCS)_4(NH_3)_2]$, in the mole ratio of 1:1 gave a complex of the composition $[H_3PLGT][Cr(NCS)_4(NH_3)_2]_2\cdot 2CH_3OH$, whereas the complexes:

$[H_3PLGT]_2[Fe^{II}(CN)_6]\cdot 3H_2O$, $[H_3PLGT]_3[Fe^{III}(CN)_6]_2\cdot 2H_2O$ and
$[H_3PLGT][Fe^{III}(CN)_5NO]\cdot 3H_2O$
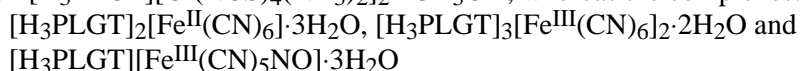
were obtained by mixing a methanolic solution of the ligand with aqueous solutions of $K_4[Fe(CN)_6]$, $K_3[Fe(CN)_6]$ and $Na_2[Fe(CN)_5NO]\cdot 2H_2O$, respectively, in a mole ratio of 1:1.[41]

In continuation of their study of the synthesis of new derivatives of the Girard-T reagent, Leovac *et al.* investigated the possibility of the preparation of the Schiff bases of this reagent and acetylacetone (Hacac), *i.e.*, of Hacac mono- and bis(Girard-T hydrazone).[45] To this end, they performed the reactions in methanolic solutions of the Girard-T reagent and acetylacetone in the molar ratios of 1:1 and 2:1 in the presence of acetic acid. To such solutions, they added methanolic solutions of $CuCl_2$, which, instead of a complex with the desired Schiff base, resulted in a mixture of monocrystals: brown $[Cu(acac)_2]\cdot 2[Cu(3,5-Me_2pz)_2Cl_2]$ (3,5-Me_2pz = 3,5-dimethylpyrazole), green $[Cu(3,5-Me_2pz)_2Cl_2]_2$, and blue $Cu(acac)_2$, the identity and structural analysis of which were established by X-ray structural analysis, while the latter two complexes were previously characterized.[49,50]

Here, a cyclization reaction occurred between the condensed hydrazide moiety of the Girard-T reagent and acetylacetone, resulting in the formation of a pyrazole derivative and elimination of the trimethylammoniumacetyl moiety in the presence of metal ions because of the weaker NH–CO bond due to the coordination. The formation of a complex with the above pyrazole derivative is not surprising since the reactions of acetylacetone and hydrazine derivatives are known to result in the corresponding pyrazole derivatives.[51]

Novaković *et al.*,[46] by reaction of a methanolic solution of 2,3,4-trihydroxy-benzaldehyde Girard-T hydrazone with $ZnCl_2$ obtained white monocrystals, the crystal structure of which contained the tetrachloridozincate ion and two Girard-T hydrazone cations.

It is known that 2,6-diacetylpyridine is an excellent precursor for the synthesis of a number of bis(Schiff base) ligands in which they act as planar pentadentate ligands,[52] promoting thus the formation of heptacoordinated pentagonal-bipyramidal complexes. A number of manganese(II) complexes have been synthesized in which bis(hydrazone) chelating agents may participate with different sets of donor atoms, including the N_3O_2 set,[52–56] involved also in the title ligand. In a study[57] the ligands, 2,6-diacetylpyridine bis(Girard-T/P hydrazone) dichloride were obtained in the form of anhydrous salts, although they were recrystallized from water–ethanol systems. However, neither physico-chemical characterization of the given hydrazone Girard-T ligand nor elemental analysis data were given in the paper. The authors only showed that the listed ligands were suitable for chromatographic determinations of Ti(IV), U(VI), Fe(III) and V(V).[57] Leovac *et al.*[32] described a simpler method for the synthesis of 2,6-diacetylpyridine bis(Girard-T hydrazone)dichloride ligand in the form of the tetrahydrate salt, $[[(CH_3)_3N^+–CH_2–C(=O)NH–N=C(CH_3)]_2C_5H_3N)]Cl_2$, $[H_2dap(GT)_2]Cl_2·4H_2O$. This ligand was obtained in high yield by the reaction of a warm methanolic solution of the stoichiometric amounts of the Girard-T reagent and 2,6-diacetylpyridine, the result being white fibrous crystals, stable in air.

Yellow, plate-like single crystals of the $[Mn(H_2dap(GT)_2)(NCS)_2](NCS)_2·$ $·CH_3OH$[32] complex were obtained by mild heating of a MeOH solution of the ligand and $MnCl_2$ in a mole ratio of 1:1 in the presence of an excess of NH_4NCS. The complex had pentagonal-bipyramidal coordination geometry, with the pentadentate N_3O_2 ligand in the equatorial plane and two isothiocyanato groups in the axial positions (*vide infra*).

Finally, as examples of non-hydrazonic Girard-T derivatives, 4-ethyl/benzoyl-1-[2-(trimethylammonio)acetyl]thiosemicarbazide chlorides, $[(CH_3)_3N^+–$ $–CH_2–C(=O)NH–NH–C(=S)NH–R]Cl$, (R = $–C_2H_5$ or $–C(=O)C_6H_5$; [H_2GTETS] Cl, [H_2GTBzIT]Cl, respectively) are mentioned. They are obtained in the reaction of the Girard-T reagent and ethyl/benzoyl isothiocyanate and gave several mono- and bi-nuclear complexes, which were characterized by spectroscopic me-

thods.[58,59] Thus, [H_2GTETS]Cl gave binuclear complexes of cobalt(II) and copper(II) of the formulas [Co_2(GTETS)(OAc)(OH)(H_2O)$_3$]Cl·C_2H_5OH and [Cu_2(HGTETS)(OH)$_3$(H_2O)]Cl·0.5C_2H_5OH.[58] As can be seen from Fig. 6, one cobalt atom is situated in an octahedral and the other in a square-planar environment, and the bridging ONS ligand is coordinated in its thiol form. An identical coordination mode, but involving a thione form, was also found in the copper complex. In addition to these complexes, the same paper also describes a mononuclear octahedral complex of copper(II) with the formula [Cu(H_2GTETS)-(H_2O)$_2$$Cl_2$]Cl·1.5$H_2O$, involving NS coordination of the ligand in its thione form, as well as a tetrahedral complex of cobalt(II) with the formula [Co(H_2GTETS)(H_2O)Cl_2]Cl·C_2H_5OH, involving an S-coordination of the ligand.

Fig. 6. Proposed structure for [Co_2(GTETS)(OAc)(OH)(H_2O)$_3$]$^+$.

In contrast to this ligand, in the case of the cation [H_2GTBzIT]$^+$, thanks to the presence of another oxygen atom as ligator, the IR spectra indicated that, apart from one nitrogen atom, both oxygen atoms were involved in the coordination.[59] Such a coordination mode was also found in the mononuclear Cr(HGTBzIT)Cl_3·3H_2O, Ni(GTBzIT)Cl·5H_2O, and Cd(H_2GTBzIT)Cl_3·3H_2O complexes, in the binuclear complex Co_2(GTBzIT)Cl_3·4H_2O and in the trinuclear complexes of Cu(II) and Zn(II) of the formula M_3(HGTBzIT)(GTBzIT)Cl_5·3H_2O. The only exception from such a coordination mode of [H_2GTBzIT]$^+$ that has hitherto been reported is the bis(ligand) complex Mn(H_2GTBzIT)$_2$$Cl_4$, in which the bidentate coordination of the ligand involves the OS or NS ligator atoms.[59] In addition to the spectroscopic characterization of the above complexes, their stability in both the solid state and solution were also investigated.
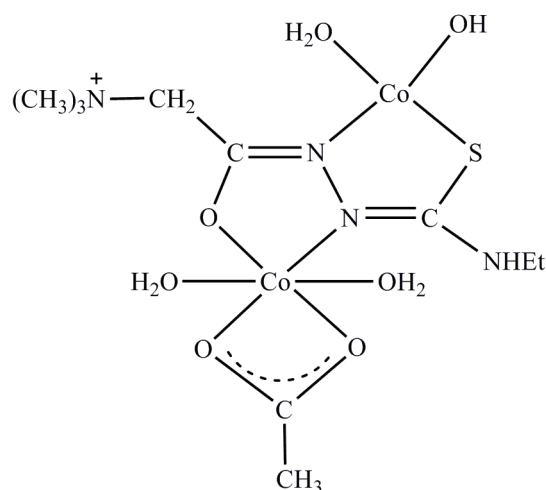
3.2.2. *Complexes with Girard-D hydrazones*

Of the complexes with Girard-D hydrazones, to the best of our knowledge, only complexes with the diacetylmonoxime Girard-D hydrazone, [$(CH_3)_2N^+H$––CH_2–$C(=O)NH$–$N=C(CH_3)$–$C(CH_3)=NOH$]Cl, [HDMGD]Cl have been reported. Thus, mono-ligand complexes [$M(HDMGD)Cl_2$]Cl (M(II) = Cd or Hg), and bis(ligand) complexes [$Cu(HDMGD)_2Br_2$]Cl_2 and [$M(DMGD)_2(H_2O)_2$]$Cl_2\cdot$ $\cdot nH_2O$, (M = Ni(II), Cu(II) or $U^{VI}O_2$) were synthesized by Mostafa *et al.*[36] In the complexes of cadmium(II) and mercury(II), NO bidentate coordination was ascribed to the hydrazone ligand, which was realized by coordination of the carbonyl oxygen atom and the azomethine nitrogen atom. In view of the participation of two chlorine atoms in the coordination, the authors supposed that these complexes had a tetrahedral geometry. For the octahedral bis(ligand) complexes [$M(DMGD)_2(H_2O)_2$]$Cl_2\cdot nH_2O$, which were obtained in the presence of sodium acetate, the authors also supposed a bidentate coordination of the ligand, but with the participation of the oxygen atom of the enol form. In contrast to these complexes, in which this hydrazone ligand is coordinated bidentately, for the bis(ligand) complex of copper(II), [$Cu(HDMGD)_2Br_2$]Cl_2, based on IR spectral analysis, monodentate ligand coordination was proposed, which involved two azomethine nitrogen atom of two HDMGD cations that, together with two bromine atoms, formed a square-planar environment around the copper(II).[36]

3.2.3. *Complexes with Girard-P hydrazones*

In contrast to the Girard-P reagent, with which, to the best of our knowledge, no metal complexes have been reported up to now, several complexes of its hydrazones have been described. Thus, Wang *et al.*[28,60] described the syntheses, spectroscopic properties and X-ray structures of the neutral square-pyramidal VO_2^+ and monocationic octahedral MoO_2^{2+} complexes with the ONO salicylaldehyde Girard-P hydrazone, [$C_5H_5N^+$–CH_2–$C(=O)NH$–$N=CH$–C_6H_4–OH]Cl, [H_2SalGP]Cl, of the formula [$VO_2(SalGP)$]$\cdot CH_3OH$ and [$MoO_2(SalGP)$] (CH_3OH)]Cl, respectively. In addition to the mentioned complexes, the same authors[61] also synthesized and structurally characterized the square-pyramidal VO_2^+ complex with tridentate ONO benzoylacetone Girard-P hydrazone, of the formula [$VO_2(BAGP)$]$\cdot CH_3CH_2OH$ ($H_2BAGP = C_5H_5N^+$–CH_2–$C(=O)NH$– –$N=C(CH_3)$–CH_2–$C(=O)$–C_6H_5) (*vide infra*). The complexes were obtained in reaction of alcoholic solutions of $MoO_2(acac)_2$ or NEt_4VO_3 with the corresponding Schiff bases.

Several complexes of the general formula [$M(SalGP)(H_2O)$]Cl·nH_2O (M = = Ni(II), Co(II) or Zn(II)), as well as the copper(II) complex [$Cu(SalGP)$]$_2Cl_2$, involving the same ligand, have been described in the literature.[62]

With a ligand similar to that above, *i.e.*, *o*-hydroxyacetophenone Girard-P hydrazone, [$C_5H_5N^+$–CH_2–$C(=O)NH$–$N=C(CH_3)$–C_6H_4–OH]Cl, [H_2AFGP]Cl,

several complexes of the formula $M(AFGP)(H_2O)Cl$ (M = Co(II), Ni(II), Cu(II) or Zn(II)) have been reported.[37] In these complexes, in addition to the tridentate ONO coordination of the doubly deprotonated ligand, the fourth coordination site is ascribed to a water molecule. There appeared an interesting possibility of thermal dehydrohalogenation of these complexes. Namely, the results of differential thermal analysis showed the formation of stable complexes of non-electrolyte type, $[M(AFGP–H)]\cdot H_2O$.

Finally, a series of metal complexes with the derivatives of Girard-P reagent and 4-benzoylthiosemicarbazide, *i.e.*, with 4-benzoyl-1-(2-pyridinioacetyl)thiosemicarbazide chloride, $[C_5H_5N^+–CH_2–C(=O)NH–NH–C(=S)NH–C(=O)–$ $–C_6H_5]Cl$, $[H_2GPBzIT]Cl$ have been described.[63] The IR spectra of the complex $Mn(HGPBzIT)_2Cl_2\cdot2H_2O$ showed that the ligand behaves as a bidentate chelate. It coordinates *via* CS in the thione form and the enolized carbonyl oxygen of the benzoyl moiety with the displacement of a hydrogen atom from the latter group. Furthermore, in the complexes, $Cr(HGPBzIT)Cl_3\cdot H_2O$, $Co(HGPBzIT)Cl_2$ and $Zn(HGPBzIT)Cl_2\cdot2H_2O$, the ligand $[H_2GPBzIT]Cl$ behaves as a tridentate chelate. In $Ni(GPBzIT)Cl\cdot H_2O$, $Cu_2(GPBzIT)Cl_3\cdot2H_2O$ and $Cd_2(GPBzIT)Cl-(OAc)_2\cdot2H_2O$, the ligand behaves as a tridentate chelate, involving the enolic oxygen of both CO groups and the nitrogen of the NH group. In addition to spectroscopic methods (IR and UV–Vis), the obtained complexes were also characterized by thermal analysis and by determination of the stability constants.

4. STRUCTURAL CHARACTERISTICS

The structural properties of the Girard reagent-based compounds are reviewed based on information available in the Cambridge Structural Database (CSD).[64] The CSD search revealed only 22 such compounds, of which 14 were complexes the crystal structures of which were characterized by X-ray structural analysis. Out of all the reported crystal structures, 19 are derivatives of the Girard-T reagent, while only three are Girard-P reagent-based compounds. To the best of knowledge, no structural data concerning the Girard-D reagent are available. An overview of the compounds and their selected structural parameters is given in Tables I and II. The general atom-numbering scheme of the moieties of the Girard reagents employed in this work was retained from the reports of Leovac *et al.*[30–32,45,46] (see Fig. 7a).

The crystal structures reported can be divided into four groups:

– Non-coordinated Girard-T reagent,[10] both unmodified or with the substituted amino H, all present as cations with the bulky $[BPh_4]^-$ as a counterion (structures **1**–**3**);

– Non-coordinated Schiff bases Girard-T hydrazones. Hitherto, the Schiff bases of salicylaldehyde (**4**),[31] 5-bromosalicylaldehyde (**5**),[33] indole-2,3-dione

(**6**),[65] 2,3,4-trihydroxybenzaldehyde (**7**),[46] as well as of isobutyraldehyde (**8**),[10] have been reported;

– Coordination compounds with Girard-T hydrazones (**9–19**);[28,30–34,40,45]
– Coordination compounds with Girard-P hydrazones (**20–22**).[28,60,61]

TABLE I. Selected bond distances (Å) in the crystal structures of Girard-based compounds

Compound	C1–O1	N1–N2	N2–C1	C1–C10	N3–C10	M–O1	M–N1	M–X	Ref.
[H$_2$GT]BPh$_4$ (**1**)	1.21	1.43	1.34	1.50	1.50	–	–	–	10
[PhNHCO-HGT]BPh$_4$ (**2**)	1.21	1.38	1.34	1.51	1.49	–	–	–	10
[CH$_3$CO-HGT]BPh$_4$ (**3**)	1.22	1.37	1.33	1.52	1.50	–	–	–	10
[H$_2$SalGT]Cl (**4**)	1.22	1.37	1.34	1.52	1.50	–	–	–	31
[5-BrH$_2$SalGT]Cl (**5**)	1.22	1.38	1.35	1.53	1.51	–	–	–	33
[Indole-2,3-dione GT]Cl (**6**)	1.21	1.36	1.36	1.51	1.50	–	–	–	65
[C$_{12}$H$_{18}$N$_3$O$_4$]^a$_2$[ZnCl$_4$]·CH$_3$OH (**7**)^b	1.21	1.37	1.35	1.51	1.49	–	–	–	46
	1.20	1.37	1.35	1.52	1.51	–	–	–	–
[*i*-BuGT]BPh$_4$ (**8**)	1.21	1.38	1.34	1.51	1.50	–	–	–	10
[Cu(HSalGT)Cl$_2$]·H$_2$O (**9**)	1.28	1.35	1.29	1.50	1.50	2.05	1.98	1.90	31
[Cu(HSalGT)Br$_2$]·H$_2$O (**10**)	1.24	1.38	1.32	1.51	1.51	2.03	1.97	1.91	31
[VO$_2$(SalGT)] (**11**)	1.29	1.40	1.28	1.49	1.53	2.00	2.13	1.90	28
[MoO$_2$(SalGT)(CH$_3$OH)]I (**12**)	1.31	1.46	1.23	1.56	1.54	2.00	2.22	1.92	40
[Fe(5-BrSalGT)Cl$_2$] (**13**)	1.29	1.41	1.30	1.51	1.52	1.98	2.09	1.91	33
[Fe(5-BrSalGT)(NCS)$_2$(H$_2$O)] (**14**)	1.31	1.41	1.30	1.51	1.48	2.00	2.08	1.93	33
[Co(HPLGT)(NO$_2$)$_3$]·H$_2$O (**15**)	1.28	1.40	1.30	1.51	1.50	1.89	1.88	1.86	30
[Cu(HPLGT)(NCS)$_2$] (**16**)	1.26	1.39	1.31	1.53	1.48	1.96	1.92	1.91	45
[Fe(2-PyGT)Cl$_3$] (**17**)^a	1.28	1.38	1.32	1.50	1.51	2.01	2.12	2.17	34
	1.29	1.38	1.30	1.52	1.48	2.02	2.12	2.16	
[Cu(2-PyGT)Cl$_2$]·H$_2$O (**18**)	1.28	1.38	1.33	1.51	1.52	2.01	1.94	2.03	34
[Mn(H$_2$dap(GT)$_2$)(NCS)$_2$]-	1.23	1.37	1.23	1.51	1.49	2.31	2.32	–	32
(NCS)$_2$·CH$_3$OH (**19**)^a	1.24	1.37	1.24	1.52	1.51	2.31	2.30	2.29	
[VO$_2$(SalGP)]·CH$_3$OH (**20**)	1.30	1.41	1.29	1.50	1.48	1.97	2.14	1.89	28
[MoO$_2$(SalGP)(CH$_3$OH)]Cl (**21**)	1.34	1.41	1.29	1.48	–	2.02	2.24	1.91	60
[VO$_2$(BAGP)]·CH$_3$CH$_2$OH (**22**)	1.27	1.41	1.30	1.51	1.46	1.98	2.13	1.98	61

^{a}[C$_{12}$H$_{18}$N$_3$O$_4$]$^+$ = 2,3,4-trihydroxybenzaldehyde Girard-T hydrazone cation; ^{b}the structure contains two Girard reagent fragments or two independent molecules

In the solid state, all non-coordinated ligands appeared as cations, with the positive charge located on the quaternary ammonium group. The fragment C2−N1−N2H−C1(O1)−C10−N3 within the Schiff base is planar or slightly deviating from planarity. In fact, in the case of **4** (Fig. 7a) and its 5-bromo derivative **5**, all atoms of the structure, except for two methyl groups attached to the terminal N3, lie in the mirror plane. In most of the structures, the carbonyl O1 atom is placed *cis* to the azomethine N1 (*Z* configuration with respect to the C−N bond). The exceptions are the structures **6** (Fig. 7b) and **8**, in which the *trans* position of these atoms was observed (*E* configuration). As previously explained for the case of the Schiff bases of thiosemicarbazide,[43] the configuration of the

ligands is mostly influenced by the formation of intramolecular hydrogen bonds. Thus, in the case of **4** (Fig.7a), the *Z* configuration is stabilized by the interaction of the phenolic hydroxyl and the azomethine N1, while in **6,** in the *E* configuration (Fig. 7b), an intramolecular interaction between the carbonyl O2 and the hydrazine N2H group could be expected. The *Z* configuration of the Girard hydrazones provides a suitable arrangement of the donor atoms for coordination to metal ions. Therefore, in all reported complexes, the Girard-T or Girard-P fragments coordinate *via* the azomethine N1 and carbonyl O1 atoms. In most of the structures, the Girard-based hydrazones coordinate as tridentate ligands involving the third donor atom from the condensed carbonyl moiety. The exception is the pentadentate ligand 2,6-diacetylpyridine bis(Girard-T hydrazone) in the Mn(II) complex **19**, which is, up to now, the only reported crystal structure comprising a Girard reagent-based ligand with a denticity larger than three.

TABLE II. Selected bond angles (°) and torsion angles (°) for crystal structures of the Girard reagent-based compounds (T1 = O1–C1–C10–N4; T2= N1–N2–C1–O1; T3 = C1–N2–N1––C2; T4 = C1–O1–M–N1; T5 = X–M–N1–C2)

Compound	O1–M–N1	N1–M–X	T1	T2	T3	T4	T5	Ref.
1	–	–	20.9	8.8	–	–	–	10
2	–	–	13.0	–1.6	–72.8	–	–	10
3	–	–	–59.6	–4.7	–163.9	–	–	10
4	–	–	8.9	169.3	–173.7	–	–	31
5	–	–	0.0	0.0	0.0	–	–	33
6	–	–	0.0	0.0	0.0	–	–	65
7	–	–	–0.49	–175.3	175.3	–	–	46
			21.6	4.5	–170.1	–	–	
8	–	–	–17.8	2.0	174.4	–	–	10
9	79.6	90.9	82.7	–2.0	178.6	–9.3	–2.5	31
10	79.8	90.8	–80.6	4.9	–179.9	9.9	4.2	31
11	73.5	82.2	89.5	0.2	179.4	4.1	6.3	28
12	73.6	79.4	73.4	–7.1	–176.8	–3.7	–13.7	40
13	75.4	85.1	–	–	–	–	–	33
14	76.6	86.2	–	–	–	–	–	33
15	83.2	94.8	–93.3	0.2	177.8	–1.6	1.9	30
16	80.8	91.0	–71.1	0.2	–176.5	5.9	4.6	45
17	75.0	73.6	82.2	–0.8	–176.6	–5.0	–4.7	34
	73.8	73.8	–11.6	–1.1	–179.9	2.2	1.4	
18	78.8	81.1	78.5	–5.1	179.9	–11.6	–3.9	34
19	68.5	67.8	–63.0	2.3	179.8	12.4	5.1	32
	66.2	68.3	–41.0	–2.9	178.3	7.4	6.8	
20	73.6	82.3	177.5	–0.4	177.8	–4.9	–29.1	28
21	73.5	81.9	–	–	–	–	–	60
22	73.5	82.0	–162.7	2.5	–178.3	11.3	15.6	61

It is worth mentioning that within the extracted complexes, the Girard reagent-based ligands behave as:

– neutral – in which the positive charge of the quaternary ammonium group is neutralized by deprotonation of the H atom belonging to the condensed carbonyl moiety (**9** and **10**), or by the deprotonation of the enolic H atom, formally belonging to the hydrazine N2H group (**17** and **18**), or both (**15** and **16**);

– negatively charged (−1) – in which the H atom belonging to the condensed carbonyl moiety and the enolic H atom are both dissociated (**11–14** and **20–22**);

– positively charged (+2) – in which only a positive charge exists that is located on the quaternary ammonium fragments (**19**).
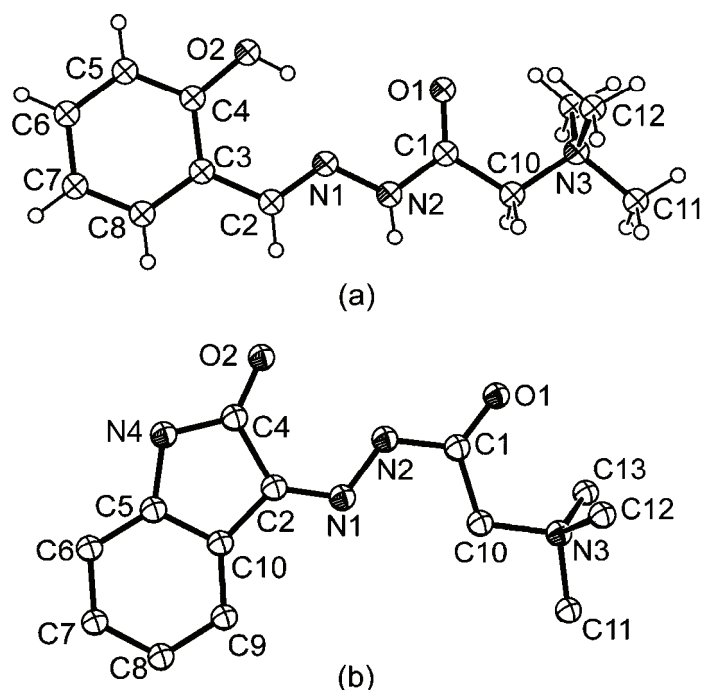
Fig. 7. The molecular structure of ligands a) [H$_2$SalGT]Cl (**4**) and b) [indole-2,3-dione GT]Cl (**6**) displaying *Z* and *E* configuration, respectively (the CIF file does not contain information concerning the H atoms in compound **6**).

Up to now, metal complexes with salicylaldehyde Girard-T and Girard-P hydrazones as ligands represent the largest family of compounds. These Schiff bases can coordinate in the neutral form *via* the deprotonated phenolic O2, azomethine N1 and carbonyl O1 (**9** and **10**) or as an anion, where the latter atom participates in the deprotonated enol form (**11**, **12**, **20** and **21**). The crystal structures of the two isostructural complexes **9** and **10** with the neutral HSalGT ligand have been reported (Fig. 8).[31] The Cu(II) ion is here located in a square-pyramidal en-

vironment (the τ values are 0.20 and 0.19 in **9** and **10**, respectively) formed by the chelating ligand, one halogen atom in the basal plane and the second halogen in the apical position.
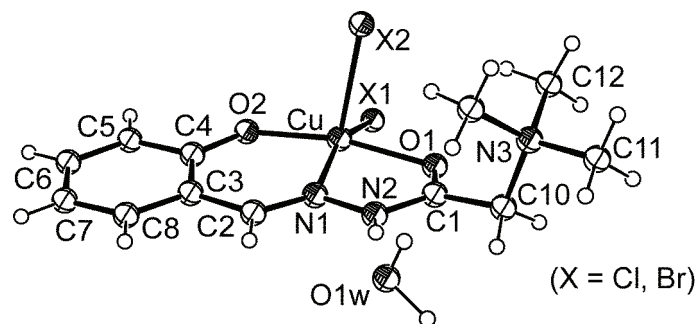
Fig. 8. The molecular structure of complexes [Cu(HSalGT)Cl$_2$]·H$_2$O (**9**) and [Cu(HSalGT)Br$_2$]·H$_2$O (**10**).

The same (ONO) coordination mode of the ligand, but involving the carbonyl O1 in a deprotonated enol form, was reported for the dioxovanadium(V) complex[28] **11** and dioxomolybdenum(VI) complex[40] **12**, as well as for their Girard-P analogues, **20**[28] and **21**.[60] According to the τ value of 0.44, the geometry of the VO$_2^+$ complex **11** can be described as very deformed square-pyramidal or trigonal-bipyramidal. The analogue complex **20**, on the other hand, displays a more regular, square-pyramidal configuration, with a τ value of 0.08. The cationic MoO$_2^{2+}$ complex **12** and the analogous complex **21** have a similar octahedral geometry, where the oxygen atoms of the Schiff base occupy the axial positions while the azomethine N1 takes one of the equatorial sites.

Similarly to the VO$_2^+$ complex **20**, which is one of the three complexes with Girard-P hydrazones characterized by X-ray crystallography, complex **22** has square-pyramidal geometry[61] ($\tau = 0.12$) (Fig. 9). In this complex, the monoanionic ligand benzoylacetone Girard-P hydrazone is coordinated *via* the enolized carbonyl O1 and O2 atoms, and the azomethine N1 atom. Revenco *et al.*[33] reported the crystal structures of Fe(III) complexes with the tridentate ONO 5-bromo derivative of the [H$_2$SalGT]Cl ligand (**13** and **14**), which also coordinates to the metal as a monoanion. The coordination polyhedron of complex **13** was described as a much distorted square-pyramid ($\tau = 0.38$), while complex **14** has an octahedral structure. The increase in the coordination number in **14** in comparison with **13** has been explained by the smaller steric hindrances of the NCS compared to the Cl anions which allowed additional coordination of the water molecule.[33]

The pyridoxal Girard-T hydrazone represents a specific ligand which can coordinate in a twice-deprotonated, and yet neutral form, as found in the case of the Co(III) (Fig. 10) and Cu(II) complexes.[30,45] This tridentate ligand coordinates

through the deprotonated carbonyl O1, the azomethine N1 and the oxygen of the deprotonated phenolic hydroxyl, forming, as above, fused five- and six-membered chelate rings. The negative charge is neutralized by the positive charges located on the quaternary ammonium and pyridoxal fragments. In the octahedral Co(III) complex **15**, the three donor atoms of the chelate ligand, together with the N-coordinated nitro group, form the equatorial plane of the polyhedron.[30] In the Cu(II) complex **16**, the chelate ligand, together with one NCS anion, forms the basal plane of a distorted square pyramid ($\tau = 0.11$).[45]
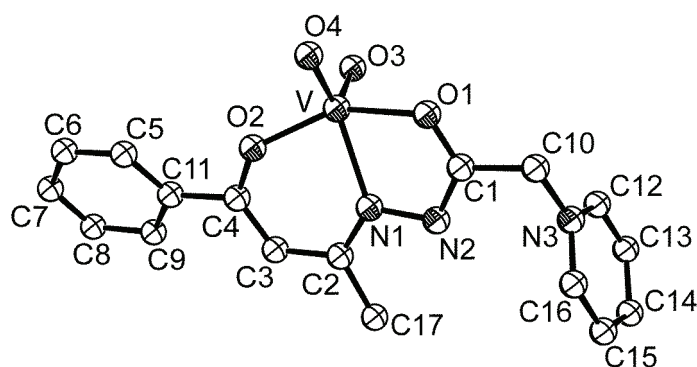
Fig. 9. The molecular structure of the complex [VO$_2$(BAGP)]·CH$_3$CH$_2$OH (**22**) (the disordered molecule of the solvent is excluded for the sake of clarity; the CIF file does not contain information concerning the H atoms).
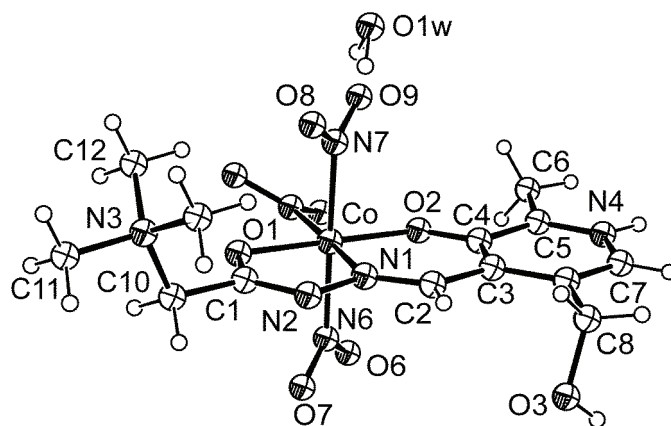
Fig. 10. The molecular structure of complex [Co(HPLGT)(NO$_2$)$_3$]·H$_2$O (**15**).

Unlike the above Schiff bases, whose coordination results in the fused five- and six-membered chelate rings, the NNO coordination of the 2-pyridinecarboxaldehyde Girard-T hydrazone results in the formation of two five-membered rings.[34] Until now, two complexes comprising this neutral tridentate ligand have

been reported, the octahedral Fe(III) complex **17** (Fig. 11) and the square-pyramidal Cu(II) complex **18** ($\tau = 0.15$).

The pentagonal-bipyramidal Mn(II) complex **19** (Fig. 12) is, to our knowledge, the only structurally characterized complex involving a pentadentate Girard reagent-based ligand.[32] This is also the only complex where the ligand is coordinated as a cation. Through the symmetric coordination, the pentadentate ligand forms two pairs of fused five-membered chelate rings, which define the equatorial plane. The pentagonal-bipyramidal coordination geometry around the Mn(II) is completed by two NCS groups that occupy the axial positions, while two remaining NCS anions, out of the coordination sphere, neutralize the complex cation.
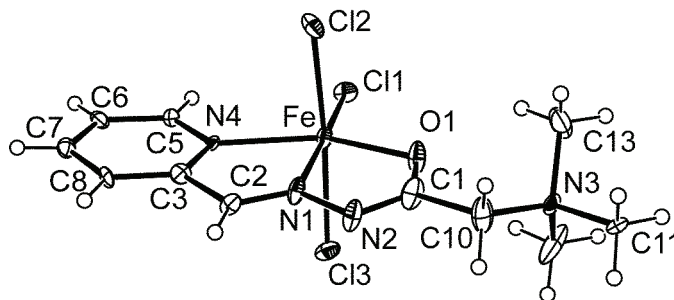
Fig. 11. The molecular structure of complex [Fe(2-PyGT)Cl$_3$] (**17**)
(one of the two independent molecules).
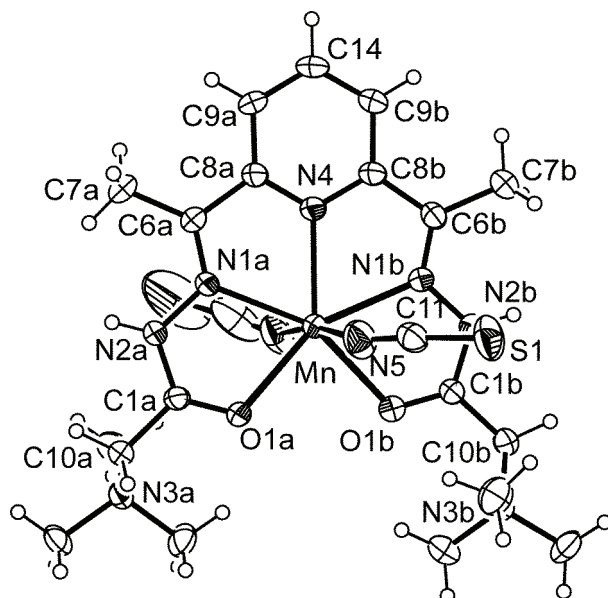
Fig. 12. The molecular structure of complex [Mn(H$_2$dap(GT)$_2$)(NCS)$_2$](NCS)$_2$·CH$_3$OH (**19**).

It is difficult to observe the straightforward differences between the geometries of the Girard reagent-based ligands when they coordinate as neutral, positively or negatively charged. As can be seen from Table I, the C1−O1 bond lengths in the free positively charged ligands have an average value of 1.22 Å, indicating a pronounced double bond character. As expected, the involvement of the O1 atom in coordination to the metal ion causes a noticeable elongation of the C1−O1 bond. The finer changes are most obvious if we compare the behavior of the ligand within the largest set of compounds *i.e.* the complexes of salicylaldehyde Girard hydrazones (Table I). Namely, the C1−O1 bond in the complexes with a neutral ligand (**9** and **10**), is noticeably shorter (C1−O1$_{(av.)}$ = 1.26 Å) compared to the same bond in the complexes with an anionic ligand (C1−O1$_{(av.)}$ = = 1.30 Å). The similar length of the C1−O1 bond for anionic ligands can be observed in the complexes of the mononegative salicylaldehyde Girard-P (C1−O1$_{(av.)}$ = 1.32 Å) and 5-bromosalicylaldehyde Girard-T (C1−O1$_{(av.)}$ = 1.30 Å) hydrazones. In contrast to these examples, the pentadentate 2,6-diacetylpyridine bis(Girard-T hydrazone) is up to now the only ligand coordinated as a cation, where the keto form of the carbonyl O1 ligator is preserved.[32] This is evidenced by the shortest lengths of the corresponding C1−O1 bonds (1.24 Å), which are closer to those found in the free ligands. Based on the data listed in Table I, it is possible to suggest that the N1−N2 bond is also affected by the deprotonation of the ligand. Namely, the average bond length in the complexes containing neutral or positively charged ligands (1.38 and 1.37 Å, respectively) is somewhat shorter than in the complexes with anionic ligands (1.41 Å). As regards the coordination sphere, it can be observed that in complexes **9, 10** and **19,** containing the ligand in its keto form, the length of the M−N1 coordination bond is shorter or similar to that of the M−O1 (Table I). In the complexes containing the ligand in the deprotonated enolic form (**11**–**14**, **17**, **18** and **20**–**22**) the coordination bond M−N1 becomes noticeably longer than the M−O1. However, the different nature of the central metal ions should be born in mind. The coordination angles O1−M−N1 and N1−M−X in most of the cases deviate significantly from 90° (Table II), which can be a consequence of the tendency of ligand to form fused chelate rings.

A most common feature of all the Girard reagent-based ligands, either neutral or charged ones, is the delocalization of the electron density within the C2−N1−N2−C1(O1) fragment. This is evidenced by the values of the bond lengths that are between the values for single and double ones (Table I). Taking into account that in most of the cases the condensed carbonyl compound represents a part of some aromatic system, the delocalization often extends to the whole hydrazone moiety. The remaining C1−C10 and C10−N3 bonds are, on the other hand, practically single bonds and thus allow for free rotation of the quaternary ammonium fragment (this important property will be described later in more detail). In accordance with the mentioned delocalization, the most of non-hydrogen

atoms in the free and coordinated ligands are approximately coplanar. As described, the coordination of the Girard reagents-based ligands result in fused chelate rings. The planarity of these rings is evidenced by the values of the T2 and T3 torsion angles (Table II, **9–22**), which are rather uniform and do not exceed |7.1| and |176.5|°, respectively. Somewhat higher twisting, and thus deformation from the planar form, can be observed from the torsion angles T4 and T5, which include the coordination bonds. The largest torsion angle (T5 = −29.1°) is found in compound **20**, in which the strong hydrogen bond existing between the complex molecule and the solvent contributes to the deformation of the chelate rings. In the analogous Girard-T derivative (**11**), which crystallizes without solvent, the value of T5 is 6.3°. The least deformation of the fused rings can be observed in the Co(III) complex with the pyridoxal Girard-T hydrazone (**15**).

Among the listed torsion angles, the largest variation in the values can be found for T1, which describes the position of the quaternary ammonium or pyridinium fragment with respect to the chelate rings. The $N(CH_3)_3^+$ group can easily change its position by rotating around the C1–C10 and C10–N3 bonds. It is important to remember that in the crystal structure of the free ligand, such as $[H_2SalGT]^+$ (Fig. 7a), the N3 atom is coplanar to the rest of the molecule, with the T1 torsion angle equal to 0°. This position of the $N(CH_3)_3^+$ group is supported by the intramolecular C–H···O1 interactions which involve the quaternary methyl groups.[31] In the corresponding complexes **9** and **10** (Fig. 8), in which the O1 atom is engaged in coordination, the $N(CH_3)_3^+$ group shifts out of the plane of the ligand and orients toward the axially bonded ligand to form the corresponding C–H···X2 intramolecular interactions (T1 is equal to 82.7 and –80.6° in **9** and **10**, respectively). Due to these interactions, the O1–Cu–X2 angle appears smaller than the other X2-coordination angles.[31] A similar, nearly orthogonal, orientation of the $N(CH_3)_3^+$ group (T1 = –93.3°), is found in the crystal structure of **15**, in which a very strong intramolecular hydrogen bond is formed between the methyl groups of the $N(CH_3)_3^+$ fragment and the axial NO_2 ligand.[30] It should be noted, however, that the intermolecular interactions can also affect the position of the $N(CH_3)_3^+$ group. This is the most obvious in the case of **17,** which crystallizes with two independent molecules in the unit cell.[34] The $N(CH_3)_3^+$ groups in these molecules display rather different orientations (the T1 values are 82.2 and −11.6°), which can be explained by the differences in their intermolecular interactions. Significant differences were also found in the orientation of the two $N(CH_3)_3^+$ groups of the symmetrically coordinated $H_2dap(GT)_2^{2+}$ in complex **19**.[32] In contrast to the Girard-T reagent-based complexes, in which the quaternary ammonium N3 atom significantly deviates from the rest of the chelate ligand, the data available for the two Girard-P reagent-based complexes (**20** and **22**) show that the corresponding quaternary pyridninum N3 atom remains more coplanar with the chelate rings (the T1 values are 177.5 and −162.7°, respecti-

vely). The pyridinium ring, however, can form different dihedral angles with respect to the nearest, five-membered chelate ring (62.3 and 83.0° in **20** and **22**, respectively), which suggests free rotation of the pyridinium fragment under the influence of the intermolecular interactions.

In general, the crystal structures of the reported Girard reagents-based compounds display extensive and diverse intermolecular interactions. In the complex compounds, the Girard reagents-based ligands have several potential hydrogen bonding binding sites. The most frequently engaged are the atom N2 (which can act as a donor or as an acceptor, depending on the deprotonation), the atom O1 (which upon coordination retains its acceptor abilities) and the possible binding sites from the condensed carbonyl moiety. In addition, as the chelate rings, together with the condensed carbonyl moiety, form extensive π-delocalized systems, the Girard reagent ligands can also engage in π···π and C–H···π interactions. The most specific fragments of these ligands, the quaternary ammonium and pyridinium groups, are highly interactive and prefer the surroundings of the strongest hydrogen bonding acceptors, such as O, N, Cl, Br and S.

5. CONCLUSIONS

Although Girard reagents have been known for more than 70 years, the first paper in the field of the coordination chemistry of these compounds, involving the Girard-T reagent, was published 33 years after the synthesis of this reagent. Nowadays, complexes with this reagent are most numerous, whereas complexes with the Girard-P reagent are, to the best of our knowledge, unknown.

Despite of the fact that a series of the Girard hydrazones are known, the number of their metal complexes is relatively small. In the complexes, Girard hydrazones behave as mono-, bi-, tri- or penta-dentate Schiff bases. Among the complexes of the Girard hydrazones, those with the tridentate Girard-T hydrazones are the most numerous.

In the crystal structures, the Girard reagents-based ligands, either free or coordinated, behave as highly delocalized systems and display considerable coplanarity of most of the constitutive atoms. The exceptions are quaternary ammonium and pyridinium groups, which can display different orientations under the influence of intra- and inter-molecular hydrogen bonds.

Since the assumptions on the different coordination modes and denticities of the non-hydrazonic Girard-T/P ligands were made based on their IR spectra,[58,59,63] it would be of interest to confirm these data by the X-ray structural analysis of the complexes.

И З В О Д

КОМПЛЕКСИ ПРЕЛАЗНИХ МЕТАЛА СА ЖИРАРОВИМ РЕАГЕНСИМА
И ЊИХОВИМ ХИДРАЗОНИМА

ЉИЉАНА С. ВОЈИНОВИЋ-ЈЕШИЋ[1], СЛАЂАНА Б. НОВАКОВИЋ[2], ВУКАДИН М. ЛЕОВАЦ[1]
и ВАЛЕРИЈА И. ЧЕШЉЕВИЋ[1]

[1]*Природно–математички факултет, Универзитет у Новом Саду, Трг Д. Обрадовића 3, 21000 Нови Сад и* [2]*Институт за нуклеарне науке Винча, Лабораторија за теоријску физику и физику кондензоване материје, Универзитет у Београду, п. п. 522, 11001 Београд*

Ово је прва ревија која описује координациону хемију комплекса метала са Жираровим реагенсима и њиховим хидразонима. У краћем уводу приказане су хемијске особине и значај ове групе органских једињења. Следећа, такође врло кратка, секција описује методе синтезе комплекса и начине координације самих Жирарових реагенаса. Последње две најопширније секције посвећене су препарацији, стереохемији и структурним карактеристикама комплекса метала са хидразонима Жирарових реагенаса, укључујући и неке њихове нехидразонске деривате.

(Примљено 4. јула, ревидирано 8. августа 2012)

REFERENCES

1. O. H. Wheeler, *Chem. Rev.* **62** (1962) 205
2. O. H. Wheeler, *J. Chem. Educ.* **45** (1968) 435
3. A. Girard, G. Sandulesco, *Helv. Chim. Acta* **19** (1936) 1095
4. N. G. Watson, *Br. J. Pharmacol.* **11** (1956) 119
5. F. Huidobro, *Bol. Soc. Biol. Santiago Chile* **5** (1948) 6
6. K. S. Dogson, B. Spenver, K. Williams, *Biochem. J.* **61** (1955) 374
7. M. Viscontini, J. Meier, *Helv. Chim. Acta* **33** (1950) 1773
8. S. Kim, H. Ko, S. Kim, T. Lee, *J. Comb. Chem.* **4** (2002) 549
9. W. Holstein, D. Severin, *Erdoel Kohle, Erdgas, Petrochem. Brennst.-Chem.* **32** (1979) 487
10. M. D. Soutullo, C. I. Odom, E. A. Salter, A. C. Stenson, R. E. Sykora, A. Wierzbicki, J. H. Davis Jr., *J. Comb. Chem.* **9** (2007) 571
11. B. Levrand, Y. Ruff, J.-M. Lehn, A. Herrmann, *Chem. Commun.* (2006) 2965
12. O. H. Wheeler, V. S. Gaind, O. Rosaldo, *J. Org. Chem.* **26** (1961) 3537
13. F. S. Sterrett, *The Essential Oils*, vol. II, E. D. Guenther, Ed., Vab Nostrand Co., New York, 1949, p. 814
14. A. Petit, S. Tallard, *Rev. Chim. Ind. (Paris)* **48** (1939) 226
15. M. Masui, H. Ohmori, *J. Chem. Soc., A* (1969) 153
16. J. Heer, K. Miescher, *Helv. Chim. Acta* **34** (1951) 359
17. D. F. Godbois, J. M. Mendelsohn, L. J. Ronsivalli, *Anal. Chem.* **37** (1965) 1776
18. W. P. McKinley, *Science* **121** (1955) 139
19. E. Lederer, M. Lederer, *Chromatography*, Elsevier, New York, 1953, p. 113
20. A. A. El-Shafei, M. N. H. Moussa, A. A. El-Far, *Mater. Chem. Phys.* **70** (2001) 175
21. M. N. H. Moussa, A. A. El-Far, A. A. El-Shafei, *Mater. Chem. Phys.* **105** (2007) 105
22. M. M. Mostafa, M. H. Abdel-Rhman, *Spectrochim. Acta, A* **56** (2000) 2341
23. A. M. A. El-Sokkary, M. M. El-Naggar, A. F. Abdel-Aziz, *Appl. Organomet. Chem.* **24** (2010) 439
24. S. P. Datta, R. Leberman, B. R. Rabin, *Trans. Faraday Soc.* **55** (1959) 1982

25. A. Petit, S. Tallard, *Ind. Parf.* **3** (1948) 75
26. M. Masui, H. Ohmori, *Chem. Pharm. Bull.* **12** (1964) 877
27. M. Masui, H. Ohmori, *J. Chem. Soc., B* (1967) 762
28. X. Wang, X. M. Zhang, H. X. Liu, *Inorg. Chim. Acta* **223** (1994) 193
29. S. P. Rao, T. A. S. Redddy, *Z. Anal. Chem.* **277** (1975) 127
30. Lj. S. Vojinović, V. M. Leovac, S. B. Novaković, G. A. Bogdanović, J. J. Csanádi, V. I. Češljević, *Inorg. Chem. Commun.* **7** (2004) 1264
31. V. M. Leovac, G. A. Bogdanović, V. I. Češljević, Lj. S. Jovanović, S. B. Novaković, Lj. S. Vojinović-Ješić, *Struct. Chem.* **18** (2007) 113
32. Lj. S. Vojinović-Ješić, V. I. Češljević, G. A. Bogdanović, V. M. Leovac, K. Mészáros Szécsényi, V. Divjaković, M. D. Joksović, *Inorg. Chem. Commun.* **13** (2010) 1085
33. M. D. Revenco, P. N. Bourosh, O. V. Palamarciuc, J. Lipkowski, M. Gdaniec, Yu. A. Simonov, *Russ. J. Inorg. Chem.* **54** (2009) 1581
34. O. V. Palamarciuc, P. N. Bourosh, M. D. Revenco, J. Lipkowski, Yu. A. Simonov, R. Clérac, *Inorg. Chim. Acta* **363** (2010) 2561
35. M. M. Mostafa, S. M. Hassan, G. M. Ibrahim, *J. Inorg. Nucl. Chem.* **42** (1980) 285
36. M. M. Mostafa, M. A. Khattab, K. M. Ibrahim, *Transition Met. Chem.* **8** (1983) 212
37. M. E. M. Emam, M. A. H. Hafez, M. N. H. Moussa, *J. Thermal. Anal.* **37** (1991) 1005 and references therein
38. M. M. Abou Sekkina, M. R. Salem, *J. Thermal. Anal.* **48** (1997) 841 and references therein
39. M. M. Mostafa, *Spectrochim. Acta, A* **66** (2007) 480 and references therein
40. X. Wang, X. M. Zhang, H. X. Liu, *J. Coord. Chem.* **33** (1994) 223
41. Lj. S. Vojinović, *Ph. D. Thesis*, Faculty of Science, University of Novi Sad, 2005 (in Serbian)
42. V. M. Leovac, K. Mészáros-Szécsényi, Lj. S. Vojinović-Ješić, V. I. Češljević, S. Markov, T. Wadsten, *J. Therm. Anal. Cal.* **86** (2006) 379
43. J. S. Casas, M. S. Garcia-Tasende, J. Sordo, *Coord. Chem. Rev.* **209** (2000) 197
44. G. Di Maio, S. Li, G. Portalone, *Acta Crystallogr., C* **50** (1994) 635
45. Lj. S. Vojinović-Ješić, G. A. Bogdanović, V. M. Leovac, V. I. Češljević, Lj. S. Jovanović, *Struct. Chem.* **19** (2008) 807
46. S. B. Novaković, B. M. Drašković, Lj. S. Vojinović-Ješić, V. I. Češljević, V. M. Leovac, *Acta Crystallogr.* **E66** (2010) m328
47. V. M. Leovac, V. S. Jevtović, Lj. S. Jovanović, G. A. Bogdanović, *J. Serb. Chem. Soc.* **70** (2005) 393
48. Lj. S. Vojinović-Ješić, V. M. Leovac, V. I. Češljević, unpublished results
49. Z. A. Starikova, E. A. Shugam, *Zh. Strukt. Khim. (Russ.)* **10** (1969) 290
50. V. Chandrasekhar, S. Kingsley, A. Vij, K. C. Lam, A. L. Rheingold, *Inorg. Chem.* **39** (2000) 3238
51. A. I. Vogel, A. R. Tatchell, B. S. Furnis, A. J. Hannaford, P. W. G. Smith, *Vogel's textbook of practical organic chemistry* 5th ed., Longman, London, 1989
52. S. Naskar, D. Mishra, S. K. Chattopadhyay, M. Corbella, A. J. Blake, *J. Chem. Soc. Dalton Trans.* (2005) 2428 and references therein
53. G. J. Palenik, D. W. Wester, *Inorg. Chem.* **17** (1978) 864
54. C. Lorenzini, C. Pelizzi, G. Pelizzi, G. Predieri, *J. Chem. Soc., Dalton Trans.* (1983) 721

55. M. R. Bermejo, A. Sousa, M. Fondo, A. M. González, O. L. Hoyos, R. Pedrido, M. A. Maestro, J. Mahia, *Z. Anorg. Allg. Chem.* **626** (2000) 506
56. K. B. Gudasi, S. A. Patil, R. S. Vadavi, R. V. Shenoz, M. Nethaji, S. W. A. Bligh, *Inorg. Chim. Acta* **359** (2006) 3229
57. M. V. Main, J. S. Fritz, *Anal. Chem.* **61** (1989) 1272
58. N. M. El-Metwally, I. M. Gabr, A. M. Shallaby, A. A. El-Asmy, *J. Coord. Chem.* **58** (2005) 1145
59. U. El-Ayaan, I. M. Kenawy, Y. G. Abu El-Reash, *J. Mol. Struct.* **871** (2007) 14
60. H. X. Liu, X. M. Zhang, X. Wang, *Polyhedron* **13** (1994) 441
61. H. X. Liu, W. Wang, X. Wang, *J. Coord. Chem.* **33** (1994) 347
62. R. M. El-Bahnasawy, *J. Therm. Anal.* **45** (1995) 1547
63. U. El-Ayaan, I. M. Kenawy, Y. G. Abu El-Reash, *Spectrochim. Acta, A* **68** (2007) 211
64. F. H. Allen, *Acta Crystallogr., B* **58** (2002) 380. The data were recovered from the August 2010 update release of the CSD (version 5.31)
65. Y.-Q. Sun, R.-S. Yang, H.-H. Zhang, R.-Q. Sun, Q.-Y. Yang, *Chin. J. Struct. Chem.* **20** (2001) 310.

Facile synthesis of bis(indolyl)methanes using iron(III) phosphate

FARAHNAZ KARGAR BEHBAHANI* and MASOUMEH SASANI

Department of Chemistry, Karaj Branch, Islamic Azad University, Karaj, Iran

Abstract: A new, convenient and high yielding procedure for the preparation of bis(indolyl)methanes in glycerol by the electrophilic substitution reaction of indole with aldehydes in the presence of catalytic amount of $FePO_4$ (5.0 mol %) as a highly stable and reusable catalyst is described.

Keywords: $FePO_4$; synthesis; bis(indolyl)alkanes; aldehyde; glycerol; catalyst.

INTRODUCTION

Lewis acids accelerate a wide range of organic reactions by binding to and thereby activating reactants. This activation often results in rate increases of many orders of magnitude compared with the thermal reaction. Transition metal Lewis acids are promising and interesting because the precursor is often structurally well-defined and steric and electronic tuning of the ligand to a particular reaction is facilitated. Iron(III) phosphate as a Lewis acid has been employed as a catalyst for the transformation of various organic functional group under heterogeneous conditions, such as the selective oxidation of CH_4 to CH_3OH,[1] benzene to phenol,[2] one-pot synthesis of dihydropyrimidinones and thiones,[3] synthesis of triarylated imidazoles,[4] acetylation of alcohols and phenols,[5] tetrahydropyranylation and tetrahydrofuranylation of alcohols and phenols,[6] synthesis of 2-substituted benzimidazoles,[7] and synthesis of polyhydroquinoline derivatives.[8]

Furthermore, the structural motifs of indole derivatives are found in numerous biologically active compounds, which are used as anti-oxidants and pharmaceuticals.[9–13] Bis(indolyl)alkanes are present in many biologically active natural products and are known to have applications in research areas, such as pharmaceuticals and materials science.[14–20] Consequently, there is an increased interest in the synthesis of compounds containing bis(indolyl)alkanes moieties due to their importance and a number of synthetic methods for the synthesis of bis(in-

---

dolyl)alkanes have been described in the literature.[21–24] However, the procedures described in the literature to access bis(indolyl)alkanes are mainly focused on the condensation of indole with carbonyl compounds in the presence of a protic acid or a Lewis acid. Also, The synthesis of bis(indolyl)alkanes by the reaction of indoles with alkynes catalyzed using $Cu(OTf)_2$ has also been reported.[25]

Lately, glycerine, which is readily available as a co-product in the production of biodiesel, has attracted attention as a versatile, cheap and renewable feedstock in synthetic organic chemistry.[26,27] In view of current interest in catalytic processes, the development of a method for the synthesis of bis(indolyl)methanes using inexpensive, mild and non-polluting reagents is highly desirable. The introduction of reusable catalysts is preferred in order to minimize environmental pollution due to the usage of hazardous solvents and their disposal. The limitations of the current methods, together with the demand for greener alternatives prompted us to develop a new method for the synthesis of bis(indolyl)methanes.

Due to our interest in developing new methodologies in catalytic organic syntheses and to show the versatility of iron(III) phosphate in organic synthesis,[1–8] the preparation of bis(indolyl)methanes by reaction of indole with aldehydes in the presence of a catalytic amount of $FePO_4$ (5.0 mol %), as an inexpensive, eco-friendly and reusable catalyst, in glycerol at 75 °C (Scheme 1) is described herein.
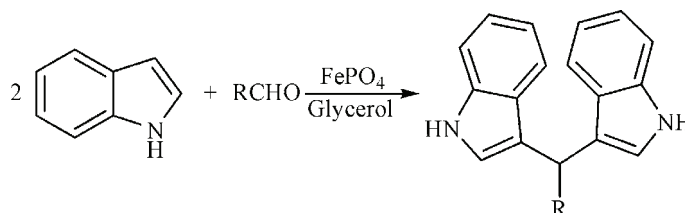
Scheme 1. The preparation of bis(indolyl)methanes by reaction of indole with aldehydes in the presence of a catalytic amount of $FePO_4$.

EXPERIMENTAL

Melting points were measured by the capillary tube method using an Thermo Scientific electrothermal 9200 apparatus. The IR spectra were recorded on a Perkin Elmer FT-IR spectrometer in the wavenumber range 4000–400 cm^{-1}. ^{1}H-NMR spectra were obtained on Bruker DRX-300MHZ NMR instrument. Chemicals shifts are reported in parts per million (δ) relative to tetramethylsilane ($\delta = 0.0$ ppm) as internal standard. GC/mass spectra were recorded on an Agilent 6890 GC Hp-5 capillary 30 m×530 μm×1.5 μm nominal operating at 70 eV. Analytical TLC of all reactions was performed on Merck pre-coated plates (silica gel 60F-254 on aluminium). All starting materials purchased from Merck Co. All products were characterized by ^{1}H-NMR, FT-IR, and comparison of their melting points with authentic samples.

*Synthesis of 3,3'-bis(indolyl)phenylmethane (**1**)*

The reaction of benzaldehyde (1 mmol) and indole (2 mmol) was used as a model reaction to determine the optimal conditions for the preparation of bis(indolyl)methanes. The

effect of varying the amount of $FePO_4$ (0–10 mol %) was studied by stirring the reactants in 4 mL glycerol for 3 h at 75 °C (Table I) After completion of the reaction (monitored by TLC), the mixture was treated with ethyl acetate and the catalyst filtered off. After evaporation of the solvent, the residue was collected and purified by recrystallization from ethanol. Using the optimal concentration (5 mol %) of $FePO_4$, the synthesis was repeated for the same time at the same temperature but in different solvents (Table II). Finally, the synthesis was performed in glycerol using the optimal concentration of $FePO_4$ by stirring for 3 h at different temperatures (25–80 °C) (Table III).

TABLE I. Effect of varying the amount of catalyst on the yield of 3,3'-bis(indolyl)phenyl-methane; benzaldehyde, 1.0 mmol, indole, 2.0 mmol, glycerol, 4.0 mL at 75 °C

Entry	Catalyst, mol %	τ / h	Yield, %
1	–	3.0	10
2	2.0	3.0	60
3	5.0	3.0	90
4	10	3.0	90

TABLE II. Effect of the solvent on the yield of 3,3'-bis(indolyl)phenylmethane; benzaldehyde, 1.0 mmol, indole, 2.0 mmol, at 75 °C in 3.0 h

Entry	Solvent (4.0 mL)	Yield, %
1	Glycerol	90
2	EtOH	70
3	H_2O	60
4	$EtOH/H_2O$	65
5	–	60

TABLE III. Synthesis of 3-[(1H-indol-3-yl)phenylmethyl]-1H-indole using $FePO_4$ in glycerol at different temperatures

Entry	t / °C	τ / h	Yield, %
1	25	3.0	30
2	50	3.0	65
3	75	3.0	90
4	80	3.0	90

Synthesis of 3,3'-bis(indolyl)methane (2–15)

Compounds **1**–**14**, Table IV, were prepared by reaction of indole (2 mmol) with the required aldehyde (1 mmol) in 4 mL glycerol at 75 °C in the presence of 5 mol % $FePO_4$. After completion of the reaction, controlled by TLC (the reaction times are given in Table IV), ethyl acetate was added, the catalyst filtered off and the solvent evaporated. The residue was recrystallized from ethanol to afford the pure compound.

Reusability of the catalyst

To test its reusability, the catalyst recovered by gravity filtration at the end of the reaction was washed with ethyl acetate and reused for 5 sequential preparations of compound **1**.

TABLE IV. FePO$_4$ catalyzed synthesis of bis(indolyl)methanes

Entry	Aldehyde	τ / h	Yield, %	M.p. / °C (found)	M.p. / °C (reported)	Ref.
1	Benzaldehyde	3	90	125	123–126	31
2	2-Chlorobenzaldehyde	8	80	72	69–71	30
3	4-Chlorobenzaldehyde	8	85	75	76–78	30
4	*Trans*-Cinnamaldehyde	7	85	100	95–97	29
5	2-Methoxybenzaldehyde	5	93	138	134–136	28
6	4-Methoxybenzaldehyde	4	92	176	178–181	28
7	3,4-Dimethoxybenzaldehyde	5	84	195–198	198–199	31
8	4-Methylbenzaldehyde	5	84	64–98	97–99	28
9	4-Dimethylaminobenzaldehyde	7	75	208–220	210–212	29
10	2-Hydroxybenzaldehyde	5	75	350	340–342	30
11	4-Hydroxybenzaldehyde	6	87	150	120–123	30
12	4-Nitrobenzaldehyde	5	84	220	216–218	32
13	Hexanal	7	76	65	67–74	30
14	Butanal	6	75	80	73–75	32
15	Furfural	8	90	340–345	322–324	29

RESULTS AND DISCUSSION

To the best of our knowledge, the preparation of bis(indolyl)methanes catalyzed by anhydrous iron(III) phosphate has not been reported previously.

The main aim of this work was to provide a new catalytic and environmentally benign protocol for the synthesis of bis(indolyl)methanes. Herein, a simple and fast method for the synthesis of bis(indolyl)methanes in glycerol using FePO$_4$ is reported.

To establish the optimum condition for this reaction, various ratios of FePO$_4$ were examined using indole and bezaldehyde in glycerol at 75 °C as a model reaction (Table I). It can be seen that very little of the desired product was obtained in the absence of catalyst and the best yields were obtained with FePO$_4$. Thus, the catalyst is an essential component for the synthesis of bis(indolyl)methanes by the reported method.

Then the effect of the solvent was examined using different solvents in the model reaction, whereby different yields were obtained (Table II). Obviously, glycerol stands out as the solvent of choice with its fast reaction rate, high yield, selectivity, cheapness and environmental acceptability.

The effect of temperature was investigated by performing the model reaction in glycerol and at different temperatures (25, 50, 75 and 80 °C). It was observed that the yield is a function of temperature with the yield increasing with increasing reaction temperature up to 75 °C. Thereafter, no further increase in the yield was registered. Therefore, all further reactions were performed in glycerol at 75 °C (Table III).

To evaluate the scope and limitations of this work, different bis(indolyl)methanes were synthesized using aliphatic, heterocyclic and aromatic aldehydes (Scheme 1, Table IV). As can be seen in Table IV, the aromatic and heterocyclic aldehydes reacted similarly to give the corresponding bis(indolyl)methanes in high yields and relatively short reaction times. The aliphatic aldehydes reacted smoothly providing the corresponding products in good to moderate yields (entries **4**, **14** and **15**).

This condensation reaction probably proceeds through the activation of a carbonyl group by FePO$_4$ as a Lewis acid to give intermediate **I**, which is followed by indole attack of **I** to give **II**. After proton rearrangement to give **III**, the other indole is added to **III** with the loss of FePO$_4$ and H$_2$O to afford **IV**, with the following step resulting in the product **V** (Scheme 2).
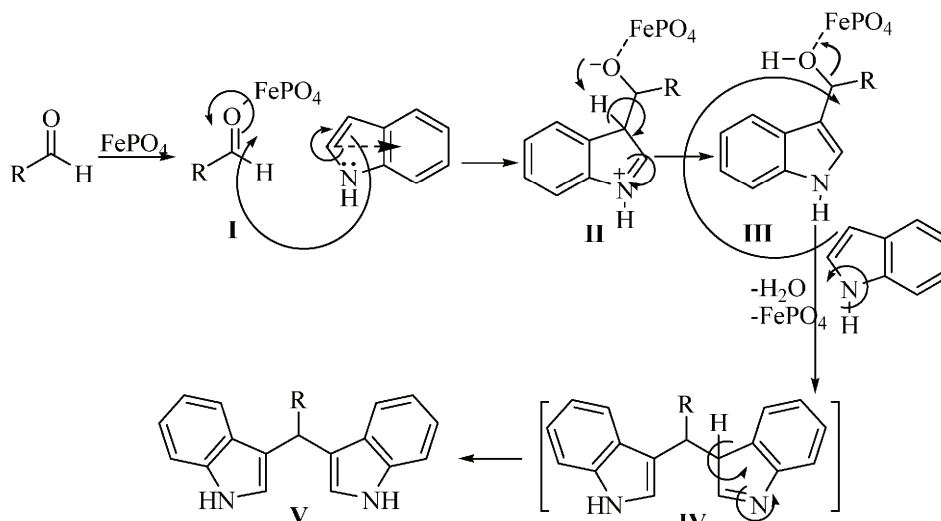
Scheme 2. Suggested mechanism for the synthesis of bis(indolyl)methanes

At the end of the reaction, the catalyst was recovered by gravity filtration and recycled after washing with ethyl acetate and employed for further preparations. The results showed that the yield of product after five runs was only slightly reduced.

CONCLUSION

In conclusion, FePO$_4$ in glycerol was found to be mild and effective catalyst for the electrophilic substitution reactions of indole with aldehydes, giving bis-(indolyl)methanes in excellent yields. The use of this inexpensive and easily available catalyst under mild conditions, the clean reaction and greater selectivity make this protocol practical and economically attractive. The procedure was

found to be general as a variety of aldehydes reacted with indole under mild reaction conditions.

SUPPLEMENTARY MATERIAL

Physical and spectral data of the synthesized compounds are available electronically from http://www.shd.org.rs/JSCS/, or from the corresponding author on request.

ИЗВОД

ЛАКА СИНТЕЗА БИС(ИНДОЛИЛ)МЕТАНА ПОМОЋУ ГВОЖЂЕ(III)-ФОСФАТА

FARAHNAZ KARGAR BEHBAHANI и MASOUMEH SASANI

Department of Chemistry, Karaj Branch, Islamic Azad University, Karaj, Iran

Описан је нов поступак за синтезу бис(индолил)метана реакцијом индола и алдехида, у глицеролу у присуству каталитичких количина $FePO_4$ (5,0 mol %). Производи се добијају у високом приносу а катализатор је стабилан и може се користити више пута.

(Примљено 27. јула, ревидирано 10. новембра 2011)

REFERENCES

1. K. Otsuka, Y. Wang, *Appl. Catal., A* **145** (2001) 222
2. T. Ren, L. Yan, X. Zhang, J. Suo, *Appl. Catal., A* **11** (2003) 244
3. M. M. Heravi, F. K. Behbahani, V. Zadsirjan, H. A. Oskooie, *Heterocycl. Commun.* **12** (2006) 369
4. F. K. Behbahani, T. Yektanezhad, A. R. Khorrami, *Heterocycl. Commun*. **81** (2010) 2315
5. F. K. Behbahani, M. Farahani, H. A. Oskooie, *Korean J. Chem. Soc*. **55** (2011) 1
6. F. K. Behbahani, M. Farahani, *Lett. Org. Chem.* **81** (2011) 436
7. F. K. Behbahani, P. Ziaei, *Chem. Heterocycl. Compd.* **7** (2012) 1088
8. F. K. Behbahani, M. Homafar, *Synth. React. Inorg. Met.-Org. Nano-Met. Chem.* **42** (2012) 291
9. R. J. Sundberg, *Indoles*, Academic Press, New York, 1996
10. J. E. Sexton, *Indoles*, Wiley, New York, 1983
11. M. Z. Wang, M. K. Wong, C. M. Che, *Chem. Eur. J.* **14** (2008) 8353
12. M. Somei, F. Yamada, *Nat. Prod. Rep*. **22** (2005) 73
13. M. Bandini, A. Melloni, S. Tommasi, A. Umani-Ronchi, *Synlett* (2005) 1199
14. S. Patil, J. K. Buolamwini, *Curr. Org. Synth*. **3** (2006) 477
15. T.-S. Kam, in: *Alkaloids from Malaysian Flora*, in *Alkaloids: Chemical and Biological Perspectives*, S. W. Pelletier, Ed., Pergamon, Amsterdam, Vol. 14, 1999, p. 285
16. G. Bifulco, I. Bruno, R. Riccio, J. Lavayre, G. J. Bourdy, *Nat. Prod*. **58** (1995) 1254
17. M. Chakrabarty, R. Basak, Y. A. Harigaya, *Heterocycles* **55** (2001) 2431
18. C. Hong, G. L. Firestone, L. Bjeldanes, *Biochem. Pharmacol*. **63** (2002) 1085
19. S. H. Benabadji, R. Wen, J. Zheng, X. Dong, S, Yuan, *Acta. Pharmacol. Sin*. **25** (2004) 666
20. A. Kamal, M. N. Khan, K. S. V. Reddy, Y. N. Srikanth, S. K. Ahmed, P. Kumark, U. S. Murthy, *J. Enzyme Inhib. Med. Chem*. **24** (2009) 559
21. M. Shiri, M. A. Zolfigol, H. G. Kruger, Z. Tanbakouchian, *Chem. Rev*. **110** (2010) 2250
22. B. Mukulesh, *Lett. Org. Chem*. **8** (2011) 461

23. H.-E. Qu , C. Xiao, N. Wang, K.-H. Yu, Q.-S. Hu, L.-X. Liu, *Molecules* **16** (2011) 3855
24. V. D. Patil, G. B. Dere, P. A. Rege, J. J. Patil, *Synth. Commun*. **41** (2011) 736
25. M. H. Xie, F. D. Xie, G. F. Lin, J. H. Zhang*, Tetrahedron Lett*. **5**1 (2010) 1213
26. C. H. C. Zhou, J. N. Beltramini, Y. X. Fana, G. Q M. Lu*, Chem. Soc. Rev*. **37** (2008) 527
27. Y. Zheng, X. Chen, Y. Shen*, Chem. Rev*. **108** (2008) 5253
28. M. A. Zolfigol, A. Khazaei, M. A. R. Zare, A. Zare*, Org. Prep. Proced. Int*. **42** (2010) 95
29. R. G. Vaghei, H. Veisi, H. Keypour, A. A. D. Firouzabadi, *Mol Divers*. **14** (2010) 87
30. R. G. Vaghei, S. M. Malekehpoor, *Org. Prep. Proced. Int*. **42** (2010) 175
31. C. C. Silveira, S. R. Mendes, F. M. Libero, E. J. Lenardao, G. Perin, *Tetrahedron Lett.* **50** (2009) 6060
32. S. R. Sheng, Q. Y. Wang, Y. Ding, X .L. Liu, M. Z. Cai, *Catal. Lett*. **128** (2009) 418.

SUPPLEMENTARY MATERIAL TO
Facile synthesis of bis(indolyl)methanes using iron(III) phosphate

FARAHNAZ KARGAR BEHBAHANI* and MASOUMEH SASANI

Department of Chemistry, Karaj Branch, Islamic Azad University, Karaj, Iran

PHYSICAL AND SPECTRAL DATA OF THE SYNTHESIZED COMPOUNDS

*3-[(1H-Indol-3-yl)(phenyl)methyl]-1H-indole (**1**)*. Yield: 90 %; m.p. 125 °C; IR (KBr, cm^{-1}): 3412 (–N–H stretching of amine), 3055 (–C–H stretching of aromatic ring), 1492, 1455 (–C=C stretching), 1092 (–C–N stretching); ^{1}H-NMR (300 MHz, DMSO-d_6, δ / ppm): 7.85 (2H, *s*, –NH), 7.43 (2H, *d*, *J* = 8.1 Hz, aromatic), 7.21–7.43 (7H, *m*, aromatic), 7.01 (2H, *t*, *J* = 7.5 Hz, aromatic), 6.6 (2H, *d*, *J* = 1.8 Hz, aromatic), 6.68 (2H, *s*, H–C–N), 5.58 (1H, *s*, –CH); ^{13}C-NMR (300 MHz, CDCl$_3$, δ / ppm): 32.6 (CH), 110.9–145.2 (aromatic); MS (*m/z*, (relative abundance, %)): 322 (M$^+$, 3.5) 116, 77 (BP, 100).

*3-[(2-Chlorophenyl)(1H-indol-3-yl)methyl]-1H-indole (**2**)*. Yield: 80 %; m.p. 72 °C; IR (KBr, cm^{-1}): 3409 (–NH stretching of amine), 3054 (–C–H stretching of aromatic ring), 1416–1455 (–C=C stretching), 1092 (–C–N stretching); ^{1}H-NMR (300 MHz, DMSO-d_6, δ / ppm): 7.83 (2H, *brs*, –NH),7.38–7.5 (4H, *m*, aromatic), 7.1–7. 22 (6H, *m*, aromatic), 7.0 (2H, *t*, *J* = 7.8 Hz, aromatic), 6.58 (2H, *s*, H–C–N), 6.31 (1H, *s*, –C–H); ^{13}C-NMR (300 MHz, CDCl$_3$, δ / ppm): 37.1 (CH), 110.4–141.5 (aromatic); MS (*m/z*, (relative abundance, %)): 356 (M$^+$, 5.7), 358 (M+2, 2) 116, 111, 113, 76 (BP, 100).

*3-[(4-Chlorophenyl)(1H-indol-3-yl)methyl]-1H-indole (**3**)*. Yield: 85 %; m.p. 75 °C; IR (KBr, cm^{-1}): 3407 (–NH stretching of amine), 3052 (–C–H stretching of aromatic ring), 1415–1453 (–C=C stretching), 1037 (–C–N stretching); ^{1}H-NMR (300 MHz, DMSO-d_6, δ / ppm): 10.85 (2H, *s*, –NH), 7.94 (2H, *d*, *J* = 7.8 Hz, aromatic), 7.01–7.95 (8H, *m*, aromatic), 6.87–6.94 (2H, *m*, aromatic), 6.84 (2H, *s*, H–C–N), 5.85 (1H, *s*, –C–H); ^{13}C-NMR (100 MHz, CDCl$_3$, δ / ppm): 38.5 (CH), 111.1–143.6 (aromatic); MS (*m/z*, (relative abundance, %)): 356 (M$^+$, 5.5), 358 (M+2, 1.8) 116, 111, 113, 76 (BP, 100).

---

* Corresponding author. E-mail: Farahnazkargar@yahoo.com

(E)-3-[1-(1H-Indol-3-yl)-3-phenylallyl]-1H-indole (4). Yield: 85 %; m.p. 100 °C; IR (KBr, cm^{-1}): 3449 (–NH stretching of amine), 3042 (–C–H stretching of aromatic ring), 1434, 1455 (–C=C stretching), 1090 (–C–N stretching); ^{1}H-NMR (300 MHz, DMSO-d_6, δ / ppm): 8.01 (2H, *s*, –NH), 7.30–7.12 (13H, *m*, aromatic), 6.96 (1H, *d*, *J* = 15.9, Ph-C**H**=CH), 6.07 (1H, t, *J* = 7.9 Hz, Ph-CH=C**H**), 6.50 (2H, *s*, H–C–N), 4.14 (1H, *d*, *J* = 7.9 Hz, –C–H); ^{13}C-NMR (300 MHz, CDCl$_3$, δ / ppm): 39.5 (CH), 111.1–136.6 (aromatic); MS (*m/z*, (relative abundance, %)): 348 (M$^+$, 4.2), 116, 77 (BP, 100).

3-[(1H-Indol-3-yl)(2-methoxyphenyl)methyl]-1H-indole (5). Yield: 93 %; m.p. 138 °C; IR (KBr, cm^{-1}): 3412 (–NH stretching of amine), 3055 (–C–H stretching of aromatic ring), 1417–1455 (–C=C stretching), 1092 (–C–N stretching); ^{1}H-NMR (300 MHz, DMSO-d_6, δ / ppm): 7.80 (2H, *brs*, –NH), 6.81–7.40 (12H, *m*, aromatic), 6.61 (2H, *s*, H–C–N), 6.32 (1H, *s*, –C–H), 3.83 (3H, *s*, –OCH$_3$); ^{13}C-NMR (300 MHz, CDCl$_3$, δ / ppm): 32.3 (CH), 56.2 (O–CH$_3$), 110–157.1 (aromatic); MS (*m/z*, (relative abundance, %)): 352 (M$^+$, 3.1), 107, 76 (BP, 100).

3-[(1H-indol-3-yl)(4-methoxyphenyl)methyl]-1H-indole (6). Yield: 92 %; m.p. 176 °C; IR (KBr, cm^{-1}): 3395 (–NH stretching of amine), 3045 (–C–H stretching of aromatic ring), 1418, 1455 (–C=C stretching), 1171 (–C–N stretching); ^{1}H-NMR (300 MHz, DMSO-d_6, δ / ppm): 7.86 (2H, *brs*, –NH), 7.38 (4H, *dd*, aromatic), 7.28 (2H, *d*, *J* = 8.43, aromatic), 7.14 (2H, *t*, *J* = 7.36, aromatic), 7.05 (2H, *t*, *J* = 7.29, aromatic), 6.81 (2H, *d*, *J* = 8.63, aromatic), 6.63 (2H, *s*, H–C–N), 5.85 (1H, *s*, –C–H), 3.79 (3H, *s*, –OCH$_3$); ^{13}C-NMR (300 MHz, CDCl$_3$, δ / ppm): 37.6 (CH) 54.8 (O–CH$_3$), 110.4–157.2 (aromatic); MS (*m/z*, (relative abundance, %)): 352 (M$^+$, 3.6), 107, 76 (BP, 100).

3-[(3,4-Dimethoxyphenyl)(1H-indol-3-yl)methyl]-1H-indole (7). Yield: 84 %; m.p. 195–198 °C; IR (KBr, cm^{-1}): 3415 (–NH stretching of amine), 3056 (–C–H stretching of aromatic ring), 1418–1456 (–C=C stretching), 1094 (–C–N stretching); ^{1}H-NMR (300 MHz, DMSO-d_6, δ / ppm): 7.86 (2H, *brs*, –NH), 7.38 (1H, *s*, aromatic), 7.28 (1H, *d*, *J* = 8.5 Hz, aromatic), 7.14 (1H, *dd*, *J* = 7.35, 2.3 Hz, aromatic), 6.81–7.05 (8H, *m*, aromatic), 6.63 (2H, *s*, H–C–N), 5.85 (1H, *s*, –C–H), 3.79 (6H, *s*, OCH$_3$); ^{13}C-NMR (100 MHz, CDCl$_3$, δ / ppm): 38.2 (CH), 55.1 (O–CH$_3$), 111.1–149.7 (aromatic); MS (*m/z*, (relative abundance, %)): 382 (M$^+$, 4.1), 137, 106, 75 (BP, 100).

3-[(1H-Indol-3-yl)(p-tolyl)methyl]-1H-indole (8). Yield: 84 % ; m.p. 64–98 °C; IR (KBr, cm^{-1}): 3408 (–NH stretching of amine), 3048 (–C–H stretching of aromatic ring), 1485, 1508 (–C=C stretching), 1453, 1336, 1182, 1039 (–C–N stretching); ^{1}H-NMR (300 MHz, DMSO-d_6, δ / ppm): 10.77 (2H, *s*, NH), 7.33––7.65 (8H, *m*, aromatic), 7.54 (2H, *d*, *J* = 8.1, aromatic), 7.9 (2H, *d*, *J* = 8.1 Hz, aromatic), 6.77 (2H, *s*, H–C–N), 5.75 (1H, *s*, –C–H), 2.21 (3H, *s*, CH$_3$); ^{13}C--NMR (300 MHz, CDCl$_3$, δ / ppm): 21.0 (CH$_3$), 39.0 (CH), 111.8–142.3 (aromatic); MS (*m/z*, (relative abundance, %)): 336 (M$^+$, 5.1), 116, 91,76 (BP, 100).

*4-[Di(1*H*-indol-3-yl)methyl]-N,N-dimethylbenzenamine (9)*. Yield: 75 %; m.p. 208–220 °C; IR (KBr, cm^{-1}): 3396 (–NH stretching of amine), 3047 (–C–H stretching of aromatic ring), 2891, 1597, 1465, 1515 (–C=C stretching), 1374, 1166 (–C–N stretching); ^{1}H-NMR (300 MHz, DMSO-d_6, δ / ppm): 7.86 (2H, *brs*, –NH), 7.38 (2H, *d*, *J* = 7.9 Hz, aromatic), 7.14 (2H, *dd*, *J* = 7.23, 2.35 Hz, aromatic), 6.81–7.05 (8H, *m*, aromatic ring), 6.63 (2H, *s*, H–C–N), 5.85 (1H, *s*, –C–H), 3.79 (6H, *s*, N(CH$_3$)$_2$); ^{13}C-NMR (300 MHz, CDCl$_3$, δ / ppm): 35.3 (CH), 22.6 (N–CH$_3$), 117.3–148.6 (aromatic); MS (*m/z*, (relative abundance, %)): 365 (M$^+$, 3.1), 76 (BP, 100).

*2-[Di(1*H*-indol-3-yl)methyl]phenol (10)*. Yield: 75 %; m.p. 350 °C; IR (KBr, cm^{-1}): 3445 (–NH stretching of amine), 3044 (–C–H stretching of aromatic ring), 1480–1616 (–C=C stretching), 1256, 1173, 1082 (–C–N stretching); 7.90–7.48 (aromatic ring); ^{1}H-NMR (300 MHz, DMSO-d_6, δ / ppm): 7.93 (2H, *brs*, –NH), 7.94 (1H, *s*, OH), 7.66 (2H, *d*, *J* = 7.36, 3.2 Hz, aromatic), 7.35 (2H, *t*, *J* = 7.35, aromatic), 7.19–7.29 (8H, *m*, aromatic), 6.72 (2H, *s*, H–C–N), 5.93 (1H, *s*, –C–H); ^{13}C-NMR (300 MHz, CDCl$_3$, δ / ppm): 38.8(CH), 136.3–111.5 (aromatic), 155.2 (O–Ar); MS (*m/z*, (relative abundance, %)): 338 (M$^+$, 3.2), 116, 93, 76 (BP, 100).

*4-[Di(1*H*-indol-3-yl)methyl]phenol (11)*. Yield: 87 %; m.p. 150 °C; IR (KBr, cm^{-1}): 3445 (–NH stretching of amine), 3052 (–C–H stretching of aromatic ring), 1424, 1613 (–C=C stretching), 1173, 1132, 1082 (–C–N stretching), 742, 796 (aromatic ring); ^{1}H-NMR (300 MHz, DMSO-d_6, δ / ppm): 7.93 (2H, *brs*, –NH), 7.64 (1H, *s*, OH), 7.56 (2H, *d*, *J* = 8.2 Hz, aromatic), 7.45 (2H, *d*, *J* = 8.2 Hz, aromatic), 7.19–7.29 (8H, *m*, aromatic), 6.75 (2H, *s*, H–C–N), 5.53 (1H, *s*, –C–H); ^{13}C-NMR (300 MHz, CDCl$_3$, δ / ppm): 38.8 (CH), 136.3–111.5 (aromatic), 155.2 (O–Ar); MS (*m/z*, (relative abundance, %)): 338 (M$^+$, 3.4), 116, 93,76 (BP, 100).

*3-[(1*H*-Indol-3-yl)(4-nitrophenyl)methyl]-1*H*-indole (12)*. Yield: 84 %; m.p. 220 °C; IR (KBr, cm^{-1}): 3448 (–NH stretching of amine), 3055 (–C–H stretching of aromatic ring), 1417, 1594 (–C=C stretching), 1342, 1218, 1012 (–C–N stretching), 735, 598 (aromatic ring); ^{1}H-NMR (300 MHz, DMSO-d_6, δ / ppm): 8.15 (2H, *s*, –NH), 7.01–7.08 (4H, *m*, aromatic), 7.36 (2H, *d*, *J* = 8.1 Hz, aromatic), 7.41 (2H, *d*, *J* = 8.1 Hz, aromatic), 7.49 (2H, *d*, *J* = 8.6 Hz, aromatic), 7.5 (2H, *d*, *J* = 8.6 Hz, aromatic), 6.68 (2H, *s*, H–C–N), 6 (1H, *s*, –C–H); ^{13}C-NMR (300 MHz, CDCl$_3$, δ / ppm): 41.6 (CH), 112.4–147.5 (aromatic), 153.6 (O$_2$N–Ar); MS (*m/z*, (relative abundance, %)): 367 (M$^+$, 4.5), 116, 76 (BP, 100).

*3-[1-(1*H*-Indol-3-yl)hexyl]-1*H*-indole (13)*. Yield: 76 % ; m.p. 65 °C; IR (KBr, cm^{-1}): 3350 (–NH stretching of amine), 3065 (–C–H stretching of aromatic ring), 1585–1615 (–C=C stretching), 1062 (–C–N stretching); ^{1}H-NMR (300 MHz, DMSO-d_6, δ / ppm): 7.87 (2H, *brs*, –NH), 7.52 (2H, *d*, *J* = 8.5 Hz, aromatic), 7.36 (2H, *d*, *J* = 8.5 Hz, aromatic), 7.02–7.18 (4H, *m*, aromatic), 6.66 (2H, *s*, H–C–N), 4.60 (1H, *t*, *J* = 6.9 Hz, CH), 4.24–1.24 (6H, *m*, CH$_2$), 0.8 (3H,

t, J = 7.3 Hz, CH$_3$); ^{13}C-NMR (300 MHz, CDCl$_3$, δ / ppm): 12.1 (CH$_3$), 20.8 (CH$_2$), 24.4 (CH$_2$), 30.2 (CH$_2$), 36.9 (CH$_2$), 40.5 (CH), 111.2–136.5 (aromatic); MS (m/z, (relative abundance, %)): 316 (M$^+$, 2.5), 116, 43 (BP, 100).

*3-[1-(1H-Indol-3-yl)butyl]-1H-indole (**14**)*. Yield: 75 %; m.p. 80 °C; IR (KBr, cm^{-1}): 3465 (–NH stretching of amine), 3028 (–C–H stretching of aromatic ring), 1495–1618 (–C=C stretching), 1009 (–C–N stretching), 782 (aromatic ring); ^{1}H-NMR (300 MHz, DMSO-d_6, δ / ppm): 7.92 (2H, brs, –NH), 7.53 (2H, d, J = 8.1 Hz, aromatic), 7.26 (2H, d, J = 8.1 Hz, aromatic), 7.06 (4H, m, aromatic), 4.47 (1H, t, J = 7.5 Hz, CH), 1.77–2.56 (4H, m, CH$_2$), 0.86 (3H, t, J = = 6.9 Hz, CH$_3$); ^{13}C-NMR (300 MHz, CDCl$_3$, δ / ppm): 17.4 (CH$_3$), 31.2 (CH$_2$), 36.9 (CH$_2$), 40.5 (CH), 111.1–138.5 (aromatic); MS (m/z, (relative abundance, %)): 288 (M$^+$, 2.3), 116, 43 (BP, 100).

*3-[Furan-2-yl(1H-indol-3-yl)methyl)-1H-indole (**15**)*. Yield: 90 % ; m.p. 340–345 °C; IR (KBr, cm^{-1}): 3409 (–NH stretching of amine), 3053 (–C–H stretching of aromatic ring), 1418, 1600 (–C=C stretching), 1093 (–C–N stretching); ^{1}H-NMR (300 MHz, DMSO-d_6, δ / ppm): 7.71 (2H, brs, –NH), 7.12–7.42 (8H, m, aromatic), 6.98 (1H, t, J = 6.8 Hz, furanyl), 6.72 (1H, d, J = 2.4 Hz, aromatic), 6.28 (1H, d, J = 2.2 Hz, aromatic), 5.95 (2H, d, J = 3.4 Hz, aromatic), 5.82 (1H, s, –CH).); ^{13}C-NMR (300 MHz, CDCl$_3$, δ / ppm): 34.6 (CH), 106.2–136.2 (aromatic), 141.2 (O–**C**–CH). MS (m/z, (relative abundance, %)): 312 (M$^+$, 2.8), 116 (BP, 100).

Microwave-assisted synthesis of novel 4*H*-chromene derivatives bearing phenoxypyrazole and their antimicrobial activity assessment

CHETAN B. SANGANI, NIMESH M. SHAH, MANISH P. PATEL
and RANJAN G. PATEL*

Department of Chemistry, Sardar Patel University, Vallabh Vidyanagar-388120, Gujarat, India

Abstract: A new series of 4*H*-chromene derivatives **4a**–**p** bearing the 5-phenoxypyrazole nucleus were synthesized under microwave irradiation by the reaction of 5-phenoxypyrazole-4-carbaldehydes **1a**–**h**, malononitrile **2** and compounds 1,3-cyclohexanedione and dimedone (**3a** and **3b**, respectively) in presence of NaOH as a basic catalyst. All the compounds were screened against three Gram-positive bacteria (*Streptococcus pneumoniae*, *Clostridium tetani* and *Bacillus subtilis*), three Gram-negative bacteria (*Salmonella typhi*, *Vibrio cholerae* and *Escherichia coli*) and two fungi (*Aspergillus fumigatus* and *Candida albicans*) using the broth microdilution minimum inhibitory concentration (MIC) method. The antimicrobial screening showed that the majority of the compounds were active against *C. tetani* and *B subtilis* as well as against *C. albicans* when compared with standard drugs.

Keywords: phenoxypyrazole; 4*H*-chromene; multi-component reaction; microwave irradiation; antimicrobial activity.

INTRODUCTION

The steadily increasing microbial resistance to existing first line drugs is a serious problem in antimicrobial cure and necessitates continuing research into new classes of antimicrobials.[1] Moreover, the progression of drug-resistant strains has contributed to the inefficiency of the straight antimicrobial therapy. This issue has provoked enormous interest in antimicrobial research and it is strongly believed that there is an urgent call for the development of new drugs with divergent and unique structures and probably with an unusual mechanism of action differing from that of existing first line drugs.

The chromene ring system is considered one of the most imperative heterocycles in nature as it has the distinction of being the parent ring in countless

---

derivatives of biological relevance. The current interest in 4*H*- and 2*H*-chromene derivatives arises from their potential application as antimicrobial,[2] anti-HIV,[3] antitubercular,[4] antioxidant,[5] anticancer,[6] antitumor,[7] cytotoxic agents,[8] antidyslipidemic agent,[9] antileishmanial,[10] anti-inflammatory,[11] anti-Helicobacter pylori agent[12] and TNF-α inhibitor.[13] On the other hand, pyrazole derivatives are also well-known for their biological properties, including antimicrobial,[14–16] anti-inflammatory (COX-2 inhibitor and ulcerogenic activity),[15] antitubercular,[16] antitumor,[17] anti-angiogenesis,[18] antiparasitic,[19] antiviral,[20] analgesic and anxiolytic activity.[21]

Moreover, the most suitable protocol for the synthesis of functionalized organic compounds could be a multicomponent reaction (MCR) because the synthesis could be performed without the isolation of the intermediates, without discharging any functional groups and within short reaction time.[22]. In addition, the conventional procedures are not found to be satisfactory with regard to operational simplicity, effectiveness and yield. An alternative synthetic approach is microwave irradiation.[23] In recent years, microwave irradiation has been demonstrated not only to dramatically accelerate many organic reactions, but also to improve yields and selectivity.

Thus, in view of biological significance of 4*H*-chromene, a modification on the 4-position on pyrane by 5-phenoxypyrazole was undertaken to check whether it may bring significant changes in the bioactivities of 4*H*-chromene derivatives. As a part of current studies in developing new antimicrobial agents *via* combination of two therapeutically active moieties,[24] the synthesis of 4*H*-chromene derivatives **4a**–**p** by MCR are reported herein.

All the compounds were characterized using elemental analysis, FT-IR, ^{1}H--NMR and ^{13}C-NMR spectroscopy, and the molecular weights of some selected compounds were confirmed by mass spectroscopy. All compounds were screened for *in vitro* antimicrobial activity against eight human pathogens, *i.e*., three Gram-positive bacteria (*Streptococcus pneumoniae*, *Clostridium tetani* and *Bacillus subtilis*), three Gram-negative bacteria (*Salmonella typhi*, *Vibrio cholera* and *Escherichia coli*) and two fungal pathogens (*Aspergillus fumigates* and *Candida albicans*) using the broth microdilution minimum inhibitory concentration (MIC) method.[25]

<div align="center">RESULTS AND DISCUSSION</div>

Chemistry

The key intermediates, 3-methyl-5-aryloxy-1-aryl-1*H*-pyrazole-4-carbaldehydes **1a**–**h** were prepared by refluxing 1-aryl-5-chloro-3-methyl-1*H*-pyrazole-4-carbaldehyde and various phenols in the presence of anhydrous potassium carbonate in dry dimethylformamide (DMF) for 3.5 h.[24a] The required 1-aryl-5-

-chloro-3-methyl-1*H*-pyrazole-4-carbaldehyde was prepared by the Vilsmeier––Haack reaction according to a literature procedure.[26]

In the present study, 4*H*-chromene derivatives **4a–p** were synthesized in moderate to good yield, *i.e.*, 68–90 %, by reaction of **1a–h**, malononitrile **2** and compounds **3a–b** under microwave irradiation in the presence of NaOH as a basic catalyst (Scheme 1).
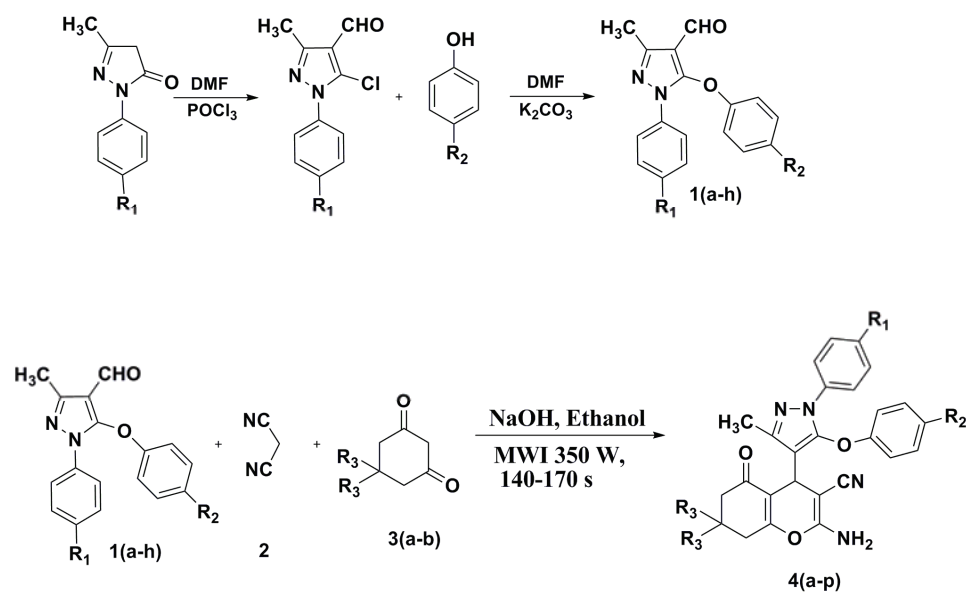
Comp.	R_1	R_2	R_3	Yield[a], %	Comp.	R_1	R_2	R_3	Yield[a], %
4a	H	H	H	78	**4i**	H	H	CH_3	90
4b	H	CH_3	H	90	**4j**	H	CH_3	CH_3	75
4c	H	OCH_3	H	84	**4k**	H	OCH_3	CH_3	87
4d	H	Cl	H	69	**4l**	H	Cl	CH_3	65
4e	CH_3	H	H	80	**4m**	CH_3	H	CH_3	88
4f	CH_3	CH_3	H	84	**4n**	CH_3	CH_3	CH_3	90
4g	CH_3	OCH_3	H	72	**4o**	CH_3	OCH_3	CH_3	92
4h	CH_3	Cl	H	64	**4p**	CH_3	Cl	CH_3	73

[a]All yields are isolated yields

Scheme 1. Synthetic pathway for the synthesis of 4*H*-chromene derivatives bearing the phenoxypyrazole core **4a–p**.

In convenient electrochemical processes, organic basic catalysts, such as piperidine and triethylamine, were used in the synthesis of many 4*H*-chromene derivatives[27] but in the present study, NaOH was used as the basic catalyst to avoid the employment of hazardous organic bases. Furthermore, during attempts to synthesize the title compounds by the conventional method, some shortcomings in this method were observed, such as longer reaction time, drastic reac-

tion conditions and poor yield. Consequently, to overcome these drawbacks, the microwave irradiation method was used in the present study for the synthesis of title compounds. In accordance with the mechanism suggested in literature,[28] the first step of this process may involve Knoevenagel condensation of the aldehyde and malononitrile to gives heterylidenenitrile derivatives, which was followed by Michael addition of **3a**–**b** to the heterylidenenitrile to afford the title compounds **4a**–**p** (Scheme 2).

Pyz-CHO = 3-Methyl-5-aryloxy-1-aryl-1*H*-pyrazole-4-carbaldehyde
R_3 = H, CH_3
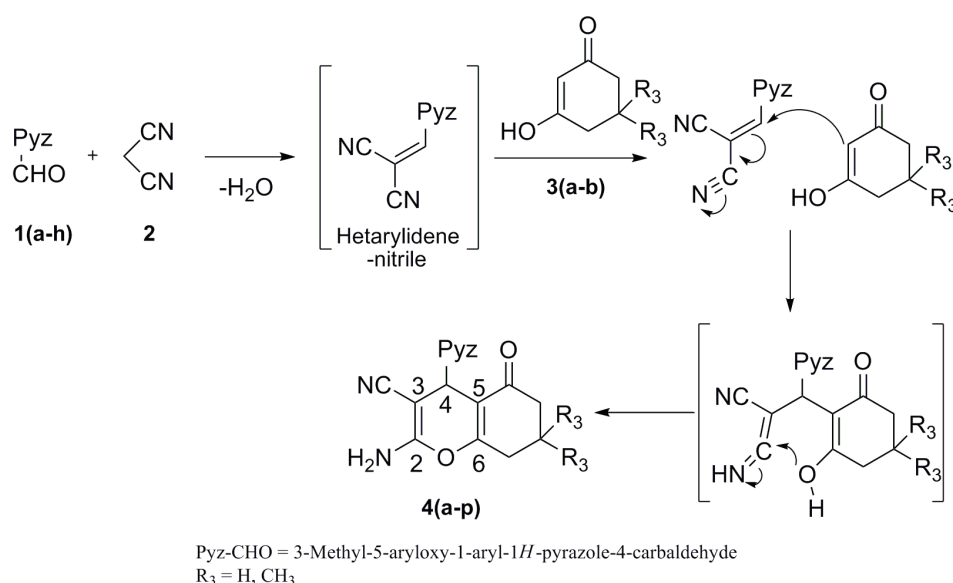
Scheme 2. Plausible mechanistic pathway of the synthesis of 4*H*-chromene derivatives **4a**–**p**.

The structures of all the newly synthesized compounds were confirmed by FTIR, ^{1}H-NMR, ^{13}C-NMR and mass spectroscopy, and elemental analysis. The physical, analytical and spectral data of all the synthesized compounds **4a**–**p** are given in the Supplementary material to this paper. The IR spectrum of title compounds **4a**–**p** revealed the presence of amino, cyano, carbonyl and ether groups through the appearance of absorption bands at around 3370–3430, 3170–3350, 2190–2220, 1630–1710 and 1190–1230 cm^{-1}, respectively. Their ^{1}H-NMR spectra indicated the presence of a singlet in the range δ 4.12–4.38 ppm of the CH proton and the disappearance of a singlet at δ 9.57–9.63 ppm of –CHO, which clearly confirmed the cyclization of the Knoevenagel intermediates. Moreover, multiplets in the range δ 6.59–7.55 ppm appeared for aromatic protons. In the ^{13}C-NMR spectral data of the title compounds **4a**–**p**, most characteristic signal around δ 24.50–25.25 ppm indicate the formation of the pyrane ring. The signal at around δ 56.20–60.64 ppm is assigned to carbon attached to carbonitrile, while signals around δ 110.20–164.50 and 196.10–196.35 ppm are attributed to all the

aromatic and carbonyl carbons, respectively, of compounds **4a**–**p**. The obtained elemental analysis values are in good agreement with theoretical data. Furthermore, the molecular weight of selected compounds, *i.e*., **4c**, **4i** and **4o**, were confirmed by mass spectral studies. The mass spectra of these compounds showed a molecular ion peak $[M+1]^+$ corresponding to the exact theoretical mass.

Biological evaluation

All the compounds were screened for their antibacterial and antifungal activity and the results are presented in Table I, expressed in the form of *MIC* in µg mL^{-1}.

TABLE I. Antimicrobial activity of compounds **4a**–**p** (minimum inhibitory concentration (*MIC*), µg mL^{-1}); Bs.: *B. subtilis*; Ct.: *C. tetani*; Sp.: *S. pneumoniae*; Ec.: *E. coli*; St.: *S. typhi*; Vc.: *V. cholerae*; Af.: *A. fumigatus*; Ca.: *C. albicans*; MTCC: microbial type culture collection; A: ampicillin; B: ciprofloxacin; C: norfloxacin; D: chloramphenicol; E: nystatin; F: griseofulvin. "–" represents "not tested"

Compound	Gram-positive bacteria			Gram-negative bacteria			Fungal species	
	Bs. MTCC 441	Ct. MTCC 449	Sp. MTCC 1936	Ec. MTCC 443	St. MTCC 98	Vc. MTCC 3906	Af. MTCC 3008	Ca. MTCC 227
4a	500	500	500	250	500	500	>1000	>1000
4b	250	500	250	500	500	100	500	500
4c	500	500	500	200	500	500	250	250
4d	1000	100	500	250	500	200	250	100
4e	250	200	250	500	250	200	500	250
4f	500	200	500	250	250	200	500	500
4g	500	250	500	250	500	100	500	200
4h	500	200	500	100	500	250	250	250
4i	250	500	250	100	100	250	1000	500
4j	500	100	500	250	62.5	250	1000	1000
4k	500	250	500	500	500	200	500	250
4l	250	200	250	250	250	200	500	250
4m	500	500	50	250	500	500	1000	500
4n	62.5	100	250	100	62.5	200	>1000	>1000
4o	500	100	500	200	500	200	500	500
4p	250	250	500	100	62.5	250	250	250
A	250	250	100	100	100	100	–	–
B	50	100	50	25	25	25	–	–
C	100	50	10	10	10	10	–	–
D	50	50	50	50	50	50	–	–
E	–	–	–	–	–	–	100	100
F	–	–	–	–	–	–	100	500

An examination of the data prescribed in Table I revealed that many of the compounds were more potent or equipotent to the standard drugs against the Gram-positive bacteria *C. tetani* and a few against *S. pneumoniae* and *B. subtilis*.

Against the Gram-positive bacteria *B. subtilis*, compound **4n** (*MIC* = 62.5 μg mL^{-1}) was found to be more potent, whereas **4b**, **4e**, **4i**, **4l**, and **4p** (*MIC* = 250 μg mL^{-1}) shows comparable activity to ampicillin (*MIC* = 250 μg mL^{-1}). Moreover, compound **4n** (*MIC* = 62.5 μg mL^{-1}) was found to more active as compared to norfloxacin (*MIC* = 100 μg mL^{-1}). Against *C. tetani*, compounds **4d**, **4j**, **4n** and **4o** (*MIC* = 100 μg/mL), and **4e**, **4f**, **4h** and **4l** (*MIC* = 200 μg mL^{-1}) were found to be more potent, whereas **4g**, **4k** and **4p** (*MIC* = 250 μg mL^{-1}) showed comparable activity to ampicillin (*MIC* = 250 μg mL^{-1}), while compounds **4d**, **4j**, **4n** and **4o** (*MIC* = 100 μg mL^{-1}) were equally potent as compared to ciprofloxacin (*MIC* = 100 μg mL^{-1}). Against *S. pneumoniae*, compound **4m** (*MIC* = 50 μg mL^{-1}) showed comparable activity to chlormphenicol and ciprofloxacin (*MIC* = 50 μg mL^{-1}).

Towards the Gram-negative strain *E. coli*, compounds **4h**, **4i**, **4n** and **4p** (*MIC* = 100 μg mL^{-1}) showed comparable activity to ampicillin (*MIC* = 100 μg mL^{-1}). Compounds **4j**, **4n** and **4p** (*MIC* = 62.5 μg mL^{-1}) were more potent, whereas **4i** (*MIC* = 100 μg mL^{-1}) showed comparable activity to ampicillin (*MIC* = 100 μg mL^{-1}) towards *S. typhi.* Also the compounds **4b** and **4g** (MIC = 100 μg/mL) show comparable activity, to ampicillin (MIC=100 μg/mL) towards *V. cholerae.*

Comparison of the data for compounds **4a–d** with those for **4e–h** showed that on replacement of H with CH$_3$, the poorly active compounds **4a**, **4b** and **4c** (*MIC* = 500 μg mL^{-1} against *C. tetani*) were converted to the highly potent **4e**, **4f** and **4g**, respectively, while the potency of compound **4d**, where R$_2$ = Cl, against *C. tetani* decreased on introduction of CH$_3$ at R$_1$. Against *B. subtilis*, comparing compound **4f** with **4n**, it was observed that the poorly active compound **4f** (*MIC* = 500 μg mL^{-1}) led to the excellent activity of **4n** (*MIC* = 62.5 μg mL^{-1}), compared to the activity of ampicillin and norfloxacin. Similarly, against the Gram-negative bacteria *S. typhi*, it was observed by comparing compound **4b** with **4j** and **4f** with **4n**, that poorly active compounds were converted to highly active ones (*MIC* = 62.5 μg mL^{-1}) as compared with ampicillin (MIC = 100 μg mL^{-1}), *i.e.*, the compound having a *gem* dimethyl group on the benzopyran ring showed increased antibacterial activity.

Against fungal pathogen *C. albicans*, compounds **4d** (*MIC* = 100 μg mL^{-1}), **4g** (*MIC* = 200 μg mL^{-1}) **4c**, **4e**, **4h**, **4k**, **4l** and **4p** (*MIC* = 250 μg mL^{-1}) showed good to excellent activity, whereas **4b**, **4f**, **4i**, **4m** and **4o** (*MIC* = 500 μg mL^{-1}) were equipotent to griseofulvin (*MIC* = 500 μg mL^{-1}). Compound **4d** (*MIC* =100 μg mL^{-1}) was found equipotent to nystatin towards *C. albicans.*

The remaining compounds showed moderate to good activity in the inhibition of the growth of bacterial pathogens and were all less effective than the standard drugs. From the antimicrobial study of the title derivatives, it is inte-

resting to note that a minor alteration in the molecular structure of the investigated compounds may have a pronounced effect on antimicrobial activity.

EXPERIMENTAL

Materials, instruments and methods

The required chemicals were obtained from S. D. Fine Chem Ltd., Vadodara, Gujarat, India. 1,3-Cyclohexanedione and dimedone were obtained from Sigma-Aldrich. The solvents were purified and dried before use. The microwave assisted reactions were conducted in a "RAGA modified electromagnetic microwave system", whereby the microwaves were generated by a magnetron at a frequency of 2450 MHz having adjustable output power levels, *i.e.*, 10 levels from 140 to 700 W and with an individual sensor for temperature control (fiber optic was used as an individual sensor for temperature control). A reflux condenser was attached to the reaction flask and the reactions were performed under constant stirring (thus avoiding the risk of high pressure development). All melting points were taken in open capillaries and are uncorrected. Thin-layer chromatography (TLC, on aluminium plates pre-coated with silica gel, 60 F254, 0.25 mm thickness) (Merck, Darmstadt, Germany) was used for monitoring the progress of all reactions, and the purity and homogeneity of the synthesized compounds. UV radiation and/or iodine were used as the visualizing agents. Elemental analysis (% C, H, N) was realized using a Perkin-Elmer 2400 Series-II elemental analyzer (Perkin-Elmer, USA) and the results for all compounds were within ±0.4 % of the theoretical values. The IR spectra were recorded in KBr on a Perkin-Elmer Spectrum GX FT-IR spectrophotometer (Perkin-Elmer, USA) and only the characteristic peaks are reported in cm^{-1}. The ^{1}H-NMR and ^{13}C--NMR spectra were recorded at 400 and 100 MHz, respectively, in DMSO-d_6 on a Bruker Avance 400F spectrometer (Bruker Scientific Corporation Ltd., Switzerland) using the solvent peak as internal standard. Chemical shifts are reported in parts per million (ppm). Mass spectra were scanned on a Shimadzu LCMS 2010 spectrometer.

*Conventional synthesis of compounds **4a**–**p***

Phenoxypyrazole-4-carbaldehyde **1a**–**h** (10 mmol), malononitrile **2** (10 mmol) and 1,3--cyclohexanedione/dimedone **3a**–**b** (10 mmol) were thoroughly mixed in ethanolic NaOH (5 mmol, 10 mL) and charged into a round bottom flask. Then the reaction mixture was refluxed for 3–3.5 h. Completion of the reaction was monitored by TLC. The solid product **4a**–**p** that separated was filtered off, washed well with ethanol (10 mL), dried and crystallized from chloroform to obtain the pure solid sample **4a**–**p**.

*Microwave-induced synthesis of compounds **4a**–**p***

Phenoxypyrazole-4-carbaldehyde **1a**–**h** (10 mmol), malononitrile **2** (10 mmol) and 1,3--cyclohexanedione/dimedone **3a**–**b** (10 mmol) were thoroughly mixed in ethanolic NaOH (5 mmol, 10 mL) and irradiated in microwave oven at 350 W (50 % of the maximum output power) for 140–170 s. After completion of the reaction (checked by TLC), the solution was cooled to room temperature, the separated solid was filtered, washed well with ethanol (10 mL), dried and crystallized from chloroform to obtain the pure solid samples **4a**–**p**.

CONCLUSIONS

A series of some new 4*H*-chromene derivatives **4a**–**p** bearing the phenolxy-pyrazole nuclei were synthesized through a facile one-pot multicomponent reaction under microwave irradiation. This synthetic strategy allowed the construc-

tion of a relatively complicated nitrogen- and oxygen-containing heterocyclic system, as well as the introduction of various aromatic and heteroaromatic substituents at the 4-position of pyrane. From the studied compounds, it was noticed that the most effective antibacterial members had a methyl group on the *N*-phenyl ring of the pyrazole moiety as well as a *gem* dimethyl group on the benzopyrane ring with either Cl or methyl substituent on the O-phenyl ring of the pyrazole moiety. The antifungal activity of the compounds shows that most of the compounds were more potent against *C. albicans* than against *A. fumigatus*. It is worth mentioning that minor changes in the molecular configuration of these compounds profoundly influenced the activity. The present study throws light on the identification of this new structural class as antimicrobials, which could be of interest for further detailed preclinical investigations.

SUPPLEMENTARY MATERIAL

Analytical, physical and spectroscopic data of the synthesized compounds are available electronically from http://www.shd.org.rs/JSCS/, or from the corresponding author on request.

И З В О Д

СИНТЕЗА НОВИХ ДЕРИВАТА ФЕНОКСИПИРАЗИНИЛ-4*H*-ХРОМЕНА ПОД УСЛОВИМА ЗРАЧЕЊА МИКРОТАЛАСИМА И ОДРЕЂИВАЊЕ ЊИХОВЕ АНТИМИКРОБНЕ АКТИВНОСТИ

CHETAN B. SANGANI, NIMESH M. SHAH, MANISH P. PATEL и RANJAN G. PATEL

Department of Chemistry, Sardar Patel University, Vallabh Vidyanagar-388120, Gujarat, India

Нова серија деривата 4*H*-хромена **4a**–**p** који садрже 5-феноксипиразол синтетисани су под условима озрачивања микроталасима, реакцијом 5-феноксипиразол-4-карбалдехида **1a**–**h**, малононитрила **2** и једињења (1,3-циклохександион, димедон) **3a**–**b** у присуству NaOH или базних катализатора. Свим једињењима испитана је активност према 3 врсте грам-позитивних бактерија (*Streptococcus pneumoniae*, *Clostridium tetani* и *Bacillus subtilis*), 3 врсте грам-негативних (*Salmonella typhi*, *Vibrio cholerae* и *Escherichia coli*) и две врсте гљива (*Aspergillus fumigatus* и *Candida albicans*) користећи поступке одређивања МИК (минимална инхибиторна концентрација разблажењем). Током испитивања антимикробне активности утврђено је да су једињења активна према *C. tetani* и *B. subtilis*, као и према *C. albicans* у поређењу са вредностима стандардних лекова.

(Примљено 2. јануара, ревидирано 27. марта 2012)

REFERENCES

1. N. Woodford, *Expert Opin. Investig. Drugs* **12** (2003) 117

2. a) B. S. Kuarm, Y. T. Reddy, J. V. Madhav, P. A. Crooks, B. Rajitha, *Bioorg. Med. Chem. Lett*. **21** (2011) 524; b) U. S. Rai, A. M. Isloor, P. Shetty, A. M. Vijesh, N. Prabhu, S. Isloor, M. Thiageeswaran, H. K. Fun, *Eur. J. Med. Chem*. **45** (2010) 2695

3. a) D. Bhavsar, J. Trivedi, S. Parekh, M. Savant, S. Thakrar, A. Bavishi, A. Radadiya, H. Vala, J. Lunagariya, M. Parmar, L. Paresh, R. Loddo, A. Shah, *Bioorg. Med. Chem. Lett*. **21** (2011) 3443; b) J. H. Park, S. U. Lee, S. H. Kim, S. Y. Shin, J. Y. Lee, C. G. Shin, K. H. Yoo, Y. S. Lee, *Arch. Pharm. Res*. **31** (2008) 1

4. N. R. Kamdar, D. D. Haveliwala, P. T. Mistry, S. K. Patel, *Med. Chem. Res*. **20** (2012) 854

5. O. M. Singh, N. S. Devi, D. S. Thokchom, G. J. Sharma, *Eur. J. Med. Chem*. **45** (2010) 2250

6. B. C. Raju, R. N. Rao, P. Suman, P. Yogeeswari, D. Sriram, T. B. Shaik, S. V. Kalivendi, *Bioorg. Med. Chem. Lett*. **21** (2011) 2855

7. W. Huang, Y. Ding, Y. Miao, M. Liu, Y. Li, G. Yang, *Eur. J. Med. Chem*. **44** (2009) 3687

8. a) T. Raj, R. K. Bhatia, A. Kapur, M. Sharma, A. K. Saxena, M. P. S. Ishar, *Eur. J. Med. Chem*. **45** (2010) 790; b) N. M. Sabry, H. M. Mohamed, E. Shawky, A. E. H. Khattab, S. S. Motlaq, A. M. El-Agrody, *Eur. J. Med. Chem*. **46** (2011) 765

9. K. V. Sashidhara, J. N. Rosaiah, G. Bhatia, J. K. Saxena, *Eur. J. Med. Chem.* **43** (2008) 2592

10. Z. Nazarian, S. Emami, S. Heydari, S. K. Ardestani, M. Nakhjiri, F. Poorrajab, A. Shafiee, A. Foroumadi, *Eur. J. Med. Chem*. **45** (2010) 1424

11. P. Gebhardt, K. Dornberger, F. A. Gollmick, U. Grafe, A. Hartl, H. Gorls, B. Schlegela, C. Hertwecka, *Bioorg. Med. Chem. Lett*. **17** (2007) 2558

12. F. Chimenti, B. Bizzarri, A. Bolasco, D. Secci, P. Chimenti, S. Carradori, A. Granese, D. Rivanera, D. Lilli, A. Zicari, M. M. Scaltrito, F. Sisto, *Bioorg. Med. Chem. Lett*. **17** (2007) 3065

13. J. Cheng, A. Ishikawa, Y. Ono, T. Arrhenius, A. Nadzan, *Bioorg. Med. Chem. Lett*. **13** (2003) 3647

14. a) I. Damljanovic, M. Colovic, M. Vukicevic, D. Manojlovic, N. Radulovic, K. Wurst, G. Laus, Z. Ratkovic, M. D. Joksovic, R. D. Vukicevic, *J. Organomet. Chem.* **694** (2009) 1575; b) I. Damljanovic, M. Vukicevic, N. Radulovic, R. Palic, E. Ellmerer, Z. Ratkovic, M. D. Joksovic, R. D. Vukicevic, *Bioorg. Med. Chem. Lett.* **19** (2009) 1093; c) O. Prakash, R. Kumar, V. Parkash, *Eur. J. Med. Chem.* **43** (2008) 435; d) O. Prakash, R. Kumar, R. Sehrawat, *Eur. J. Med. Chem.* **44** (2009) 1763

15. A. A Bekhit, H. M. A. Ashour, Y. S. A. Ghany, A. E. A. Bekhit, A. M. Baraka, *Eur. J. Med. Chem.* **43** (2008) 456

16. A. R. Trivedi, V. R. Bhuva, B. H. Dholariya, D. K. Dodiya, V. B. Kataria, V. H. Shah, *Bioorg. Med. Chem. Lett.* **20** (2010) 6100

17. M. D. Joksovic, V. Markovic, Z. D. Juranic, T. Stanojkovic, L. S. Jovanovic, I. S. Damljanovic, K. Meszaros Szecsenyi, N. Todorovic, S. Trifunovic, R. D. Vukicevic, *J. Organomet. Chem.* **694** (2009) 3935

18. A. H. Abadi, A. A. H. Eissa, G. S. Hassan, *Chem. Pharm. Bull.* **51** (2003) 838

19. P. Rathelot, N. Azas, H. El-Kashef, F. Delmas, C. D. Giorgio, P. Timon-David, J. Maldonado, P. Vanelle, *Eur. J. Med. Chem.* **37** (2002) 671

20. a) A. I. Hashem, A. S. A. Youssef, K. A. Kandeel, W. S. I. Abou-Elmagd, *Eur. J. Med. Chem.* **42** (2007) 934; b) A. Farghaly, H. El-Kashef, *ARKIVOC* (2006) 76; c) A. Farghaly, E. De Clercq, H. El-Kashef, *ARKIVOC* (2006) 137

21. S. C. Shetty, V. C. Bhagat, *Asian J. Chem.* **20** (2008) 5037

22. L. Boulard, S. BouzBouz, J. Cossy, X. Franck, B. Figadère, *Tetrahedron Lett.* **45** (2004) 6603.

23. M. A. Pasha, V. P. Jayshankara, *Indian J. Chem.*, Sect. B **46** (2007) 1328

24. a) C. B. Sangani, D. C. Mungra, M. P. Patel, R. G. Patel, *Cent. Eur. J. Chem.* **9** (2011) 635; b) C. B. Sangani, D. C. Mungra, M. P. Patel, R. G. Patel, *Chin. Chem. Lett.* **23** (2012) 57; c) N. M. Shah, M. P. Patel, R. G. Patel, *J. Heterocycl. Chem.* 49 (2012) 913; d) N. M. Shah, M. P. Patel, R. G. Patel, *J. Chem. Sci.*, accepted; e) D. C. Mungra, M. P. Patel, D. P. Rajani, R. G. Patel, *Eur. J. Med. Chem.* **46** (2011) 4192; () J. A. Makawana, M. P. Patel, R. G. Patel, *Med. Chem. Res.* (2011), doi: 10.1007/s00044-010-9568-6; f) N. J. Thumar, M. P. Patel, *Arch. Pharm.* **344** (2011) 91; g) N. K. Shah, N. M. Shah, M. P. Patel, R. G. Patel, *J. Serb. Chem. Soc.* 77 (2012) 279; h) H. G. Kathrotiya, M. P. Patel, R. G. Patel, *J. Serb. Chem. Soc.* **77** (2012) 983

25. NCCLS (National Committee for Clinical Laboratory Standards), 2002. *Performance standards for antimicrobial susceptibility testing*, Twelfth informational supplement. ISBN 1-56238-454-6, M100-S12 (M7)

26. R. A. Pawar, A. A. Patil, *Indian J. Chem., Sect. B* **33** (1994) 156

27. a) L. Fotouhi, M. M. Heravi, A. Fatehi, K. Bakhtiari, *Tetrahedron Lett.* **48** (2007) 5379; b) S. Makarem, A. A. Mohammadi, A. R. Fakhari, *Tetrahedron Lett.* **49** (2008) 7194; c) M. N. Jachak, D. B. Kendre, A. B. Avhale, R. B. Toche, V. J. Medhane, *Org. Prep. Proced. Int.* **38** (2006) 313; d) A. Shaabani, R. Ghadari, S. Ghasemi, M. Pedarpour, A. Rezayan, A. Sarvary, S. Weng Ng, *J. Comb. Chem.* **11** (2009) 956

28. J. A. Makawana, M. P. Patel, R. G. Patel, *Bioorg. Med. Chem. Lett.* **21** (2011) 6166.

Microwave-assisted synthesis of novel 4*H*-chromene derivatives bearing phenoxypyrazole and their antimicrobial activity assessment

CHETAN B. SANGANI, NIMESH M. SHAH, MANISH P. PATEL
and RANJAN G. PATEL*

Department of Chemistry, Sardar Patel University, Vallabh Vidyanagar-388120, Gujarat, India

ANALYTICAL, PHYSICAL AND SPECTROSCOPIC DATA
OF THE SYNTHESIZED COMPOUNDS

*2-Amino-4-(3-methyl-5-phenoxy-1-phenyl-1*H-*pyrazol-4-yl)-5-oxo-5,6,7,8-tetrahydro-4*H-*chromene-3-carbonitrile (4a)*. Yield: 78 %; m.p.: 159–160 °C; Anal. Calcd. for $C_{26}H_{22}N_4O_3$ (FW: 438.48): C, 71.22; H, 5.06; N, 12.78 %. Found: C, 71.13; H, 5.13; N, 12.69 %; IR (KBr, cm^{-1}): 3395 and 3310 (asym. and sym. stretching of –NH$_2$), 2200 (–C≡N stretching), 1680 (C=O str.), 1230 (C–O–C ether stretching); ^{1}H-NMR (400 MHz, DMSO-d_6, δ / ppm): 1.68–2.17 (6H, *m*, 3×CH$_2$), 2.37 (3H, *s*, CH$_3$), 4.20 (1H, *s*, CH), 6.68–7.41 (12H, *m*, Ar–H + NH$_2$); ^{13}C-NMR (100 MHz, DMSO-d_6, δ / ppm): 13.10 (CH$_3$), 19.45 (CH$_2$), 25.00 (CH), 26.48 (CH$_2$), 36.49 (CH$_2$), 56.30 (**C**–CN), 111.20, 112.54, 115.26, 115.53, 120.50, 121.49, 126.85, 129.61, 138.34, 145.63, 147.80, 150.20, 155.43, 159.00, 164.30 (Ar–C + CN), 196.19 (C=O); MS (*m/z*): 439.2 (M+1).

*2-Amino-4-[3-methyl-5-(4-methylphenoxy)-1-phenyl-1*H-*pyrazol-4-yl]-5-oxo--5,6,7,8-tetrahydro-4*H-*chromene-3-carbonitrile (4b)*. Yield: 90 %; m.p.: 217––218 °C; Anal. Calcd. for $C_{27}H_{24}N_4O_3$ (FW: 452.50): C, 71.67; H, 5.35; N, 12.38 %. Found: C, 71.83; H, 5.45; N, 12.21 %; IR (KBr, cm^{-1}): 3405 and 3200 (asym. and sym. stretching of –NH$_2$), 2190 (–C≡N stretching), 1700 (C=O str.), 1210 (C–O–C ether stretching); ^{1}H-NMR (400 MHz, DMSO-d_6, δ / ppm): 1.71––2.24 (6H, *m*, 3xCH$_2$), 2.23, 2.25 (2×3H, *s*, CH$_3$), 4.29 (1H, *s*, CH), 6.75–7.51 (11H, *m*, Ar–H + NH$_2$); ^{13}C-NMR (100 MHz, DMSO-d_6, δ / ppm): 12.95 (CH$_3$), 19.72 (CH$_2$), 20.50 (CH$_3$), 24.98 (CH), 26.55 (CH$_2$), 36.60 (CH$_2$), 57.25 (**C**–CN), 110.72, 112.22, 115.20, 115.75, 120.18, 121.39, 126.54, 129.60, 138.12, 145.57, 147.69, 150.14, 155.15, 159.17, 164.36 (Ar–C+ CN), 196.11 (C=O); MS (*m/z*): 453.2 (M+1).

---

* Corresponding author. E-mail: patelranjanben@yahoo.com

*2-Amino-4-[5-(4-methoxyphenoxy)-3-methyl-1-phenyl-1*H-*pyrazol-4-yl]-5-oxo--5,6,7,8-tetrahydro-4*H-*chromene-3-carbonitrile (**4c**)*. Yield: 84 %; m.p.: 143––145 °C; Anal. Calcd. for $C_{27}H_{24}N_4O_4$ (FW: 468.50): C, 69.22; H, 5.16; N, 11.96 %. Found: C, 69.09; H, 5.33; N, 12.03 %; IR (KBr, cm^{-1}): 3410 and 3340 (asym. and sym. stretching of $-NH_2$), 2200 ($-C≡N$ stretching), 1640 (C=O str.), 1205 (C–O–C ether stretching); ^{1}H-NMR (400 MHz, DMSO-d_6, δ / ppm): 1.73––2.13 (6H, *m*, CH_2), 2.33 (3H, *s*, CH_3), 3.65 (3H, *s*, OCH_3), 4.15 (1H, *s*, CH), 6.60–7.53 (11H, *m*, Ar–H + NH_2); ^{13}C-NMR (100 MHz, DMSO-d_6, δ / ppm): 13.19 (CH_3), 19.59 (CH_2), 25.20 (CH), 26.68 (CH_2), 36.45 (CH_2), 55.90 (OCH_3), 56.37 (**C**–CN), 111.57, 112.28, 115.26, 115.71, 120.47, 121.49, 126.84, 129.60, 138.26, 145.65, 147.73, 150.19, 155.34, 159.13, 164.36 (Ar–C + CN), 196.27 (C=O); MS (*m/z*): 469.2 (M+1).

*2-Amino-4-[5-(4-chlorophenoxy)-3-methyl-1-phenyl-1*H-*pyrazol-4-yl]-5-oxo--5,6,7,8-tetrahydro-4*H-*chromene-3-carbonitrile (**4d**)*. Yield: 69 %; m.p.: 173––174 °C; Anal. Calcd. for $C_{26}H_{21}ClN_4O_3$ (FW: 472.92): C, 66.03; H, 4.48; N, 11.85 %. Found: C, 65.90; H, 4.63; N, 12.00 %; IR (KBr, cm^{-1}): 3375 and 3320 (asym. and sym. stretching of $-NH_2$), 2190 ($-C≡N$ stretching), 1695 (C=O str.), 1215 (C–O–C ether stretching); ^{1}H-NMR (400 MHz, DMSO-d_6, δ / ppm): 1.65––2.19 (6H, *m*, CH_2), 2.43 (3H, *s*, CH_3), 4.38 (1H, *s*, CH), 6.73–7.50 (11H, *m*, Ar–H + NH_2); ^{13}C-NMR (100 MHz, DMSO-d_6, δ / ppm): 13.14 (CH_3), 19.55 (CH_2), 25.15 (CH), 26.58 (CH_2), 36.54 (CH_2), 57.25 (**C**–CN), 110.42, 112.01, 115.13, 115.65, 120.55, 121.11, 126.80, 129.13, 138.24, 145.18, 147.12, 150.00, 155.66, 159.18, 163.98 (Ar–C + CN), 196.14 (C=O); MS (*m/z*): 473.1 (M+1).

*2-Amino-4-[3-methyl-1-(4-methylphenyl)-5-phenoxy-1*H-*pyrazol-4-yl]-5-oxo--5,6,7,8-tetrahydro-4*H-*chromene-3-carbonitrile (**4e**)*. Yield: 80 %; m.p.: 189––190 °C; Anal. Calcd. for $C_{27}H_{24}N_4O_3$ (FW: 452.50): C, 71.67; H, 5.35; N, 12.38 %. Found: C, 71.75; H, 5.44; N, 12.25 %; IR (KBr, cm^{-1}): 3410 and 3240 (asym. and sym. stretching of $-NH_2$), 2210 ($-C≡N$ stretching), 1665 (C=O str.), 1215 (C–O–C ether stretching). ^{1}H-NMR (400 MHz, DMSO-d_6, δ / ppm): 1.70––2.10 (6H, *m*, CH_2), 2.35 (3H, *s*, CH_3), 4.18 (1H, *s*, CH), 6.69–7.44 (11H, *m*, Ar–H + NH_2); ^{13}C-NMR (100 MHz, DMSO-d_6, δ / ppm): 13.01 (CH_3), 19.40 (CH_2), 20.55 (CH_3), 25.23 (CH), 26.42 (CH_2), 36.38 (CH_2), 56.18 (**C**–CN), 111.40, 112.22, 115.17, 116.01, 120.53, 121.19, 126.11, 129.61, 138.27, 145.60, 147.73, 150.19, 155.16, 160.00, 164.10 (Ar–C + CN), 196.15 (C=O); MS (*m/z*): 453.2 (M+1).

*2-Amino-4-[3-methyl-5-(4-methylphenoxy)-1-(4-methylphenyl)-1*H-*pyrazol--4-yl]-5-oxo-5,6,7,8-tetrahydro-4*H-*chromene-3-carbonitrile (**4f**)*. Yield: 84 %, m.p.: 129–130 °C; Anal. Calcd. for $C_{28}H_{26}N_4O_3$ (FW: 466.53): C, 71.09; H, 5.62; N, 12.01 %. Found: C, 71.14; H, 5.70; N, 11.87 %; IR (KBr, cm^{-1}): 3400 and 3225 (asym. and sym. stretching of $-NH_2$), 2200 ($-C≡N$ stretching), 1700 (C=O str.), 1200 (C–O–C ether stretching); ^{1}H-NMR (400 MHz, DMSO-d_6,

δ / ppm): 1.73–2.22 (6H, *m*, CH$_2$), 2.20, 2.26 (2×3H, *s*, CH$_3$), 4.17 (1H, *s*, CH), 6.63–7.40 (10H, *m*, Ar–H + NH$_2$); ^{13}C-NMR (100 MHz, DMSO-d_6, δ / ppm): 12.90 (CH$_3$), 19.80 (CH$_2$), 20.54, 20.65 (2×CH$_3$), 24.70 (CH), 26.62 (CH$_2$), 36.57 (CH$_2$), 56.35 (**C**–CN), 110.35, 111.94, 115.20, 115.45, 120.59, 121.50, 126.84, 129.61, 138.11, 145.70, 147.84, 150.20, 155.55, 159.95, 163.28 (Ar–C + CN), 196.29 (C=O); MS (*m/z*): 467.2 (M+1).

*2-Amino-4-[5-(4-methoxyphenoxy)-3-methyl-1-(4-methylphenyl)-1*H-*pyrazol--4-yl]-5-oxo-5,6,7,8-tetrahydro-4*H-*chromene-3-carbonitrile (4g)*. Yield: 72 %; m.p.: 244–246 °C, Anal. Calcd. for C$_{28}$H$_{26}$N$_4$O$_4$ (FW: 482.53): C, 69.70; H, 5.43; N, 11.61 %. Found: C, 70.00; H, 5.19; N, 11.80 %; IR (KBr, cm^{-1}): 3425 and 3195 (asym. and sym. stretching of –NH$_2$), 2200 (–C≡N stretching), 1690 (C=O str.), 1190 (C–O–C ether stretching); ^{1}H-NMR (400 MHz, DMSO-d_6, δ / ppm): 1.66–2.14 (6H, *m*, CH$_2$), 2.31 (3H, *s*, CH$_3$), 3.66 (3H, *s*, OCH$_3$), 4.20 (1H, *s*, CH), 6.75–7.46 (10H, *m*, Ar–H + NH$_2$); ^{13}C-NMR (100 MHz, DMSO-d_6, δ / ppm): 13.11 (CH$_3$), 19.47 (CH$_2$), 20.72 (CH$_3$), 25.62 (CH), 26.65 (CH$_2$), 36.30 (CH$_2$), 55.88 (OCH$_3$), 58.20 (**C**–CN), 110.98, 112.03, 115.30, 115.74, 120.20, 121.67, 126.89, 129.62, 137.88, 145.12, 147.98, 149. 91, 155.35, 159.12, 164.50 (Ar–C + CN), 196.31 (C=O); MS (*m/z*): 483.2 (M+1).

*2-Amino-4-[5-(4-chlorophenoxy)-3-methyl-1-(4-methylphenyl)-1*H-*pyrazol--4-yl]-5-oxo-5,6,7,8-tetrahydro-4*H-*chromene-3-carbonitrile (4h)*. Yield: 64 %; m.p.: 153–154 °C; Anal. Calcd. for C$_{27}$H$_{23}$ClN$_4$O$_3$ (FW: 486.95): C, 66.60; H, 4.75; N, 11.51 %. Found: C, 66.45; H, 4.94; N, 11.73 %; IR (KBr, cm^{-1}): 3370 and 3330 (asym. and sym. stretching of –NH$_2$), 2215 (–C≡N stretching), 1685 (C=O str.), 1210 (C–O–C ether stretching); ^{1}H-NMR (400 MHz, DMSO-d_6, δ / ppm): 1.74–2.20 (6H, *m*, CH$_2$), 2.49 (3H, *s*, CH$_3$), 4.22 (1H, *s*, CH), 6.72––7.55 (10H, *m*, Ar–H + NH$_2$); ^{13}C-NMR (100 MHz, DMSO-d_6, δ / ppm): 13.20 (CH$_3$), 19.60 (CH$_2$), 20.63 (CH$_3$), 24.92 (CH), 26.70 (CH$_2$), 36.38 (CH$_2$), 56.25 (**C**–CN), 111.60, 111.99, 114.17, 119.12, 121.70, 123.02, 126.67, 128.72, 129.71, 138.01, 145.53, 148.27, 155.95, 158.04, 164.35 (Ar–C + CN), 196.26 (C=O); MS (*m/z*): 487.1 (M+1).

*2-Amino-7,7-dimethyl-4-[3-methyl-5-phenoxy-1-phenyl-1*H-*pyrazol-4-yl]-5--oxo-5,6,7,8-tetrahydro-4*H-*chromene-3-carbonitrile (4i)*. Yield: 90 %; m.p.: 249–250 °C; Anal. Calcd. for C$_{28}$H$_{26}$N$_4$O$_3$ (FW: 466.53): C, 72.09; H, 5.62; N, 12.01 %. Found: C, 71.84; H, 5.52; N, 12.17 %; IR (KBr, cm^{-1}): 3380 and 3180 (asym. and sym. stretching of –NH$_2$), 2200 (–C≡N stretching), 1680 (C=O str.), 1220 (C–O–C ether stretching); ^{1}H-NMR (400 MHz, DMSO-d_6, δ / ppm): 1.02, 1.04 (3H, *s*, 2xCH$_3$) 1.95, 2.13 (2×2H, *s*, CH$_2$), 2.50 (3H, *s*, CH$_3$), 4.36 (1H, *s*, CH), 6.76–7.55 (12H, *m*, Ar–H + NH$_2$); ^{13}C-NMR (100 MHz, DMSO-d_6, δ / ppm): 12.86 (CH$_3$), 24.60 (CH), 27.68, 28.77 (2×CH$_3$), 32.01 (C), 40.25, 50.43 (2×CH$_2$), 60.64 (**C**–CN), 110.20, 111.80, 114.79, 119.00, 121.81, 122.92,

126.51, 128.92, 129.76, 138.01, 145.50, 148.21, 156.45, 157.94, 161.64 (Ar–C + CN), 196.17 (C=O); MS (*m/z*): 467.2 (M+1).

2-Amino-7,7-dimethyl-4-[3-methyl-5-(4-methylphenoxy)-1-phenyl-1H-pyra-zol-4-yl]-5-oxo-5,6,7,8-tetrahydro-4H-chromene-3-carbonitrile (4j). Yield: 75 %; m.p.: 136–137 °C; Anal. Calcd. for $C_{29}H_{28}N_4O_3$ (FW: 480.56): C, 72.48; H, 5.87; N, 11.66 %. Found: C, 72.45; H, 5.98; N, 11.88 %; IR (KBr, cm^{-1}): 3415 and 3265 (asym. and sym. stretching of –NH$_2$), 2220 (–C≡N stretching), 1660 (C=O str.), 1205 (C–O–C ether stretching); ^{1}H-NMR (400 MHz, DMSO-d_6, δ / ppm): 0.95, 0.98 (2×3H, *s*, CH$_3$) 1.98, 2.08 (2×2H, *s*, CH$_2$), 2.28, 2.55 (2×3H, *s*, CH$_3$), 4.23 (1H, *s*, CH), 6.74–7.46 (11H, *m*, Ar–H + NH$_2$); ^{13}C-NMR (100 MHz, DMSO-d_6, δ / ppm): 13.25 (CH$_3$), 20.58 (CH$_3$), 25.08 (CH), 27.27, 28.89 (2×CH$_3$), 32.00 (C), 40.00 50.34 (2×CH$_2$), 58.69 (**C**–CN), 110.54, 111.48, 115.36, 115.70, 120.48, 121.51, 129.98, 135.85, 136.27, 145.54, 147.43, 150.23, 155.52, 159.00, 162.05 (Ar–C + CN), 196.22 (C=O); MS (*m/z*): 481.2 (M+1).

2-Amino-7,7-dimethyl-4-[5-(4-methoxyphenoxy)-3-methyl-1-phenyl-1H-py-razol-4-yl]-5-oxo-5,6,7,8-tetrahydro-4H-chromene-3-carbonitrile (4k). Yield: 87 %; m.p.: 179–180 °C; Anal. Calcd. for $C_{29}H_{28}N_4O_4$ (FW: 496.56): C, 70.15; H, 5.68; N, 11.28 %. Found: C, 70.24; H, 5.78; N, 11.01 %; IR (KBr, cm^{-1}): 3380 and 3210 (asym. and sym. stretching of –NH$_2$), 2195 (–C≡N stretching), 1645 (C=O str.), 1200 (C–O–C ether stretching). ^{1}H-NMR (400 MHz, DMSO-d_6, δ / ppm): 1.05, 1.07 (2×3H, *s*, CH$_3$) 1.90, 2.01 (2×2H, *s*, CH$_2$), 2.25 (3H, *s*, CH$_3$), 3.64 (3H, *s*, OCH$_3$), 4.17 (1H, *s*, CH), 6.70–7.48 (11H, *m*, Ar–H + NH$_2$); ^{13}C-NMR (100 MHz, DMSO-d_6, δ / ppm): 13.00 (CH$_3$) 25.24 (CH), 27.42, 28.80 (2×CH$_3$), 32.07 (C), 40.15 50.40 (2×CH$_2$), 55.89 (OCH$_3$), 57.31 (**C**–CN), 111.25, 112.02, 114.81, 119.06, 121.94, 123.11, 126.52, 128.62, 129.86, 138.19, 145.84, 148.28, 156.45, 157.90, 161.50 (Ar–C + CN), 196.35 (C=O); MS (*m/z*): 497.2 (M+1).

2-Amino-4-[5-(4-chlorophenoxy)-3-methyl-1-phenyl-1H-pyrazol-4-yl]-7,7-di-methyl-5-oxo-5,6,7,8-tetrahydro-4H-chromene-3-carbonitrile (4l). Yield: 65 %; m.p.: 203–205 °C; Anal. Calcd. for $C_{28}H_{25}ClN_4O_3$ (FW: 500.98): C, 67.13; H, 5.03; N, 11.18 %. Found: C, 67.02; H, 5.25; N, 11.37 %; IR (KBr, cm^{-1}): 3430 and 3190 (asym. and sym. stretching of –NH$_2$), 2210 (–C≡N stretching), 1690 (C=O str.), 1220 (C–O–C ether stretching). ^{1}H-NMR (400 MHz, DMSO-d_6, δ / ppm): 0.88, 0.93 (2×3H, *s*, CH$_3$) 1.81, 2.11 (2×2H, *s*, CH$_2$), 2.39 (3H, *s*, CH$_3$), 4.12 (1H, *s*, CH), 6.64–7.50 (11H, *m*, Ar–H + NH$_2$); ^{13}C-NMR (100 MHz, DMSO-d_6, δ / ppm): 12.80 (CH$_3$), 24.50 (CH), 27.25, 28.94 (2×CH$_3$), 31.90 (C), 39.92, 50.30 (2×CH$_2$), 60.64 (**C**–CN), 110.27, 111.18, 115.52, 115.71, 120.55, 121.87, 130.00, 135.86, 136.20, 145.54, 147.17, 150.33, 155.51, 159.17, 162.10 (Ar–C + CN), 196.13 (C=O); MS (*m/z*): 501.2 (M+1).

2-Amino-7,7-dimethyl-4-[3-methyl-1-(4-methylphenyl)-5-phenoxy-1H-pyra-zol-4-yl]-5-oxo-5,6,7,8-tetrahydro-4H-chromene-3-carbonitrile (4m). Yield: 88

%; m.p.: 240–241 °C; Anal. Calcd. for $C_{29}H_{28}N_4O_3$ (FW: 480.56): C, 72.48; H, 5.87; N, 11.66 %. Found: C, 72.63; H, 6.00; N, 11.80 %; IR (KBr, cm^{-1}): 3400 and 3340 (asym. and sym. stretching of –NH$_2$), 2200 (–C≡N stretching), 1705 (C=O str.), 1200 (C–O–C ether stretching); ^{1}H-NMR (400 MHz, DMSO-d_6, δ / ppm): 0.97, 1.01 (2×3H, *s*, CH$_3$), 1.92, 2.04 (2×2H, *s*, CH$_2$), 2.25, 2.50 (2×3H, *s*, CH$_3$), 4.30 (1H, *s*, CH), 6.76–7.45 (11H, *m*, Ar–H + NH$_2$); ^{13}C-NMR (100 MHz, DMSO-d_6, δ / ppm): 13.18 (CH$_3$), 20.75 (CH$_3$), 25.25 (CH), 27.48, 28.91 (2×CH$_3$), 32.10 (C), 40.20 50.45 (2×CH$_2$), 57.91 (**C**–CN), 110.94, 111.81, 114.78, 118.79, 121.75, 122.88, 126.44, 128.90, 129.70, 138.00, 145.51, 148.12, 156.51, 157.88, 162.25 (Ar–C + CN), 196.28 (C=O); MS (*m/z*): 481.2 (M+1).

2-Amino-7,7-dimethyl-4-[3-methyl-5-(4-methylphenoxy)-1-(4-methylphenyl)- -1H-pyrazol-4-yl]-5-oxo-5,6,7,8-tetrahydro-4H-chromene-3-carbonitrile **(4n)**. Yield: 90 %; m.p.: 223–224 °C; Anal. Calcd. for $C_{30}H_{30}N_4O_3$ (FW: 494.58): C, 72.85; H, 6.11; N, 11.33 %. Found: C, 72.70; H, 6.20; N 11.45 %; IR (KBr, cm^{-1}): 3420 and 3300 (asym. and sym. stretching of –NH$_2$), 2205 (–C≡N stretching), 1680 (C=O str.), 1225 (C–O–C ether stretching); ^{1}H-NMR (400 MHz, DMSO-d_6, δ / ppm): 1.01, 1.03 (2×3H, *s*, CH$_3$) 1.97, 2.09 (2×2H, *s*, CH$_2$), 2.25, 2.27, 2.32 (3×3H, *s*, CH$_3$), 4.18 (1H, *s*, CH), 6.71–7.43 (10H, *m*, Ar–H + NH$_2$); ^{13}C-NMR (100 MHz, DMSO-d_6, δ / ppm): 12.92 (CH$_3$), 20.60, 20.90 (CH$_3$), 25.03 (CH), 27.32, 28.75 (2×CH$_3$), 31.94 (C), 40.10 50.37 (2×CH$_2$), 57.91 (**C**–CN), 110.94, 111.24, 115.38, 115.64, 120.23, 121.94, 130.56, 135.84, 136.20, 145.55, 147.39, 150.21, 155.30, 159.18, 162.25 (Ar–C + CN), 196.28 (C=O); MS (*m/z*): 495.2 (M+1).

2-Amino-4-[5-(4-methoxyphenoxy)-3-methyl-1-(4-methylphenyl)-1H-pyrazol- -4-yl]-7,7-dimethyl-5-oxo-5,6,7,8-tetrahydro-4H-chromene-3-carbonitrile **(4o)**. Yield: 92 %; m.p.: 149–150 °C; Anal. Calcd. for $C_{30}H_{30}N_4O_4$ (FW: 510.58): C, 70.57; H, 5.92; N, 10.97 %. Found: C, 70.69; H, 6.04; N, 11.13 %; IR (KBr, cm^{-1}): 3385 and 3230 (asym. and sym. stretching of –NH$_2$), 2205 (–C≡N stretching), 1710 (C=O str.), 1195 (C–O–C ether stretching); ^{1}H-NMR (400 MHz, DMSO-d_6, δ / ppm): 0.90, 0.93 (2×3H, *s*, CH$_3$) 1.85, 2.07 (2×2H, *s*, CH$_2$), 2.23, 2.30 (2×3H, *s*, CH$_3$), 3.66 (3H, *s*, OCH$_3$), 4.16 (1H, *s*, CH), 6.59–7.40 (10H, *m*, Ar–H + NH$_2$); ^{13}C-NMR (100 MHz, DMSO-d_6, δ / ppm): 13.10 (CH$_3$), 20.86 (CH$_3$), 25.03 (CH), 27.29, 28.95 (2×CH$_3$), 31.98 (C), 39.90 50.31 (2×CH$_2$), 55.88 (OCH$_3$), 56.20 (**C**–CN), 111.18, 111.24, 115.36, 115.69, 120.43, 121.44, 130.04, 135.91, 136.21, 145.50, 147.40, 150.16, 155.26, 159.08, 162.24 (Ar–C + CN), 196.14 (C=O); MS (*m/z*): 511.2 (M+1).

2-Amino-4-[5-(4-chlorophenoxy)- 3-methyl-1-(4-methylphenyl)-1H-pyrazol- -4-yl]-7,7-dimethyl-5-oxo-5,6,7,8-tetrahydro-4H-chromene-3-carbonitrile **(4p)**. Yield: 73 %; m.p.: 168–169 °C; Anal. Calcd. for $C_{29}H_{27}ClN_4O_3$ (FW: 515.00): C, 67.63; H, 5.28; N, 10.88 %. Found: C, 67.76; H, 5.44; N, 10.92 %; IR (KBr, cm^{-1}): 3390 and 3300 (asym. and sym. stretching of –NH$_2$), 2200 (–C≡N stretch-

ing), 1685 (C=O str.), 1200 (C–O–C ether stretching); ^{1}H-NMR (400 MHz, DMSO-d$_6$, δ / ppm): 1.03, 1.06 (2×3H, *s*, CH$_3$) 1.83, 2.15 (2×2H, *s*, CH$_2$), 2.28, 2.45 (2×3H, *s*, CH$_3$), 4.14 (1H, *s*, CH), 6.67–7.53 (10H, *m*, Ar–H + NH$_2$); ^{13}C--NMR (100 MHz, DMSO-d$_6$, δ / ppm): 13.07 (CH$_3$), 20.80 (CH$_3$), 25.11 (CH), 27.50, 28.93 (2×CH$_3$), 32.05 (C), 40.25 50.41 (2×CH$_2$), 59.11 (**C**–CN), 111.15, 111.39, 115.40, 115.70, 120.73, 121.60, 130.11, 135.85, 136.17, 145.44, 147.35, 150.00, 155.15, 159.08, 161.50 (Ar–C + CN), 196.20 (C=O); MS (*m/z*): 515.2 (M+1).

Efficient one-pot, four-component synthesis of *N,N*-dibenzyl--1-(5-aryl-1,3,4-oxadiazol-2-yl)cyclobutylamine derivatives from the reaction of (isocyanoimino)triphenylphosphorane, dibenzylamine, an aromatic carboxylic acid and cyclobutanone

NAHID SHAJARI*, ALI REZA KAZEMIZADEH and ALI RAMAZANI

Research Laboratory of MCRs, *Department of Chemistry, Zanjan Branch, Islamic Azad University, P. O. Box 49195-467, Zanjan, Iran*

Abstract: The four-component reaction of cyclobutanone, dibenzylamine and (isocyanoimino)triphenylphosphorane in the presence of aromatic carboxylic acids proceeds smoothly at room temperature under neutral conditions to afford *N,N*-dibenzyl-1-(5-aryl-1,3,4-oxadiazol-2-yl)cyclobutylamine derivatives in high yields.

Keywords: multicomponent reaction; isocyanide; 1,3,4-oxadiazole; heterocycles.

INTRODUCTION

There is increasing interest in the chemistry of heterocyclic compounds because of their vast distribution in natural compounds, their applications in pharmaceuticals, agrochemicals, and industrial chemicals, *etc*. 1,3,4-Oxadiazole derivatives are an important class of heterocycles, which possess pharmaceutical and biological activities, such as antimicrobial,[1-3] antimycobacterial,[4] anti-inflammatory,[5] anti-allergic,[6] antifungal and genotoxic activities.[7] Nowadays, many organic compounds can be synthesized in multicomponent reactions (MCRs).[8] An important class of MCRs are the isocyanide-based multicomponent reactions (IMCRs). IMCRs are especially interesting because they are more diverse and versatile than non-IMCRs.[9–18] Several methods have been reported in the literature for the synthesis of 1,3,4-oxadiazoles. These protocols are multi-step in nature.[19–21] In recent years, a one-pot method for the synthesis of 1,3,4--oxadiazole derivatives from (isocyanoimino)triphenylphosphorane has been established.[22–26] In connection with interest in the synthesis of heterocycles,[27–30] the synthesis of *N,N*-dibenzyl-1-(5-aryl-1,3,4-oxadiazol-2-yl)cyclobutylamine derivatives *via* a four-component reaction of cyclobutanone, dibenzylamine, and

* Corresponding author. E-mail: n_shajari120@yahoo.com

(isocyanoimino)triphenylphosphorane in the presence of aromatic carboxylic acids, in high yields and fairly mild reaction conditions, is reported herein (Scheme 1).
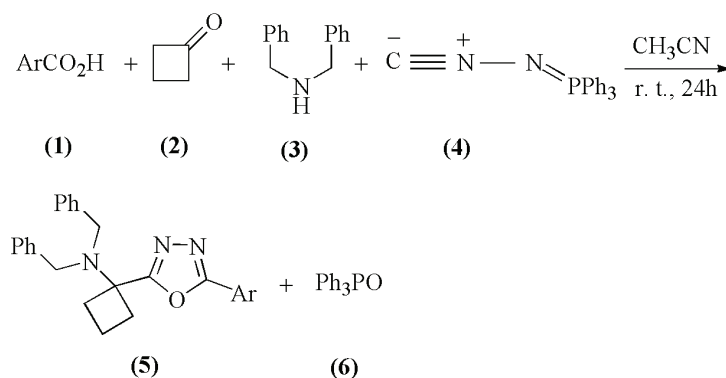
Scheme 1. Four-component reaction of carboxylic acids, cyclobutanone, dibenzylamine and (isocyanoimino)triphenylphosphorane.

RESULTS AND DISCUSSION

The four-component reactions of cyclobutanone (**2**), dibenzylamine (**3**) and (isocyanoimino)triphenylphosphorane (**4**) in the presence of aromatic carboxylic acids (**1**) led to *N,N*-dibenzyl-1-(5-aryl-1,3,4-oxadiazol-2-yl)cyclobutylamine derivatives (**5**) in high yields, under fairly mild reaction conditions (Scheme 1 and Table I). A mechanistic rationalization for this reaction is provided in Scheme 2. The imine intermediate generated by the reaction of cyclobutanone (**2**) and dibenzylamine (**3**) is protonated with aromatic carboxylic acid (**1**) to produce iminium intermediate (**7**). Nucleophilic addition of the (isocyanoimino)triphenylphosphorane (**4**) to the iminium ion (**7**) leads to a nitrilium intermediate (**9**). The intermediate **9** may be attacked by the carboxylate anion (**8**) to form adduct **10**. The adduct **10** may undergo an intramolecular aza-Wittig reaction of an iminophosphorane moiety with the ester carbonyl group to afford the 1,3,4-oxadiazole derivatives (**5**) by the removal of triphenylphosphine oxide (**6**) from intermediate (**11**).

The structures of the products were deduced from their ^{1}H-NMR, ^{13}C-NMR, mass, IR spectra, and elemental analysis. For example the ^{1}H-NMR spectrum of **5a** exhibited distinct signals at δ_H 1.71–1.92, 2.17–2.38 and 2.40–2.61 ppm (6H, 3*m*) arising from the 3CH$_2$ groups of cyclobutane, δ_H 3.65 ppm (4H, *s*) from the 2CH$_2$ groups of benzyl and at δ_H 7.12–8.18 ppm (15H, *m*) of the aromatic CH groups. The ^{13}C-NMR spectrum of **5a** showed 14 distinct resonances arising from the 3CH$_2$ of cyclobutane (δ_c 14.47 and 33.05 ppm), the 2CH$_2$ of benzyl (δ_c 53.85 ppm), C$_{ipso}$ of cyclobutane (δ_c 62.66 ppm), aromatic carbons (δ_c 124.09, 126.88, 126.95, 128.01, 129.00, 129.12, 131.74 and 139.65 ppm), 2C=N (δ_c

165.47 and 168.55 ppm). The mass spectrum of **5a** displayed a molecular ion peak at $m/z = 395$. The analytic and spectral data for all the synthesized compounds are given in the Supplementary material to this paper.

TABLE I. Synthesis of *N,N*-dibenzyl-1-(5-aryl-1,3,4-oxadiazol-2-yl)cyclobutylamine derivatives

Entry	Ar	Product
1	C_6H_5	**5a**
2	2-Thienyl	**5b**
3	$4\text{-}ClC_6H_4$	**5c**
4	$3\text{-}ClC_6H_4$	**5d**
5	$4\text{-}BrC_6H_4$	**5e**
6	$4\text{-}FC_6H_4$	**5f**
7	$4\text{-}MeC_6H_4$	**5g**
8	$3\text{-}MeC_6H_4$	**5h**
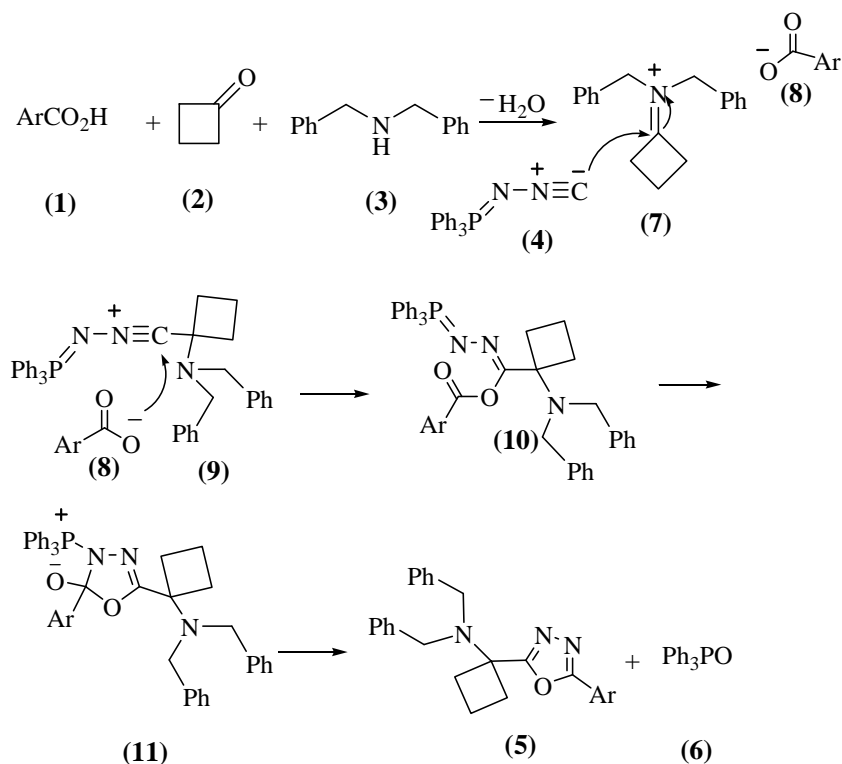
Scheme 2. The proposed mechanism for the formation of **5**.

EXPERIMENTAL

The starting materials and solvents were obtained from Merck (Germany) and Fluka (Switzerland) and were used without further purification. The melting points were measured

on an electrothermal 9100 apparatus and are uncorrected. The IR spectra were recorded on a Jasco FT-IR 6300 spectrometer. The ^{1}H- and ^{13}C-NMR spectra were measured (CDCl$_3$ solution) with a Bruker DRX-250 Avance spectrometer at 250.0 and 62.5 MHz, respectively. The mass spectra were recorded on a HP (Agilent Technologies) 5937 mass selective detector at an ionization potential of 70 eV. The elemental analyses were realized using a Heraeus CHN--O-rapid analyzer.

General procedure

To a magnetically stirred solution of cyclobutanone (**2**, 1 mmol), dibenzylamine (**3**, 1 mmol) and an aromatic carboxylic acid (**1**, 1 mmol) in CH$_3$CN (5 mL) was added dropwise a solution of (isocyanoimino)triphenylphosphorane (**4**, 1 mmol) in CH$_3$CN (5 mL) at room temperature over 15 min. The mixture was stirred for 24 h. The solvent was removed under reduced pressure and the viscous residue was purified by preparative layer chromatography (silica gel; petroleum ether–ethyl acetate (10:3)). The solvent was removed under reduced pressure and the products **5a**–**h** were obtained.

CONCLUSIONS

The reported method offers a mild, simple, and efficient route for the preparation of *N,N*-dibenzyl-1-(5-aryl-1,3,4-oxadiazol-2-yl)cyclobutylamine derivatives *via* a four-component reaction of cyclobutanone, dibenzylamine and (isocyanoimino)triphenylphosphorane in the presence of an aromatic carboxylic acid in high yields and under fairly mild reaction conditions.

SUPPLEMENTARY MATERIAL

Analytical and spectral data of the synthesized compounds are available electronically from http://www.shd.org.rs/JSCS/, or from the corresponding author on request.

ИЗВОД

ЕФИКАСНА СИНТЕЗА ДЕРИВАТА *N,N*-ДИБЕНЗИЛ-1-(5-АРИЛ-1,3,4-ОКСА-ДИАЗОЛ-2-ИЛ)ЦИКЛОБУТИЛАМИНА У ЈЕДНОМ РЕАКЦИОНОМ КОРАКУ ЧЕТВОРОКОМПОНЕНТНЕ РЕАКЦИОНЕ СМЕШЕ – (ИЗОЦИЈАНО-ИМИНО)ТРИФЕНИЛФОСФОРАН, ДИБЕНЗИЛАМИН, АРОМАТИЧНА КАРБОКСИЛНА КИСЕЛИНА И ЦИКЛОБУТАНОН

NAHID SHAJARI, ALI REZA KAZEMIZADEH и ALI RAMAZANI

Research Laboratory of MCRs*, Department of Chemistry, Zanjan Branch, Islamic Azad University, P O Box 49195-467, Zanjan, Iran*

Реакциона смеша која садржи (изоцијаноимино)трифенилфосфоран, дибензиламин и циклобутанон, у присуству ароматичних карбоксилних киселина, при собној температури, као производ даје деривате *N,N*-дибензил-1-(5-арил-1,3,4-оксадиазол-2-ил)цикло-бутиламина у високом приносу.

REFERENCES

1. S. Rollas, N. Gulerman, H. Erdeniz, *Farmaco* **57** (2002) 171
2. G. Şahin, E. Palaska, M. Ekizoğlu, M. Özalp, *Farmaco* **57** (2002) 539
3. B. S. Holla, R. Gonsalves, S. Shenoy, *Eur. J. Med. Chem*. **35** (2000) 267
4. M. G. Mamolo, D. Zampieri, L. Vio, M. Fermeglia, M. Ferrone, S. Pricl, G. Scialino, E. Banfi, *Bioorg. Med. Chem*. **13** (2005) 3797
5. E. Palaska, G. Şahin, P. Kelicen, N. T. Durlu, G. Altinok, *Farmaco* **57** (2002) 101
6. J. H. Musser, R. E. Brown, B. Loev, K. Bailey, H. Jones, R. Kahen, F. Huang, A. Khandwala, M. Leibowitz, *J. Med. Chem.* **27** (1984) 121
7. A. O. Maslat, M. Abussaud, H. Tashtoush, M. AL-Talib, *Pol. J. Pharmacol*. **54** (2002) 55
8. J. Zhu, *Multicomponent Reactions*, Wiley-VCH, Weinheim, Germany, 2005
9. a) J. Zhu, *Eur. J. Org. Chem*. (2003) 1133; b) A. Dömling, *Chem. Rev*. **106** (2006) 17
10. a) C. Hulme, V. Gore, *Curr. Med. Chem.* **10** (2003) 51; b) M. A. Mironov, *QSAR Comb. Sci*. **25** (2006) 423; c) L. Banfi, R. Riva, A. Basso, *Synlett* (2010) 23
11. a) A. Shaabani, A. Maleki, A. H. Rezayan, A. Sarvary, *Mol. Divers*. **15** (2011) 41; b) M. T. Maghsoodlou, G. Marandi, N. Hazeri, S. M. Habibi Khorassani, A. A. Mirzaei, *Mol. Divers*. **15** (2011) 227
12. a) A. Ramazani, A. Rezaei, A. Tofangchi Mahyari, M. Rouhani, M. Khoobi, *Helv. Chim. Acta* **93** (2010) 2033; b) A. Ramazani, A. Tofangchi Mahyari, M. Rouhani, A. Rezaei, *Tetrahedron Lett*. **50** (2009) 5625
13. a) I. Yavari, G. Khalili, A. Mirzaei, *Tetrahedron Lett*. **51** (2010) 1190; b) A. A. Esmaeili, R. Hosseinabadi, A. Habibi, *Synlett* (2010) 1477; c) M. Adib, E. Sheikhi, N. Rezaei, *Tetrahedron Lett*. **52** (2011) 3191
14. a) E. Ahmadi, A. Ramazani, M. Nekomanesh Haghighi, *Tetrahedron Lett*. **48** (2007) 5954; b) J. Azizian, A. Ramazani, M. Haji, *Helv. Chim. Acta* **94** (2011) 371
15. a) S. Sadjadi, M. M. Heravi, *Tetrahedron* **67** (2011) 2707; b) M. M. Heravi, S. Moghimi, *J. Iran. Chem. Soc*. **8** (2011) 306
16. a) A. Ramazani, A. Mahyari, *Helv. Chim. Acta* **93** (2010) 2203; b) E. Ahmadi, A. Tofangchi Mahyari, A. Ramazani, M. Nekomanesh Haghighi, *Lett. Org. Chem*. **5** (2008) 540
17. a) A. R. Kazemizadeh, A. Ramazani, *Asian J. Chem.* **23** (2011) 4613; b) S. M. Shoaei, A. R. Kazemizadeh, A. Ramazani, *Chin. J. Struct. Chem*. **30** (2011) 568
18. a) A. R. Kazemizadeh, A. Ramazani, *Arkivoc* **xv** (2008) 159; b) A. R. Kazemizadeh, A. Ramazani, *J. Braz. Chem. Soc*. **20** (2009) 309
19. a) I. R. Baxendale, S. V. Ley, M. Martinelli, *Tetrahedron* **61** (2005) 5323; b) C. T. Brain, S. A. Brunton, *Synlett* (2001) 382
20. a) B. J. Brown, I. R. Clemens, J. K. Neesom, *Synlett* (2000) 131; b) C. T. Brain, J. M. Paul, Y. Loong, P. J. Oakley, *Tetrahedron Lett*. **40** (1999) 3275
21. F. T. Coppo, K. A. Evans, T. L. Graybill, G. Burton, *Tetrahedron Lett*. **45** (2004) 3257
22. a) A. Ramazani, Y. Ahmadi, R. Tarasi, *Heteroat. Chem*. **22** (2011) 79; b) A. Ramazani, Y. Ahmadi, M. Rouhani, N. Shajari, A. Souldozi, *Heteroat. Chem*. **21** (2010) 368
23. a) A. Ramazani, A. Rezaei, *Org. Lett*. **12** (2010) 2852; b) A. Souldozi, A. Ramazani, *Tetrahedron Lett*. **48** (2007) 1549
24. a) A. Ramazani, N. Shajari, A. Mahyari, Y. Ahmadi, *Mol. Divers.* **15** (2011) 521; b) A. Ramazani, F. Zeinali Nasrabadi, A. Mashhadi, Y. Ahmadi, *Monatsh. Chem.* **142** (2011) 625

25. a) A. Ramazani, M. Rouhani, A. Rezaei, N. Shajari, A. Souldozi, *Helv. Chim. Acta* **94** (2011) 282; b) B. Ahankar, A. Ramazani, A. Amini, Y. Ahmadi, A. Souldozi, *Heteroat. Chem.* **22** (2011) 612; c) A. Ramazani, N. Shajari, A. Tofangchi Mahyari, M. Khoobi, Y. Ahmadi, A. Souldozi, *Phosphorus, Sulfur Silicon Relat. Elem.* **185** (2010) 2496

26. a) F. Zeinali Nasrabadi, A. Ramazani, Y. Ahmadi, *Mol. Divers.* **15** (2011) 791; b) A. Ramazani, F. Zeinali Nasrabadi, Z. Karimi, M. Rouhani, *Bull. Korean Chem. Soc.* **32** (2011) 2700

27. a) A. Souldozi, A. Ramazani, *Tetrahedron Lett.* **48** (2007) 2617; b) A. Ramazani, A. Morsali, B. Ganjeie, A. R. Kazemizadeh, E. Ahmadi, R. Kempe, I. Hertle, *Z. Naturforsch.* **60b** (2005) 569; c) A. Ramazani, F. Marandi, A. R. Kazemizadeh, *Phosphorus, Sulfur Silicon Relat. Elem.* **180** (2005) 1541

28. a) A. Ramazani, E. Ahmadi, A. R. Kazemizadeh, L. Dolatyari, N. Noshiranzadeh, I. Eskandari, A. Souldozi, *Phosphorus, Sulfur Silicon Relat. Elem.* **180** (2005) 2419; b) B. Ganjeie, A. Ramazani, A. R. Kazemizadeh, *Phosphorus, Sulfur Silicon Relat. Elem.* **182** (2007) 1703; c) A. Ramazani, A. Morsali, B. Ganjeie, A. R. Kazemizadeh, E. Ahmadi, *Phosphorus, Sulfur Silicon Relat. Elem.* **180** (2005) 2439

29. a) M. Rahnema, M. R. Bigdeli, A. R. Kazemizadeh, A. Ramazani, *Phosphorus, Sulfur Silicon Relat. Elem.* **182** (2007) 1683; b) A. Ramazani, A. Souldozi, F. Marandi, A. R. Kazemizadeh, *Asian J. Chem.* **17** (2005) 293; c) A. Ramazani, A. R. Kazemizadeh, B. Ganjeie, E. Ahmadi, *Phosphorus, Sulfur Silicon Relat. Elem.* **180** (2005) 2569

30. a) A. Ramazani, E. Ahmadi, B. Ganjeie, A. R. Kazemizadeh, A. Morsali, *Asian J. Chem.* **17** (2005) 2371; b) A. Ramazani, A. R. Kazemizadeh, B. Ganjeie, E. Ahmadi, *Asian J. Chem.* **17** (2005) 2375; c) M. Rimaz, J. Khalafy, K. Tavana, K. Slepokura, T. Lis, A. Souldozi, A. Tofangchi Mahyari, N. Shajari, A. Ramazani, *Z. Naturforsch.* **64b** (2009) 1065 d) N. Shajari, A. Ramazani, *Phosphorus, Sulfur Silicon Relat. Elem.* **185** (2010) 1850.

Efficient one-pot, four-component synthesis of *N,N*-dibenzyl--1-(5-aryl-1,3,4-oxadiazol-2-yl)cyclobutylamine derivatives from the reaction of (isocyanoimino)triphenylphosphorane, dibenzylamine, an aromatic carboxylic acid and cyclobutanone

NAHID SHAJARI*, ALI REZA KAZEMIZADEH and ALI RAMAZANI

Research Laboratory of MCRs*, Department of Chemistry, Zanjan Branch, Islamic Azad University, P. O. Box 49195-467, Zanjan, Iran*

ANALYTICAL AND SPECTRAL DATA OF THE SYNTHESIZED COMPOUNDS

N,N-*Dibenzyl-1-(5-phenyl-1,3,4-oxadiazol-2-yl)cyclobutylamine* *(5a)*. Yellow crystal, Yield: 81 %; m.p. 99.8–102.6 °C; Anal. Calcd. for $C_{26}H_{25}N_3O$: C, 78.96; H, 6.37; N, 10.62 %. Found: C, 79.04; H, 6.42; N, 10.58 %; IR (KBr, cm^{-1}): 1554, 1447, 1363, 1257, 1076, 750, 698; ^{1}H-NMR (250 MHz, CDCl$_3$, δ / ppm): 1.71–1.92 (2H, *m*, cyclobutane), 2.17–2.38 (2H, *m*, cyclobutane), 2.40–2.61 (2H, *m*, cyclobutane), 3.65 (4H, *s*, 2CH$_2$ of benzyl), 7.12–8.18 (15H, *m*, aromatic CH); ^{13}C-NMR (62.5 MHz, CDCl$_3$, δ / ppm): 14.47 and 33.05 (3CH$_2$, cyclobutane), 53.85 (2CH$_2$ of benzyl), 62.66 (C$_{ipso}$, cyclobutane), 124.09, 126.88, 126.95, 128.01, 129.00, 129.12, 131.74 and 139.65 (aromatic carbons), 165.47 and 168.55 (2C=N); MS, *m*/*z* (%): 395 (M$^+$, 7), 304 (69), 276 (29), 250 (17), 196 (9), 173 (12), 130 (9), 91 (100), 65 (13), 41 (2).

N,N-*Dibenzyl-1-[5-(2-thienyl)-1,3,4-oxadiazol-2-yl]cyclobutylamine* *(5b)*. Yellow crystal, yield: 85 %; m.p. 57.6–59.8 °C; Anal. Calcd. for $C_{24}H_{23}N_3OS$: C, 71.79; H, 5.77; N, 10.47 %. Found: C, 71.72; H, 5.79; N, 10.53 %; IR (KBr, cm^{-1}): 1553, 1450, 1363, 1254, 1075, 749, 696; ^{1}H-NMR (250 MHz, CDCl$_3$, δ / ppm): 1.70–2.04 (2H, *m*, cyclobutane), 2.15–2.40 (2H, *m*, cyclobutane), 2.42––2.62 (2H, *m*, cyclobutane), 3.65 (4H, *s*, 2CH$_2$ of benzyl), 7.05–7.87 (13H, *m*, aromatic CH); ^{13}C-NMR (62.5 MHz, CDCl$_3$, δ / ppm): 14.44 and 33.02 (3CH$_2$, cyclobutane), 53.88 (2CH$_2$ of benzyl), 62.67 (C$_{ipso}$, cyclobutane), 125.51 (C$_{ipso}$, thiophene), 126.86, 127.98, 128.16, 128.97, 129.68, 130.05 and 139.62 (aromatic carbons), 161.24 and 167.97 (2C=N); MS, *m*/*z* (%): 401 (M$^+$, 2), 310 (51), 282

* Corresponding author. E-mail: alirezakazemizadeh@yahoo.com; aliramazani@yahoo.com

(29), 264 (6), 196 (10), 173 (18), 149 (7), 132 (12), 106 (38), 91(100), 65 (21), 41 (6).

N,N-*Dibenzyl-1-[5-(4-chlorophenyl)-1,3,4-oxadiazol-2-yl]cyclobutylamine (5c)*. Yellow crystal, yield: 80 %; m.p. 89.0–91.5 °C; Anal. Calcd. for $C_{26}H_{24}ClN_3O$: C, 72.63; H, 5.63; N, 9.77 %. Found: C, 72.70; H, 5.58; N, 9.70 %; IR (KBr, cm^{-1}): 1541, 1452, 1363, 1257, 1076, 748, 696; ^{1}H-NMR (250 MHz, CDCl$_3$, δ / ppm): 1.75–1.92 (2H, *m*, cyclobutane), 2.23–2.40 (2H, *m*, cyclobutane), 2.42–2.58 (2H, *m*, cyclobutane), 3.67 (4H, *s*, 2CH$_2$ of benzyl), 6.98––7.38 (10H, *m*, aromatic CH), 7.54 (2H, *d*, $^3J_{HH}$ = 8.0 Hz, aromatic CH), 8.02 (2H, *d*, $^3J_{HH}$ = 8.0 Hz, aromatic CH); ^{13}C-NMR (62.5 MHz, CDCl$_3$, δ / ppm): 14.39 and 32.98 (3CH$_2$, cyclobutane), 53.76 (2CH$_2$ of benzyl), 62.67 (C$_{ipso}$, cyclobutane), 122.62, 126.89, 128.00, 128.20, 128.94, 129.46, 137.91 and 139.51 (aromatic carbons), 164.20 and 168.88 (2C=N); MS, *m/z* (%): 429 (M$^+$, 2), 338 (59), 310 (39), 290 (7), 263(5), 196 (13), 173(22), 149 (10), 130 (12), 91 (100), 65 (17), 41 (4).

N,N-*Dibenzyl-1-[5-(3-chlorophenyl)-1,3,4-oxadiazol-2-yl]cyclobutylamine (5d)*. Yellow crystal, yield: 83 %; m.p. 131.1–133.2 °C; Anal. Calcd. for $C_{26}H_{24}ClN_3O$: C, 72.63; H, 5.63; N, 9.77 %. Found: C, 72.57; H, 5.67; N, 9.70 %; IR (KBr, cm^{-1}): 1551, 1438, 1364, 1259, 1080, 749, 696; ^{1}H-NMR (250 MHz, CDCl$_3$, δ / ppm): 1.72–1.96 (2H, *m*, cyclobutane), 2.22–2.43 (2H, *m*, cyclobutane), 2.45–2.61 (2H, *m*, cyclobutane), 3.68 (4H, *s*, 2CH$_2$ of benzyl), 7.03––8.09 (14H, *m*, aromatic CH); ^{13}C-NMR (62.5 MHz, CDCl$_3$, δ / ppm): 14.39 and 32.99 (3CH$_2$, cyclobutane), 53.76 (2CH$_2$ of benzyl), 62.68 (C$_{ipso}$, cyclobutane), 125.04, 125.75, 126.90, 128.00, 128.90, 128.94, 130.44, 131.68, 135.19 and 139.48 (aromatic carbons), 163.72 and 169.07 (2C=N).

N,N-*Dibenzyl-1-[5-(4-bromophenyl)-1,3,4-oxadiazol-2-yl]cyclobutylamine (5e)*. Yellow crystal, yield: 82 %; m.p. 121.3–123.1 °C; Anal. Calcd. for $C_{26}H_{24}BrN_3O$: C, 65.83; H, 5.10; N, 8.86 %. Found: C, 65.89; H, 5.13; N, 8.83 %; IR (KBr, cm^{-1}): 1563, 1452, 1361, 1257, 1080, 758, 703; ^{1}H-NMR (250 MHz, CDCl$_3$, δ / ppm): 1.81–1.98 (2H, *m*, cyclobutane), 2.28–2.48 (2H, *m*, cyclobutane), 2.52–2.68 (2H, *m*, cyclobutane), 3.73 (4H, *s*, 2CH$_2$ of benzyl), 7.12––7.98 (10H, *m*, aromatic CH), 8.01 (2H, *d*, $^3J_{HH}$ = 8.5 Hz, aromatic CH), 8.19 (2H, *d*, $^3J_{HH}$ = 8.5 Hz, aromatic CH); ^{13}C-NMR (62.5 MHz, CDCl$_3$, δ / ppm): 14.47 and 33.07 (3CH$_2$, cyclobutane), 53.96 (2CH$_2$ of benzyl), 62.78 (C$_{ipso}$, cyclobutane), 123.31, 126.87, 127.13, 128.00, 129.00, 129.08, 132.88 and 139.69 (aromatic carbons), 165.22 and 168.72 (2C=N).

N,N-*Dibenzyl-1-[5-(4-fluorophenyl)-1,3,4-oxadiazol-2-yl]cyclobutylamine (5f)*. Yellow crystal, yield: 80%; m.p. 91.3–93.5 °C; Anal. Calcd. for $C_{26}H_{24}FN_3O$: C, 75.52; H, 5.85; N, 10.16. Found: C, 75.50; H, 5.89; N, 10.12; IR (KBr, cm^{-1}): 1560, 1497, 1364, 1235, 1067, 745, 697; ^{1}H-NMR (250 MHz, CDCl$_3$, δ / ppm): 1.76–1.95 (2H, *m*, cyclobutane), 2.26–2.44 (2H, *m*, cyclobu-

tane), 2.46–2.61 (2H, *m*, cyclobutane), 3.68 (4H, *s*, 2CH$_2$ of benzyl), 7.02–7.45 and 8.05–8.16 (14H, 2*m*, aromatic CH); ^{13}C-NMR (62.5 MHz, CDCl$_3$, δ / ppm): 14.39 and 32.99 (3CH$_2$, cyclobutane), 53.82 (2CH$_2$ of benzyl), 62.68 (C$_{ipso}$, cyclobutane), 116.41 (2CH of aromatic carbons, *d*, $^2J_{CF}$ = 22.5 Hz), 120.52 (C, *d*, aromatic , $^4J_{CF}$ =3.6 Hz), 126.88, 127.99, 128.94 and 139.56 (aromatic carbons), 129.19 (2CH of aromatic carbons, *d*, $^3J_{CF}$ = 8.1 Hz), 164.58 (C, *d*, aromatic, $^1J_{CF}$ = 231.1 Hz), 164.20 and 168.70 (2C=N).

N,N-*Dibenzyl-1-[5-(4-methylphenyl)-1,3,4-oxadiazol-2-yl]cyclobutylamine (5g)*. Yellow crystal, yield: 82 %; m.p. 55.5–57.9 °C; Anal. Calcd. for C$_{27}$H$_{27}$N$_3$O: C, 79.19; H, 6.65; N, 10.26 %. Found: C, 79.24; H, 6.62; N, 10.29 %; IR (KBr, cm^{-1}): 1560, 1454, 1364, 1258, 1078, 747, 696; ^{1}H-NMR (250 MHz, CDCl$_3$, δ / ppm): 1.75–1.91 (2H, *m*, cyclobutane), 2.22–2.62 (4H, 2*m*, cyclobutane), 2.47 (3H, *s*, CH$_3$), 3.67 (4H, *s*, 2CH$_2$ of benzyl), 7.12–7.45 (10H, *m*, aromatic CH), 7.33 (2H, *d*, $^3J_{HH}$ = 8.0 Hz, aromatic CH), 7.99 (2H, *d*, $^3J_{HH}$ = 8.0 Hz, aromatic CH); ^{13}C-NMR (62.5 MHz, CDCl$_3$, δ / ppm): 14.44 and 33.03 (3CH$_2$, cyclobutane), 21.66 (CH$_3$), 53.95 (2CH$_2$ of benzyl), 62.71 (C$_{ipso}$, cyclobutane), 121.42, 126.83, 126.90, 127.97, 128.98, 129.78, 139.73 and 142.17 (aromatic carbons), 165.16 and 168.28 (2C=N).

N,N-*Dibenzyl-1-[5-(3-methylphenyl)-1,3,4-oxadiazol-2-yl]cyclobutylamine (5h)*. Yellow crystal, yield: 81 %; m.p. 100.1–102.3 °C; Anal. Calcd. for C$_{27}$H$_{27}$N$_3$O: C, 79.19; H, 6.65; N, 10.26 %. Found: C, 79.25; H, 6.67; N, 10.22 %; IR (KBr, cm^{-1}): 1556, 1454, 1363, 1255, 1071, 750, 695; ^{1}H-NMR (250 MHz, CDCl$_3$, δ / ppm): 1.72–1.92 (2H, *m*, cyclobutane), 2.23–2.61 (4H, 2*m*, cyclobutane), 2.49 (3H, *s*, CH$_3$), 3.67 (4H, *s*, 2CH$_2$ of benzyl), 7.12–7.50 and 7.85––7.96 (14H, 2*m*, aromatic CH); ^{13}C-NMR (62.5 MHz, CDCl$_3$, δ / ppm): 14.45 and 33.03 (3CH$_2$, cyclobutane), 21.40 (CH$_3$), 53.97 (2CH$_2$ of benzyl), 62.72 (C$_{ipso}$, cyclobutane), 124.03, 124.09, 126.85, 127.46, 127.97, 128.40, 128.98, 132.48, 138.97 and 139.70 (aromatic carbons), 165.17 and 168.47 (2C=N).

Trichloroisocyanuric acid as an efficient homogeneous catalyst for the chemoselective synthesis of 2-substituted oxazolines, imidazolines and thiazolines under solvent-free condition

SEYEDEH FATEMEH HOJATI* and SEYEDE ATEFE NEZHADHOSEINY

Department of Chemistry, Sabzevar Tarbiat Moallem University, Sabzevar 9617976487, Iran

Abstract: Trichloroisocyanuric acid, as a commercially available and inexpensive catalyst, was used in a new, facile and efficient procedure for the synthesis of 2-oxazolines, 2-imidazolines and 2-thiazolines through the reaction of nitriles with 2-aminoethanol, ethylenediamine or 2-aminoethanethiol under solvent-free conditions.

Keywords: trichloroisocyanuric acid; oxazoline; imidazoline; thiazoline; solvent-free condition.

INTRODUCTION

Developing new and efficient methods for the synthesis of heterocyclic biologically active natural compounds has received considerable attention in organic chemistry. This importance is due to their great applications in medicine. Oxazolines, imidazolines and thiazolines are important substructures in a large number of biologically active natural products.[1,2] Many derivatives of these heterocycles have shown antihypertensive,[3,4] antidepressive,[5] antihypercholesterolemic,[6] antidiabetic,[7] antitumor[8] and anti-inflammatory[9] properties. In addition to these serious affairs, they are also known as valuable intermediates in organic transformations.[10,11] Furthermore, optically active mono- and bis-derivatives of these heterocycles have been widely used as both auxiliaries and ligands in asymmetric syntheses.[12–14]

Numerous methods have been reported for the synthesis of 2-oxazolines, 2-imidazolines and 2-thiazolines from various precursors.[15–25] Although some of these procedures have been successfully used for the synthesis of these heterocycles, most of them suffer from disadvantages such as: strong acidic conditions, long reaction times, low yields of products, use of complex and expensive re-

---

* Corresponding author. E-mail: sfhojati@sttu.ac.ir

1181

agents and toxic solvents. Therefore, the introduction of a new efficient method for the synthesis of these useful moieties is still in demand.

Trichloroisocyanuric acid (1,3,5-trichloro-1,3,5-triazine-2,4,6(1*H*,3*H*,5*H*)-tri-one or TCCA) is an *N*-halo compound which has been known since 1902 (Fig. 1). It has been used primarily as a disinfectant in swimming pools and water treatment.[26] Recently, TCCA has become attractive candidate as a homogeneous catalyst in organic transformations[27–35] due to its lack of volatility, commercial availability, low cost and ease of handling.
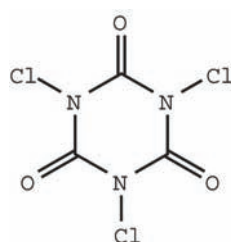
Fig. 1. Structure of trichloroisocyanuric acid.

Consequently, in continuation of our interest in the synthesis of 2-oxazoline, 2-imidazoline and 2-thiazoline derivatives,[36–38] the catalytic activity of TCCA in this field was investigated (Scheme 1).
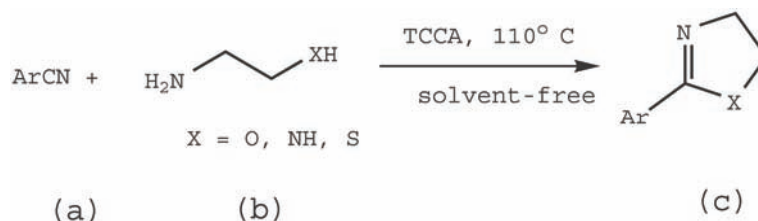
Scheme 1. Synthesis of 2-oxazoline, 2-imidazoline and 2-thiazoline derivatives using TCCA as catalyst.

EXPERIMENTAL

General procedure for the conversion of nitriles to 2-oxazolines, 2-imidazolines and 2-thiazolines

A mixture of a nitrile (1 mmol), 2-aminoethanol (6 mmol), ethylenediamine (4 mmol) or 2-aminoethanethiol (1.2 mmol) and TCCA (0.03 mmol for oxazoline, 0.1 mmol for imida-zoline and 0.01 mmol for thiazoline synthesis) was stirred at 110 °C for an appropriate time, according to Table I. The reaction was performed under solvent-free conditions. After com-pletion of the reaction, monitored by TLC (eluent: *n*-hexane:EtOAc, 2:1 for oxazolines and thiazolines, EtOAc:methanol, 10:1 for imidazolines), the reaction mixture was cooled to room temperature and the crude product (**1c**–**24c**) was purified by column chromatography to afford the pure products in high yields (Table I).

TABLE I. Synthesis of 2-oxazolines, 2-imidazolines and 2-thiazolines from nitriles catalyzed by TCCA
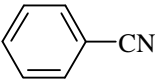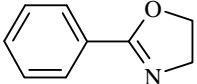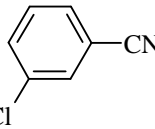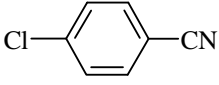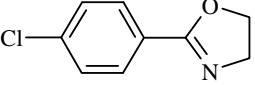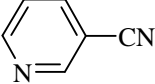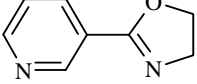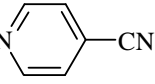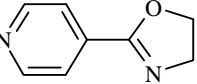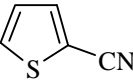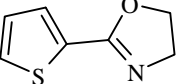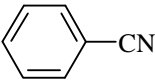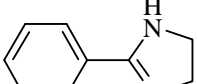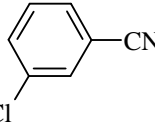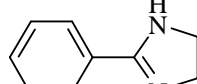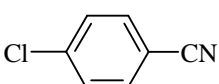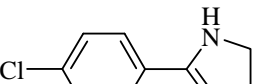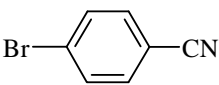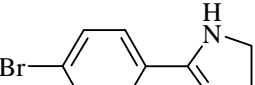
No.	Nitrile (a)	Product (c)[a]	Time, min	Yield[b], %
1c			60	95
2c			30	90
3c			120	98
4c			60	90
5c			20	94
6c			140	93
7c			240	90
8c			120	85
9c			180	93
10c			150	93

TABLE I. Continued
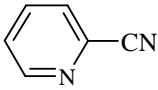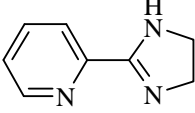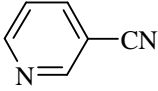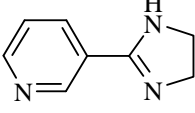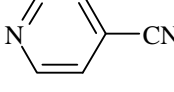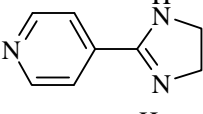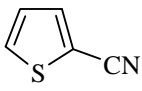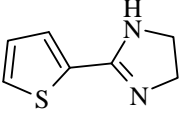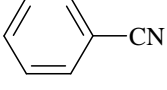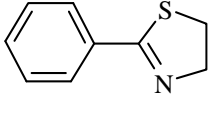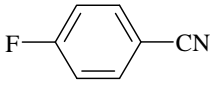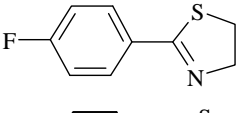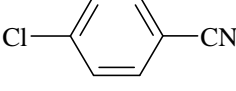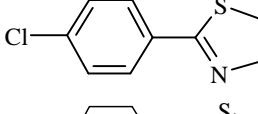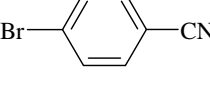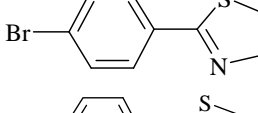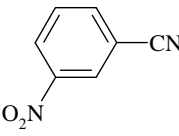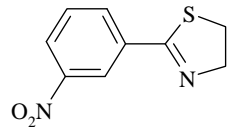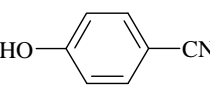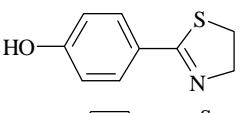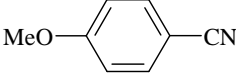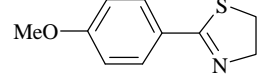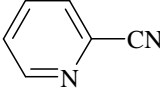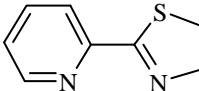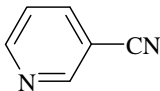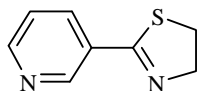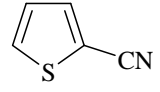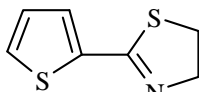
Entry	Nitrile (a)	Product (c)[a]	Time, min	Yield[b], %
11c			8	98
12c			150	95
13c			15	94
14c			120	90
15c			2	95
16c			1	96
17c			5	97
18c			2	80
19c			2	98
20c			3	60
21c			2	50

TABLE I. Continued

Entry	Nitrile (a)	Product (c)[a]	Time, min	Yield[b], %
22c			1	98
23c			3	97
24c			2	98

[a]The products were identified by comparison of their physical and spectral data with those of authentic samples;
[b]isolated yield

General method for the conversion of dinitriles to mono- and bis-oxazolines, mono-imidazolines and bis-thiazolines

To a mixture of a dinitrile (1 mmol) and 2-aminoethanol (10 mmol), ethylenediamine (8 mmol) or 2-aminoethanethiol (2.5 mmol), TCCA (0.06 mmol for oxazoline, 0.15 mmol for imidazoline and 0.02 mmol for thiazoline synthesis) was added. The reaction mixture was stirred at 110 °C without solvent. The progress of the reaction was followed by TLC (eluent: *n*-hexane:EtOAc, 2:1 for mono- and bis-oxazolines and bis-thiazolines, EtOAc:methanol, 10:1 for mono-imidazolines). After the appropriate time according to Table II, the pure products (**1f**–**8f**) were gained by column chromatography.

RESULTS AND DISCUSSION

In continuation of our work to recommend new catalysts for organic syntheses,[36–42] now TCCA as a highly efficient homogeneous catalyst for the preparation of 2-oxazolines, 2-imidazolines and 2-thiazolines from nitriles is presented (Scheme 1).

In order to find the optimum reaction conditions, benzonitrile was reacted with 2-aminoethanol in the presence of TCCA. The model reaction was performed using different molar ratios of substrates and catalyst, at various temperatures and in different polar and non-polar solvents. With the goal of performing the synthesis in the absence of solvent as a special advantage of the method, the model reaction was also investigated under solvent-free conditions. The best result was obtained in the reaction of benzonitrile (1 mmol), 2-aminoethanol (6 mmol) and TCCA (0.03 mmol) at 110 °C under solvent-free conditions (Table I, entry 1). Using these optimized conditions, a variety of aromatic and heteroaromatic nitriles were reacted with 2-aminoethanol and corresponding 2-oxazolines were generated in high yields (Table I, entries 1–6).

Similarly, the model reaction of benzonitrile with ethylenediamine was performed in the presence of TCCA for optimization of 2-phenylimidazoline syn-

thesis. After several experiments, 1:4:0.1 molar ratio of benzonitrile: ethylene-diamine: catalyst at 110 °C in the absence of solvent was selected as the best re-action conditions (Table I, entry 7). Subsequently, heterocyclization of a great variety of aromatic and heteroaromatic nitriles with ethylenediamine were per-formed to prepare the corresponding 2-imidazoline products (Table I, entries 7––14).

Furthermore, cyclocondensation of benzonitrile with 2-aminoethanethiol was performed in the presence of different amounts of TCCA. The effects of tem-perature and solvent were also investigated. The best result was obtained with 1:1.2:0.01 molar ratios of benzonitrile:2-aminoethanethiol:TCCA at 110 °C under solvent-free conditions. Various aromatic and heteroaromatic nitriles were re-acted with 2-aminoethanethiol in the presence of TCCA under the optimum re-action conditions. The corresponding 2-substituted thiazolines were generated in good to excellent yields (Table I, entries 15–24).

Extensive applications of both chiral and achiral bis-oxazolines, bis-imi-dazolines and bis-thiazolines as ligands in various complex structures promoted the use of the present method for the synthesis of these useful ligands from di-nitriles. Therefore, dicyanobenzene derivatives were reacted with 2-aminoetha-nol, ethylenediamine or 2-aminoethanethiol in the presence of TCCA at 110 °C under solvent-free conditions (Table II). As given in Table II, the conversion of dinitriles to mono-oxazolines (10–20 min) and bis-oxazolines (300–390 min) is a special time-dependent chemo-selective procedure. It is also important to note that the synthesis of mono-imidazolines and bis-thiazolines is a chemo-selective, but not a time-dependent reaction (Table II). Mono-imidazolines were satisfac-torily produced after 20–30 min (Table II, **5f** and **6f**) and prolonging the reaction time did not lead to the production of the corresponding bis-imidazolines. Whereas, bis-thiazolines were exclusively obtained from the reactions of dinit-riles with 2-aminoethanethiol after 7–10 min (Table II, **7f** and **8f**).

TABLE II. Synthesis of mono- and bis-derivatives of oxazolines, imidazolines and thiazolines from dinitriles catalyzed by TCCA
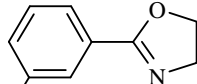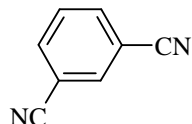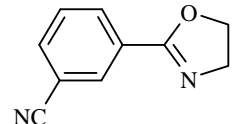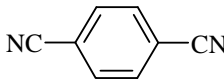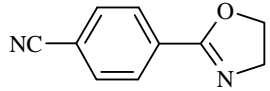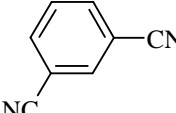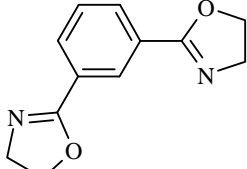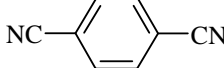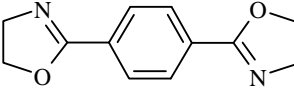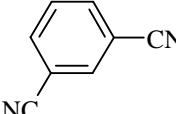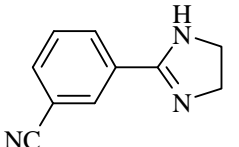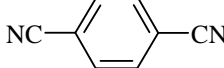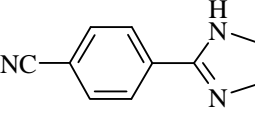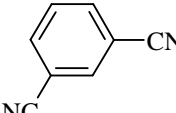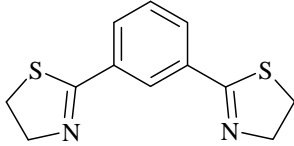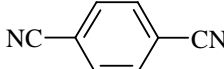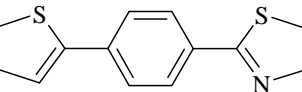
Entry	Dinitrile (e)	Product (f)[a]	Time, min	Yield[b], %
1f			10	95
2f			20	92

TABLE II. Continued

Entry	Dinitrile (e)	Product (f)[a]	Time, min	Yield[b], %
3f			300	80
4f			390	97
5f			20	92
6f			30	95
7f			7	95
8f			10	92

[a]The products were identified by comparison of their physical and spectral data with those of authentic samples;
[b]isolated yield

It is noteworthy that the method is selective for the reaction of aromatic nitriles as aliphatic nitriles are unreactive under these conditions.

In order to show the superiority of TCCA over other catalysts, the results obtained in the present study for the synthesis of 2-phenyloxazoline are compared with some other results reported in the literature in Table III. It is note-

TABLE III. Comparison of some other procedures with the present method for the synthesis of 2-phenyloxazoline (**1c**)

Entry	Catalyst amount, mol %	Temperature, °C	Time, h	Yield, %	Ref.
1	TCCA (3)	110	1	95	–
2	Bi(OTf)$_3$ (5)	100	3.5	88	31
3	ZrOCl$_2$.8H$_2$O (10)	100	5	90	33
4	H$_3$PW$_{12}$O$_{40}$ (1)	100	3.5	85	–
5	ZnCl$_2$ (1.25)	130, under N$_2$	12	74	34

worthy that the catalytic activity of TCCA was greater than those of some active Lewis acids or solid acids, as given in Table III.

CONCLUSIONS

In summary, TCCA was employed as a novel and highly efficient catalyst for the synthesis of 2-oxazolines, 2-imidazolines and 2-thiazolines from nitriles in high yields. This homogeneous catalyst is commercially available, inexpensive and non-volatile and is a chemical commonly found in organic laboratories. Furthermore, the efficiency and chemoselectivity of the protocol was also investigated in the selective preparation of aromatic and heteroaromatic mono- and bis-oxazolines, mono-imidazolines and bis-thiazolines. In addition, the absence of hazardous and non-green solvents, easy work-up and approximately short reaction times are another noteworthy advantage of the reported protocols.

SUPPLEMENTRY MATERIAL

The physical and spectral data of the prepared compounds are available electronically from http://www.shd.org.rs/JSCS/, or from the corresponding author on request.

И З В О Д

ТРИХЛОРИЗОЦИЈАНУРНА КИСЕЛИНА КАО ЕФИКАСАН ХОМОГЕНИ КАТАЛИЗАТОР У ХЕМОСЕЛЕКТИВНОЈ СИНТЕЗИ 2-СУПСТИТУИСАНИХ ОКСАЗОЛИНА, ИМИДАЗОЛИНА И ТИАЗОЛИНА У РЕАКЦИЈАМА БЕЗ РАСТВАРАЧА

SEYEDEH FATEMEH HOJATI и SEYEDE ATEFE NEZHADHOSEINY

Department of Chemistry, Sabzevar Tarbiat Moallem University, Sabzevar 9617976487, Iran

Трихлоризоцијанурна киселина је комерцијално доступан и приступачан реагенс, који је употребљен као катализатор у синтези 2-оксазолина, 2-имидазолина и 2-ти-азолина, у реакцији 2-аминоетанола, етилендиамина или 2-аминоетантиола у одсуству растварача.

(Примљено 31. октобра 2011, ревидирано 21. марта 2012)

REFERENCES

1. B. S. Davidson, *Chem. Rev.* **93** (1993) 1771
2. C. Dardonville, I. Rozas, *Med. Res. Rev.* **24** (2004) 639
3. M. Schorderet, *Pharmacologie: Des Concepts Fondamentaux aux Applications Thérapeutiques,* Frison-Roche, Paris, 1992, p. 130–153
4. P. Blancafort, *Drugs Future* **3** (1978) 592
5. E. S. Vizi, *Med. Res. Rev.* **6** (1986) 431
6. H. Y. Li, S. Drummond, I. Delucca, G. A. Boswell, *Tetrahedron* **52** (1996) 11153
7. L. Crane, M. Anastassiadou, S. El Hage, J. L. Stigliani, G. Baziard-Mouysset, M. Payard, J. M. Leger, J. G. Bizot-Espiard, A. Ktorza, D. H. Caignard, P. Renard, *Bioorg. Med. Chem.* **14** (2006) 7419

8. L. T. Vassilev, B. T. Vu, B. Graves, D. Carvajal, F. Podlaski, Z. Filipovic, N. Kong, U. Kammlott, C. Lukacs, C. Klein, N. Fotouhi, E. A. Liu, *Science* **303** (2004) 844

9. M. Ueno, K. Imaizumi, T. Sugita, I. Takata, M. Takeshita, *Int. J. Immunopharmacol.* **17** (1995) 597

10. T. G. Gant, A. I. Meyers, *Tetrahedron* **50** (1994) 2297

11. D. Yang, M.-K. Wong, Y.-C. Yip, X.-C. Wang, M.-W. Tang, J.-H. Zheng, K.-K. Cheung, *Tetrahedron Lett.* **38** (1997) 7083

12. Y. Jiang, Q. Jiang, G. Zhu, X. Zhang, *Tetrahedron Lett.* **38** (1997) 215

13. J. Zhou, Y. Tang, *Chem. Soc. Rev.* **34** (2005) 664

14. H. Liu, D.-M. Du, *Adv. Synth. Catal.* **351** (2009) 489

15. R. Ghorbani-Vaghei, S. Akbari-Dadmahaleh, M. Amiri, *J. Iran. Chem. Soc.* **7** (2010) 301

16. A. R. Katritzky, C. Cai, K. Suzuki, S. K. Singh, *J. Org. Chem.* **69** (2004) 811

17. L. N. Pridgen, *J. Org. Chem.* **47** (1982) 4319

18. M. C. Pirrung, L. N. Tumey, *J. Comb. Chem.* **2** (2000) 675

19. B. George, E. P. Papadopoulos, *J. Org. Chem.* **42** (1977) 441

20. T. Kumagai, Y. Kawamura, T. Mukai, *Tetrahedron Lett.* **24** (1983) 2279

21. C. Lixin, X. Yahong, *J. Mat. Sci. Lett.* **22** (2003) 953

22. H. Salgado-Zamora, E. Campos, R. Jimenez, H. Cerantes, *Heterocycles* **47** (1998) 1043

23. I. Mohammadpoor-Baltork, M. Abdollahi-Alibeik, *Bull. Korean Chem. Soc.* **24** (2003) 1354

24. R. D. Crouch, *Tetrahedron* **65** (2009) 2387

25. V. Mirkhani, M. Moghadam, S. Tangestaninejad, H. Kargar, *Tetrahedron Lett.* **47** (2006) 2129

26. H. Fujioka, K. Murai, O. Kubo, Y. Ohba, Y. Kita, *Tetrahedron* **63** (2007) 638

27. U. Tilstam, H. Weinmann, *Org. Process Res. Dev.* **4** (2002) 384

28. J. Ye, Y. Wang, R. Liu, G. Zhang, Q. Zhang, J. Chen, X. Liang, *Chem. Commun.* (2003) 2714

29. J. Ye, Y. Wang, J. Chen, X. Liang, *Adv. Synth. Catal.* **346** (2004) 691

30. J. C. Barros, *Synlett* (2005) 2115

31. H. Veisi, *Synthesis* (2010) 2631

32. H. Veisi, *Tetrahedron Lett.* **51** (2010) 2109

33. H. Veisi, R. Ghorbani-Vaghei, *Tetrahedron* **66** (2010) 7445

34. H. Veisi, *Curr. Org. Chem.* **15** (2011) 2438

35. H. Veisi, R. Golbedaghi, J. Malakootikhah, A. R. Sedrpoushan, B. Maleki, D. Kordestani, *J. Heterocycl. Chem.* **47** (2010) 1398

36. I. Mohammadpoor-Baltork, A. R. Khosropour, S. F. Hojati, *Synlett* (2005) 2747

37. I. Mohammadpoor-Baltork, M. Moghadam, S. Tangestaninejad, V. Mirkhani, S. F. Hojati, *Polyhedron* **27** (2008) 750

38. I. Mohammadpoor-Baltork, A. R. Khosropour, S. F. Hojati, *Catal. Commun.* **8** (2007) 200

39. S. F. Hojati, I. Mohammadpoor–Baltork, B. Maleki, M. Gholizadeh, F. Shafiezadeh, M. Haghdost, *Can. J. Chem.* **88** (2010) 135

40. S. F. Hojati, M. Gholizadeh, M. Haghdoust, F. Shafiezadeh, *Bull. Korean Chem. Soc.* **31**, 2010, 3238

41. S. F. Hojati, B. Maleki, Z. Beykzadeh, *Monatsh. Chem.* **142**, 2011, 87

42. I. Mohammadpoor-Baltork, M. Moghadam, S. Tangestaninejad, V. Mirkhani, S. F. Hojati, *Catal.Commun.* **9** (2008) 1153.

Trichloroisocyanuric acid as an efficient homogeneous catalyst for the chemoselective synthesis of 2-substituted oxazolines, imidazolines and thiazolines under solvent-free condition

SEYEDEH FATEMEH HOJATI* and SEYEDE ATEFE NEZHADHOSEINY

Department of Chemistry, Sabzevar Tarbiat Moallem University, Sabzevar 9617976487, Iran

PHYSICAL AND SPECTRAL DATA OF SOME PRODUCTS

2-Phenyl-4,5-dihydro-1,3-oxazole (1c). Oil; IR (neat, cm^{-1}): 1648 (C=N stretching); ^{1}H-NMR (500 MHz, CDCl$_3$, δ / ppm): 4.05 (2H, *t*, *J* = 9.5 Hz, CH$_2$–O), 4.41 (2H, *t*, *J* = 9.5 Hz, CH$_2$-N), 7.40 (2H, *t*, *J* = 7.5 Hz, aromatic), 7.46 (1H, *t*, *J* = 7.5 Hz, aromatic), 7.95 (2H, *d*, *J* = 7.5 Hz, aromatic).

2-(3-Chlorophenyl)-4,5-dihydro-1,3-oxazole (2c). m.p. 40–42 °C; IR (KBr, cm^{-1}): 1644 (C=N stretching); ^{1}H-NMR (500 MHz, CDCl$_3$, δ / ppm): 4.04 (2H, *t*, *J* = 9.5 Hz, CH$_2$–O,), 4.41 (2H, *t*, *J* = 9.5 Hz, CH$_2$-N), 7.32 (2H, t, aromatic, *J* =7.9 Hz), 7.42 (1H, dd, aromatic, *J* = 0.8 and 7.9 Hz), 7.81 (1H, *dd*, *J* = 0.8 and 7.9 Hz, aromatic), 7.92 (1H, *s*, aromatic).

2-(4-Chlorophenyl)-4,5-dihydro-1,3-oxazole (3c). m.p. 77–79 °C; IR (KBr, cm^{-1}): 1646 (C=N stretching); ^{1}H-NMR (500 MHz, CDCl$_3$, δ / ppm): 4.05 (2H, *t*, *J* = 9.5 Hz, CH$_2$–O), 4.43 (2H, *t*, *J* = 9.5 Hz, CH$_2$-N), 7.8 (2H, *d*, *J* =8.3 Hz, aromatic), 7.88 (2H, *d*, *J* = 8.3 Hz, aromatic).

2-(3-Pyridyl)-4,5-dihydro-1,3-oxazole (4c). m.p. 66–68 °C; IR (KBr, cm^{-1}): 1648 (C=N stretching); ^{1}H-NMR (500 MHz, CDCl$_3$, δ / ppm): 4.06 (2H, *t*, *J* = = 9.6 Hz, CH$_2$–O), 4.44 (2H, *t*, *J* = 9.6 Hz, CH$_2$-N), 7.33 (1H, *dd*, *J* =7.9 and 4.7 Hz, aromatic), 8.20 (1H, *dd*, *J* = 1.8 and 7.9 Hz, aromatic), 8.68 (1H, *dd*, *J* = 1.8 and 4.7 Hz, aromatic), 9.13 (1H, *s*, aromatic).

2-(4-Pyridyl)-4,5-dihydro-1,3-oxazole (5c). m.p. 109–111 °C; IR (KBr, cm^{-1}): 1648 (C=N stretching); ^{1}H-NMR (500 MHz, CDCl$_3$, δ / ppm): 4.05 (2H, *t*, *J* = = 9.6 Hz, CH$_2$–O), 4.42 (2H, *t*, *J* = 9.4 Hz, CH$_2$–N), 7.74 (2H, *d*, *J* = 5.7 Hz, aromatic), 8.67 (2H, *d*, *J* = 5.7 Hz, aromatic).

2-(2-Thienyl)-4,5-dihydro-1,3-oxazole (6c). m.p. 58–60 °C; IR (KBr, cm^{-1}): 1642 (C=N stretching); ^{1}H NMR (500 MHz, CDCl$_3$, δ / ppm): 4.03 (2H, *t*, CH$_2$–O,

---

* Corresponding author. E-mail: sfhojati@sttu.ac.ir

J = 9.4 Hz), 4.42 (2H, *t*, CH$_2$–N, J = 9.4 Hz), 7.06 (1H, dd, aromatic, J =3.6 and 4.7 Hz), 7.44 (1H, *d*, aromatic, J = 4.7 Hz), 7.60 (1H, *d*, aromatic, J = 3.6 Hz).

2-Phenyl-4,5-dihydro-1H-imidazole (7c). m.p. 100–102 °C; IR (KBr, cm^{-1}): 3190 (NH stretching), 1598 (C=N stretching); ^{1}H-NMR (80 MHz, CDCl$_3$, δ / ppm): 3.75 (4H, *s*, 2CH$_2$), 4.8 (1H, *s*, NH), 7.3–7.4 (3H, *m*, aromatic), 7.7–7.8 (2H, *m*, aromatic).

2-(3-Chlorophenyl)-4,5-dihydro-1H-imidazole (8c). m.p. 134–136 °C; IR (KBr, cm^{-1}): 3140 (NH stretching), 1595 (C=N stretching); ^{1}H-NMR (80 MHz, CDCl$_3$, δ / ppm): 3.76 (4H, *s*, 2CH$_2$), 4.25 (1H, *s*, NH), 7.22–7.75(4H, *m*, aromatic).

2-(4-Chlorophenyl)-4,5-dihydro-1H-imidazole (9c). m.p. 186–188 °C; IR (KBr, cm^{-1}): 3140 (NH stretching), 1590 (C=N stretching); ^{1}H-NMR (80 MHz, CDCl$_3$, δ / ppm): 3.75 (4H, *s*, 2CH$_2$), 4.22 (1H, *s*, NH), 7.30 (2H, *d*, aromatic), 7.93 (2H, *d*, aromatic).

2-(4-Bromophenyl)-4,5-dihydro-1H-imidazole (10c). m.p. 242–246 °C; Anal. Calcd. For C$_9$H$_9$N$_2$Br: C, 48.17; H, 4.06; N, 12.45. Found: C, 48.21; H, 4.02; N, 12.50; IR (KBr, cm^{-1}): 3130 (NH stretching), 1590 (C=N stretching); ^{1}H-NMR (80 MHz, CDCl$_3$, δ / ppm): 3.90 (4H, *s*, 2CH$_2$), 7.70–7.80 (4H, *m*).

2-(2-Pyridyl)-4,5-dihydro-1H-imidazole (11c). m.p. 100–102 °C; IR (KBr, cm^{-1}): 3240 (NH stretching), 1594 (C=N stretching); ^{1}H-NMR (80 MHz, CDCl$_3$, δ / ppm): 3.81 (4H, *s*, 2CH$_2$), 5.38 (1H, *s*, NH), 7.22-7.38 (1H, *m*, aromatic), 7.62-7.85 (1H, *m*, aromatic), 8.12 (1H, *d*, aromatic). 8.55 (1H, *d*, aromatic).

2-(3-Pyridyl)-4,5-dihydro-1H-imidazole (12c). m.p. 106–108 °C; IR (KBr, cm^{-1}): 3150 (NH stretching), 1586 (C=N stretching); ^{1}H-NMR (80 MHz, CDCl$_3$, δ / ppm): 3.78 (4H, *s*, 2CH$_2$), 4.54 (1H, *s*, NH), 7.2–7.38 (1H, *m*, aromatic), 8.02––8.15 (1H, *m*, aromatic), 8.6–8.67 (1H, *m*, aromatic), 8.92 (1H, *s*, aromatic).

2-(4-Pyridyl)-4,5-dihydro-1H-imidazole (13c). m.p. 133–135 °C; IR (KBr, cm^{-1}): 3180 (NH stretching), 1594 (C=N stretching); ^{1}H-NMR (80 MHz, CDCl$_3$, δ / ppm): 3.79 (4H, *s*, 2CH$_2$), 4.3 (1H, *s*, NH), 7.61 (2H, *d*, aromatic), 8.65 (2H, *d*, aromatic).

2-(2-Thienyl)-4,5-dihydro-1H-imidazole (14c). m.p. 174–176 °C; IR (KBr, cm^{-1}): 3140 (NH stretching), 1597 (C=N stretching); ^{1}H NMR (80 MHz, CDCl$_3$, δ / ppm): 3.75 (4H, *s*, 2CH$_2$), 4.25 (1H, *s*, NH), 6.9–7.05 (1H, *m*, aromatic), 7.35––7.4 (2H, *m*, aromatic).

2-Phenyl-4,5-dihydro-1,3-thiazole (15c). m.p. 126–128 °C; ^{1}H-NMR (500 MHz, CDCl$_3$, δ / ppm): 3.40 (2H, *t*, CH$_2$–S, J = 8.3 Hz), 4.46 (2H, *t*, CH$_2$–N, J = = 8.3 Hz), 7.38–7.49 (3H, *m*, aromatic), 7.85 (2H, dd, aromatic, J = 1.6 and 7.6 Hz).

2-(4-Fluorophenyl)-4,5-dihydro-1,3-thiazole (16c). Oil; Anal. Calcd. For C$_9$H$_8$NSF: C, 59.64; H, 4.45; N, 7.72. Found: C, 59.67; H, 4.42; N, 7.73; ^{1}H--NMR (500 MHz, CDCl$_3$, δ / ppm): 3.44 (2H, *t*, CH$_2$–S, J = 8.3 Hz), 4.46 (2H, *t*, CH$_2$–N, J = 8.3 Hz), 7.07–7.13 (2H, *m*, aromatic), 7.82–7.87 (2H, *m*, aromatic).

*2-(4-Chlorophenyl)-4,5-dihydro-1,3-thiazole (**17c**)*. m.p. 53–55 128 °C; ^{1}H--NMR (500 MHz, CDCl$_3$, δ / ppm): 3.45 (2H, *t*, CH$_2$–S, *J* = 8.4 Hz), 4.47 (2H, *t*, CH$_2$–N, *J* = 8.4 Hz), 7.40 (2H, *d*, aromatic, *J* = 8.6 Hz), 7.79 (2H, *d*, aromatic, *J* = 8.6 Hz).

*2-(4-Bromophenyl)-4,5-dihydro-1,3-thiazole (**18c**)*. m.p. 60–62 °C; ^{1}H-NMR (500 MHz, CDCl$_3$, δ / ppm): 3.33 (2H, *t*, CH$_2$–S, *J* = 8.35 Hz), 4.44 (2H, *t*, CH$_2$–N, *J* = 8.4 Hz), 7.54 (2H, *d*, aromatic, *J* = 8.55 Hz), 7.69 (2H, *d*, aromatic, *J* = 8.5 Hz).

*2-(3-Nitrophenyl)-4,5-dihydro-1,3-thiazole (**19c**)*. m.p. 135–137 °C; Anal. Calcd. For C$_9$H$_8$N$_2$SO$_2$: C, 51.94; H, 3.81; N, 13.44. Found: C, 51.92; H, 3.85; N, 13.46; ^{1}H-NMR (500 MHz, CDCl$_3$, δ / ppm): 3.53 (2H, *t*, CH$_2$–S, *J* = 8.4 Hz), 4.53 (2H, *t*, CH$_2$–N, *J* = 8.4 Hz), 7.63 (1H, *t*, aromatic, *J* = 8.0 Hz), 8.19 (1H, *d*, aromatic, *J* = 7.8 Hz), 8.34 (1H, *dd*, aromatic, *J* = 1.3 and 8.2 Hz), 8.70 (1H, *s*, aromatic, *J* = 1.8 Hz).

*2-(4-Hydroxyphenyl)-4,5-dihydro-1,3-thiazole (**20c**)*. m.p. 176–178 °C; ^{1}H--NMR (500 MHz, CDCl$_3$, δ / ppm): 3.43 (2H, *t*, CH$_2$–S, *J* = 8.3 Hz), 3.85 (1H, *s*, OH), 4.44 (2H, *t*, CH$_2$–N, *J* = 8.3 Hz), 6.84 (2H, *d*, aromatic, *J* = 8.5 Hz) 7.73 (2H, *d*, aromatic, *J* = 8.5 Hz); MS (*m/z*): 179 (M[+]), 177 (M[+]–2H), 151 (M[+]––C$_2$H$_4$).

*2-(4-Methoxyphenyl)-4,5-dihydro-1,3-thiazole (**21c**)*. m.p. 53–55 °C; ^{1}H--NMR (500 MHz, CDCl$_3$, δ / ppm): 3.42 (2H, *t*, CH$_2$–S, *J* = 8.2 Hz), 3.86 (3H, *s*, O–CH$_3$), 4.44 (2H, *t*, CH$_2$–N, *J* = 8.2 Hz), 6.93 (2H, *d*, aromatic, *J* = 8.3 Hz), 7.81 (2H, *d*, aromatic, *J* = 8.3 Hz).

*2-(2-Pyridyl)-4,5-dihydro-1,3-thiazole (**22c**)*. m.p. 92–94 °C; ^{1}H-NMR (500 MHz, CDCl$_3$, δ / ppm): 3.32 (2H, *t*, CH$_2$–S, *J* = 8.6 Hz), 4.48 (2H, *t*, CH$_2$–N, *J* = 8.6 Hz), 7.28–732 (1H, *m*, aromatic), 7.71 (1H, *dt*, aromatic, *J* = 1.7 and 7.7 Hz), 8.01 (1H, *d*, aromatic, *J* = 7.9 Hz), 8.60 (1H, *d*, aromatic, *J* = 4.8 Hz).

*2-(3-Pyridyl)-4,5-dihydro-1,3-thiazole (**23c**)*. m.p. 111–113 °C; ^{1}H-NMR (500 MHz, CDCl$_3$, δ / ppm): 3.37 (2H, *t*, CH$_2$–S, *J* = 8.4 Hz), 4.39 (2H, *t*, CH$_2$–N, *J* = 8.4 Hz), 7.27 (1H, *dd*, aromatic, *J* = 4.8 and 8.0 Hz), 8.02 (1H, *dt*, aromatic, *J* = 1.9 and 8.0 Hz), 8.60 (1H, *dd*, aromatic, *J* = 1.4 and 4.8 Hz), 8.96 (1H, *d*, aromatic, *J* = 1.9 Hz).

*2-(2-Thienyl)-4,5-dihydro-1,3-thiazole (**24c**)*. m.p. 40–42 °C; ^{1}H-NMR (500 MHz, CDCl$_3$, δ / ppm): 3.37 (2H, *t*, CH$_2$–S, *J* = 8.4 Hz), 4.39 (2H, *t*, CH$_2$–N, *J* = 8.4 Hz), 7.27 (1H, *dd*, aromatic, *J* = 4.8 and 8.0 Hz), 8.02 (1H, *dt*, aromatic, *J* = 1.9 and 8.0 Hz), 8.60 (1H, *dd*, aromatic, *J* = 1.4 and 4.8 Hz), 8.96 (1H, *d*, aromatic, *J* = 1.9 Hz).

*3-(4,5-Dihydro-1,3-oxazole-2-yl)benzonitrile (**1f**)*. m.p. 98–100 °C; IR (KBr, cm[-1]): 1647 (C=N stretching); ^{1}H-NMR (500 MHz, CDCl$_3$, δ / ppm): 4.08 (2H, *t*, CH$_2$–O, *J* = 9.6 Hz), 4.47 (2H, *t*, CH$_2$–N, *J* = 9.4 Hz), 7.53 (1H, *t*, aromatic, *J* =7.8), 7.74 (1H, *d*, aromatic, *J* = 7.7 Hz), 8.18 (1H, *d*, aromatic, *J* = 7.8 Hz), 8.22 (1H, *s*, aromatic).

*4-(4,5-Dihydro-1,3-oxazol-2-yl)benzonitrile (**2f**)*. m.p. 112–114 °C; IR (KBr, cm^{-1}): 1641 (C=N stretching); ^{1}H-NMR (500 MHz, CDCl$_3$, δ / ppm): 4.09 (2H, *t*, CH$_2$–O, *J* = 9.6 Hz), 4.426 (2H, *t*, CH$_2$–N, *J* = 9.6 Hz), 7.68 (2H, *d*, aromatic, *J* =8.3 Hz), 8.03 (2H, *d*, aromatic, *J* = 8.3 Hz).

*2,2'-(1,3-Phenylene)bis[4,5-dihydrooxazole] (**3f**)*. m.p. 137–139 °C; IR (KBr, cm^{-1}): 1657 (C=N stretching); ^{1}H-NMR (500 MHz, CDCl$_3$, δ / ppm): 4.09 (4H, *t*, 2CH$_2$–O, *J* = 9.5 Hz), 4.46 (4H, *t*, 2CH$_2$–N, *J* = 9.5 Hz), 7.48 (1H, *t*, aromatic, *J* = 7.8 Hz), 8.10 (2H, *dd*, aromatic, *J* = 1.4 and 7.8 Hz), 8.50 (1H, *s*, aromatic).

*2,2'-(1,4-Phenylene)bis[4,5-dihydrooxazole] (**4f**)*. m.p. 238–240 °C; IR (KBr, cm^{-1}): 1640 (C=N stretching); ^{1}H-NMR (500 MHz, CDCl$_3$, δ / ppm): 4.10 (4H, *t*, 2CH$_2$–O, *J* = 9.6 Hz), 4.48 (4H, *t*, 2CH$_2$–N, *J* = 9.6 Hz), 8.01 (4H, *s*, aromatic).

*3-(4,5-Dihydro-1H-imidazol-2-yl)benzonitrile (**5f**)*. m.p. 133–134 °C; ^{1}H--NMR (500 MHz, CDCl$_3$, δ / ppm): 3.81 (4H, *s*, 2CH$_2$), 4.2 (1H, *s*, NH), 7.51 (1H, *t*, aromatic, *J* = 7.8 Hz), 7.71 (1H, *d*, aromatic, *J* = 7.7 Hz), 8.01 (1H, *d*, aromatic, *J* = 7.9 Hz), 8.05 (1H, *s*, aromatic); MS (*m/z*): 171 (M$^+$), 169 (M$^+$–2H), 142 (M$^+$–C$_2$H$_5$).

*4-(4,5-Dihydro-1H-imidazole-2-yl)benzonitrile (**6f**)*. m.p. 207–209 °C; ^{1}H--NMR (500 MHz, CDCl$_3$, δ / ppm): 3.83 (4H, *s*, 2CH$_2$), 4.2 (1H, *s*, NH), 7.71 (2H, *d*, aromatic, *J* = 8.4 Hz), 7.90 (2H, *d*, aromatic, *J* = 8.4 Hz); MS (*m/z*): 171 (M$^+$), 169 (M$^+$–2H), 142 (M$^+$–C$_2$H$_5$).

*2,2'-(1,3-Phenylene)bis[4,5-dihydrothiazole] (**7f**)*. m.p. 111–113 °C; ^{1}H-NMR (500 MHz, CDCl$_3$, δ / ppm): 3.46 (4H, *t*, 2CH$_2$–S, *J* = 8.4 Hz), 4.49 (4H, *t*, 2CH$_2$–N, *J* = 8.4 Hz), 7.48 (1H, *dd*, aromatic, *J* = 7.8 and 8.0 Hz), 7.95 (2H, *dd*, aromatic, *J* = 1.5 and 7.8 Hz), 8.27 (1H, *s*, aromatic); MS (*m/z*): 248 (M$^+$), 246 (M$^+$–2H), 244 (M$^+$–4H), 220 (M$^+$–C$_2$H$_4$), 192 (M$^+$–2C$_2$H$_4$).

*2,2'-(1,4-Phenylene)bis[4,5-dihydrothiazole] (**8f**)*. m.p. 105–107 °C; ^{1}H-NMR (500 MHz, CDCl$_3$, δ / ppm): 3.45 (4H, *t*, 2CH$_2$–S, *J* = 8.3 Hz), 4.49 (4H, *t*, 2CH$_2$–N, *J* = 8.3 Hz), 7.88 (4H, *s*, aromatic).

Application of membrane processes for the concentration of *Symphytum officinale* and *Geranium robertianum* extracts to obtain compounds with high anti-oxidative activity

GABRIELA PAUN[1*], ELENA NEAGU[1], SIMONA CARMEN LITESCU[1], PINCU ROTINBERG[2] and GABRIEL LUCIAN RADU[3]

[1]*Centre of Bioanalysis, National Institute for Research-Development of Biological Sciences, 296 Spl. Independentei, P. O. Box 17–16, 060031, Bucharest 6, Romania,* [2]*Biological Research Institute – National Institute of Research-Development, Lascar Catargi Street 47, Iassy, Romania and* [3]*Faculty of Applied Chemistry and Materials Science, Polytechnic University of Bucharest, 313 Spl. Independentei, 060042, Bucharest, Romania*

Abstract: The paper reports the successful application of membranes processes to obtain good quality extracts with compounds of high antioxidative activity and therapeutic value. In this study, the phenolic compounds from two plant species used in Romanian ethno-medicine were investigated and their antioxi/-dant and cytotoxic activities evaluated. Three extracts prepared from *Geranium robertianum* and *Symphytum officinale* were concentrated by microfiltration and ultrafiltration. The levels of phenolic compounds and flavonoids were determined by UV–Vis spectroscopy and high-pressure liquid chromatography (HPLC). The free-radical scavenging activity of the concentrated extracts was determined by the 2,2-diphenyl-1-picrylhydrazyl radical (DPPH) method. The preliminary tests of cytotoxic activity for the concentrated extracts were performed on human epidermoid laryngeal carcinoma cell line (Hep-2p) and normal monkey kidney cells (RM). The results showed that all the concentrated extracts had a very low cytotoxicity against healthy cells, but a significant cytotoxic effect on Hep-2p tumor cells. The concentrated extracts had a high anti-oxidant activity (% DPPH inhibition > 80 %).

Keywords: antioxidant compounds; cytotoxicity; ultrafiltration; *Geranium robertianum*; *Symphytum officinale*; free-radical scavenger.

INTRODUCTION

The major therapeutical activity of phytochemicals is described in relation to their biologically active polyphenol components, such as flavonoids and phenolic acids, which possess significant antioxidant activity.[1–4] Antioxidant substances

---

block the action of free radicals involved in the pathogenesis of many diseases, including atherosclerosis, ischemic heart disease, Alzheimer's disease, Parkinson's disease, cancer and the aging process.[5] With respect to this, in recent years, considerable attention has been paid to plants as sources of antioxidants.

In the present study, interest was focused on medicinal plants extracts obtained from *Symphytum officinale* and *Geranium robertianum* L. (Geraniaceae), both of them known for a long time as remedies in traditional medicine.[6–9] *S. officinale* L. – comfrey (Boraginaceae family) is used in the traditional medicine of Romania to treat different human and animal diseases, such as ulcerations in the gastrointestinal tract, lung congestion, and joint inflammation, and to promote wound healing.[6,7] *G. robertianum* (herb Robert) is used as an anti-inflammatory, haemostatic, anti-diabetic, antibacterial, immunomodulatory and anti-cancer remedy in popular medicine, although very little information is available on the constituents.[8,9]

Medicinal plants have been used for centuries in the cure of human diseases due to their content of components with therapeutic value.[10] Moreover, the wide use of plant extracts in the food, cosmetic and pharmaceutical industries suggests that a systematic study of medicinal plants is very important to identify the active compounds.[10]

Previous studies revealed that ultrafiltration could be used for the concentration of medicinal plant extracts.[4,11] Ultrafiltration processes offer more benefits over conventional technologies. Its application in the phyto-pharmaceutical industry raises particular interest, since membrane processes occur at mild temperatures, avoiding damages caused by thermal processes, thus maintaining the original characteristics of the processed products. Compared with other purification and concentration techniques, including evaporation and dialysis, ultrafiltration has the capability to process larger amounts at greater speeds and it is a very efficient process. Vacuum evaporation is a slower process and is feasible only with small volumes of samples.

The major aim of the present study was to apply various membrane techniques to obtain good quality extracts with high value antioxidant compounds and therapeutic value. The second aim was to determine the cytotoxic effect of *S. officinale* and *G. robertianum* extracts for application as herbal medicine in extract preparation.

In addition, in various research studies, the level of minerals present in medicinal plants were investigated, since these are essential for human nutrition.[12,13] Recently, the importance of the determination of toxic metals level in aqueous extracts and on the phyto-products made from medicinal plants,[14] has been emphasized not only for their benefits, but also for their safe use.

In this study, the metal ions present in the extracts, considering both essential and non-essential ions to the human body, were also determined. The analysis

was performed using flame atomic absorption spectroscopy. The levels of phenolic compounds and flavonoids were determined by UV–Vis spectroscopy and reversed phase-high pressure liquid chromatography (RP-HPLC). To the best of our knowledge, there are no experimental data reported in the literature on the content of microelements and the cytotoxic effect of *S. officinale* and *G. robertianum* extracts.

EXPERIMENTAL

Chemicals and equipments

All chemicals and solvents were purchased from Sigma Aldrich (Germany), Fluka (Switzerland) and Roth (Germany). Deionized water was used for all the performed analysis (Millipore, Bedford, MA).

Microfiltration membranes with 0.45 μm pores and ultrafiltration membranes from regenerated cellulose (MWCO 10000 Da and 1000 Da) were purchased from Millipore (SUA).

The medicinal plants (*S. officinale* and *G. robertianum*) were obtained from a provider specialized in medicinal and aromatic plants – Phytogentec srl (Romania).

Determinations of Ca, Mg, Mn, Zn, Fe, Ni and Pb were performed using a flame atomic absorption spectrometer – FAAS SOLAAR 969 AA (ATI Unicam). All of the absorbance measurements were realized in the area integration mode. Samples were prepared in triplicate and their signals were subtracted from their blanks.

The experiments are performed in a KMS Laboratory Cell CF-1 (Koch Membrane – Germany) with a type cross-flow lab-scale filtration unit.

The rejection, R, was calculated using Eq. (1):

$$R\ \% = 100\ (1 - c_P/c_f) \tag{1}$$

where c_f and c_p are the polyphenols/flavones concentrations in the feed and permeate, respectively.

Preparation and concentration of the extracts

Three extracts were prepared by maceration: *G. robertianum* aqueous extract using cold distilled water as the solvent and for *S. officinale* and *G. robertianum*, alcoholic extracts using 50 % aqueous ethanol (v/v) as the solvent. The dried root (comfrey) and dried leaves (herb Robert) were ground into powder using mill equipment (Grindomix G200), and then mixed with the selected solvent. The herbal mass concentration in the solvent was 6 % (w/v).

The extracts were then successively filtered through Whatman 1 (Medium-fast) filter paper, and microfiltered through 0.45 μm pore size membrane (Millipore), to remove any fine solid particles that could cause membrane fouling during the ultrafiltration (UF).

The concentration experiments were realized on a two-stage membrane filtration set. First, the microfiltration (MF) extracts are treated using a UF1 membrane (cut-off 10000 Da), then the permeate obtained from UF1 was introduced into the cross-flow circuits for UF2 membrane (cut-off 1000 Da) treatment. Each of the flat sheet membranes used in the experiment had an effective area of 0.0028 m^2.

The concentration ratio in ultrafiltration processes (expressed as permeate and concentrate volume ratio) was 2:1. All ultrafiltration experiments were performed at room temperature (*ca*. 23 °C).

Determination of phenolic compounds

The phenolic total content (TPC) was determined by the Folin–Ciocalteu method.[15] Gallic acid (GAE) was used to calibrate the standard curve; the total polyphenols content was obtained from the regression equation of the calibration curve of gallic acid ($y = 0.0036x +$ $+ 0.0203$, $R^2 = 0.9954$) and is expressed as gallic acid (GAE) equivalent.

The characterization of the bioactive phenolic compounds was effected by UV–Vis spectroscopy and HPLC.

Determination the total flavonoid compounds (TFC)

The total flavonoid content was determined according to the aluminum chloride colorimetric method with slight modifications.[16] Rutin was chosen as the standard in the concentration range: 0.005 to 0.1 mg mL^{-1} and the total flavonoid content is expressed as microgram rutin per mL. Total flavonoid content was obtained from the regression equation of the calibration curve of rutin ($y = 0.00989x + 0.01975$, $R^2 = 0.9977$).

HPLC analysis of the extracts for polyphenols and flavones

The analysis of extracts for polyphenols and flavones was performed with a Shimadzu HPLC system equipped with a binary pump (LC-20Adsp), a CTO-20AC column thermostat and a diode-array detector (DAD: SPD-M20A). The spectral data for all peaks were recorded in the range 220–800 nm. Samples were injected at ambient temperature (20 °C) onto a reverse-phase KROMASIL C$_{18}$ column, 4.6 mm×150 mm, 5.1 µm. An auto injector was used to inject 15 µL of the test solution into the HPLC system. The binary mobile phase consisted of solvent A (water acidified with 1 % formic acid, pH 3.0) and B (acetonitrile acidified with 1 % formic acid, pH 3.0). The gradient elution started with 5 % B and changed to 50 % B in 50 min, then reached 5 % B in 5 min. The flow rate was 1.0 mL min^{-1}. The quantitative determinations were made by the calibration curves for caffeic acid, gallic acid, coumaric acid, ferulic acid, chlorogenic acid, rosmarinic acid, rutin, quercetin and kaempferol.

Determination of free radical scavenging activity

The free radical scavenging activities of the feed (extracts), permeate and retentate were studied by the DPPH method – based on the decrease in the maximum absorbance at 519 nm of the 2,2-diphenyl-1-picrylhydrazyl radical (DPPH) (Sigma–Aldrich) in the presence of an antioxidant.[17-19] DPPH· is a stable radical that can readily undergo reduction by an antioxidant (AH), which occurs by the reaction:

$$DPPH^{\bullet} + AH \rightarrow DPPH–H + A^{\bullet}$$
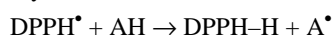
The decreasing of the DPPH radical absorption by the action of antioxidants could be used as a measure the antioxidative activity.

The antioxidant activity (radical scavenging activity) was calculated using the expression:

$$I\% = 100\,((A_0 – A_s)/A_0) \tag{3}$$

where A_0 is the blank absorbance and A_s the sample absorbance.

Cytotoxic activity analysis

The preliminary tests of the cytotoxic activity of the concentrated extracts were performed on the human epidermoid laryngeal carcinoma cell line (Hep-2p) and normal monkey kidney cells (RM).

The cellular cultures of human neoplasm origin (Hep-2p cells) were cultured in DMEM medium (Dulbeco's modified essential medium, Biochrom AG, Germany) supplemented with

10 % fetal bovine serum (Sigma, Germany), 100 μg mL^{-1} streptomycin (Biochrom, Germany), 100 IU mL^{-1} penicillin (Biochrom, Germany) and 50 μg mL^{-1} amphotericin B (Biochrom, Germany), at a density of 5×10^5 cells mL^{-1} flasks, in a humidified 5 % CO_2 atmosphere at 37 °C. When the cells reached confluence, they were detached from the flask with 0.25 % trypsin + 0.02 % ethylenediaminetetraacetic acid (EDTA, Biochrom, Germany) in normal medium and then centrifuged at 1800 rpm for 2 min. The cells were seeded at a density of 1×10^5 cells mL^{-1} in experimental tubes containing 2 mL DMEM medium. The medium of the 24 h cell cultures was replaced either by a normal one (control cultures) or by one containing the vegetal extracts (treated cultures), in a variable dose. After 24 and 48 h of *in vitro* treatment, the total cell number (cytometry), the dead cells/living cells (exclusion test with Trypan Blue) and the cell cultures development were estimated. The cytotoxic property of the studied biopreparations was calculated using the expression:[20]

$$\text{Cytotoxicity level} = 100(N_{tct} - N_{cat})/N_{tc} \tag{4}$$

where N_{tct} = total number of treated cells, N_{cat} = number of treated living cells and N_{tcc} = control cell total number.

Statistical analysis

The measurements were performed in triplicate and Excel 2007 was used for statistical processing, standard deviation (*SD*) was < 10 %.

RESULTS AND DISCUSSION

The microfiltration (MF) process is performed for feed clarification and sterilization, while the ultrafiltration (UF) processes were employed to concentrate the bioactive compounds in the extracts from *S. officinale* and *G. robertianum.*

As plant phenolics represent one of the major groups of compounds acting as primary antioxidants or free radical scavengers, it was important to determine their total amount in the selected plant extracts. The total contents of polyphenols (Fig. 1) and flavones (Fig. 2) were determined in the permeate and retentate after ultrafiltration of the extracts.

The obtained results for the concentration of the extracts by ultrafiltration (after UF2) ranged between 72–78 % for the polyphenols retention, while for flavonoids, the retention ranged between 46–61 %. The degree of retention of polyphenols was between 19–33 % when the extracts were processed using the UF1 membrane. The retention of polyphenols by the UF1 membrane (cut-off 10000 Daltons) was probably due to colloids, which were clustered together with the colloidal matter on the membrane.

The contents of the individual polyphenolic compounds (flavones and polyphenol carboxylic acids) in the extracts were determined by RP-HPLC, after processing by MF–UF. The obtained values are presented in Tables I and II.

Quantitative and qualitative analysis showed that pure water was not the best solvent for the extraction of phenolic compounds (*G. robertianum* aqueous extract compared with *G. robertianum* aqueous alcoholic extract). This is in concordance with previous studies, which reported that aqueous alcohol solvent is the best solvent for the extraction of phenolic compounds from plant materials.[21,22]
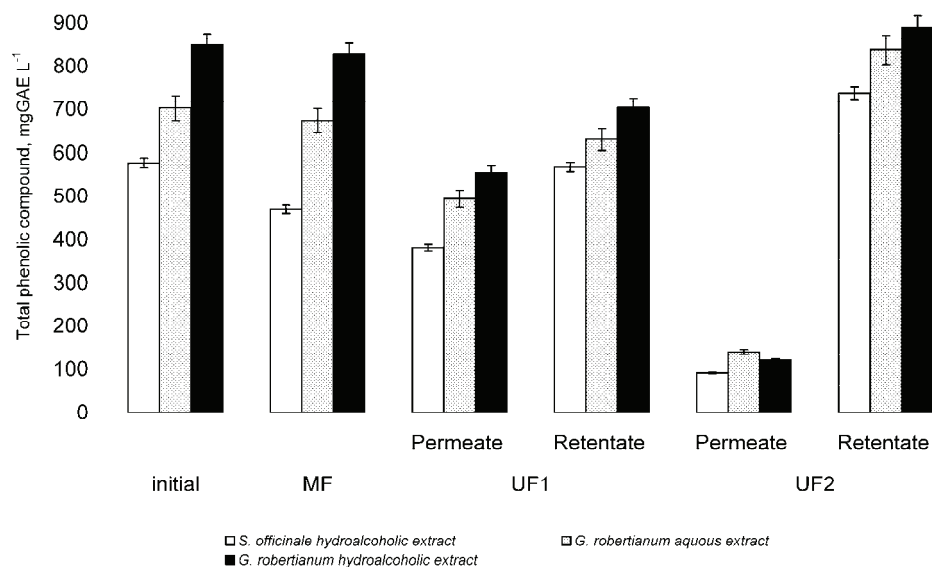
Fig. 1. Total phenolic compounds in *S. officinale* and *G. robertianum* extracts concentrated by ultrafiltration.
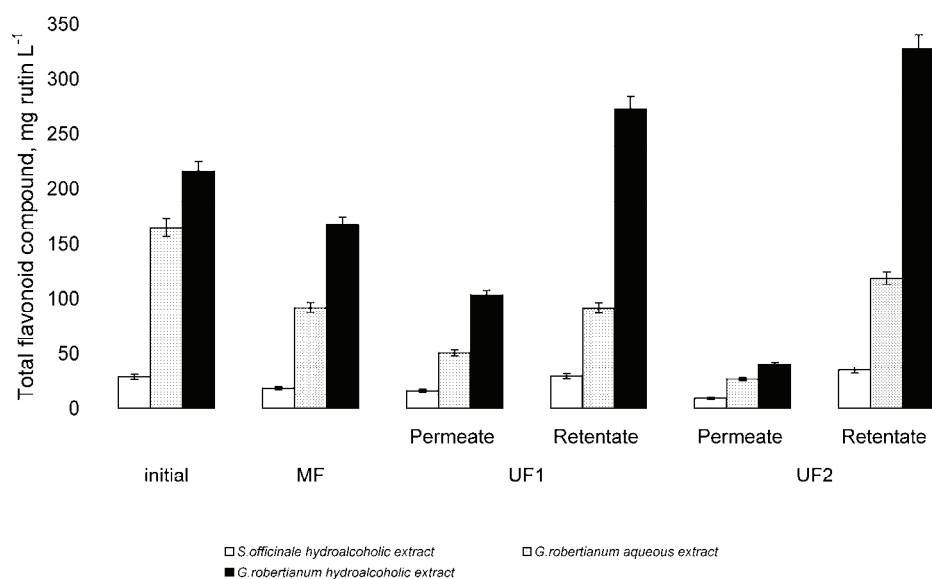
Fig. 2. Total flavonoid compounds in *S. officinale* and *G. robertianum* extracts concentrated by ultrafiltration.

The most important compound identified in the comfrey extract was rosmarinic acid (146.3 mg kg^{-1} in the microfiltrate and 198.66 mg kg^{-1} in the final concentrate extract) and a less important one was luteolin (1.11 mg kg^{-1} in the

microfiltrate and 1.23 mg kg^{-1} in the final concentrate extract). In the *G. robertianum* aqueous alcoholic extract, kaempferol (284.57 mg kg^{-1} in the microfiltrate and 402.83 mg kg^{-1} in the final concentrated extract) and quercetin (54.6 mg kg^{-1} in the microfiltrate and 74 mg kg^{-1} in the final concentrate extract) were the major compounds identified. *p*-Coumaric (9.22 mg kg^{-1} in the microfiltrate and 21.05 mg kg^{-1} in the final concentrate extract) followed by ferulic acid (11 mg kg^{-1} in the microfiltrate and 18.12 mg kg^{-1} in the final concentrate extract) were of minor importance.

TABLE I. Contents of phenolic acids (mg kg^{-1}) and flavonoids in *S. officinale* extracts

Sample	Chloro-genic acid	Caffeic acid	Ferulic acid	*p*-Cou-maric acid	Rutin	Rosmari-nic acid	Lute-olin	Quer-cetin	Kaem-pferol	Apige-nin
MF	3.23	13.35	3.51	8.51	7.86	146.30	1.11	1.50	1.49	1.81
UF1 permeate	1.58	7.43	1.99	2.43	2.23	41.05	0.96	0.42	1.28	1.63
UF1 retentate	2.25	9.97	4.12	5.30	4.89	137.37	1.04	1.48	1.43	1.72
UF2 retentate	4.11	12.58	8.51	11.51	10.45	198.66	1.23	1.75	1.53	1.78

TABLE II. Contents of phenolic acids (mg kg^{-1}) and flavonoids in *G. robertianum* extracts

Sample		Rutin	Caffeic acid	*p*-Coumaric acid	Ferulic acid	Quercetin	Kaempferol
G. robertianum aqueous extract							
MF		2.67	8.18	0.77	1.18	4.83	0.00
UF1	Retentate	10.72	10.97	0.52	3.63	0.00	0.00
	Permeate	1.75	7.85	0.43	1.23	4.83	0.00
UF2	Retentate	1.87	8.32	0.50	1.25	5.60	0.00
G. robertianum aqueous alcoholic extract							
MF		38.95	20.18	9.22	11.00	54.60	284.57
UF1	Retentate	42.78	25.28	22.80	12.58	66.90	375.30
	Permeate	11.73	13.97	6.80	4.27	40.20	188.27
UF2	Retentate	26.97	24.48	21.05	18.12	74.00	402.83

The polyphenol-rich extracts were obtained by combining the two retentate fractions.

The total phenolic contents in the *G. robertianum* and *S. officinale* concentrated extracts were proportional to their free-radical scavenging-linked antioxidant activities.

The results obtained by the DPPH method showed 90 % DPPH inhibition by the *G. robertianum* concentrated extracts (Fig. 3) and over 80 % DPPH inhibition by the comfrey concentrated extract (Fig. 4). The retentate from the aqueous alcoholic and aqueous *G. robertianum* extracts showed the highest antioxidant

activity. The results indicate that the antioxidant activity of the all concentrated extracts is higher than that of Trolox (6-hydroxy-2,5,7,8-tetramethylchroman-2--carboxylic acid).
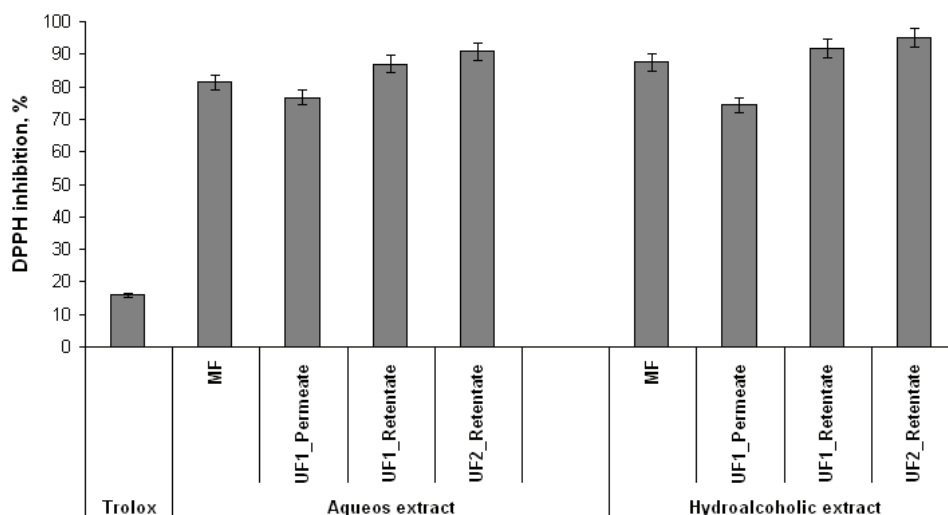
Fig. 3. Comparison of the DPPH radical scavenging activity of the concentrated *G. robertianum* extracts and that of Trolox.
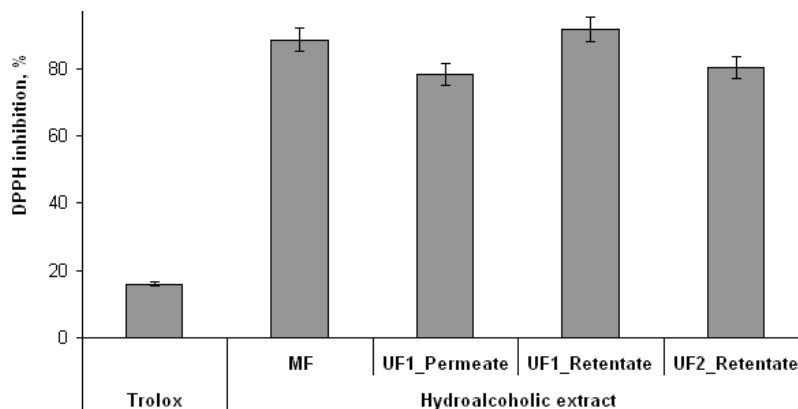
Fig. 4. Comparison of the DPPH radical scavenging activity of the concentrated *Symphytum officinale* extracts and that of Trolox.

A good correlation coefficient (Pearson's correlation coefficient $r \geq 0.98$) between TPC and DPPH scavenging activity was observed.

The strong correlation observed in this study between the total phenolics and the total antioxidant capacity, together with the lack of the cytotoxicity, indicates

the necessity for the use of comfrey and herb Robert, in order to increase health benefits.

There is a direct relationship between the quality of phytotherapeutic products and the bioprocessing of herbals based on the latest developed methods. The present research contributes to the field of medicinal and aromatic plant processing, as the ultrafiltration process showed good results in concentration and purification processes of the active principles with high antioxidant activity from *S. officinale* (comfrey) and *G. robertianum* (herb Robert).

The contents of microelements in the extracts, expressed as mg L^{-1}, are given in Table III. Some metals, such as Ca, Mg, Mn, Zn and Fe, are reported as essential for human health, whereas others, such as Pb and Ni, have been identified as toxic.

TABLE III. Contents of microelements in comfrey (*S. officinale*) and herb Robert (*G. robertianum*) extracts; DL = detection limit; MF = microfiltrate: UF = ultrafiltrate

Sample		Content of microelements, mg L^{-1}						
		Ca	Mg	Mn	Zn	Fe	Ni	Pb
S. officinale	MF	0.052± 0.004	0.054± 0.005	< DL	0.079± 0.009	0	0.050± 0.004	0.354± 0.011
	Permeate UF1	0.052± 0.005	0.053± 0.004	< DL	0.072± 0.008	0	0.041± 0.003	0.298± 0.02
	Permeate UF2	< DL	< DL	< DL	0.030± 0.001	0	0.048± 0.003	1.22± 0.09
	Retentate UF2	0.051± 0.004	0.052± 0.003	< DL	0.082± 0.007	0	0.023± 0.001	0.196± 0.02
G. robertianum aqueous extract	MF	0.935± 0.08	10.4± 0.3	0.893± 0.07	0.071± 0.006	3.2± 0.1	0.051± 0.003	< DL
	Permeate UF1	0.89± 0.07	9.4± 0.6	0.734± 0.06	0.071± 0.006	2.3± 0.1	0.043± 0.003	< DL
	Permeate UF2	0.705± 0.06	8.82± 0.4	0.236± 0.01	0.050± 0.004	0.7± 0.05	0.042± 0.003	< DL
	Retentate UF2	1.72± 0.1	12.8± 0.9	0.919± 0.08	0.097± 0.008	5.6± 0.3	0.044± 0.004	< DL
G. robertianum Aqueous alcoholic extract	MF	0.927± 0.08	9.78± 0.7	0.819± 0.07	0.069± 0.006	1.8± 0.1	0.047± 0.003	< DL
	Permeate UF1	0.896± 0.07	9.12± 0.6	0.729±0 .06	0.064± 0.006	1.3± 0.09	0.041± 0.003	< DL
	Permeate UF2	0.792± 0.05	7.69± 0.6	0.254± 0.01	0.031± 0.004	0.3± 0.03	0.037± 0.003	< DL
	Retentate UF2	1.34± 0.09	11.7± 0.9	1.273± 0.09	0.11± 0.009	2.9± 0.2	0.046± 0.004	< DL

The concentrations of Ca, Mg, and Fe in permeate of the *S. officinale* extract after the UF2 were below the detection limit of the instrument. Mn was an exception as its concentration was below the detection limit even in the microfil-

tration step. In the case of the *G. robertianum* extracts, only Pb was below the detection limit even in the microfiltration step.

The elemental studies of the plants showed that they contained large amounts of nutrients (Mg, Ca and Fe); WHO limits for these metals have not been established.

On comparing the two extracts, it could be observed that the concentrations of the toxic heavy metals (Pb and Ni) in the UF2 retentate were higher in the *S. officinale* extracts. The Pb concentration levels ranged from 0.196 to 0.354 mg L^{-1} and Ni concentration levels from 0.023 to 0.05 mg L^{-1} but they did not exceed the limits of 10 mg kg^{-1} Pb and 8 mg kg^{-1} Ni recommended for medicinal plants.[23] The concentrations of all the microelements determined in the studied medicinal plants were well below the critical limits.

Determination of the cytotoxic action of the studied extracts on the viability of Hep-2p tumor cell cultures and the normal RM cell cultures was based on the calculation of viability percentage of the treated cell cultures, in relation to the controls. The obtained results are presented in Tables IV–VI.

TABLE IV. The cytotoxic impact of *S. officinale* aqueous alcoholic extract processed by MF-UF on Hep-2p tumor cells and RM normal cells; ES = standard deviation; NS = no significant

Sample	Number of alive cells		Number of dead cells		Cytotoxicity, %
	$(X \pm ES) \times 10^{-4}$	p	$(X \pm ES) \times 10^{-4}$	p	
Hep-2p cells					
Control	94.60±5.34(5)	–	3.90±1.08(5)	–	4.0
Retentate UF2	32.85±1.97(5)	NS	5.25±2.34(5)	NS	13.8
70 % Ethanol	1.11±0.6(5)	<0.001	4.8±1.2(5)	<0.001	81.2
RM cells					
Control	39.90±3.10(5)	–	3.00±1.26(5)	–	6.9
Retentate UF2	39.30±2.83(5)	<0.001	2.50±0.97(5)	<0.001	6.0
70% Ethanol	0.18±0.2(5)	<0.001	1.11±0.4(5)	<0.001	86.0

The comparative analysis of the number of alive and dead cells from the Hep-2p cell cultures/normal RM cell cultures, control and treated for 48 h with extracts, at a dose of 1.5 mg mL^{-1}, emphasized the different behavior of these two types of cell cultures. Thus, the control cultures were characterized by a greater number of living cells than dead ones, while the treated cultures showed a greater number of dead cells than living ones.

It is highly important that all concentrated extracts, namely the ethanolic extract of *S. officinale* and *G. robertianum*, and the aqueous extract of *G. robertianum* showed very low cytotoxicity against healthy cells, but selective cytotoxicity against the Hep-2p tumor cells. The low cytotoxic potential of the aqueous extracts is of great significance for their traditional use in the treatment of various disorders, other than cancer.

TABLE V. The cytotoxic impact of *G. robertianum* aqueous extract processed by MF-UF on Hep-2p tumor cells and RM normal cells; MF = microfiltrate extract, ES = standard deviation; NS = no significant

Sample	Number of alive cells		Number of dead cells		Cytotoxicity, %
	$(X \pm ES) \times 10^{-3}$	*p*	$(X \pm ES) \times 10^{-3}$	*p*	
Hep-2p cells					
Control	314.89±9.98(5)	–	10.11±0.32(5)		3.1
MF	271.85±7.60(5)	<0.01	21.47±0.60(5)	<0.001	7.3
UF1 Permeate	320.44±9.04(5)	NS	2.77±0.08(5)	<0.001	0.9
UF1 Retentate	101.53±3.91(5)	<0.001	48.97±1.89(5)	<0.001	32.5
UF2 Retentate	319.58±7.18(5)	NS	19.20±0.07(5)	<0.001	5.7
RM cells					
Control	214.15±11.72(5)	–	6.87±0.38(5)	–	3.1
MF	176.41±9.40(5)	<0.05	7.17±0.38(5)	NS	3.9
UF1 Permeate	210.72±6.79(5)	NS	3.29±0.11(5)	<0.001	1.5
UF1 Retentate	124.98±5.26(5)	<0.001	12.72±0.54(5)	<0.001	9.2
UF2 Retentate	195.93±7.68(5)	NS	10.43±0.41(5)	<0.001	5.1

TABLE VI. The cytotoxic impact of *G. robertianum* aqueous alcoholic extract processed by MF-UF on Hep-2p tumors cells and RM normal cells; MF = microfiltrate extract, ES = standard deviation; NS = no significant

Sample	Number of alive cells		Number of dead cells		Cytotoxicity, %
	$(X \pm ES) \times 10^{-3}$	*p*	$(X \pm ES) \times 10^{-3}$	*p*	
Hep-2p cell					
Control	318.70±10.10(5)	–	6.30±0.20(5)	–	1.9
MF	251.60±7.63(5)	<0.001	71.70±2.17(5)	<0.001	22.2
HA	239.66±3.85(5)	<0.001	15.58±0.25(5)	<0.001	6.1
UF1 Permeate	247.61±3.61(5)	<0.001	19.77±0.29(5)	<0.001	7.4
UF1 Retentate	92.73±1,70(5)	<0.001	32.37±0.60(5)	<0.001	25.9
UF2 Retentate	167.66±2.73(5)	<0.001	41.49±0.67(5)	<0.001	19.8
RM cell					
Control	214.15±11.72 (5)	–	6.87±0.38 (5)	–	1.9
HA	157.42±7.24 (5)	<0.002	53.47±2.46 (5)	<0.001	25.4
MF	182.18±3.91 (5)	<0.02	15.96±0.34 (5)	<0.001	8.1
UF1 Permeate	195.55±3.92 (5)	NS	9.73±0.20 (5)	<0.001	4.7
UF1 Retentate	118.44±1.79 (5)	<0.001	34.06±0.51 (5)	<0.001	22.3
UF2 Retentate	185.30±3.40 (5)	<0.02	10.75±0.20 (5)	<0.001	5.5

The concentrated aqueous alcoholic extract from *G. robertianum* was the most cytotoxic on Hep-2 cell lines, 19.8 % cytotoxicity for the UF2 retentate and 25.9 % cytotoxicity for the UF1 retentate, while the cytotoxicity of the concentrated aqueous extracts from *G. robertianum* were 32.5 % for the UF1 retentate and 5.7 % for UF2 retentate.

Comparison of the cytotoxicity of *S. officinale* and *G. robertianum* may lead to the conclusion that this effect is mainly related to their phenolic compounds.

The cytotoxic effect of the comfrey extract concentrate may also be associated with the toxic metal level (Pb and Ni).

This information helps to establish modern complementary and alternative medicine treatment methods, which may offer efficient cures to large populations suffering from different diseases, including cancer.

CONCLUSIONS

This study showed that it is possible to obtain concentrated comfrey and herb Robert extracts with high antioxidant activity by membrane processes.

Moreover, the *Geranium* aqueous and aqueous alcoholic extracts, both purified and concentrated by membrane processes, and the concentrated *Symphytum* aqueous alcoholic extract diminished the viability of tumor cells. This proved that these extracts had a moderate cytotoxic potential.

The present study evidenced that the heavy metal and minerals contents of the selected medicinal plants were within safe limits. Thus, it was proven that the health of the human body is unlikely to be affected by the extracts of these medicinal plants containing such low contents of heavy metals.

It should be stressed that, hitherto, no reports on the microelements and cytotoxic effect of extracts of *S. officinale* and *G. robertianum* exist in the available literature.

И З В О Д

ПРИМЕНА МЕМБРАНСКОГ ПРОЦЕСА ЗА КОНЦЕНТРОВАЊЕ ЕКСТРАКАТА БИЉАКА *Symphytum officinale* И *Geranium robertianum* РАДИ ДОБИЈАЊА ЈЕДИЊЕЊА ВЕЛИКЕ АНТИОКСИДАТИВНЕ АКТИВНОСТИ

GABRIELA PAUN[1], ELENA NEAGU[1], SIMONA CARMEN LITESCU[1], PINCU ROTINBERG[2] и GABRIEL LUCIAN RADU[3]

[1]Centre of Bioanalysis, National Institute for Research – Development of Biological Sciences, 296 Spl. Independentei, P. O. Box 17–16, 060031, Bucharest 6, Romania, [2]Biological Research Institute – National Institute of Research-Development, Lascar Catargi Street 47, Iassy, Romania и [3]Faculty of Applied Chemistry and Materials Science, Polytechnic University of Bucharest, 313 Spl. Independentei, 060042, Bucharest, Romania

У раду је описана примена мембранског процеса за добијање екстраката једињења велике антиоксидативне активности и могуће примене у терапији. Испитивана су фенолна једињења биљних врста које се користе у румунској етномедицини и утврђена је њихова антиоксидативна и цитотоксична активност. Екстракти добијени из *Geranium robertianum* и *Symphytum officinale* су концентровани микрофилтрацијом и ултрафилтрацијом. Концентрације фенолних једињења и флавоноида су одређене UV–Vis спектроскопијом и методом HPLC. Способност хватања слободних радикала концентрованих екстраката утврђена је методом DPPH. Прелиминарни тестови цитотоксичности изведени су на ћелијској линији епидермоидног карцинома (Hep-2p) и на нормалним буб-

режним ћелијама мајмуна. Резултати су показали да концентровани екстракти испољавају ниску цитотоксичност спрам здравих ћелија, док је цитотоксичност спрам Нер-2р туморских ћелија значајна. Концентровани екстракти су испољили и велику антиоксидативну активност (DPPH инхибиција је преко 80 %).

(Примљено 6. јануара, ревидирано 22. фебруара 2012)

REFERENCES

1. K. D. Croft, *Ann. N. Y. Acad. Sci.* **854** (1998) 435
2. P. G. Pietta, *J. Nat. Prod.* **63** (2000) 1035
3. A. Banerjee, N. Dasgupta, B. De, *Food Chem.* **90** (2005) 727
4. R. G. Paun, E. Neagu, G. L. Radu, *Rev. Chim-Bucharest* **61** (2010) 877
5. O. I. Aruoma, *Mutat. Res.* **523** (2003) 9
6. M. Adams, T. Berset, C. Kessler, M. Hamburger, *J. Ethnopharm.* **121** (2009) 343
7. D. Rode, *Trends Pharmacol. Sci.* **23** (2002) 497
8. M. Bnouham, H. Mekhfi, A. Legssyer, A. Ziyyat, *Int. J. Diabetes Metab.* **10** (2002) 33
9. Z. Amirghofran, M. Azadbakht, M. H. Karimi, *J. Ethnopharm.* **72** (2000) 167
10. A. Nostro, M. P. Germanò, V. D'Angelo, A. Marino, M. A. Cannetelli, *Lett. Appl. Microbiol.* **30** (2000) 379
11. E. Neagu, G. Paun, V. Moroeanu, G. L. Radu, *Rev. Roum. Chim.* **55** (2010) 321
12. P. L. Fernandez, F. Pablos, M. J. Martin, A. G. Gonzalez, *Food Chem.* **76** (2002) 483
13. M. N. Rashed, *J Arid Environ.* **29** (1995) 185
14. V. F. Veiga-Junior, A. C. Pinto, M. A. M. Maciel, *Quim. Nova* **28** (2005) 519
15. V. L. Singleton, R. Orthofer, R. M. Lamuela-Raventos, *Methods Enzymol.* **299** (1999) 152
16. J.-Y. Lin, C.-Y. Tang, *Food Chem.* **101** (2007) 140
17. W. Brand-Williams, M. E. Cuvelier, C. Berset, *Lebensm. Wiss. Technol.* **28** (1995) 25
18. S. C. Litescu, G. L. Radu, *Eur. Food Res. Technol.* **211** (2000) 218
19. E. N. Frankel, A. S. Meyer, *J. Sci. Food Agric.* **80** (2000) 1925
20. A. Doyle, J. B. Griffiths, Cell Quantification, in *Cell and Tissue Culture: Laboratory Procedures in Biotechnology*, Wiley, Chichester, UK, 1998, p. 57
21. WHO, *Monographs on Selected Medicinal Plants*, Vol. 1, World Health Organization, Geneva, 1999
22. W. Zheng, S.Y. Wang, *J. Agric. Food Chem.* **49** (2001) 5165
23. R. G. Marwah, M. O. Fatope, R. A. Mahrooqi, G. B. Varma, H. A. Abadi, S. K. S. Al-Burtamani, *Food Chem.* **101** (2007) 465.

SHORT COMMUNICATION

Synthesis and characterization of *cis*-dioxomolybdenum(VI) complexes having furil as a precursor molecule

DEVENDRA PRATAP RAO[1]*, HARDEO SINGH YADAV[2],
ASHOK KUMAR YADAVA[2], SANJAY SINGH[3] and UMA SHANKER YADAV[4]

[1]*Department of Chemistry, D.A-V. (P.G.) College, Kanpur 208001, Uttar Pradesh, India,* [2]*Department of Chemistry, North Eastern Regional Institute of Science and Technology (NERIST), Nirjuli, Arunachal Pradesh, India,* [3]*Department of Chemistry, M.G.P.G. College, Gorakhpur, Uttar Pradesh, India* and [4]*Department of Chemistry, J. P. University, Chapra, Bihar, India*

Abstract: The syntheses of some new dioxomolybdenum(VI) complexes having the general formula $[MoO_2(mac)](acac)_2$, (where mac = tetraazamacrocyclic ligands derived from the condensation of furil with 1,2-diaminobenzene or 2,3-diaminopyridine and their reaction with β-diketones) using the dioxometal ion as a kinetic template are reported. The prepared complexes were characterized by molar conductance, elemental analyses, infrared and electronic data. The spectral data indicate that the ligands act as tetradentate chelating agents. Due to their biological relevance, molybdenum catalyzed oxygen transfer reactions are of great interest. All the dioxomolybdenum(VI) complexes had octahedral geometry with six coordination.

Keywords: dioxomolybdenum(VI); condensation; amines; macrocyclic complexes.

INTRODUCTION

The versatile nature of molybdenum is due to its multiple oxidation states, which range from –2 to +6, and coordination numbers, which vary from four to eight.[1] In the second transition series, only molybdenum is considered as a biometal that is important for animals, plants and microorganisms. There are many reports on the use of dioxomolybdenum(VI) complexes, which act as catalysts in some biological processes[2,3] and in some industrial processes.[4–6] Due to their relevance in biological processes, molybdenum-catalyzed oxygen-transfer reactions have attracted considerable interest. Mo(VI) is present as a simple molybdate ($MoO_4^{2–}$) ion in aqueous solution depending on its concentration and the pH

---

of the solution. The coordination chemistry of Mo(VI) is an actively pursued area of current research because of its catalytic properties and biological activities.[7–10] Furil is a versatile chelating ligand having two reactive carbonyl groups capable of undergoing Schiff base condensation with a variety of di- and polyamines. Thus, furil has played an important role in the design of macrocyclic ligands. In this context, some dioxomolybdenum(VI) complexes with new high denticity ligands derived from the condensation of furil with 1,2-diaminobenzene or 2,3-diaminopyridine, capable of undergoing cyclization with *β*-diketones *via* the metal template effect, were prepared, characterized and their tentative structures ascertained.

Herein, the synthesis of these complexes and their tentative structures, based on molar conductivity, elemental analysis, and electronic and IR spectroscopy, are reported.

EXPERIMENTAL

Materials and methods

All the employed chemicals and solvents were of reagent grade. The *β*-diketones *viz.* acetylacetone, benzoylacetone, thenoyltrifluoroacetone and dibenzoylmethane were SRL products and the diamines used were reagent grade products. Furil was obtained from Aldrich. Dioxomolybdenum(VI) acetylacetonate was prepared by the standard method using sodium molybdate and acetylacetone.

Analytical methods and physical measurements

The microanalysis of carbon, hydrogen and nitrogen for the complexes were realized at the Central Research Facility, NERIST, Nirjuli-791109, Itanagar, Arunachal Pradesh, India. Molybdenum was estimated gravimetrically after decomposing the complex with concentrated nitric acid by the standard method.[11] Sulphur was estimated as barium sulphate.[12] The standard technique of melting point (uncorrected) determination using a sulphuric acid bath was employed. The electronic spectra of the complexes were recorded on a Beckmann DU-2 spectrophotometer and c Ф10 Russian spectrophotometer in the ranges 2000–185 nm and 700–400 nm. The infrared spectra of the complexes were recorded in the region 4000–200 cm^{-1} in pressed KBr pellets on a Perkin-Elmer 621 and a Beckmann Acculab-9 spectrophotometers.

In-situ *preparation of dioxomolybdenum(VI) complexes with ligands derived by condensation of furil with 1,2-diaminobenzene or 2,3-diaminopyridine*

Molybdenyl acetylacetonate (2 mmol) dissolved in methanol (20 mL) was added to a refluxing solution of furil (2 mmol) and 1,2-diaminobenzene (4 mmol) or 2,3-diaminopyridine (4 mmol) in ethanol (20 mL). The mixture was allowed to react under mild reflux for 6 h, when the colour of the solution turned yellow (Scheme 1). The solvent was removed under vacuo at room temperature and the dirty yellow colour product was isolated. The complex was thoroughly washed with methanol/ethanol mixture. The yield was 70 %.

In situ *preparation of macrocyclic complexes of dioxomolybdenum(VI)*

Molybdenyl acetylacetonate (2 mmol) dissolved in methanol (20 mL) was added to a refluxing solution of furil (2 mmol) and 1,2-diaminobenzene or 2,3-diaminopyridine (4 mmol) in ethanol (25 mL). The mixture was subjected to mild reflux for 6 h, when the colour of the solution intensified and turned yellow (Scheme 2). To this reaction mixture, an ethanolic

solution (10 mL) of acetylacetone (2 mmol) and glacial acetic acid (5 mL) were added. The reaction mixture was refluxed for about 6 h whereby a yellow precipitate was obtained. The filtered precipitate of the complex was purified by washing with 10 mL of a mixture of methanol/ethanol (1:1). The yield was 60 %. The same procedure was adopted for the synthesis of other dioxomolybdenum(VI) macrocyclic complexes using benzoylacetone, thenoyltrifluoroacetone and dibenzolylmethane.
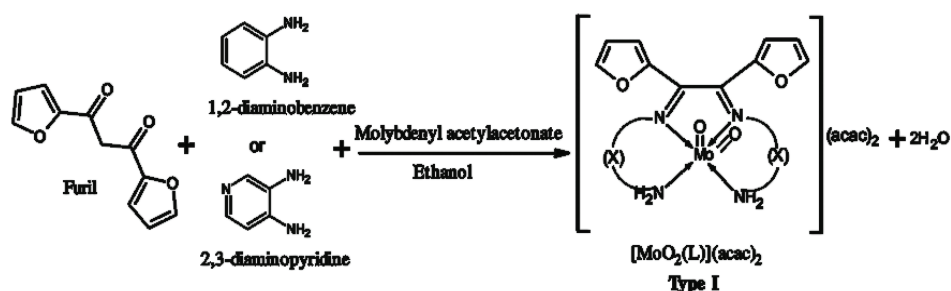
Scheme 1. Preparation of dioxomolybdenum(VI) complexes; X = 1,2-diaminobenzene or 2,3-diaminopyridine; L^1 = furil + 1,2 diaminobenzene; L^2 = furil + 2,3-diaminopyridine.
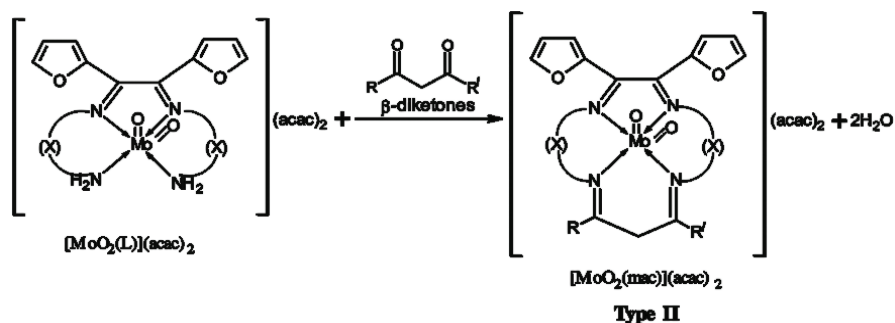
Scheme 2. Preparation of macrocyclic complexes of dioxomolybdenum(VI); mac = tetraazamacrocyclic ligands derived from the condensation of L^1 or L^2 with β-diketones in presence of the dioxmolybdenum(VI) cation; R = CH_3, C_6H_5, C_4H_3S, C_6H_5; R' = CH_3, CH_3, CF_3 or C_6H_5; β-diketone = acetylacetone, benzoylacetone, thenoyltrifluroacetone or dibenzoylmethane.

RESULTS AND DISCUSSION

The dioxomolybdeum(VI) complexes were synthesized using an *in-situ* method by refluxing the reaction mixture of furil, diamines and molybdenyl acetylacetonate in 1:2:1 molar ratio in aqueous ethanol, as shown in Scheme 1, which resulted in the macrocyclic complexes according to Scheme 2.

Physical and analytical data of the molybdenum complexes

The physical and analytical data of the complexes are given in the Supplementary material to this paper. The elemental analyses of the complexes agreed

with the theoretical values and showed 1:1 metal to ligand stoichiometry. The molar conductivity of dioxmolybdenum(VI) complexes in dimethylformamide showed values of Λ_M between 125–140 ohm^{-1} cm^2 mol^{-1}, which indicate their electrolytic nature.

Infrared spectra

The characteristic infrared spectral bands for the complexes are listed in the Table given in the Supplementary material to this paper. The macrocyclic complexes of dioxomolybdenum(VI) exhibit >C=N absorption around 1625–1610 cm^{-1}, which normally appears at 1660 cm^{-1} in free ligands.[13–15] The lowering of this band in the complexes (Type-I) indicates coordination of the nitrogen atoms of the azomethine groups to the molybdenum.[13–16] The presence of a band at around 300 cm^{-1} may be assigned to ν(Mo–N) vibrations.[17] The appearance of >C=N band and the absence of the >C=O band around 1700 cm^{-1} is conclusive evidence for the condensation of the diamines with the two keto groups of furil.[18,19] The bands appearing at 3350 and 3180 cm^{-1} may be assigned to asymmetrical and symmetrical N–H stretching modes of the coordinated terminal amino group.[18] The dioxomolybdenum(VI) complexes prefer to form a *cis*-dioxo group due to the maximum utilization of the d-orbital for bonding. The *cis*-dioxo configuration in the dioxomolybdenum(VI) moiety[20–22] is characterized by two infra-red bands, ν_{asym}(O=Mo=O) and ν_{sym}(O=Mo=O) in C_{2V} symmetry. The presence of two infra-red bands in the 898–910 cm^{-1} and 935–945 cm^{-1} regions are assigned to ν_{asym}(O=Mo=O) and ν_{sym}(O=Mo=O) vibrations, respectively. The bands appearing at 1562 and 1515 cm^{-1} are assigned to ν(C=O) and ν(C=C) vibrations of the acetylacetonate group present in the outer coordination sphere.[23] The infrared spectra of macrocyclic complexes of Type-II show the same pattern of bands but the asymmetrical and symmetrical N–H stretching modes of the terminal amino groups are absent due to condensation of these amino groups with the carbonyl group of the β-diketones in cyclization reactions.[24,25]

Electronic spectra

These spectra are similar to other dioxomolybdenum(VI) complexes involving nitrogen donor atoms. The electronic spectra of the complexes were recorded in 10^{-3} mol L^{-1} solution in DMF and these spectral bands are interpreted according to earlier reported energy level scheme.[26,27] The high intensity peaks observed in the region 295–360 nm of the dioxomolybdenum(VI) complexes seem to appear due to intra-ligand n → π*/π → π* transitions. A medium intensity peak appearing in the region 343 and 394 nm may be assigned as a ligand to metal charge-transfer transition between the lowest empty molybdenum d-orbital and highest occupied ligand molecular orbital.[28]

The above details support the tentative structures of dioxomolybdenum(VI) complexes of Type (I) and macrocyclic complexes of type (II), as shown in the Schemes 1 and 2.

CONCLUSIONS

The spectral data show that the Schiff base condensation of furil, a versatile chelating agent, with diamines and their cyclization reaction with β-diketones were achieved by virtue of the kinetic template effect of the dioxomolybdenum(VI) cation in aqueous ethanol medium. The Schiff bases behave as tetradentate ligands by bonding to the metal ion through the azomethine nitrogen atoms. The analytical data show the presence of one metal ion per ligand molecule and suggest a mononuclear structure for the complexes. The analytical and electronic data support the octahedral structure for the dioxomolybdenum(VI) complexes.

SUPPLEMENTARY MATERIAL

Physical and analytical data of the synthesized molybdenum complexes are available electronically from http://www.shd.org.rs/JSCS/, or from the corresponding author on request.

ИЗВОД

СИНТЕЗА И КАРАКТЕРИЗАЦИЈА *cis*-ДИОКСОМОЛИБДЕН(VI) КОМПЛЕКСА КОЈИ САДРЖЕ ФУРИЛ КАО ПРЕКУРСОРСКИ МОЛЕКУЛ

DEVENDRA PRATAP RAO[1], HARDEO SINGH YADAV[2], ASHOK KUMAR YADAVA[2], SANJAY SINGH[3] и UMA SHANKER YADAV[4]

[1]Department of Chemistry, D.A-V. (P.G.) College, Kanpur 208001, Uttar Pradesh, India, [2]Department of Chemistry, North Eastern Regional Institute of Science and Technology (NERIST), Nirjuli, Arunachal Pradesh, India, [3]Department of Chemistry, M.G.P.G. College, Gorakhpur, Uttar Pradesh, India u [4]Department of Chemistry, J. P. University, Chapra, Bihar, India

Полазећи од диоксомолибден(VI) јона템플атном методом синтетисани су нови комплекси опште формуле $[MoO_2(mac)](acac)_2$ (mac = тетраазамакроциклични лиганди добивени кондензацијом фурила са 1,2-диаминобензеном или 2,3-диаминопиридином и њиховом реакцијом са β-дикетонима). Синтетисани комплекси су окарактерисани на основу кондуктометријских мерења, резултата елементалне анализе, инфрацрвених и електронских апсорпционих спектара. На основу спектроскопских мерења нађено је да координациони број диоксомолибдена(VI) износи шест и да комплекси имају октаедарску геометрију са тетрадентатном координацијом испитиваних лиганада.

(Примљено 30. новембра 2011, ревидирано 7. фебруара 2012)

REFERENCES

1. D. C. Crans, *Pure Appl. Chem.* **77** (2005) 1407
2. L. Rousso, N. Friedman, M. Sheves, M. Ottolenghi, *Biochemistry* **34** (1995) 12059
3. T. Bassov, M. Sheves, *Biochemistry* **25** (1980) 5249

4. M. Mancka, W. Plass, *Inorg. Chem. Commun.* **10** (2007) 677
5. Z. Petrovski, A. A. Valente, M. Pillinger, A. S. Dias, S. S. Rodrigues, C. C. Romao, I. S. Goncalves, *J. Mol. Catal. A: Chem.* **249** (2006) 166
6. F. E. Kuhn, J. Zhao, M. Abrantes, W. Sun, C. A. M. Afonso, L. C. Branco, I. S. Goncalves, M. Pillinger, C. C. Romao, *Tetrahedron Lett.* **46** (2005) 47
7. H. Mimoum, I. S. D. Roch, L. Sajus, *Tetrahedron* **26** (1970) 37
8. V. Conte, F. D. Furia, *Catalytic Oxidations with Hydrogen Peroxide as Oxidant*, Kluwer, Berlin, Germany, 1992
9. H. Mimoum, L. Saussine, E. Daire, M. Postel, J. Fisher, R. Weiss, *J. Am. Chem. Soc.* **105** (1983) 3101
10. M. L. Harikumaran Nair, D. Thankamani, *Indian J. Chem., A* **48** (2009) 1212
11. A. I. Vogel, *A Text Book of Quantitative Inorganic Analysis,* 4th ed., Longmans Green, London, 1978
12. A. I. Vogel, *A Text Book of Practical Organic Chemistry,* 4th ed., Longmans Green, London, 1978
13. V. B. Rana, D. P. Singh, P. Singh, M. P. Teotia, *Transition Met. Chem.* **7** (1982) 174
14. S. Chandra, K. K. Sharma, *Transition Met. Chem.* **8** (1983) 1
15. W. U. Malik, R. Bembi, R. Singh, *Inorg. Chim. Acta* **68** (1983) 223
16. T. G. Gowaik, L. J. J. M. Sobczak, J. J. Z. Kowski, *Inorg. Chim. Acta* **356** (2003) 387
17. J. R. Ferraro, *Low Frequency Vibrations of Inorganic and Coordination Compounds*, Plenum, New York, 1971
18. J. R. Dyer, *Applications of Absorption Spectroscopy of Organic Compounds*, Prentice-Hall, Englewood Cliffs, NJ, 1965
19. D. P. Rao, H. S. Yadav, S. Singh, A. K. Yadava, *Curr. Res. Chem.* **3** (2011) 106
20. B. I. Ceylan, Y. D. Kurt, B. Ulkuseven, *J. Coord. Chem.* **62** (2009) 757
21. R. C. Maurya, R. Verma, T. Singh, *Synth. React. Inorg. Met-Org. Chem.* **33** (2003) 309
22. X. Wang, X. M. Zhang, H. X. Liu, *J. Coord. Chem.* **33** (1994) 223
23. H. Gehrke Jr., J. Veal, *Inorg. Chim. Acta* **3** (1969) 623
24. H. S. Yadav, *Polyhedron* **12** (1993) 313
25. K. Nakamoto, *IR and Raman Spectra of Inorganic and Coordination Compounds, parts A and B*, Wiley, New York, USA, 1998
26. D. P. Rao, H. S. Yadav, A. K. Yadava, S, Singh, U. S. Yadav, *J. Coord. Chem.* **64** (2011) 293
27. K. Sakata, M. Kuroda, S. Yanagida, M. Hashimoto, *Inorg. Chim. Acta* **156** (1989) 107
28. R. Garg, M. K. Saini, N. Fahmi, R. V. Singh, *Transition Met. Chem.* **31** (2006) 362.

Synthesis and characterization of *cis*-dioxomolybdenum(VI) complexes having furil as a precursor molecule

DEVENDRA PRATAP RAO[1]*, HARDEO SINGH YADAV[2],
ASHOK KUMAR YADAVA[2], SANJAY SINGH[3] and UMA SHANKER YADAV[4]

[1]Department of Chemistry, D.A-V. (P.G.) College, Kanpur 208001, Uttar Pradesh, India,
[2]Department of Chemistry, North Eastern Regional Institute of Science and Technology
(NERIST), Nirjuli, Arunachal Pradesh, India, [3]Department of Chemistry, M.G.P.G.
College, Gorakhpur, Uttar Pradesh, India and [4]Department of Chemistry,
J. P. University, Chapra, Bihar, India

PHYSICAL AND ANALYTICAL DATA OF THE MOLYBDENUM COMPLEXES

*[MoO$_2$(L^1)](acac)$_2$ (**1**).* Yield: 62 %; m.p. 306 °C; Anal. Calcd. for C$_{32}$H$_{32}$MoN$_4$O$_8$ (FW 696.57): C, 55.2; H, 4.6; N, 8.1; Mo, 13.8 %. Found: C, 55.1; H, 4.5; N, 8.0; Mo, 13.7 %.

*[MoO$_2$(L^2)](acac)$_2$ (**2**).* Yield: 64 %; m.p. 304 °C; Anal. Calcd. for C$_{30}$H$_{30}$MoN$_6$O$_8$ (FW 698.54): C, 51.6; H, 4.3; N, 12.0; Mo, 13.7 %. Found: C, 51.5; H, 4.2; N, 12.0; Mo, 13.7 %.

*[MoO$_2$(mac^1)](acac)$_2$ (**3**).* Yield 65 %; m.p. 305 °C; Anal. Calcd. for C$_{37}$H$_{36}$MoN$_4$O$_8$ (FW 760.66): C, 58.4; H, 4.7; N, 7.4; Mo, 12.6 %. Found: C, 58.3; H, 4.6; N, 7.3; Mo, 12.5 %.

*[MoO$_2$(mac^2)](acac)$_2$ (**4**).* Yield: 62 %; m.p. 308 °C; Anal. Calcd. for C$_{42}$H$_{38}$MoN$_4$O$_8$ (FW 822.73): C, 61.3; H, 4.6; N, 6.8; Mo, 11.7 % . Found: C, 61.2; H, 4.5; N, 6.7; Mo, 11.6 %.

*[MoO$_2$(mac^3)](acac)$_2$ (**5**).* Yield: 65 %; m.p. 306 °C; Anal. Calcd. for C$_{40}$H$_{33}$F$_3$MoN$_4$O$_8$S (FW 882.73): C, 54.4; H, 3.7; N, 6.3; Mo, 10.9; S, 3.7 %. Found: C, 54.3; H, 3.6; N, 6.2; Mo, 10.8; S, 3.6 %.

*[MoO$_2$(mac^4)](acac)$_2$ (**6**).* Yield 67 %; m.p. 305 °C; Anal. Calcd. for C$_{47}$H$_{40}$MoN$_4$O$_8$ (FW 884.80): C, 63.8; H, 4.6; N, 6.3; Mo, 10.8 %. Found: C, 63.7; H, 4.5; N, 6.2; Mo, 10.8 %.

*[MoO$_2$(mac^5)](acac)$_2$ (**7**).* Yield: 65 %; m.p. 304 °C; Anal. Calcd. for C$_{35}$H$_{34}$MoN$_6$O$_8$ (FW 762.63): C, 55.1; H, 4.5; N, 11.0; Mo, 12.6 %. Found: C, 55.0; H, 4.4; N, 11.0; Mo, 12.5 %.

* Corresponding author. E-mail: devendrapratprao@yahoo.com

[MoO$_2$(mac^6)](acac)$_2$ (8). Yield: 67 %; m.p. 306 °C; Anal. Calcd. for C$_{40}$H$_{36}$MoN$_6$O$_8$ (FW 824.70): C, 58.3; H, 4.4; N, 10.2; Mo, 11.6 %. Found: C, 58.2; H, 4.3; N, 10.1; Mo, 11.5 %.

[MoO$_2$(mac^7)](acac)$_2$ (9). Yield: 62 %; m.p. 308 °C; Anal. Calcd. for C$_{38}$H$_{31}$F$_3$MoN$_6$O$_8$S (FW 884.70): C, 51.6; H, 3.5; N, 9.5; Mo, 10.8; S, 3.6 %. Found: C, 51.5; H, 3.4; N, 9.4; Mo, 10.7; S, 3.5 %.

[MoO$_2$(mac^8)](acac)$_2$ (10). Yield: 65 %; m.p. 304 °C; Anal. Calcd. for C$_{45}$H$_{38}$MoN$_6$O$_8$ (FW 886.77): C, 61.0; H, 4.3; N, 9.5; Mo, 10.8 %. Found: C, 60.9; H, 4.2, N, 9.5; Mo, 10.7 %.

L^1 = ligand derived by condensation of furil with 1,2-diaminobenzene (1:2); L^2 = ligand derived by condensation of furil with 2,3-diaminopyridine(1:2); mac^1 = macrocyclic ligand derived by condensation of L^1 with acetylacetone; mac^2 = macrocyclic ligand derived by condensation of L^1 with benzoylacetone; mac^3 = macrocyclic ligand derived by condensation of L^1 with thenoyltrifluoroacetone; mac^4 = macrocyclic ligand derived by condensation of L^1 with dibenzoylmethane; mac^5 = macrocyclic ligand derived by condensation of L^2 with acetylacetone; mac^6 = macrocyclic ligand derived by condensation of L^2 with benzoylacetone; mac^7 = macrocyclic ligand derived by condensation of L^2 with thenoyltrifluoroacetone; mac^8 = macrocyclic ligand derived by condensation of L^2 with dibenzoylmethane.

INFRARED DATA

TABLE S-I. Infrared spectral bands (ν / cm^{-1}) of the molybdenum complexes. All spectra were recorded in KBr pellets in the range 4000–200 cm^{-1}

Complex	>C=N	Mo–N	>C=O	>C=C<	ν_{asym}	ν_{sym}	ν_{asym}	ν_{sym}
			of acetylacetonate		O=Mo=O		N–H	
[MoO$_2$(L^1)](acac)$_2$	1622	302	1560	1517	906	938	3352	3182
[MoO$_2$(L^2)](acac)$_2$	1620	300	1564	1515	904	936	3350	3180
[MoO$_2$(mac^1)](acac)$_2$	1622	301	1562	1513	903	943	–	–
[MoO$_2$(mac^2)](acac)$_2$	1616	304	1560	1517	904	940	–	–
[MoO$_2$(mac^3)](acac)$_2$	1618	304	1562	1513	905	942	–	–
[MoO$_2$(mac^4)](acac)$_2$	1622	303	1560	1515	904	943	–	–
[MoO$_2$(mac^5)](acac)$_2$	1624	301	1564	1517	908	940	–	–
[MoO$_2$(mac^6)](acac)$_2$	1616	302	1562	1513	906	942	–	–
[MoO$_2$(mac^7)](acac)$_2$	1618	300	1560	1515	904	936	–	–
[MoO$_2$(mac^8)](acac)$_2$	1622	303	1564	1517	905	944	–	–

Synthesis of thiadiazolobenzamide, *via* cyclization of thioxothiourea, and its Ni and Pd complexes

FOROGH ADHAMI[1]*, NASIM NABILZADEH[1], FRANZISKA EMMERLING[2],
MINA GHIASI[3] and MAJID M. HERAVI[3]

[1]*Department of Chemistry, Shahr-rey, IAU, 18155-144, Tehran, Iran,* [2]*BAM Federal
Institute for Materials Research and Testing, Berlin, Germany and*
[3]*Department of Chemistry, Alzahra University, Vanak, Tehran, Iran*

Abstract: In this study, a compound, *N*-(3-methyl-4-oxo-4*H*-[1,3,4]thiadiazo-
lo[2,3-*c*][1,2,4]triazin-7-yl)benzamide, was obtained *via* two different reac-
tions: 1) reaction of 4-amino-6-methyl-3-(methylthio)-1,2,4-triazin-5(4*H*)-one
with benzoyl isothiocyanate under removal of methanethiol and 2) reaction of
4-amino-3,4-dihydro-6-methyl-3-thioxo-1,2,4-triazin-5(2*H*)-one with benzoyl
isothiocyanate under elimination of hydrogen sulfide. In both reactions, a new
bond between sulfur and nitrogen atoms was formed and a five-membered ring
was created. The oxo thiadiazolo benzamide was characterized by IR, ^{1}H-NMR
and ^{13}C-NMR spectroscopy, and mass spectrometry. X-Ray crystallography
was used to shed light on the structure of this new compound. Two new com-
plexes could be generated by coordination of the oxo thiadiazolo benzamide to
Pd(II) and Ni(II) ions. These complexes were analyzed by IR, ^{1}H-NMR and [13]C-
-NMR spectroscopy, conductometry and thermal gravimetry (TGA). The theo-
retical QM calculation GIAO was also applied to predict the structure of the Pd
complex.

Keywords: nucleophilic addition reaction; Pd complexes; QM calculations; GIAO.

INTRODUCTION

The chemistry of isocyanates and isothiocyanates have been greatly investi-
gated.[1,2] Isocyanate and isothiocyanate compounds undergo two kinds of reac-
tions: cycloaddition,[3–5] such as [2+2],[6,7] [3+2],[8,9] [4+2],[10,11] [2+2+2],[12,13] and
nucleophilic addition, such as to thiosemicarbazide,[14] thiosemicarbazone,[15] urea[16]
and thiourea.[17] The nucleophilic addition of an amine group to an isothiocyanate
results in the formation of thiourea, thiosemicarbazide and, in some cases, to

---

1211

benzamide derivatives.[18] Properties such as cytotoxic and antibacterial have been reported for some of these compounds.[19–21] These compounds, as neutral or anionic ligands, can also connect to metal cations and form numerous complexes.[22–24]

In this study, the compounds produced by the nucleophilic addition reaction of benzoyl isothiocyanate with two thiotriazine derivatives were analyzed. In addition, these compounds were used as ligands to produce their nickel(II) and palladium(II) complexes. The biological activities of the obtained complexes were also investigated. The prepared compounds and complexes were analyzed by different techniques and quantum mechanical calculations were employed to confirm additionally the experimental data.

EXPERIMENTAL

4-Amino-6-methyl-3-(methylthio)-1,2,4-triazin-5(4*H*)-one (AMMSTO) and 4-amino-3,4-dihydro-6-methyl-3-thioxo-1,2,4-triazin-5(2*H*)-one (AMTTO) were prepared according to literature procedures.[25] Benzoyl isothiocyanate and the solvents were purchased from Fluka and Merck. All chemicals were used without further purification.

Ultrasonic (Elmasonic S) and microwave (CEM MDS-2000) radiation were applied in the experiments. Melting points were determined using an Electro Thermal IA 9000 instrument. The infrared spectra (on a Nicolet 5SXC employing the KBr disk technique, 4000–400 cm^{-1}) and ^{1}H-NMR and ^{13}C-NMR spectra (on a Bruker Advance 500 spectrometer using DMSO-d_6 and TMS as the internal reference) were recorded at room temperature.

Synthesis of N-*(3-methyl-4-oxo-4*H-*[1,3,4]-thiadiazolo[2,3-c][1,2,4]triazin-7-yl)benzamide (1)*

Benzoyl isothiocyanate (0.156 cm^3, 1 mmol) was gradually added to a solution of 4-amino-6-methyl-3-(methylthio)-1,2,4-triazin-5(4*H*)-one (AMMSTO) (0.2 g, 1 mmol) in acetonitrile (15 cm^3). The mixture was stirred for 7 h at 70–80 °C. The milky precipitate of **1** was filtered, washed with methanol and dried in an oven at 80 °C. Yield: 76 %. The reaction was repeated with the same reactant ratio under other conditions: 1) microwave 360 W, 15 min; 600 W, 3 min in solvent and 600 W, 2 min without solvent, 2) ultrasonic 75 °C, 2 h. The maximum yield of about 81 % was obtained by using microwave 600 W and without solvent.

Synthesis of N-*{[(2,5-dihydro-6-methyl-5-oxo-3-thioxo-1,2,4-triazin-4(3*H*)-yl)amino]thioxomethyl}benzamide (2)*

Benzoyl isothiocyanate (0.156 cm^3, 1 mmol) was gradually added to a solution of 4-amino-3,4-dihydro-6-methyl-3-thioxo-1,2,4-triazin-5(2*H*)-one (AMTTO) (0.158 g, 1 mmol) in ethanol (15 cm^3). The mixture was stirred for 6 h at 70–80 °C. The white precipitate of **2** was filtered, washed with methanol and acetone, and dried in an oven at 80 °C. Yield: 36 %. This reaction was also repeated with the same reactant ratio under the other conditions. The highest yield of 42 % was afforded using microwave 360 W radiation for 15 min and solvent-free.

Synthesis of the Pd and Ni complexes

Synthesis of the palladium complex with N-*(3-methyl-4-oxo-4*H-*[1,3,4]-thiadiazolo[2,3-c][1,2,4]triazin-7-yl)benzamide (1), complex C1.* Complex **C1** was synthesized from palladium(II) chloride (0.04 g, 0.2 mmol) and **1** (0.105 g, 0.3 mmol) in 8 cm^3 acetonitrile. After 1 hour, 1 cm^3 methanol was added and the mixture was stirred under reflux for 4 h. The ob-

tained brown precipitate was filtered, washed with methanol and dried in a vacuum oven. The yield was 82 %. With the same ratio of reactants in DMSO under the other employed conditions, microwave 180 W radiation for 15 min afforded the highest yield of 92 %.

Synthesis of the nickel complex with N-*{[(2,5-dihydro-6-methyl-5-oxo-3-thioxo-1,2,4-triazin-4(3*H*)-yl)amino]thioxomethyl}benzamide (2), Complex **C2***. Complex **C2** was synthesized from nickel(II) acetylacetonate (0.051 g, 0.20 mmol) and **2** (0.064 g, 0.20 mmol) in 4 cm^3 ethanol. The mixture was stirred gently at 70 °C for 10 h. The obtained green precipitate was filtered, washed several times with methanol and dried in a vacuum oven. Repetition of the reaction under the other conditions had no effect on the yield.

Thermal gravimetric analysis and conductivity

Thermal analysis and conductivity of complexes were measured by Module STA 1500 and Metrohm, respectively.

The conductivity of 0.20–0.80 M solutions of complexes in *N,N*-methylformamide was measured at room temperature. No conductivity has been detected. Thermal analysis was performed in air within 100–950 °C temperature range; the heating rate was 40 °C min^{-1}.

X-Ray crystallography

Suitable single crystals of compounds **1** and **2** were obtained by dissolving the corresponding precipitate in a mixture of methanol and acetonitrile (1:1) or methanol and *N,N*-dimethylformamide (1:1), respectively. The data collection for the crystal was realized on a Bruker AXS SMART diffractometer at room temperature using MoK$_\alpha$ radiation (λ = 0.71073 Å) monochromatized by a graphite crystal. Data reduction was completed using the Bruker AXS SAINT and SADABS software packages. The structure of compounds **1** and **2** were solved by direct methods and refined by full-matrix least-squares calculation using SHELX-97. An empirical absorption correction (Ψ-scan) was applied. All non-hydrogen atoms were refined anisotropically. The positions of the hydrogen atoms were calculated corresponding to their geometric conditions and refined using the riding model. Isotropic displacement parameters of hydrogen atoms were derived from the parent atoms.

RESULTS AND DISCUSSION

On reaction of AMMSTO with benzoyl isothiocyanate, methanethiol was released,[26] a five-membered ring was formed and finally *N*-(3-methyl-4-oxo-4*H*--[1,3,4]-thiadiazolo[2,3-*c*][1,2,4]triazin-7-yl)benzamide (**1**) was afforded. *N*-{[(2,5--di–hydro-6-methyl-5-oxo-3-thioxo-1,2,4-triazin-4(3*H*)-yl)amino]thioxomethyl}-benzamide (**2**) was synthesized directly through the reaction of AMTTO with benzoyl isothiocyanate (Scheme 1).

Spectral data for the synthesized compounds and complexes

N-*(3-methyl-4-oxo-4*H-*[1,3,4]-thiadiazolo[2,3-*c*][1,2,4]triazin-7-yl)benzamide (1)*. Decomposed at 300 °C. FTIR (KBr, cm^{-1}): 3212 (NH stretching), 3109 (CH stretching of aromatic ring), 2921 (CH stretching of aliphatic group), 1702 (C=O stretching), 1673 (C=O stretching), 1598, 1566 (NH bending), 1529 (C=N and C=C stretching), 1487 (C=N and C=C stretching), 1296 (C–N– stretching), 1252 (N–N stretching), 1068 (C–N stretching), 713 (C–S stretching). ^{1}H-NMR (500 MHz, DMSO-d_6, δ / ppm): 2.42 (3H, *s*, CH$_3$), 7.58 (2H, *t*, *J* = 7.3 Hz, C2H and

C4H), 7.70 (1H, *t*, *J* = 7.3 Hz, C3H), 8.14 (2H, *d*, *J* = 7.35 Hz, C1H and C5H), 13.76 (1H, *s*, NH). ^{13}C-NMR (125 MHz, DMSO-d_6, δ / ppm): 17.29 (CH$_3$), 128.51 (C2 and C4), 128.77 (C1 and C5), 130.41 (C3), 133.70 (C6), 147.92 (C9), 152.97 (C11), 153.57 (C7), 157.42 (C8), 166.89 (C10). MS (*m/z*, (relative abundance, %)): 211 (C$_6$H$_4$N$_5$O2S$^+$+1, 75), 105 (C$_6$H$_5$CO$^+$, 100), 77 (C$_6$H$_5$$^+$, 88), 51 (C$_4H_3$$^+$, 30). Scheme 1 indicates the C numbering.
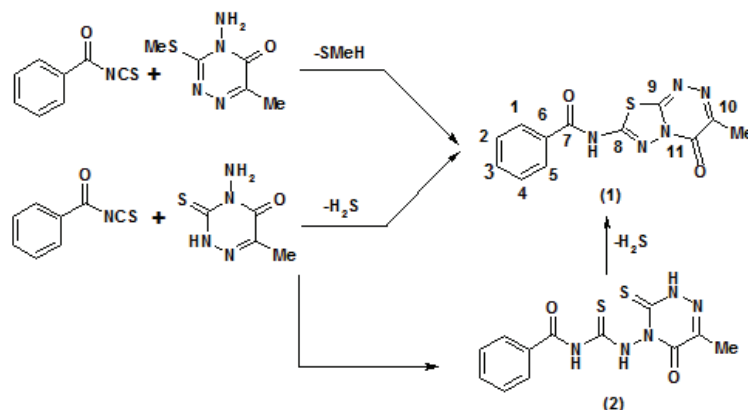
Scheme 1. Reaction pathways of the reactants to **1** and **2**. The C atom numbering is indicated.

N-{[(2,5-di–hydro-6-methyl-5-oxo-3-thioxo-1,2,4-triazin-4(3*H*)-yl)amino]thioxomethyl}benzamide *(2)*. Decomposed at 330 °C. FTIR (KBr, cm^{-1}): 3328 (NH stretching), 3169 (CH stretching of aromatic ring), 2956 (CH stretching of aliphatic group), 1713 (C=O stretching), 1698 (C=O stretching), 1599 (NH bending), 1519 (C=N and C=C stretching), 1490 (C=N and C=C stretching), 1376 (C=S stretching), 1324 (C=S stretching), 1297 (C–N stretching), 1269 (N–N stretching), 1094 (C–N stretching). ^{1}H-NMR (500 MHz, DMSO-d_6, δ / ppm): 2.43 (3H, *s*, CH$_3$), 7.59 (2H, *t*, *J* = 7.3 Hz, C2H and C4H), 7.71 (1H, *t*, *J* = 7.3 Hz, C3H), 8.14 (2H, *d*, *J* = 7.3 Hz, C1H and C5H), 13.71 (1H, *s*, NH). ^{13}C-NMR (125 MHz, DMSO-d_6, δ / ppm): 17.00 (CH$_3$), 128.49 (C2 and C4), 128.77 (C1 and C5), 130.28 (C3), 133.74 (C6), 147.90 (C9), 153.00 (C11), 153.44 (C7), 157.39 (C8), 166.79 (C10). MS (*m/z*, (relative abundance, %)): 321 (C$_{12}$H$_{11}$N$_5$O$_2$S$_2$$^+$, 14.5), 287 (C$_{12}H_9N_5O_2S^+$, 8.5), 158 (C$_4H_5N_4OS^+$+1, 36.5), 105 (C$_6H_5CO^+$, 100), 77 (C$_6H_5$$^+$, 83), 51 (C$_4H_3$$^+$, 23). Scheme 1 indicates the C numbering.

Spectral data for the prepared Ni and Pd complexes

Complex C1. Decomposed at 320 °C. FTIR (KBr, cm^{-1}): 3245 (NH stretching), 3109 (CH stretching of aromatic ring), 2956 (CH stretching of aliphatic group), 1710 (C=O stretching), 1680 (C=O stretching), 1597, 1563 (NH bending), 1492 (C=N and C=C stretching), 1460 (C=N and C=C stretching), 1297 (C–N stretching), 1254 (N–N stretching), 1099 (C–N stretching), 706 (C–S stretching).

^{1}H-NMR (500 MHz, DMSO-d_6, δ / ppm): 2.42 (3H, *s*, CH$_3$), 7.58 (2H, *t*, *J* = 7.3 Hz, C2H and C4H), 7.71 (1H, *t*, *J* = 7.3 Hz, C3H), 8.13 (2H, *d*, *J* = 7.3 Hz, C1H and C5H), 13.70 (1H, *s*, NH). ^{13}C-NMR (125 MHz, DMSO-d_6, δ / ppm): 16.99 (CH$_3$), 128.51 (C2 and C4), 128.78 (C1 and C5), 130.14 (C3), 133.78 (C6), 147.86 (C9), 153.02 (C11), 153.37 (C7), 157.41 (C8), 166.73 (C10). Scheme 1 indicates the C numbering.

Complex C2. Yield: 63 %; decomposed at 220 °C. FTIR (KBr, cm^{-1}): 3365 (NH stretching), 3072 (CH stretching of aromatic ring), 2924 (CH stretching of aliphatic group), 1630 (C=O stretching), 1594 (C=O stretching), 1557 (NH bending), 1525 (C=N and C=C stretching), 1504 (C=N and C=C stretching), 1264 (N–N stretching), 1071 (C–N stretching), 734 (C–S stretching). ^{1}H-NMR (500 MHz, DMSO-d_6, δ / ppm): 2.29 (3H, *s*, CH$_3$), 7.39 (3H, *s*, C2H, C3H and C4H), 8.06 (2H, *s*, C1H and C5H), 2.48 (12H, *s*, CH$_3$, acetylacetonate), 5.42 (2H, *s*, CH, acetylacetonate). ^{13}C-NMR (125 MHz, DMSO-d_6, δ / ppm): 17.05 (CH$_3$), 126.09 (C2 and C4), 126.69 (C1 and C5), 128.88 (C3), 136.29 (C6), 146.06 (C9), 159.85 (C11), 171.57 (C10), 15.52 (CH$_3$, acetylacetonate), 54.41 (CH, acetylacetonate), 196.30 (CO, acetylacetonate). Scheme 1 indicates the C numbering.

IR spectroscopy and mass spectrometry confirmed the synthesis of compound **2** as well as compound **1**. However, although **1** and **2** differed in the absorbance bands in their IR spectra and the peaks in the mass spectra differed significantly, both exhibited the same ^{1}H- and ^{13}C-NMR spectra and X-ray single crystal data. This indicated the instability of **2** in solution and its conversion to **1** by loss of hydrogen sulfide (Scheme 1). The analysis of complex **C2** showed that this conversion also occurred in this complex.

The observed decrease in the wavelength numbers of absorbance bands of carbonyl group in the complex **C2** could be due to the dislocation of the electronic cloud in acetylacetonate and thiadiazolo benzamide. In the NMR spectrum, the resonances of the methyl groups and carbonyl groups of acetylacetonate ions appeared at 15.52 and 196.30 ppm, respectively. The sharp resonances of complexes **C1** and **C2** demonstrated that the Ni(II) and Pd(II) ions with d[8] electronic configuration have diamagnetic properties.

The conductivities of the complexes were measured in *N,N*-dimethylformamide and no conductivity could be detected. The lack of conductivity certified the neutral structure of the complexes. This is evidence for the location of the ligands and the anionic parts in the inner sphere of both complexes.

X-Ray diffraction analysis

The same structures were deduced for **1** and **2**. The relevant crystallographic information on **1** is summarized in Table I and Fig. 1. In the crystal lattice, three interactions were observed between sulfur and nitrogen atoms (S1···N6, medium, 3.161 Å) and sulfur and oxygen atoms (S2···O1, strong, 2.566 Å and S2···O4,

strong, 2.602 Å). Finally, two intermolecular hydrogen bonds joined the molecules together (N5–H5···O3, strong, 2.834 Å and N10–H10A···N3, medium, 3.004 Å).

Thermal analysis

The thermal gravimetric analysis (TGA) and differential thermal analysis (DTA) data for complexes **C1** and **C2** are listed in Table II.

TABLE I. Crystallographic and structure refinement data of **1**

Empirical formula	$C_{12}H_9N_5O_2S$
Formula weight	287.30
T / K	296(2)
Wavelength, Å	0.71073
Crystal system	Monoclinic
Space group	$P2_1/c$
a / Å	7.2750(4)
b / Å	26.6492(15)
c / Å	13.1837(7)
β / °	100.962(4)
V / Å^3	2509.3(2)
Z	8
D / g cm^{-3}	1.521
μ / mm^{-1}	0.267
% Completeness to θ, R(int)	97.5 ($\theta = 34.89°$), 0.0582
Final R indices $(I > 2\sigma(I))$	$R1 = 0.1010$, $wR2 = 0.1329$
R indices (all data)	$R1 = 0.0471$, $wR2 = 0.1143$
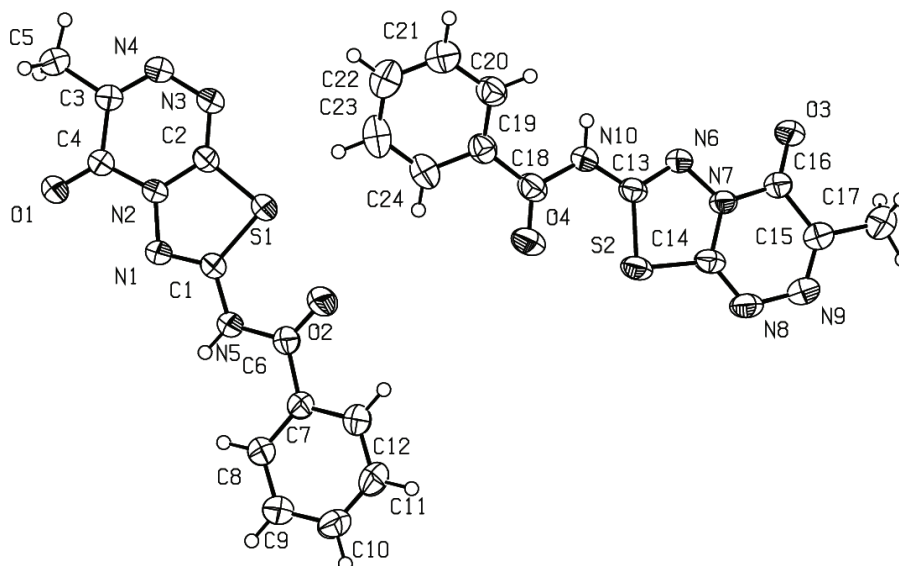
Fig. 1. Molecular structure of compound **1** (50 % probability level).

Thermal gravimetric analyses indicated different behavior of **C1** and **C2** even though both had **1** as the ligand. For both complexes, weight loss occurred in two steps. In the first step complex, **C1** lost two chloride ions above 340 °C and in the second step, compound **1** was lost above 360 °C. On the other hand, in the first step, **C2** lost compound **1** in temperature region 220–414 °C, then the two acetylacetonate ions above 420 °C. This difference could be related to the different number and kinds of bonds between compound **1** and Pd and Ni ions in complexes **C1** and **C2**.

TABLE II. Results of TGA and DTA of **C1** and **C2**

Complex (molecular mass)	TG range, °C	Lost	Residue	Weight loss, %		Reaction pathway
				Found	Calcd.	
C1=PdLCl$_2$ (463.3)	340→358	2Cl	PdL	16	15.34	Endothermic
	360→398	L	PdO	60	62.01	Exothermic
	398→500	PdO	PdO	26	26.33	Endothermic
C2=NiL(acac)$_2$ (543)	220→414	L	Ni(acac)$_2$	51	52.86	Exothermic
	415→498	2acac	NiO	33	36.33	Exothermic
	500→900	NiO	NiO	16	13.75	Exothermic

From the obtained results, the empirical formulas [Pd**1**Cl$_2$] and [Ni**1**(acac)$_2$] could be suggested for complexes **C1** and **C2**, respectively.

THEORETICAL SECTION

Computational details

Ab initio *molecular orbital calculation.* All calculations were performed using Gaussian 98.[27] The energies and geometries of compound **1** and complex **C1** were calculated and optimized with the Lee, Yang and Parr (LYP)[28] correlation functional, denoted B3LYP,[29] of which the most successful one is based on the hybrid functional method.[30] The spin-unrestricted version of B3LYP (U B3LYP) was used with an open-shell singlet electronic configuration of species. The 6-311G** basis set was employed in the geometry optimization and energy calculations. Full optimizations of all the compounds were addressed without any symmetry constraint. Vibration frequency calculations confirmed the stationary geometries.

Solvation calculations were performed on DMSO ($\varepsilon = 46.7$) with the optimized geometries, using the polarized continuum (overlapping spheres) model (PCM) of Tomasi and co-workers.[31]

*Optimization of compound **1***

The structure of compound **1** was fully optimized by the B3LYP method using the 6-311G** basis set with no initial symmetry restrictions and assuming C$_1$ point group.

The optimized geometry of compound **1** in the gas phase was re-optimized considering the solvent effect ($\varepsilon = 46.7$) using polarized continuum (overlapping spheres) model (PCM). The optimized structure of compound **1** in DMSO solvent is shown in Fig. 2. Calculations of the vibrational frequencies have confirmed stationary points with no negative eigen value observed in the force constant matrix.
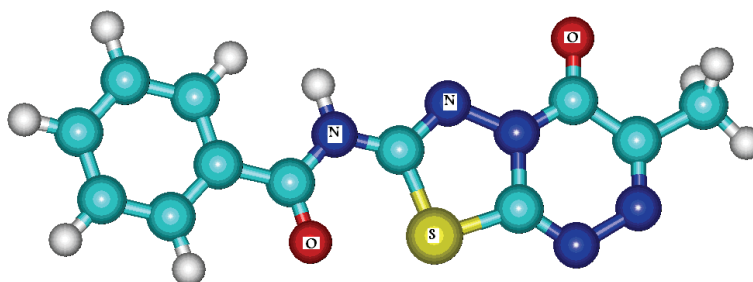
Fig. 2. The optimized structure of compound **1**.

A selection of calculated bond distances, bond angles and dihedral angles of compound **1** are compared with the X-ray data in Table III.

TABLE III. Selected bond distances, Å, and bond and dihedral angles, °, of compound **1** from X-ray analysis and DFT calculations

Bond	X-ray	Calcd.	Bond	X-ray	Calcd.
S1–C2	1.7401(14)	1.757	N1–C1	1.2973(16)	1.297
S2–C14	1.7419(15)		N6–C13	1.2999(18)	
S1–C1	1.7440(13)	1.753	N1–N2	1.3821(15)	1.379
S2–C13	1.7465(13)		N6–N7	1.3857(14)	
O1–C4	1.2093(18)	1.212	N5–C1	1.3775(16)	1.377
O3–C16	1.2215(17)		N10–C13	1.3673(17)	
O2–C6	1.2186(17)	1.221	N5–C6	1.3798(17)	1.380
O4–C18	1.2184(18)		N10–C18	1.3835(18	
Bond angle, °					
C2–S1–C1	87.20(6)	86.32	C1–N5–C6	122.06(11)	124.52
C14–S2–C13	86.95(6)		C13–N10–C18	122.00(12)	
C2–N2–N1	117.37(10)	117.35	N1–C1–S1	118.16(10)	117.20
C14–N7–N6	116.87(11)		N6–C13–S2	118.41(10)	
C2–N3–N4	116.55(11)	116.61	N3–C2–N2	125.55(12)	125.80
C14–N8–N9	116.48(12)		N8–C14–N7	124.98(13)	
Dihedral angle, °					
S1–C1–N5–C6	6.9(2)	0	C1–N5–C6–C7	–179.71(14)	0
N1–C1–N5–C6	–175.03(15)[a]	180.0	N5–C6–C7–C8	1.7(2)[a]	180.0
N1–C1–S1–C2	0.07(13)	0	–	–	–

[a]The direction of the plane was different

Calculation of chemical shifts of compound 1

NMR computations of the absolute shielding were performed using the GIAO method[32] with the DFT optimized structure in the presence of solvent. The ^{1}H- and ^{13}C-NMR chemical shifts were calculated using the corresponding absolute shieldings calculated for Me_4Si at the same level of theory. The obtained calculated values together with the experimental values are given in Table IV. The impressive agreement between the experimental and theoretical chemical shifts confirmed the reliability of DFT calculations for these series of molecules and predicted theoretical results.

TABLE IV. Comparison of some experimental and theoretical ^{1}H-NMR and ^{13}C-NMR chemical shifts, ppm, of **1**

^{1}H	Calcd.	Exp.	^{13}C	Calcd.	Exp.
CH$_3$	2.54	2.42	CH$_3$	19.31	17.29
C2H and C4H	7.73	7.58	C2 and C4	129.24	128.51
C3H	7.93	7.70	C1 and C5	129.52	128.77
C1H and C5H	8.26	8.14	C3	131.25	130.41
NH	13.97	13.76	C6	134.75	133.70
			C10	149.24	147.92
			C11	154.12	152.97
			C7	154.91	153.57
			C8	158.24	157.42
			C9	168.24	166.89

Optimization of the geometries of the Pd(II) complex with 1 in different spin states

The geometry of the [Pd(II)**1**Cl$_2$] complex was estimated for two different coordination modes; complex **A** with S and O atoms coordinated to the Pd ion and complex **B** with N and O atoms coordinated to the Pd ion, Fig. 3. Both complexes were optimized in the singlet and triplet spin states with no symmetry constraint imposed and re-optimized in DMSO solvent by the PCM method. The calculated results showed that the low spin states ($S = 1$) were more stable than high spin states ($S = 3$) in complex **A**, 5.78 kcal mol^{-1} and complex **B**, 6.5 kcal mol^{-1}. Comparison of the energy values between the low spin states of the two complexes indicated **A** (with a six-membered heterocycle) is about 15.5 kcal mol^{-1} more stable than **B** (with a five-membered heterocycle).

The calculated geometrical parameters are presented in Fig. 3 considering its optimized structure at the B3LYP/6-311G** level and the solvent effect.

Given these points, the agreement between the theoretical and experimental results confirmed the suggested structure of complex **C1** and its coordination.

CONCLUSIONS

Compounds **1** and **2** were synthesized through nucleophilic addition reactions and analyzed by IR, NMR and mass spectrometry. Compound **1** was also

characterized by quantum mechanical calculations. In addition, X-ray crystallography was used to determine the structures of compounds. This analysis indicated the cinversion of compound **2** to compound **1** in solution.
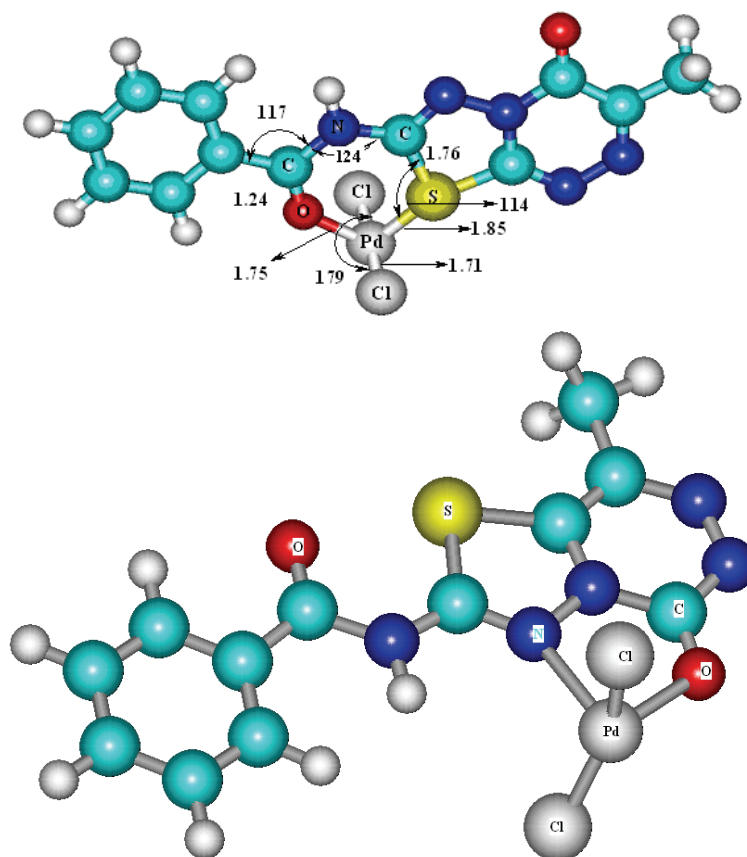
Fig. 3. The optimized structure of the complex **C1** [Pd**1**Cl2] at the B3LYP/6-311G** level in DMSO for the two different possible geometries; complex **A**, O and S atoms connected to Pd, complex **B**, O and N atoms connected to Pd.

In complex **C1**, the Pd(II) ion was surrounded by compound **1** as a new non-ionic ligand and two chloride ions. During the synthesis of complex **C2** of compound **2** and Ni(II) acetylacetonate, conversion of compound **2** to compound **1** occurred, consequently complex **C2** consists also of compound **1**.

Considering the obtained experimental and theoretical data, the following structures are suggested as the most adequate for these complexes:

Complex **C1**: two chloride ions and compound **1** as the bidentate ligand are coordinated to Pd(II) ion forming a square planar complex.

Complex **C2**: a) two acetylacetonate ions and compound **1** as a monodentate ligand are coordinated to Ni(II) ions producing a square pyramidal complex, b) two acetyl acetonate ions and compound **1** as bidentate ligand are connected to Ni(II) ions constructing a distorted octahedral complex.

SUPPLEMENTRY MATERIAL

CCDC 758812 contains the supplementary crystallographic data. Data can be obtained free of charge via http://www.ccdc.cam.ac.uk/conts/retrieving.html or from the Cambridge Crystallographic Data Centre, 12 Union Road, Cambridge CB2 1EZ, UK; fax: (+44) 1223-336-033). Conductivity diagram of complexes and Crystal packing with hydrogen bonding of compound **1** are available electronically from http://www.shd.org.rs/JSCS/, or from the corresponding author on request.

И З В О Д

СИНТЕЗА ТИЈАДИАЗОЛО-БЕНЗАМИДА У РЕАКЦИЈИ ЦИКЛИЗАЦИЈЕ ТИОКСОТИОУРЕЕ И ЊЕГОВИХ Ni(II) И Pd(II) КОМПЛЕКСА

FOROGH ADHAMI[1], NASIM NABILZADEH[1], FRANZISKA EMMERLING[2], MINA GHIASI[3] и MAJID M. HERAVI[3]

[1]Department of Chemistry, Shahr-rey, IAU, 18155-144, Tehran, Iran, [2]BAM Federal Institute for Materials Research and Testing, Berlin, Germany и [3]Department of Chemistry, Alzahra University, Vanak, Tehran, Iran

У овом раду, једињење *N*-(3-метил-4-оксо-4*H*-[1,3,4]тијадиазоло[2,3-*c*][1,2,4]три-азин-7-ил)бензамид добијено је на два различита начина: 1) у реакцији између 4-амино--6-метил-3-(метилтио)-1,2,4-триазин-5(4*H*)-она и бензоил-изотиоцијаната уз елимина-цију метантиола и 2) у реакцији између 4-амино-3,4-дихидро-6-метил-3-тиоксо-1,2,4--тризин-5(2*H*)-она и бензоил-изотиоцијаната уз елиминацију водониксулфида. У овим реакцијама долази до грађења нове везе између атома сумпора и азота, при чему се формира петочлани прстен. Добијени оксотијадиазоло-бензамид је окарактерисан при-меном IR, ^{1}H- и ^{13}C-NMR спектроскопије, као и масене спектрометрије. Поред тога, структура новог једињења је потврђена применом рендгенске структурне анализе. Коор-динацијом оксотијадиазоло-бензамида за Pd(II) и Ni(II) јоне настају два нова комплекса, који су карактерисани применом IR, ^{1}H- и ^{13}C-NMR спектроскопије, као и помоћу кон-дуктометрије и термалне гравиметрије (TGA). Поред тога, структура Pd(II) комплекса је предвиђена применом теоријских квантномеханичких (QM) израчунавања GIAO.

REFERENCES

1. H. Ulrich, *Chemistry and Technology of Isocyanates*, Wiley, New York, USA, 1996
2. L. Drobnica, P. Kristian, J. Augustin, *The Chemistry of Cyanates and their Thio Derivatives*, Wiley, New York, USA, 1977, p. 1003
3. A. K. Mukerjee, R. Ashare, *Chem. Rev.* **91** (1991) 1
4. G. Labbe, K. Buelens, *J. Heterocycl. Chem.* **27** (1990) 199
5. I. Devi, H. N. Borah, P. J. Bhuyan, *Tetrahedron Lett.* **45** (2004) 2405
6. O. Tsuge, S. Kanemasa, K. Matsuda, *J. Org. Chem.* **49** (1984) 2688
7. H. Ulrich, R. Richter, B. Tucker, *Chem. Ber.* **120** (1986) 849
8. G. Labbe, I. Sannen, A. Vandendriessche, *J. Heterocycl. Chem.* **29** (1992) 69
9. X. Yuanyuan, C. Xiaodong, S. Weike, *J. Chem. Res.* (2009) 129

10. G. Abbiati, A. C. Carvalho, E. Rossi, *Tetrahedron* **59** (2003) 7397
11. A. S. Valueva, G. N. Nikonov, R. M. Kamalov, N. A. Khailova, M. A. Pudovik, *Russ. Chem. Bull*. **40** (1991) 1088
12. K. Tanaka, A. Wada, K. Noguchi, *Org. Lett*. **8** (2006) 907
13. Y. Yamamoto, H. Takagishi, K. Itoh, *J. Am. Chem. Soc.* **124** (2002) 28
14. F. F. Jian, Z. S. Bai, H. L. Xiao, K. Li, *Acta Crystallogr., E* **61** (2005) 653
15. M. A. Kaldrikyan, L. A. Grigoryan, R. G. Melik-Ogandzhanyan, F. G. Arsenyan, *Pharm. Chem. J*. **43** (2009) 242
16. V. Antochshuk, O. Olkhovyk, M. Jaroniec, I. S. Park, R. Ryoo, *Langmuir* **19** (2003) 3031
17. J. L. J. Blanco, C. S. Barría, J. M. Benito, C. O. Mellet, J. Fuentes, F. S. González, J. M. G. Fernández, *Synthesis* (1999) 1907
18. F. T. Coppo, M. M. Fawzi, *J. Heterocycl. Chem*. **34** (1997) 1351
19. A. E. Souza, K. Pissinate, M. G. Nascimento, N. F. Grynberg, A. Echevarria, *Bioorg. Med. Chem*. **14** (2006) 492
20. X. Xiong, H. Liu, L. Fu, L. Li, J. Li, X. Luo, C. Mei, *Chemotherapy* **54** (2008) 463
21. S. A. Khan, N. Singh, K. Saleem, *Eur. J. Med. Chem*. **43** (2008) 2272
22. E. Labisbal, K. D. Haslow, A. S. Pedrares, J. V. Martínez, S. H. Ortega, D. X. West, *Polyhedron* **22** (2003) 2831
23. V. V. Pavlishchuk, S. V. Kolotilov, A .W. Addison, R. J. Butcher, E. Sinn, *J. Chem. Soc., Dalton Trans*. (2000) 335
24. A. Tadjarodi, F. Adhami, Y. Hanifehpour, M. Yazdi, Z. Moghaddamfard, G. Kickelbick, *Polyhedron* **26** (2007) 4609
25. A. Dornow, H. M. Enzel, P. Marx, *Chem. Ber*. **97** (1964) 2173
26. P. Molina, M. Alajarin, R. Benzal, *Synthesis* **9** (1983) 759
27. Gaussian (Revision-B), Gaussian, Inc., Pittsburgh, PA, 2003
28. A. D. Beck, *J. Chem. Phys*. **98** (1993) 5648
29. R.G. Parr, W. Yang, *Density-Functional Theory of Atoms and Molecules*, Oxford University Press, New York, USA, 1989
30. E. M. Siegbahn, *Faraday Discuss*. **289** (2003) 124
31. V. Barone, M. Cossi, J. Tomasi, *J. Comput. Chem*. **19** (1998) 404
32. K. Wolinski, J. F. Hilton, P. Pulay, *J. Am. Chem. Soc*. **112** (1990) 8251.

SUPPLEMENTARY MATERIAL TO

Synthesis of thiadiazolobenzamide, *via* cyclization of thioxothiourea, and its Ni and Pd complexes

FOROGH ADHAMI[1]*, NASIM NABILZADEH[1], FRANZISKA EMMERLING[2], MINA GHIASI[3] and MAJID M. HERAVI[3]

[1]*Department of Chemistry, Shahr-rey, IAU, 18155-144, Tehran, Iran*, [2]*BAM Federal Institute for Materials Research and Testing, Berlin, Germany and* [3]*Department of Chemistry, Alzahra University, Vanak, Tehran, Iran*
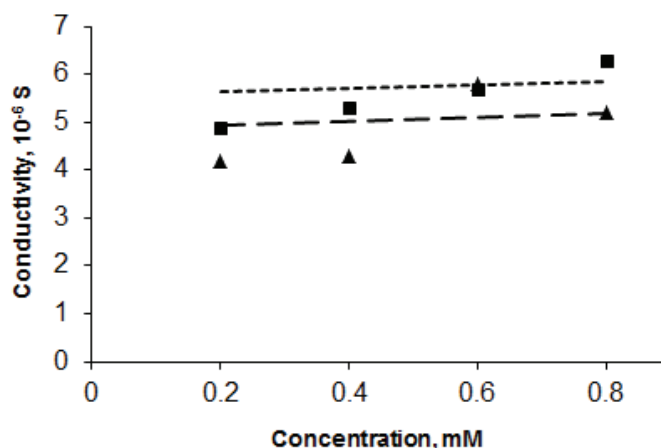
Fig. S1. Conductivity diagram of the complexes.

* Corresponding author. E-mail: fadhami@iausr.ac.ir
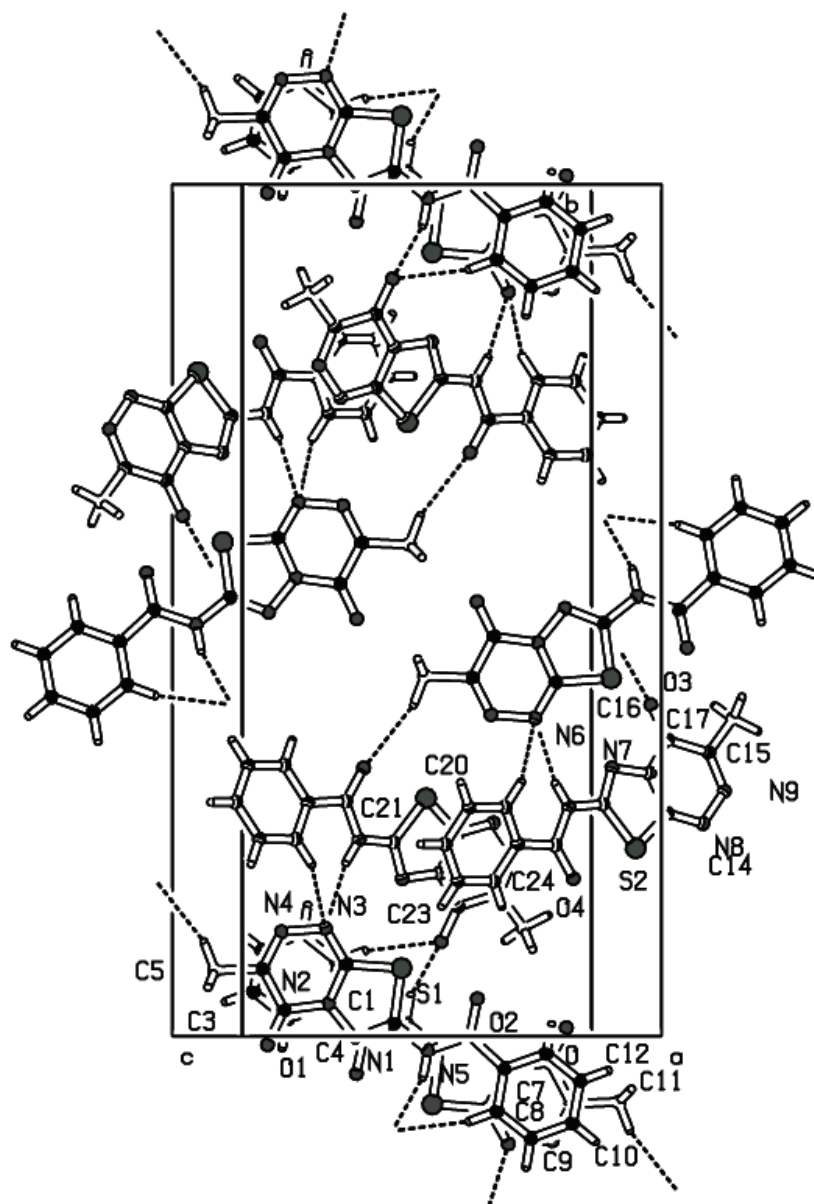
Fig. S2. Crystal packing with hydrogen bonding of compound **1.**

Synthesis and photovoltaic properties of octacarboxy-metallophthalocyanine dyes applied in dye-sensitized solar cells

LING JIN, WEI CHEN and DAJUN CHEN*

State Key Laboratory for Modification of Chemical Fibers and Polymer Materials, College of Materials Science and Engineering, Donghua University, Shanghai 201620, China

Abstract: A series of octacarboxy-metallophthalocyanine dyes with different central metal ions, *i.e*., MgOCPc, MnOCPc, FeOCPc and ZnOCPc, were designed and synthesized by microwave irradiation. The effects of the introduction of different metal ions with variant 3d orbitals ($3d^0$, $3d^5$, $3d^6$, and $3d^{10}$, respectively) in the centre of the phthalocyanine rings on the thermal, photophysical, and electrochemical properties of octacarboxy-metallophthalocyanines were characterized and evaluated in detail. The results showed that ZnOCPc and MgOCPc, with closed-shell metal ions, and FeOCPc, with an open-shell metal ion, had excellent thermal properties. However, MnOCPc, with a half-full-shell metal ion, exhibited the lowest decomposition temperature and largest Q-band red shifts. The energy gaps of MgOCPc, MnOCPc, FeOCPc and ZnOCPc were theoretically calculated to be 0.11, 0.10, 0.20 and 0.22V, respectively. Applied in TiO_2 nanocrystalline dye-sensitized solar cells (DSSC), the photovoltaic properties of the four dyes were obtained under AM1.5 irradiation (100 mW cm^{-2}).

Keywords: octacarboxy-metallophthalocyanine dyes; 3d orbital; photophysical properties; electrochemical properties; energy gaps; DSSC.

INTRODUCTION

Owing to their extensively delocalized 18-π electron system consisting of four isoindole subunits linked together through nitrogen atoms,[1,2] phthalocyanines (Pcs) possess interesting properties, such as high thermal and chemical stability, efficient light absorption from the red to the near infrared region(NIR) of the optical spectrum, and both semi- and photoconducting characteristic.[3] Pcs and their metallo-derivatives have received considerable attention in recent years and have been intensively applied as optical recording media,[4] liquid crystals,[5]

1223

photodynamic therapy for cancer,[6] nonlinear optical materials (NLO),[7] electro-catalytic detection,[8] photovoltaic cells[9–11] and many other fields.

Pcs are of interest as NIR photosensitizers for employment in dye-sensitized solar cells (DSSC) due to their above-mentioned excellent properties. DSSC are based on photo-induced electron injection from excited molecules into the conduction band of a nanocrystalline metal oxide film.[1] Thus, the current is generated when photons absorbed by dye molecules that are placed over a layer of a wide band-gap semiconducting material such as a mesoporous metal oxide, *e.g.*, TiO_2.[1,12] However, for a long time, the applications of Pc dyes in DSSC was restricted due to their poor solubility in organic solvents and other factors.[13] To improve their water solubility, Pcs were functionalized with carboxy-,[14–17] sulfo-[9] and ester groups.[18] Grätzel and Nazeeruddin *et al.*[9] reported on the use of different substituted zinc(II) and aluminum(III) phthalocyanines using the tetracarboxylate functionality as efficient charge transfer sensitizers. They and Hagfeldt *et al.*[14] designed a new type of zinc phthalocyanines with tyrosine substituents (ZnPcTyr) and glycine substituents (ZnPcGly) to make the dyes ethanol-soluble and enhance significantly the solar cell performance. Boston[19] and co-workers first reported the synthesis of copper phthalocyanine octacarboxylic acid. Matemadombo and Nyokong[20] used cobalt octacarboxy phthalocyanine (CoOCPc) adsorbed onto glassy carbon electrodes for the electrocatalytic detection of nitrite, L-cysteine and melatonin. Masilela and Nyokong[21] synthesized water-soluble octacarboxylated Ga phthalocyanine and discussed its photophysical properties. However, there are hardly any reports describing the application of octacarboxy-metallophthalocyanines for DSSC.

Conventional heating methods, involving the use of an oil bath or muffle furnace that heat the reactor wall by convection, result in slow and time-consuming syntheses of metallophthalocyanines. However, using a microwave heating system, which is able to heat target compounds and produce more uniform thermal energy making molecules dramatically collide, heat is generated from inside the target compounds in contrast with the conventional heating methods where heat is transferred from outside to inside.[22,23] Thus, the synthesis time is remarkably reduced and the yield of reaction product greatly increased when a microwave heating system is employed.

In this work, four octacarboxy-metallophthalocyanine dyes (MOCPc) containing different central metals (Mg, Mn, Fe and Zn) were designed and synthesized by microwave irradiation. Herein, the effect of the introduction of different metal ions with variant 3d orbitals ($3d^0$, $3d^5$, $3d^6$ and $3d^{10}$, respectively) in the centre of the phthalocyanine rings on the thermal, photophysical and electrochemical properties of octacarboxy-metallophtalocyanines were investigated. Moreover, the four dyes were applied in nanocrystalline TiO_2–dye-sensitized solar cells and their photovoltamic performances were measured.

EXPERIMENTAL

Materials

Pyromellitic dianhydride, urea, hexaammonium heptamolybdate tetrahydrate, zinc chloride, iron(II) chloride tetrahydrate, manganese(II) chloride tetrahydrate, magnesium chloride hexahydrate, potassium hydroxide, tetrabutylammonium perchlorate (TBAP) and hydrochloric acid (37 %) of analytical grade were purchased from Sinopharm Chemical Reagent Co., Ltd.. The acetone and dimethylsulfoxide (DMSO) used in this work were of reagent grade and were used without further purification.

Synthesis of the octacarboxy-metallophthalocyanine dyes

The MOCPc were synthesized by microwave irradiation from pyromellitic dianhydride, metal halide and urea, as shown in Scheme 1.
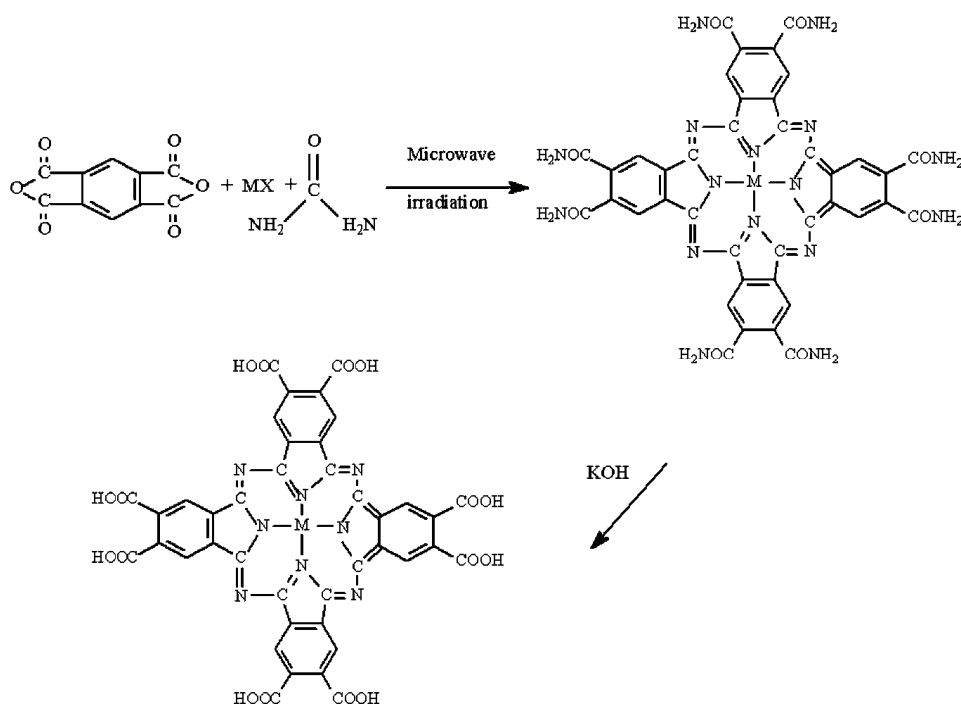
Scheme 1. Molecular structures and synthesis of the octacarboxy-metallophthalocyanine dyes.

Synthesis of octacarboxy-metallophthalocyanine of zinc: pyromellitic dianhydride (5.05 g, 23.1 mmol), urea (26.0 g, 0.430 mol), $ZnCl_2$ (6.28 g, 46.2 mmol) and hexaammonium heptamolybdate tetrahydrate (0.2 g) were ground together in a 500 ml beaker and irradiated in a microwave oven at 320 W for 10 min. The black solid was then cooled and washed with water, acetone, and dried in air. Next, the crushed solid was stirred in 6 M HCl solution (200 ml) for 30 min. This procedure was repeated three times and the supernatant liquid was decanted each time. Finally, the solid was hydrolyzed in 10 % NaOH water solution (250 ml), and the mixture was heated for 8–10 h at 85 °C with stirring. The reaction mixture was then diluted with distilled water (100 ml), filtered through a No. 5 sintered glass funnel, and the

filtrate was slowly acidified to pH ≥ 3 with concentrated HCl (12 M). At this point, the product completely precipitated as a blue, flocculent solid and was washed with the distilled water and acetone until the mixture solution was a clear color. This was allowed to settle, and most of the supernatant liquid was decanted. The blue product that precipitated was separated from the liquor using a centrifuge and then dried in a vacuum drying oven at 30 °C. The solid reaction product was quite soluble in water, although it dissolved slowly, and somewhat soluble in acetone. It was, however, insoluble in acidic aqueous solutions. The same procedure was adopted in the preparation of the respective magnesium, manganese, and iron octacarboxy phthalocyanines, M(OCPc) (M = Mn or Fe). Their IR spectra and NMR spectra were similar to those of ZnOCPc.

Characterizations

IR spectra (KBr pellets) were recorded on a Nicolet 8700 FTIR spectrometer. ^{1}H-NMR spectra were obtained using a Bruker AV 400 MHz NMR spectrometer. Thermal properties were tested on an Iris 209 F1 thermo gravimetric analyzer at a heating rate of 10 °C min^{-1} under nitrogen. The UV–Vis spectra were investigated on a Lambda A35 UV–Vis/NIR spectrophotometer. Fluorescence excitation and emission spectra were recorded on a FP-6600 spectrofluorometer. The samples were contained in 1 cm path-length quartz cells. The electrochemical properties were measured with a CIMPS-1 electrochemical workstation. In addition, cyclic voltammetry measurements (CV) were realized in a three-electrode measuring cell with a glassy carbon working electrode, a Pt wire counter electrode and an Hg/Hg_2Cl_2 reference electrode. The supporting electrolyte was 0.1 M TBAP in DMSO.

ZnOCPc. Yield: 35 %; Anal. Calcd. for $C_{40}H_{16}N_8O_{16}Zn$ ($16H_2O$): C, 40.51; H, 4.05; N, 9.45 %. Found: C, 39.11; H, 3.83; N, 8.53 %; IR (KBr, cm^{-1}): 3388 (O–H stretching of COOH group), 3144 (C–H stretching of aromatic ring), 1701 (C=O stretching of COOH group), 1302 (C–O stretching of COOH group), 1624 (C=N or C=C stretching of phthalocyanine ring), 1353, 1094 (C–C or C–N stretching of phthalocyanine ring), 739 (C–H stretching of aromatic ring); ^{1}H-NMR (400 MHz, DMSO-d_6, δ / ppm): 8.78 (8H, *s*, terminal phenyl), 10.07 (8H, *s*, COOH); ^{13}C-NMR (100 MHz, DMSO-d_6, δ / ppm): 138.30 (C_{quat}), 136.43 (C_{quat}), 171.44 (COO), 171.13 (COO), 170.08 (COO), 169.46 (COO), 155.94 (CN), 142.99 (CN), 141.25 (CN), 128.80 (CH), 128.03 (CH).

FeOCPc. Yield: 40 %; Anal. Calcd. for $C_{40}H_{16}N_8O_{16}Fe$ ($16H_2O$): C, 40.82; H, 4.08; N, 9.52 %. Found: C, 39.32; H, 3.93; N, 8.69 %; IR (KBr, cm^{-1}): 3398 (O–H stretching of COOH group), 3168 (C–H stretching of aromatic ring), 1710 (C=O stretching of COOH group), 1312 (C–O stretching of COOH group), 1620 (C=N or C=C stretching of phthalocyanine ring), 1359, 1094 (C–C or C–N stretching of phthalocyanine ring), 748 (C–H stretching of aromatic ring).

MnOCPc. Yield: 25 %; Anal. Calcd. for $C_{40}H_{16}N_8O_{16}Mn$ ($16H_2O$): C, 40.85; H, 4.09; N, 9.53 %. Found: C, 39.37; H, 3.92; N, 8.63 %; IR (KBr, cm^{-1}): 3406 (O–H stretching of COOH group), 3163 (C–H stretching of aromatic ring), 1702 (C=O stretching of COOH group), 1304 (C–O stretching of COOH group), 1623 (C=N or C=C stretching of phthalocyanine ring), 1362, 1088 (C–C or C–N stretching of phthalocyanine ring), 719 (C–H stretching of aromatic ring).

MgOCPc. Yield: 15%; Anal. Calcd. for $C_{40}H_{16}N_8O_{16}Mg$ ($16H_2O$): C, 41.96; H, 4.20; N, 9.79 %. Found: C, 40.31; H, 3.98; N, 8.78 %; IR (KBr, cm^{-1}): 3415 (O–H stretching of COOH group), 3169 (C–H stretching of aromatic ring), 1706 (C=O stretching of COOH group), 1304 (C–O stretching of COOH group), 1621 (C=N or C=C stretching of phthalocyanine ring), 1358, 1083 (C–C or C–N stretching of phthalocyanine ring), 735 (C–H stretch-

ing of aromatic ring); ^{1}H-NMR (400 MHz, DMSO-d_6, δ / ppm): 7.50 (8H, *s*, terminal phenyl), 9.76 (8H, *s*, COOH); ^{13}C-NMR (100 MHz, DMSO-d_6, δ / ppm): 138.04 (C_{quat}), 170.97 (COO), 170.04 (COO), 169.68 (COO), 152.68 (CN), 127.70 (CH).

Fabrication of dye-sensitized solar cells

The DSSC consisted of a dye-adsorbed TiO_2 electrode, a counter electrode, and an organic electrolyte. The electrolyte solution was a mixture of DMPII/LiI/I_2/TBP/GuSCN. The TiO_2 electrodes with a 0.23 cm^2 working area were purchased from Dalian HeptaChroma Solar-Tech Co. They were heated at 450 °C for 30 min and then allowed to cool to 80–90 °C before immersion in the dye solutions. The dye solutions were prepared in DMSO at a concentration of 1.8×10^{-5} M. The TiO_2 electrodes were immersed into the dye solutions for 6 h at room temperature. Finally, the dye-adsorbed TiO_2 electrodes were rinsed several times with DMSO and ethanol to remove non-adsorbed dye and then dried quickly under a N_2 flow. As a counter electrode, a thin Pt layer was deposited on FTO conducting glass. The photovoltaic performance of the DSSC device was measured using a Keithley 2400 digital source meter under 100 mW cm^{-2} simulated air mass (AM) 1.5 solar light illumination.

The fill factor (*FF*) is defined by the following equation:[24]

$$FF = j_m V_m / j_{sc} V_{oc} \tag{1}$$

where j_m and V_m are the photocurrent density and voltage for maximum power output, respectively, and j_{sc} and V_{oc} are the short circuit photocurrent density and open circuit voltage, respectively.

The solar energy-to-electricity conversion efficiency (η) of a DSSC is calculated from j_{sc}, V_{oc}, *FF* and the intensity of the incident light (P_{in}) according to the following equation:[25]

$$\eta = j_{sc} V_{oc} FF / P_{in} \tag{2}$$

RESULTS AND DISCUSSION

Thermal properties

The incorporation of a metal ion into the central cavity affects thermal stability of phthalocyanines, which could be due to how different metals interact with phthalocyanine rings. The thermal properties of the four dyes are shown in Fig. 1. The valence electron distribution and ionic radius of metal ion and the data of the decomposition temperature of the four dyes are collected in Table I. The decomposition temperature of MnOCPc with a half-full-shell metal ion is lower than that of the other dyes. As Table 1 shows, the ionic radius of Mn^{2+} with a $3d^5$ orbital is the largest, which may result in the central metal interacting weakly with the phthalocyanine ring giving rise to the lowest decomposition temperature.[26–28] The decomposition temperature of FeOCPc with an open-shell metal ion is the highest due to the strong interaction between the metal and the Pc ligand. On the other hand, ZnOCPc and MgOCPc with closed-shell metal ions may form outer-orbital complexes, while FeOCPc is an inner-orbital complex, which leads to the thermal stability of ZnOCPc and MgOCPc being slightly lower than that of FeOCPc.
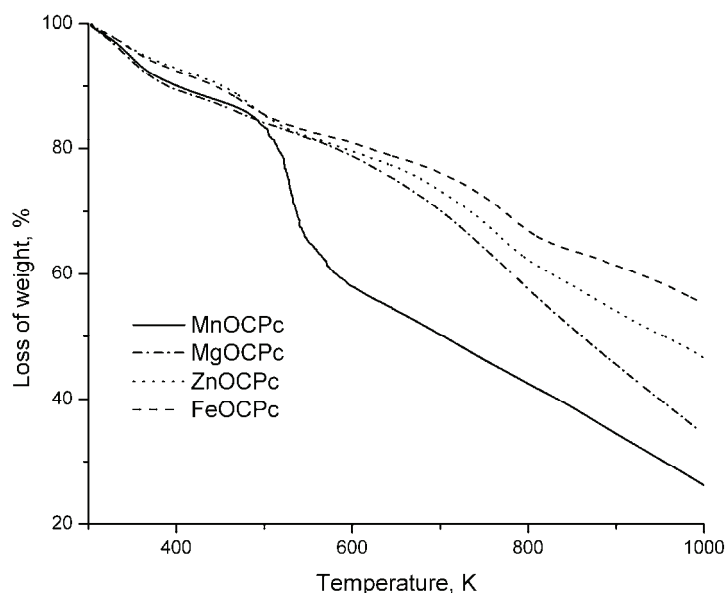
Fig. 1. Thermal properties of the four dyes.

TABLE I. Valance electron distribution of the metal ion and thermal decomposition tempe-rature of the four dyes

Dye	Metal ion	Ionic radius pm	Valence electron distribution	Decomposition temperature, K
MgOCPc	Mg^{2+}	66	$1s^22s^22p^6$	748
MnOCPc	Mn^{2+}	90	$1s^22s^22p^63d^5$	529
FeOCPc	Fe^{2+}	85	$1s^22s^22p^63d^6$	777
ZnOCPc	Zn^{2+}	83	$1s^22s^22p^63d^{10}$	765

Photophysical properties

The UV–Vis spectra of the octacarboxy-metallophthalocyanine dyes in DMSO solution are displayed in Fig. 2, and the Q band maximum absorption wavelength and the molar extinction coefficient of the four dyes are summarized in Table II.

The absorption bands of the four as-synthesized dyes are similar and exhibit the features typical of a phthalocyanine ring, with a Soret band (B-band) in the range 300–400 nm. The Q band in the NIR region 600–800 nm is assigned to a ligand-centered π–π^* transition from the highest occupied molecular orbital (HOMO) to the lowest unoccupied molecular orbital (LUMO) in the main con-jugation system of the phthalocyanine macro-ring. The position of the Q band and the shape of the spectral curve are determined by the nature of the metal, substituents on the benzene rings, solvent, concentration, and other factors.[29] It is evident that the Q bands of the four dyes have different red shifts following the

order MnOCPc > MgOCPc > ZnOCPc > FeOCPc. In DMSO, the absorption spectrum of MnOCPc has a Q band peak at 725 nm, while the Q band of MnOCPc is strongly red-shifted 38 nm when compared to FeOCPc and 22 nm when compared to that of MgOCPc. The observed red shifts could be attributed to the linear combination of the atomic orbitals (LCAO) coefficient in MnOCPc of the HOMO being greater than are those of ZnOCPc and FeOCPc, resulting in the HOMO level of MnOCPc being destabilized more than are those of ZnOCPc and FeOCPc. As a result, the energy gap between the HOMO and LOMO becomes smaller leading to the generated red shifts.
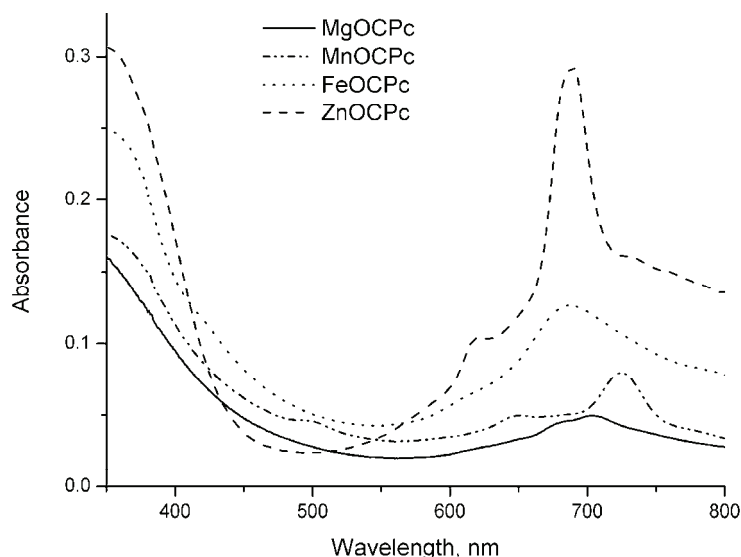
Fig. 2. UV–Vis absorption spectra of the four dyes in DMSO solution at concentrations of about 7.2×10^{-6} M.

TABLE II. The absorption and the molar extinction coefficient data for the four dyes

Dye	Q band, λ_{max} / nm	ε_{max}[a] / M^{-1} cm^{-1}
MgOCPc	703	6856
MnOCPc	725	11022
FeOCPc	687	17576
ZnOCPc	689	40697

[a]ε_{max} is the molar extinction coefficient at λ_{max} of absorption

The four dyes (MgOCPc, MnOCPc, FeOCPc and ZnOCPc) showed similar fluorescence behavior in DMSO. The fluorescence emission and excitation spectra for the four dyes measured in DMSO are shown in Fig. 3 and the maximum emission and excitation data are summarized in Table III. In DMSO, the emission peaks were observed at 709 (MgOCPc), 725 (MnOCPc), 695 (FeOCPc) and

698 nm (ZnOCPc). The excitation spectra of the four dyes were mirror images of the fluorescent spectra in DMSO except for the spectra of MnOCPc. This can be explained by MnOCPc as an intermediate-spin complex[26] has an unable excitation state. The observed Stokes shift were typical of the four dyes in DMSO and were similar, *i.e.*, 6 (MgOCPc), 5 (MnOCPc), 6 (FeOCPc) and 9 nm (ZnOCPc).

A

B
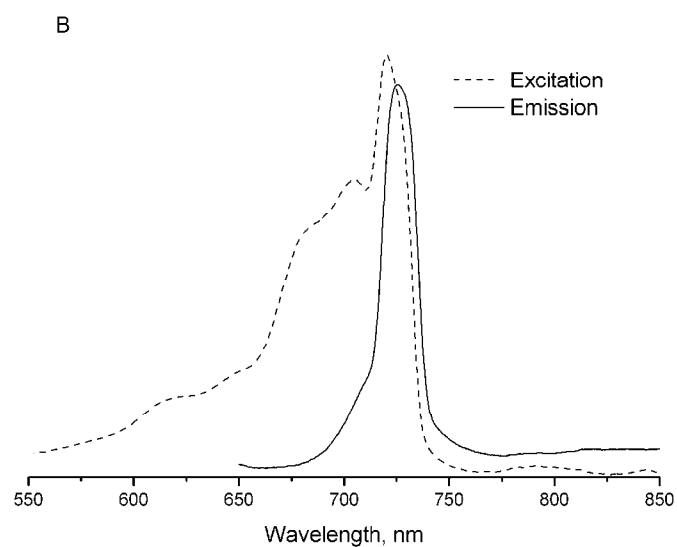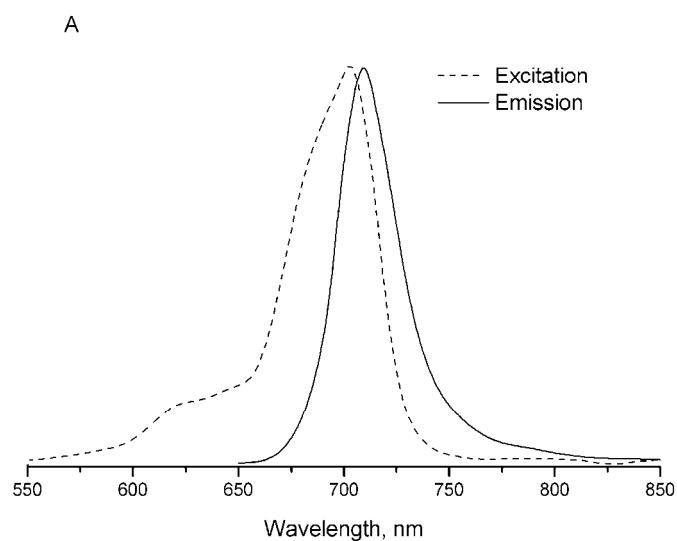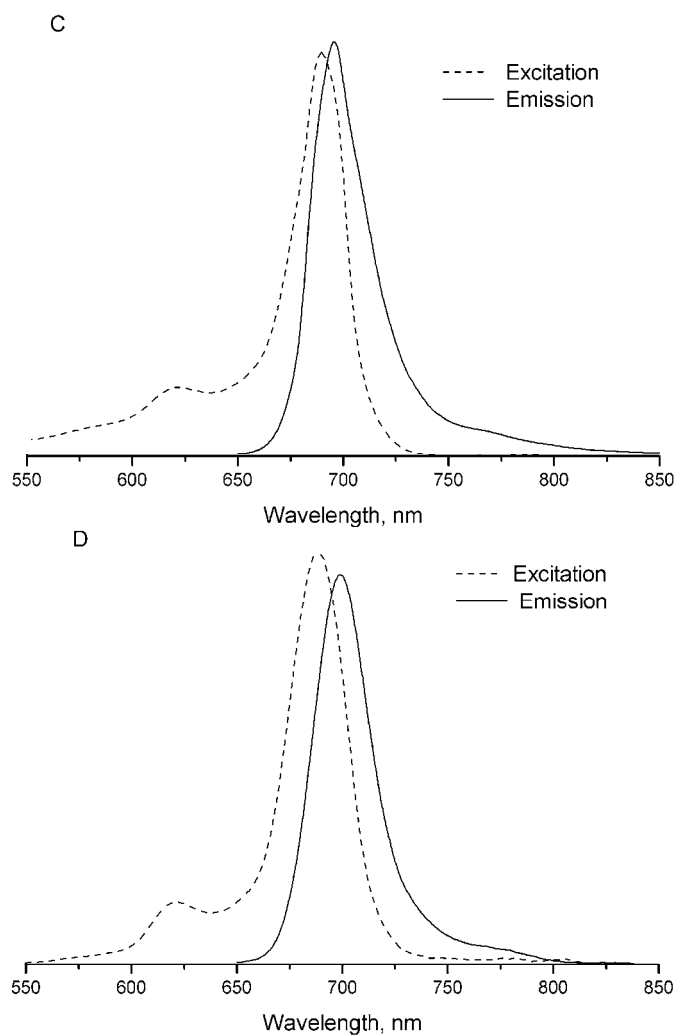
Fig. 3. Emission and excitation spectra of the four dyes in DMSO solution: A) MgOCPc; B) MnOCPc; C) FeOCPc; D) ZnOCPc. The solution concentrations of samples were about 7.2×10^{-6} M.

TABLE III. Fluorescence emission and excitation spectral parameters of the four dyes

Dye	Emission, λ_{em} / nm	Excitation, λ_{ex} / nm	Stokes shift, Δ_{Stokes}
MgOCPc	709	703	6
MnOCPc	725	720	5
FeOCPc	695	689	6
ZnOCPc	698	689	9

Electrochemical properties

To judge the possibilities of electron transfer from the excited molecules of the dyes to the conduction band of TiO_2 and the regeneration of the dyes, their excited-state redox potentials, which play an important role in the electron-injection process, were measured *via* CV,[30] as shown in Fig. 4. The value can be derived from the ground-state oxidation potential and the zero-zero excitation energy ($E_{(0–0)}$), according to the following equation:

$$E_{(S^+/S^*)} = E_{(S^+/S)} - E_{(0–0)} \tag{3}$$
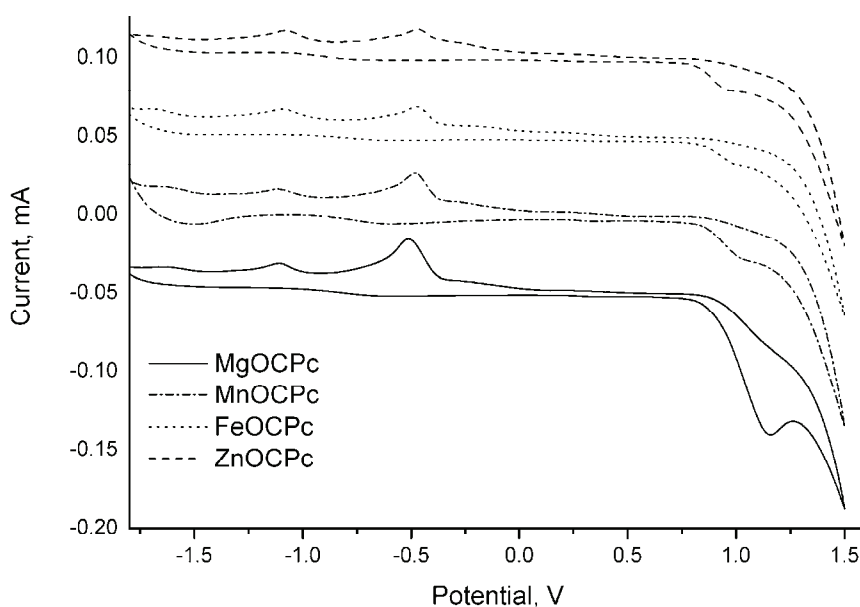
Fig. 4. Electrochemical properties of the four dyes from cyclic voltammetry.

As shown in Table IV, the $E_{(0–0)}$ energies of 1.76, 1.71, 1.79 and 1.78 eV were extracted for MgOCPc, MnOCPc, FeOCPc and ZnOCPc, respectively, from the intersection between the absorption and emission spectra. The energy levels of the four dyes in comparison to the TiO_2 conduction band and the redox couple I^-/I_3^- are illustrated in Fig. 5. It is well known that the efficiency of a dye-sensitized solar cell depends on the balance between the electron injection into the conduction band and the back transfer of injected electrons from the conduction band of TiO_2 to the dye cation radical. The HOMO levels of the four dyes, ranging from 1.15 to 1.06 V *vs.* NHE, were more positive than that of the I^-/I_3^- redox couple (≈ 0.4 V *vs.* NHE), ensuring that sufficient driving force exits for the efficient regeneration of the dyes through the recapture of the injected electrons from I^- by the dyes cation radical.[31] Furthermore, provided that an energy gap of 0.2

eV is necessary for efficient electron injection, these thermodynamic driving forces are sufficient for efficient charge injection. Thus, the electron injection process from the excited dye molecule to the TiO_2 conduction band and the sub-sequent dye regeneration are energetically permitted.[30] From Table IV, it is clear that the energy gaps of MgOCPc, MnOCPc, FeOCPc and ZnOCPc are 0.11, 0.10, 0.20 and 0.22 V, respectively. Therefore, for MgOCPc and MnOCPc the driving force is not sufficient for charge injection from the dyes to the TiO_2 conduction band.

TABLE IV. Electrochemical data for the four dyes

Dye	$E_{(0-0)}$[a] / eV	$E_{(S+/S)}$[b] / V vs. NHE	$E_{(S+/S*)}$[c] / V vs. NHE	E_{gap}[d] / V
MgOCPc	1.76	1.15	–0.61	0.11
MnOCPc	1.71	1.11	–0.60	0.10
FeOCPc	1.79	1.09	–0.70	0.20
ZnOCPc	1.78	1.06	–0.72	0.22

[a]The E_{0-0} value was calculated from $E_{(0-0)} = 1240/\lambda$, and λ was obtained from the intersection between the absorption and emission spectra; [b]the ground-state energy oxidation potentials ($E_{(S+/S)}$) of the four dyes, describing the highest occupied molecular orbital (HOMO), were measured in DMSO with 0.1 M TBAP as the electrolyte (scanning rate, 30 mV s^{-1}) using glassy carbon as the working electrode, a Pt wire as the counter electrode and an Hg/Hg_2Cl_2 electrode as the reference electrode; [c]the excited state energy ($E_{(S+/S*)}$), reflecting the lowest unoccupied molecular orbital (LUMO); [d]E_{gap} is the energy gap between the $E_{(S+/S*)}$ of the dyes and the conduction band (CB) level of TiO_2 (–0.5 V vs. normal hydrogen electrode (NHE))
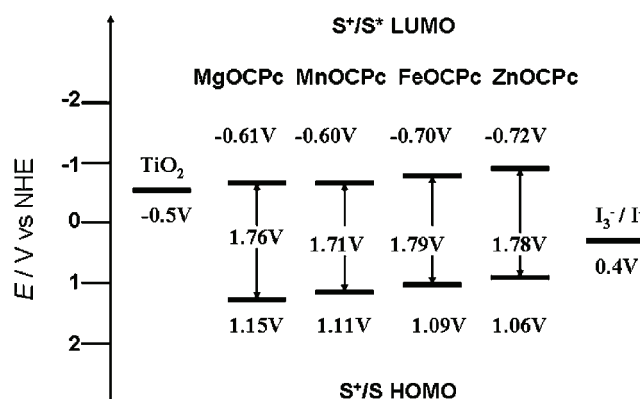
Fig. 5. Energy levels diagram from the electrochemical data.

Photovoltaic performance of DSSC

To manufacture DSSC, the TiO_2 electrodes were immersed into a DMSO solution of the four dyes. The absorption spectra of the four dyes adsorbed on the TiO_2 electrodes are shown in Fig. 6, and the trend of absorption intensity follows the order: ZnOCPc > FeOCPc > MnOCPc > MgOCPc, showing no difference in comparison to the spectra in Fig. 6. However, the spectra were broadened in contrast to the spectra in DMSO solution, which may be ascribed to aggregation of the dyes on the TiO_2 surface.
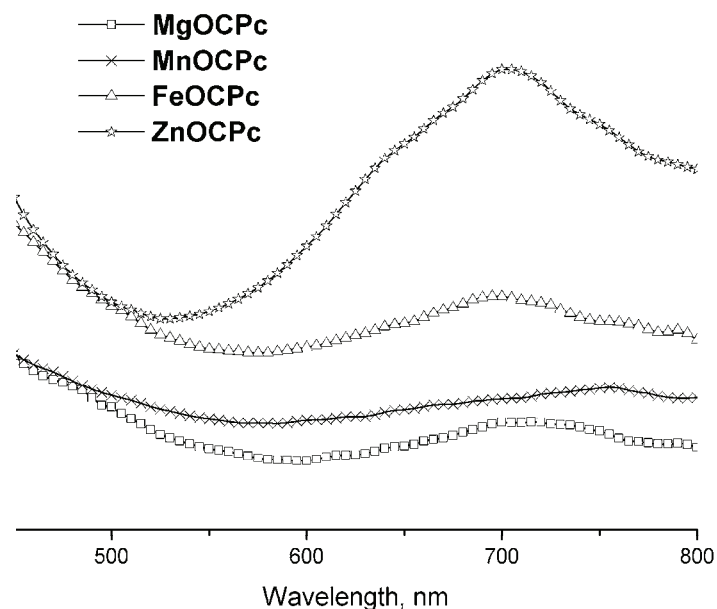
Fig. 6. Absorption spectra of the four dyes adsorbed on TiO$_2$ electrodes.

The four dye-sensitized TiO$_2$ electrodes were employed as working electrodes in the DSSC and the effects of the four dyes with different metal ions possessing variant 3d orbital on the photovoltaic performance of the four DSSC devices could be estimated with the aid of photocurrent–voltage characteristics. The *I–V* curves of the DSSCs based on the four dyes are shown in Fig. 7. The detailed parameters are summarized in Table V.

When comparing the photovoltaic performance of the four DSSC devices, it is seen that *η* assumes the following order: ZnOCPc > FeOCPc > MgOCPc > MnOCPc. The DSSC based on ZnOCPc exhibits the best properties with a short circuit photocurrent density of 0.409 mA cm^{-2}, an open circuit voltage of 0.429 V, and a fill factor of 0.74, corresponding to an overall light to electricity conversion efficiency of 0.13 % under AM 1.5 irradiation (100 mW cm^{-2}). This can be explained by the more negative LUMO level observed for ZnOCPc with the closed-shell metal ion (3d^{10}) among the four dyes, which gives a larger driving force for electron injection from this metallophthalocyanine. This trend matches the photovoltaic efficiency trend, which indicates that the factor is crucial to the photovoltaic performance of the DSSC. In addition, ZnOCPc gives stronger absorption than that of the other dyes. However, the MnOCPc-based DSSC device exhibited a lowest efficiency, which is consistent with the lowest *j*$_{sc}$ value of 0.205 mA cm^{-2} and FF value of 0.60 for this device. The reason is probably due to the poor electron injection and low absorption.
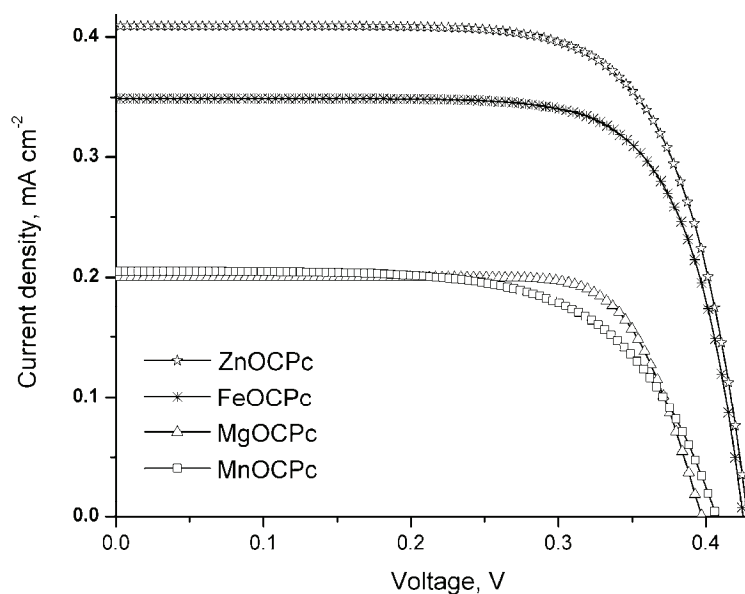
Fig. 7. Current–voltage characteristics for DSSC from the four dyes under illumination of simulated solar light (AM1.5, 100 mW cm^{-2}).

TABLE V. Photovoltaic performance of DSSC based on the four dyes

Dye	j_{sc} / mA cm^{-2}	V_{oc} / V	FF	η / %
MgOCPc	0.200	0.397	0.76	0.06
MnOCPc	0.205	0.406	0.60	0.05
FeOCPc	0.348	0.426	0.74	0.11
ZnOCPc	0.409	0.429	0.74	0.13

CONCLUSIONS

In summary, four octacarboxy-metallophthalocyanines (MgOCPc, MnOCPc, FeOCPc and ZnOCPc) were prepared by microwave irradiation, and the resultant dyes possessed excellent solubility in DMSO solution. The decomposition temperature of the four dyes ranged from 256 to 504 °C. The maximum absorption peaks of MnOCPc, FeOCPc and ZnOCPc were all between 687 nm and 725 nm and their red shift wavelength increased with destabilized HOMO of the metal–ligand. Especially, ZnOCPc had a high molar extinction coefficient. Subsequently, the four dyes were anchored to TiO$_2$ electrodes and their photovoltaic properties applied in DSSC were investigated. It was found that the DSSC device based on ZnOCPc exhibited the best photovoltaic properties with an open circuit voltage of 0.429 V, a short circuit photocurrent density of 0.409 mA cm^{-2} and a fill factor of 0.74 under AM 1.5 irradiation (100 mW cm^{-2}) when compared to the other three dyes. The considerably excellent conversion efficiency obtained with the ZnOCPc-based TiO$_2$ nanocrystalline dye-sensitized solar cells revealed that

ZnOCPc with a closed-shell metal ion ($3d^{10}$) among the four dyes had an excellent excited state giving the largest driving force for electron injection into the TiO_2 conduction band.

И З В О Д

СИНТЕЗА И ФОТОНАПОНСКЕ КАРАКТЕРИСТИКЕ ОКТАКАРБОКСИ-МЕТАЛФТАЛОЦИЈАНИНСКИХ БОЈА ЗА ПРИМЕНУ У СОЛАРНИМ ЋЕЛИЈАМА СЕНЗИБИЛИСАНИМ БОЈОМ

LING JIN, WEI CHEN и DAJUN CHEN

State Key Laboratory for Modification of Chemical Fibers and Polymer Materials, College of Materials Science and Engineering, Donghua University, Shanghai 201620, China

Низ октакарбокси-металфталоцијанинских боја са различитм централним јонима метала, MgOCPc, MnOCPc, FeOCPc и ZnOCPc, је дизајниран и синтетисан уз помоћ микроталасног зрачења. Детаљно је испитан утицај увођења металних јона са различитом попуњеношћу 3d орбитала ($3d^0$, $3d^5$, $3d^6$ и $3d^{10}$) у центар фталоцијанинског прстена на термичке, фото-физичке и електрохемијске особине октакарбокси-металфталоцијанина. Резултати су показали да ZnOCPc и MgOCPc који имају метални јон са затвореном љуском и FeOCPc код којег метални јон има отворену љуску поседују одличне термичке особине. Међутим, MnOCPc са металним јоном који има делимично попуњену љуску има најнижу температуру разлагања и највећи црвени помераj Q траке. Теоријски је израчунато да енергетски процепи за MgOCPc, MnOCPc, FeOCPc и ZnOCPc износе 0,11, 0,10, 0,20 и 0,22V, респективно. Фотонапонске карактеристике поменуте четири боје, примењене у TiO_2 нанокристалној и бојом сензибилисаној соларној ћелији, одређене су AM1.5 зрачењем снаге 100 mW cm^{-2}.

(Примљено 10. јула 2011, ревидирано 19. марта 2012)

REFERENCES

1. C. G. Claessens, U. Hahn, T. Torres, *Chem. Rec.* **8** (2008) 75
2. N. Masilela, T. Nyokong, *Dyes Pigm.* **84** (2010) 242
3. J. Andzelm, A. M. Rawlett, J. A. Orlicki, J. F. Snyder, *J. Chem. Theory Comput.* **3** (2007) 870
4. M. G. Martín, M. L. Rodríguez-Méndez, J. A. Saja, *Langmuir* **26** (2010) 19217
5. G. Bottari, J. A. Suanzes, O. Trukhina, T. Torres, *J. Phys. Chem. Lett.* **2** (2011) 905
6. M. Kuruppuarachchi, H. Savoie, A. Lowry, C. Alonso, R. W. Boyle, *Mol. Pharmaceutics* **8** (2011) 920
7. G. Torre, P. Vázquez, F. Agulló-López, T. Torres, *Chem. Rev.* **104** (2004) 3723
8. F. Matemadombo, N. Sehlotho, T. Nyokong, *J. Porphyrins Phthalocyanines* **13** (2009) 986
9. M. K. Nazeeruddin, R. Humphry-Baker, M. Grätzel, D. Wöhrle, G. Schnurpfeil, G. Schneider, A. Hirth, N. Trombach, *J. Porphyrins Phthalocyanines* **3** (1999) 230
10. J. J. He, G. Benkö, F. Korodi, T. Polivka, R. Lomoth, B. Åkermark, L. C. Sun, A. Hagfeldt, V. Sundström, *J. Am. Chem. Soc.* **124** (2002) 4922
11. J. J. Cid, J. H. Yum, S. R. Jang, M. K. Nazeeruddin, E. Martínez-Ferrero, E. Palomares, J. Ko, M. Grätzel, T. Torres, *Angew. Chem.* **119** (2007) 8510
12. B. O'Regan, M. Grätzel, *Nature* **353** (1991) 737

13. A. Hagfeldt, G. Boschloo, L. C. Sun, L. Kloo, H. Pettersson, *Chem. Rev.* **110** (2010) 6595
14. S. Eu, T. Katoh, T. Umeyama, Y. Matanoa, H. Imahori, *Dalton Trans.* **40** (2008) 5476
15. H. Imahori, T. Umeyama, S. Ito, *Acc. Chem. Res.* **42** (2009) 1809
16. P. Y. Reddy, L. Giribabu, C. Lyness, H. J. Snaith, C. Vijaykumar, M. Chandrasekharam, M. Lakshmikantam, J.-H. Yum, K. Kalyanasundaram, M. Grätzel, M. K. Nazeeruddin, *Angew. Chem. Int. Ed.* **46** (2007) 373
17. J. H. Yum, S. R. Jang, R. Humphry-Baker, M. Grätzel, J.-J. Cid, T. Torres, M. K. Nazeeruddin, *Langmuir* **24** (2008) 5636
18. V. Aranyos, J. Hjelm, A. Hagfeldt, H. Grennberg, *J. Porphyrins Phthalocyanines* **5** (2001) 609
19. D. R. Boston, J. C. Bailar, Jr., *Inorg. Chem.* **11** (1972) 1579
20. F. Matemadombo, N. Sehlotho, T. Nyokong, *J. Porphyrins Phthalocyanines* **13** (2009) 986
21. N. Masilela, T. Nyokong, *Dyes Pigm.* **84** (2010) 242
22. L. C. Liu, C. C. Lee, A. T. Hu, *J. Porphyrins Phthalocyanines* **5** (2001) 806
23. Y. Ma, E. Vileno, S. L. Suib, P. K. Dutta, *Chem. Mater.* **9** (1997) 3023
24. L. Giribabu, Ch. Vijay Kumara, V. Gopal Reddy, P. Yella Reddy, Ch. Srinivasa Rao, S.-R. Jang, J.-H. Yum, M. K. Nazeeruddin, M. Grätzel, *Sol. Energ. Mat. Sol. C.* **91** (2007) 1611
25. W. Xu, B. Peng, J. Chen, M. Liang, F. S. Cai, *J. Phys. Chem. C* **112** (2008) 874
26. M. S. Liao, J. D. Watts, M. J. Huang, *Inorg. Chem.* **44** (2005) 1941
27. U. Mazur, K. W. Hipps, *J. Phys. Chem. C* **103** (1999) 9721
28. J. Krzystek, J. Telser, L. A. Pardi, D. P. Goldberg, B. M. Hoffman, L. C. Brunel, *Inorg. Chem.* **38** (1999) 6121
29. G. P. Shaposhnikov, V. E. Maizlish, V. P. Kulinich, *Russ. J. Gen. Chem.* **75** (2005) 1480
30. G. Li, K. J. Jiang, Y. F. Li, S. L. Li, L. M. Yang, *J. Phys. Chem. C* **112** (2008) 11591
31. D. P. Hagberg, J. H. Yum, H. J. Lee, F. D. Angelis, T. Marinado, K. M. Karlsson, R. Humphry-Baker, L. C. Sun, A. Hagfeldt, M. Grätzel, M. K. Nazeeruddin, *J. Am. Chem. Soc.* **130** (2008) 6259.

Epitaxial growth by monolayer-restricted galvanic displacement[●]

RASTKO VASILIĆ*

Faculty of Environmental Governance and Corporate Responsibility, Educons University, Vojvode Putnika 87, 21208 Sremska Kamenica, Serbia

Abstract: The development of a new method for epitaxial growth of metals in solution by galvanic displacement of layers pre-deposited by underpotential deposition (UPD) was discussed and experimentally illustrated throughout the lecture. Cyclic voltammetry (CV) and scanning tunneling microscopy (STM) were employed to perform and monitor a "quasi-perfect", two-dimensional growth of Ag on Au(111), Cu on Ag(111), and Cu on Au(111) by repetitive galvanic displacement of underpotentially deposited monolayers. A comparative study emphasizes the displacement stoichiometry as an efficient tool for thickness control during the deposition process and as a key parameter that affects the deposit morphology. The excellent quality of the layers deposited by monolayer-restricted galvanic displacement was manifested by steady UPD voltammetry and ascertained by the flat and uniform surface morphology that was maintained during the entire growth process.

Keywords: underpotential deposition; crystal growth; surface morphology; STM.

Epitaxial growth by monolayer-restricted galvanic displacement is realized utilizing a concept for submonolayer to monolayer surface modification assisted by the irreversible galvanic displacement of an underpotentially deposited (UPD) less-noble metal by a more-noble metal.[1] This protocol functions in homo- and hetero-epitaxial systems where the displaced UPD metals are displaced not only on the substrate, but also on the growing metal of interest; hence, the "building block" reaction could be repeated as many times as desired. Similar pathways have been technically employed in electrochemical atomic layer epitaxy (EC ALE) for the growth of epitaxial compound semiconductor layers with a wide spectrum of applications in the electronics industry.[2] The electroless nature of the

displacement reaction allows for decoupling of mutually dependent growth controlling factors in a typical electrodeposition scenario, thus improving the overall deposition control.

The development of a new method for hetero-epitaxial growth by monolayer restricted galvanic displacement was presented in the lecture. Although the epitaxial growth of Ag on Au(111) was the system under detailed consideration, complementary results for Cu epitaxial growth on Ag(111) and on Au(111) suggest that this method can be applied to a number of other systems. The main limitation of the proposed method is manifested by the requirement that the selected underpotentially deposited metals have to feature UPD on both the substrate and the growing metal. The newly developed method for epitaxial growth of thin films enables the substrate with a metal underpotentially deposited on it to be transferred into a solution that contains ions of a more noble metal than the UPD metal. A naturally ensuing galvanic displacement results in stoichiometric exchange between the UPD atomic layer and the metal ions of interest. This building block reaction can be repeated as many times as desired. The unique property that warrants success of the proposed strategy is associated with the fact that UPD is a reversible process and galvanic displacement is not. Therefore, a metal that displaces the UPD layer remains on the surface awaiting another layer "to come" in the next cycle. The continuous accumulation of new epitaxial layers eventually results in a thin epitaxial film with perfectly controlled thickness. The driving force for the displacement step is the formation of the corrosion potential between the UPD metal and the substrate.

Kinetic factors that govern the feasibility of the described procedure and provide hand-on knowledge for precise control of the growth are associated with the stability of an underpotentially deposited metal layer at the open circuit potential (OCP). A comprehensive kinetic study performed during this work identified oxygen reduction reaction (ORR), hydrogen evolution reaction (HER) and nitrate electroreduction as typical oxidizing agents that compete with the displacing metal ions in any working environment.[3] The completed kinetic study served as a base for the development of an analytical model. Assuming Langmuir and/or Frumkin type UPD behavior, the derived equation enables a quantitative prediction of the stability of the UPD layer at the OCP and precise kinetics control of the galvanic displacement based on readily measurable experimental parameters. A fitting of the experimental results for the systems Pb/Cu(111) and Pb/Ag(111) with the model equation showed an excellent prediction of the stability of the UPD layer at the OCP and renders the model applicable for a variety of kinetic studies.[4]

The most important result of this research is manifested by work focused on initial trials, procedure optimization, a stoichiometric study and the successful implementation of the galvanic displacement as a tool for epitaxial thin film

growth.[5,6] Furthermore, both qualitative and quantitative examination of deposited thin films ascertained the applicability of the proposed strategy in metal epitaxy. A systematic study of thin film morphology as a function of the oxidation state of the UPD metal suggested growth of Ag by displacement of a Tl UPD layer (1:1 displacement) as preferred, considering the surface roughness and uniformity. Subsequent stripping experiments validated the proposed working formula for galvanic displacement that takes into account not only the stoichiometric arguments, but also the crystallographic parameters of the participating elements. High-resolution X-ray photoelectron spectroscopy (XPS) experiments suggested not even a trace of Tl and Pb was present in the respectively grown Ag layers, thus confirming the purity of the deposit. At the same time, the surface confined intermixing between Ag and Bi, undoubtedly demonstrated by CV and XPS, could be envisioned as a fundament of the new strategy for the deposition of multi-functional ordered surface alloys (Ag–Bi, Au–Bi and Pt–Bi) with immediate application in fuel cell catalysis.[7] The results obtained for the Cu/Ag(111) and Cu/Au(111) systems prove epitaxial growth by monolayer restricted galvanic displacement as a viable method for obtaining epitaxial thin films of excellent quality.[8] The long term fundamental goals of presented research are related to the implementation of monolayer restricted galvanic displacement to other systems, such as Au/Pt(111), Ag/Pt(111), Pd/Pt(111), and further expansion towards the growth of "perfectly layered" metal composites.

ИЗВОД

ЕПИТАКСИЈАЛНИ РАСТ КРИСТАЛА ПРИМЕНОМ МЕТОДЕ ГАЛВАНСКЕ ИЗМЕНЕ ОГРАНИЧЕНЕ НА МОНОСЛОЈ

РАСТКО ВАСИЛИЋ

Факулшеш зашшише живошне средине, Универзишеш Едуконс, Војводе Пушника 87, 21208 Сремска Каменица

У овом предавању су приказане основне идеје и резултати примене нове методе епитаксијалног раста кристала галванском изменом ограниченом на монослој. Метода је заснована на спонтаном, иреверзибилном, редокс процесу при коме се подпотенцијално депоновани слој замењује слојем (електрохемијски) племенитијих металних јона из раствора, који се редукују на кристалној површини. У одређеном броју система, понављање овог корака резултира формирањем танких филмова који прате морфологију субстрата. Представљени су резултати добијени за систем Ag/Au(111), Cu/Ag(111) и Cu/Au(111). Посебна пажња је посвећена испитивању утицаја стехиометрије галванске измене у систему Ag/Au(111), када је подпотенцијално депоновани слој формиран од атома Tl, Pb и Bi, редом. Карактеризација овако добијених танких филмова показује да се методом галванске измене ограничене на монослој стиче максимална контрола униформности раста уз минимум спољашње контроле. Танки епитаксијални филмови добијени на овај начин су супериорни у односу на танке филмове добијене уобичајеним техникама електродепозиције.

REFERENCES

1. S. R. Brankovic, J. X. Wang, R. R. Adzic, *Surf. Sci.* **474** (2001) L173
2. J. L. Stickney, *Advances in Electrochemical Science and Engineering,* Vol. 7, R. Alkire, D. Kolb, Eds., Wiley-VCH, Weinheim, 2001, p. 1
3. R. Vasilić, N. Vasiljević, N. Dimitrov, *J. Electroanal. Chem.* **580** (2005) 203
4. N. Dimitrov, R. Vasilić, N. Vasiljević, *Electrochem. Solid-State Lett.* **10** (2007) D79
5. R. Vasilić, N. Dimitrov, *Electrochem. Solid-State Lett.* **8** (2005) C173
6. R. Vasilić, L. T. Viyannalage, N. Dimitrov, *J. Electrochem. Soc.* **153** (2006) C648
7. D. Volpe, E. Casado-Rivera, L. Alden, C. Lind, K. Hagerdon, C. Downie, C. Korzeniewski, F. J. Di Salvo, H. D. Abruna, *J. Electroanal. Chem.* **151** (2004) A971
8. L. T. Viyannalage, R. Vasilić, N. Dimitrov, *J. Phys. Chem.* **111** (2007) 4036.

Journal of the Serbian Chemical Society

Vapour pressures and vapour–liquid equilibria of binary systems of *n*-propyl acetate and isobutyl acetate with ethanol or 2-propanol at 0.15 MPa

PEDRO SUSIAL*, JOSÉ J. RODRÍGUEZ-HENRÍQUEZ, JOSÉ C. APOLINARIO,
VICTOR D. CASTILLO and ESTEBAN J. ESTUPIÑAN

*Escuela de Ingenierias Industriales y Civiles, Universidad de
Las Palmas de Gran Canaria, Canary Islands, Spain*

Abstract: The vapour pressures of *n*-propyl acetate, *iso*-butyl acetate and 2-propanol from 0.004 to 1.6 MPa absolute pressure and vapour–liquid equilibria (VLE) data for the binary systems *n*-propyl acetate+ethanol, *n*-propyl acetate+2-propanol, *iso*-butyl acetate+ethanol and *iso*-butyl acetate+2-propanol at 0.15 MPa were determined. The experimental VLE data were verified with the van Ness Test and the Fredenslund Criterion. The *n*-propyl acetate+ethanol and +2-propanol binary systems have an azeotropic point at 0.15 MPa. Different versions of the universal quasichemical functional group activity coefficients and analytical solutions of groups contribution models were applied.

Keywords: vapour–liquid equilibria isobaric data; phase equilibrium; binary system; esters; alcohols.

INTRODUCTION

Esters, including *n*-propyl acetate and *iso*-butyl acetate, are used in fermentation processes for the synthesis of antibiotics, as solvents for paints, lacquers and varnishes, and in various applications in the graphic arts industry. These substances generate azeotropic mixtures with some alcohols. However, the components of the azeotropic mixtures can be separated by modifying the pressure in the process, in order to obtain pure substances. For this reason, it may be of interest to know the operating conditions under which the azeotropic point disappears. Thus, laboratory data becomes necessary, meaning that ebulliometers and components of experimental facilities must be analyzed.

The construction of a metallic ebulliometer for the determination of the vapour–liquid equilibrium (VLE) data at moderate pressures was previously re-

---

* Corresponding author. E-mail: psusial@dip.ulpgc.es

1243

ported.[1,2] Considering this, together with the necessity for reliable data, different modifications were accomplished in the experimental installation,[2] which are verified in this study.

The VLE of the binary system *n*-propyl acetate+ethanol (PAE) was studied at 101.3 and 160.0 kPa,[3] and the system *n*-propyl acetate+2-propanol (PA2P) at 101.32 kPa.[4] The azeotropic point was described for these two systems.[3–5] Therefore, both systems could be used as references in the analysis of the modifications introduced in the experimental equipment. For this purpose, VLE data of the binary system PAE and PA2P at 0.15 MPa were determined. The experimental data for the isobutyl acetate+ethanol (IBAE) and isobutyl acetate+2-propanol (IBA2P) systems, which have not been described in literature, are also presented in this paper at 0.15 MPa.

On the other hand, the thermodynamic validation of VLE data depends on the vapour pressures of the pure substances. Accordingly, the vapour pressures of *n*-propyl acetate, isobutyl acetate and 2-propanol, which are required for the application of the point-to-point test, were determined in this study over a wide temperature range.[6] The data used for ethanol was published in previously.[2] The VLE data obtained at 0.15 MPa for the binary systems PAE, PA2P, IBAE and IBA2P met the consistency criteria established in literature.[7] After the thermodynamic consistency was proven, the experimental data were predicted with the universal quasichemical functional group activity coefficients (UNIFAC)[8–10] and *a*nalytical *s*olutions of *g*roups and analytical solutions of groups (ASOG)[11] group contribution models for the activity coefficients.

EXPERIMENTAL

Chemicals and apparatus

The physical properties, normal boiling point, density at 298.15 K, and refractive index at 298.15 K, determined for *n*-propyl acetate (Alfa Aesar GmbH & Co. with a purity of 99 %), *iso*-butyl acetate (Panreac Química S.A. with a purity of 99 %) and 2-propanol (99.8 % purity from Panreac Química S.A.), and a comparison with values from literature are given in Table I. The physical properties of ethanol (Panreac Química S.A. of 99.8 % purity) are not different from those previously published.[2] These chemicals were used without further purification. The normal boiling point at 0.1 MPa was determined with a stainless steel ebulliometer.[1,2] A Kyoto Electronics DA-300 vibrating tube density meter with an uncertainty of ± 0.1 kg·m^{-3} and a Zusi 315RS Abbe refractometer with an uncertainty of ± 0.0002 units were used for density and refractive index determinations, respectively.

Equipment and procedure

The experimental work in this paper was performed with a dynamic ebulliometer equipped with a Cottrell pump and where the recirculation of both phases is verified, as was previously described.[1] Dostmann Electronic GmbH Pt100 probes, to which a nut and welded ring were included, were placed in the experimental equipment.[1] The electrical system was later assembled inside a sheath, allowing the probe to be screwed to the stainless-steel ebulliometer. The digital Dostmann Electronic GmbH p655 probes used allowed temperature measu-

rements with a ±0.02 K uncertainty. The welding of the ring to the sheath and the calibration of the system was realised by Dostmann Electronic GmbH. National Physical Laboratory (NPL) and National Institute of Standards and Technology (NIST) standards were applied during calibration of the device. After the probes had been installed, their correct operation was verified by measurement of the boiling point of distilled water.

TABLE I. Physical properties of pure substances and the Antoine constants; tw – this work

T_{bp} / K	ρ / kg·m^{-3}	n_D	A	B	C	ΔT / K	$\sigma(p_i^0)$ / MPa
			2-Propanol				
355.53[(tw)]	781.3[tw]	1.3751[tw]	6.4727[tw]	1162.30[tw]	95.25[tw]	303–452	0.001
355.30[4]	781.33[4]	1.3752[4]	6.87294[4]	1365.38[4]	70.04[4]	330–370	–
355.41[12]	781.26[12]	1.3752[12]	6.86618[12]	1360.13[12]	75.56[12]	–	–
			n-Propyl acetate				
374.61[tw]	882.4[tw]	1.3825[tw]	6.2797[tw]	1371.09[tw]	55.27[tw]	302–503	0.002
374.686[12]	883.03[12]	1.3828[12]	6.14362[4]	1284.08[4]	64.364[4]	–	–
374.55[3]	882.40[3]	1.3816[3]	6.50975[12]	1523.13[12]	36.38[12]	320–430	–
			Isobutyl acetate				
389.44[tw]	866.2[tw]	1.3882[tw]	6.4101[tw]	1487.45[tw]	51.07[tw]	300–516	0.001
389.80[12]	867.7[12]	1.3880[12]	6.3546[4]	1462.4[4]	53.45[4]	–	–
389.85[13]	866.06[14]	1.3876[13]	6.4088[12]	1500.59[12]	49.088[12]	307–392	–

In order to determine work pressure, a digital display pressure transmitter type 8311 from Burket Fluid control systems (0.0–4.0 MPa range, ±0.002 MPa uncertainty) was included in the experimental installation.[2] A controller valve (Binks MFG Co.) was included in the experimental setup in order to control dry nitrogen flow into the equipment during continuous operation and for the determination of the experimental VLE data. However, for the determination of vapour pressure, a controller valve with a 0.6–2.4 MPa range from Truflo International and a discharge pressure regulator with a 0.035–2.8 MPa range from Fairchild Ind. Prod. Co., were employed. The experimental installation[2] was also equipped with a Bourdon manometer with a –0.1–0.15 MPa range and ±0.001 MPa uncertainty.

The mixtures studied in this work were kept under boiling conditions for 90 min to ensure a stationary state. After recirculation of both phases, the liquid and vapour condensate samples were extracted from the ebulliometer into external sealed recipients. Once the sample was extracted, the equipment was recharged with a small amount of one of the compounds, in order to modify the composition of the mixture inside the ebulliometer in a continuous operation. The composition of the liquid and vapour phases in the collected samples was determined by density measurement at 298.15 K. A calibration curve composition *vs.* density had previously been obtained. The greatest uncertainty found for these systems by this composition analysis method was better than 0.002 units in the mole fraction of vapour phase.

RESULTS AND DISCUSSION

The vapour pressures of n-propyl acetate, *iso*-butyl acetate and 2-propanol in this work were obtained previously with the stainless-steel ebulliometer,[1] and the new equipment included in the installation previously detailed.[2] The vapour pressures and temperature data (Table S-I, Supplementary material) were correlated to the Antoine Equation:

$$\log_{10}\left(p_i^0 \; / \; \text{kPa}\right) = A - \frac{B}{T \; / \; \text{K} - C} \tag{1}$$

and the Nelder and Mead[15] procedure was used. The constants obtained are given in Table I together with literature data.

The vapour pressures were verified by calculating the enthalpy of vaporization using the Clapeyron Equation:[16]

$$\frac{\mathrm{d}p^0}{\mathrm{d}T} = \frac{\Delta H_{\text{vap}}}{T(v_i^G - v_i^L)} \tag{2}$$

and introducing the Antoine Equation into Eq. (2) as follows:

$$\Delta H_{\text{vap}} = \frac{(v_i^G - v_i^L)p^0 B T}{(T - C)^2} \tag{3}$$

The constants of Eq. (1) given in Table I and the vapour pressures from Table S-I were applied in Eq. (3). Data of the critical properties[7] were employed in the determination of the vapour and liquid molar volumes of the pure compounds using the Hayden and O'Connell[18] method and the Yen and Woods Equation,[19] respectively. When considering as a reference all the data in Table II for each of the substances and the Antoine constants from the literature,[12] the results show that the average errors in the enthalpy of vaporization were less than 2.6, 1.4 and 0.4 %, for 2-propanol, *n*-propyl acetate and isobutyl acetate, repetitively. On the other hand, the application of Eq. (3) together with the normal boiling points and the Antoine constants of this work returns deviations of less than 1.3, 1.6 and 1.4 % for 2-propanol, *n*-propyl acetate and isobutyl acetate, respectively, when considering as a reference the enthalpy of vaporization from literature.[17] The acentric factor was obtained using the properties in the literature[7] and from the correlation of the experimental data from Table S-I, as reduced properties in the Antoine Equation. The acentric factors showed values of 0.665; 0.411 and 0.441 with deviations of less than 5.6, 4.1 and 2.9 % for 2-propanol, *n*-propyl acetate and isobutyl acetate, respectively; literature data[17] were taken for comparison.

The VLE data $T–x_1–y_1$ of PAE, PA2P, IBAE and IBA2P at 0.15 MPa are shown in Tables S-II and S-III (Supplementary material). The experimental data were verified to evaluate the thermodynamic consistency using the method described by Fredenslund *et al.*[7] To develop the test, a three-term Legendre polynomial was used to correlate the excess Gibbs free energy. According to this criterion, the experimental data are consistent if the mean absolute deviation between calculated and measured mole fractions of component 1 in the vapour phase is less than 0.01. In the present study, the values obtained were $\delta y = 0.0089$

for the PAE system, $\delta y = 0.0092$ for the PA2P system, $\delta y = 0.0032$ for the IBAE system and $\delta y = 0.0079$ for the IBA2P system.

Data treatment

The activity coefficients of the liquid phase for each system were determined using the following equation:

$$\gamma_i = \frac{y_i p}{x_i p_i^0} \exp\left[\frac{p}{RT}\left(2\sum_j y_i B_{ij} - \sum_i \sum_j y_i y_j B_{ij}\right) - \frac{p_i^0 B_{ii}}{RT} + \frac{\left(p_i^0 - p\right)v_i^L}{RT}\right] \quad (4)$$

The virial state equation truncated at the second term was employed and the second virial coefficients were obtained by means of the Hayden and O'Connell[18] method. The liquid molar volumes of the pure compounds were estimated using the Yen and Woods equation.[19]

The activity coefficients of the liquid phase (Tables S-II and S-III), calculated from the VLE data applying the previous procedure showed a positive deviation from ideal behaviour, probably due to molecular association. The negative deviation observed is possibly a consequence of the experimental uncertainty in the temperature and pressure measurements.

After the thermodynamic consistency of the experimental data had been verified, the calculated activity coefficients were correlated using the excess Gibbs free energy with the relation G^E/RT *vs.* x_1 in the following thermodynamic models: Wilson, non-random two-liquid (NRTL) and universal quasichemical (UNIQUAC). To obtain the interaction parameters for the activity–coefficient models, the simplex method[15] was applied, using the minimization of the objective function (*OF*) as follows:[20]

$$OF = \sum_1^n \left(\gamma_1^{\text{exp}} - \gamma_1^{\text{calc}}\right)_i^2 + \sum_1^n \left(\gamma_2^{\text{exp}} - \gamma_2^{\text{calc}}\right)_i^2 \quad (5)$$

Good correlations were obtained with the thermodynamic models (Table II), and acceptable deviations were observed in the prediction of temperature and vapour phase mole fractions.

Correlation of data and prediction

As in previous studies,[1,2] the experimental data from every system were correlated to a fitting function (FF) with a polynomial structure:

$$(y_1 - x_1)\left[x_1(1 - x_1)\right]^{-1} = \sum_{k=0}^m A_k \left\{x_1\left[x_1 + R_T(1 - x_1)\right]^{-1}\right\}^k \quad (6)$$

$$\left[T - x_1 T_{\text{bp1}} - (1 - x_1)T_{\text{bp2}}\right]\left[x_1(1 - x_1)\right]^{-1} = \sum_{k=0}^m A_k \left\{x_1\left[x_1 + R_T(1 - x_1)\right]^{-1}\right\}^k \quad (7)$$

$$\left[T - y_1 T_{bp1} - (1 - y_1) T_{bp2} \right] \left[y_1 (1 - y_1) \right]^{-1} = \sum_{k=0}^{m} A_k \left\{ x_1 \left[x_1 + R_T (1 - x_1) \right]^{-1} \right\}^k \quad (8)$$

The data correlations were performed using the simplex method.[15] The results from the treatment of experimental data are given in Table III. The same process was applied to literature data[3,4] (Figs. 1–3). It can be observed that the experimental results at 0.15 MPa present good agreements with literature data at 0.1013 and 0.160 MPa for the PAE and PA2P systems studied in this work. For these reason, it seems obvious that the new apparatus for temperature and pressure control are appropriate.

TABLE II. Correlation parameters for G^E/RT with average and standard deviations and predictions of the azeotropic points:

$$\delta(F) = \frac{1}{n} \sum_{1}^{n} \left| F_{exp} - F_{cal} \right| \; ; \; \sigma(F) = \sqrt{\frac{\sum_{1}^{n} \left(F_{exp} - F_{cal} \right)^2}{n - m}} \; ; \; \bar{e}(F) = \frac{100}{n} \sum_{1}^{n} \frac{\left| F_{exp} - F_{cal} \right|}{F_{exp}}$$

Model	Parameters, J mol⁻¹		$\delta(y_1)$	$\delta(T)$ / K	$\sigma(G^E/RT)$
n-Propyl acetate (1) + ethanol (2) at 0.15 MPa					
Wilson	$\Delta\lambda_{12} = 4339.4$	$\Delta\lambda_{21} = -1193.7$	0.005	0.77	0.02
NRTL ($\alpha = 0.47$)	$g_{12} = 954.0$	$g_{21} = 2250.5$	0.005	0.90	0.03
UNIQUAC ($Z = 10$)	$\Delta u_{12} = 1959.4$	$\Delta u_{21} = -411.2$	0.005	0.81	0.03
n-Propyl acetate (1) + 2-propanol (2) at 0.15 MPa					
Wilson	$\Delta\lambda_{12} = 3754.0$	$\Delta\lambda_{21} = -1368.0$	0.009	0.24	0.02
NRTL ($\alpha = 0.47$)	$g_{12} = -553.6$	$g_{21} = 3129.3$	0.011	0.30	0.02
UNIQUAC ($Z = 10$)	$\Delta u_{12} = 397.2$	$\Delta u_{21} = 344.5$	0.009	0.23	0.02
Isobutyl acetate (1) + ethanol (2) at 0.15 MPa					
Wilson	$\Delta\lambda_{12} = 5113.0$	$\Delta\lambda_{21} = -1508.3$	0.003	0.18	0.01
NRTL ($\alpha = 0.47$)	$g_{12} = 1060.2$	$g_{21} = 2536.9$	0.003	0.22	0.01
UNIQUAC ($Z = 10$)	$\Delta u_{12} = 2365.7$	$\Delta u_{21} = -548.5$	0.003	0.25	0.01
Isobutyl acetate (1) + 2-propanol (2) at 0.15 MPa					
Wilson	$\Delta\lambda_{12} = 4183.1$	$\Delta\lambda_{21} = -1866.8$	0.005	0.54	0.02
NRTL ($\alpha = 0.47$)	$g_{12} = -269.5$	$g_{21} = 2598.1$	0.004	0.51	0.02
UNIQUAC ($Z = 10$)	$\Delta u_{12} = 778.2$	$\Delta u_{21} = -12.9$	0.004	0.49	0.02
Azeotropic data					

n-Propyl acetate (1) + ethanol (2) at 0.15 MPa				
Model	This work	Wilson	NRTL	UNIQUAC
$x_{1az\,exp}$	0.051	0.046	0.049	0.046
$T_{az\,exp}$ / K	361.93	361.61	361.60	361.64

n-Propyl acetate (1) + 2-propanol (2) at 0.15 MPa				
Model	This work	Wilson	NRTL	UNIQUAC
$x_{1az\,exp}$	0.011	0.024	0.028	0.023
$T_{az\,exp}$ / K	365.77	365.70	365.69	365.71

The symmetrical behaviour of the T *vs.* x_1 curves in for systems, as well as the influence of pressure, are shown in Figs. 1 and 2. However, the effect of pressure on the vapour phase of the substances seems to create a certain asymmetry in the T *vs.* y_1 curves, which is highlighted at higher system pressures and ester composition. The different development between the IBAE and IBA2P systems as a consequence of the differences in the boiling points of these alcohols is shown in Fig. 3.

TABLE III. Coefficients and standard deviations obtained in the correlation of the VLE data using the FF equations

FF Equation	R_T	A_0	A_1	A_2	A_3	Condition
n-Propyl acetate (1) + ethanol (2) at 0.15 MPa						
(6)	2.22	0.12	–4.26	5.89	–6.26	$\sigma(y_1–x_1) < 0.003$
(7)	2.11	–29.85	2.42	–88.99		$\sigma(T) = 0.17$ K
(8)	0.60	–38.33	45.79	–0.40		$\sigma(T) = 0.11$ K
n-Propyl acetate (1) + 2-propanol (2) at 0.15 MPa						
(6)	1.99	–0.13	–1.57	0.69	–1.62	$\sigma(y_1–x_1) < 0.003$
(7)	3.52	–23.12	–50.04	18.06	–49.11	$\sigma(T) = 0.13$ K
(8)	1.24	–24.00	–14.98	112.41	–90.11	$\sigma(T) = 0.12$ K
Isobutyl acetate (1) + ethanol (2) at 0.15 MPa						
(6)	2.94	–0.21	–4.58	5.24	–7.47	$\sigma(y_1–x_1) < 0.003$
(7)	9.60	–38.66	–249.20	0.65		$\sigma(T) = 0.11$ K
(8)	0.85	–56.50	178.59	–136.64		$\sigma(T) = 0.22$ K
Isobutyl acetate (1) + 2-propanol (2) at 0.15 MPa						
(6)	9.29	–0.42	–7.15	5.58	–0.01	$\sigma(y_1–x_1) < 0.003$
(7)	11.06	–31.53	–237.47	262.30		$\sigma(T) = 0.18$ K
(8)	0.07	6.05	–144.42	148.93		$\sigma(T) = 0.17$ K

The VLE data for the binary systems PAE, PA2P, IBAE and IBA2P at 0.15 MPa were predicted using the following group contribution methods to calculate the liquid-phase activity coefficients: the ASOG[11] method; the original UNIFAC[7] method, with the structural and group-interaction parameters recommended by Hansen *et al*.,[9] the UNIFAC-Lyngby[8] method; and the UNIFAC-Dortmund[10] method. The mean errors and average deviations between the experimental VLE data and those predicted by the different group contribution models are listed in Table IV.

It should be noted that, globally, the ASOG[11] method and UNIFAC-1987[8] version provide the best results in the prediction of the activity coefficients, temperature and vapour phase mole fraction. However, the best method for the prediction of the vapour phase mole fraction at 0.15 MPa was UNIFAC-1991[9] in the IBAE system. The experimental data for PAE and for PA2P both at 0.15 MPa, together with the data fitting curves predicted with the different group contribution models are shown in Fig. 4. For the PAE and the PA2P systems at 0.15 MPa,
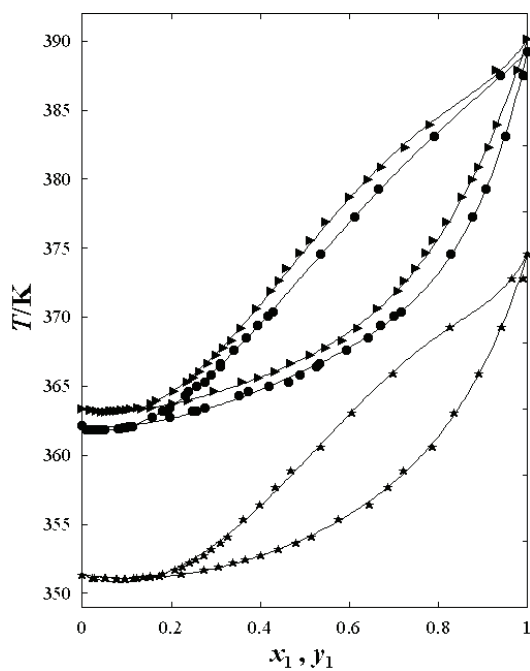
Fig. 1. Plot of experimental VLE data and curves for *n*-propyl acetate (1) + ethanol (2) at 0.15 MPa (●). Fitting curves and literature data[3] for 0.1013 (★) and 0.1600 MPa (▲).
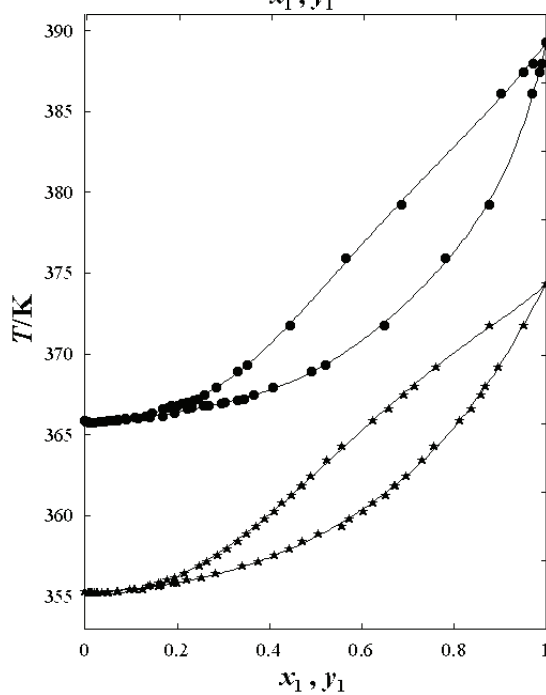
Fig. 2. Isobaric VLE representation of *n*-propyl acetate (1) + 2-propanol (2) at 0.15 MPa (●) with literature data[4] at 0.10132 MPa (★) and fitting curves.
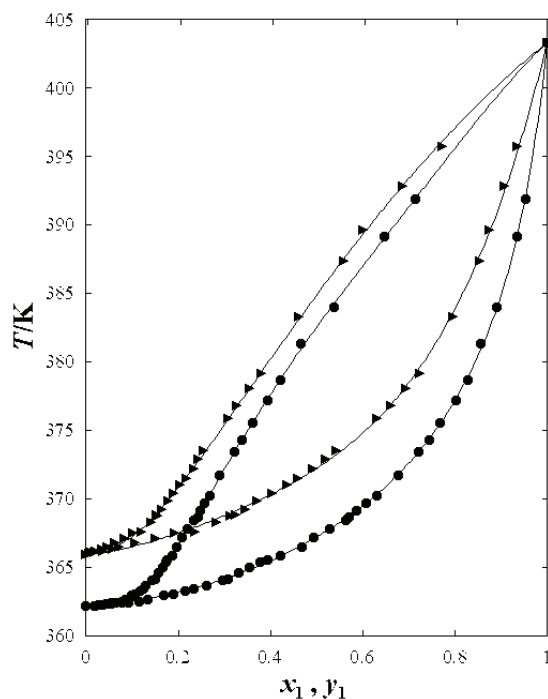
Fig. 3. Plot of experimental VLE data for isobutyl acetate (1) + ethanol (2) (●) and isobutyl acetate (1) + 2-propanol (2) (▲), at 0.15 MPa.

the UNIFAC-1991[9] and UNIFAC-1987[8] methods gave lower mean deviations for the ester vapour phase mole fraction, as shown in Fig. 4; however, the ASOG[11] model globally represents the behaviour of these systems acceptably (see the inset in Fig. 4). The UNIFAC-1991[9] version was the best model to predict the IBAE system and the IBA2P system was well represented by the UNIFAC-1987[8] model, as shown in Fig. 5. However, the ASOG[11] model gave a good prediction for the IBA2P system at 0.15 MPa, as can be seen in the inset of Fig. 5.

TABLE IV. Mean errors and average deviations in the prediction of the VLE data using the ASOG and UNIFAC models

Parameter	UNIFAC-1987[8] OH/COOC	UNIFAC 1991[9] OH/COOC	UNIFAC 1993[10] OH/COOC	ASOG[11] OH/COO
n-Propyl acetate (1) + ethanol (2) at 0.15 MPa				
$\delta(y_1)$	0.012	0.006	0.018	0.013
$\bar{e}(\gamma_1)$	4.89	4.80	7.42	4.89
$\delta(T)$ / K	0.47	1.26	0.73	0.50
Azeotropic data				
$x_{1az\,exp} = 0.051$	0.030	0.059	0.018	0.034
$T_{az\,exp}$ / K = 361.93	361.68	361.51	361.70	361.68

TABLE IV. Continued

Azeotropic data			
n-Propyl acetate (1) + 2-propanol (2) at 0.15 MPa			
$\delta(y_1)$	0.007	0.013	0.013	0.009
$\bar{e}(\gamma_1)$	4.61	8.51	10.18	5.78
$\delta(T)$ / K	0.44	0.47	1.23	0.19
Azeotropic data			
$x_{1az\ exp} = 0.011$	0.012	0.049	0.002	0.031
$T_{az\ exp}$ / K = 365.77	365.77	365.61	365.87	365.67
Isobutyl acetate (1) + ethanol (2) at 0.15 MPa			
$\delta(y_1)$	0.014	0.004	0.022	0.017
$\bar{e}(\gamma_1)$	5.85	1.89	10.48	7.87
$\delta(T)$ / K	1.24	0.41	2.21	1.59
Isobutyl acetate (1) + 2-propanol (2) at 0.15 MPa			
$\delta(y_1)$	0.003	0.017	0.014	0.005
$\bar{e}(\gamma_1)$	2.20	8.58	8.66	2.61
$\delta(T)$ / K	0.45	1.26	1.78	0.30
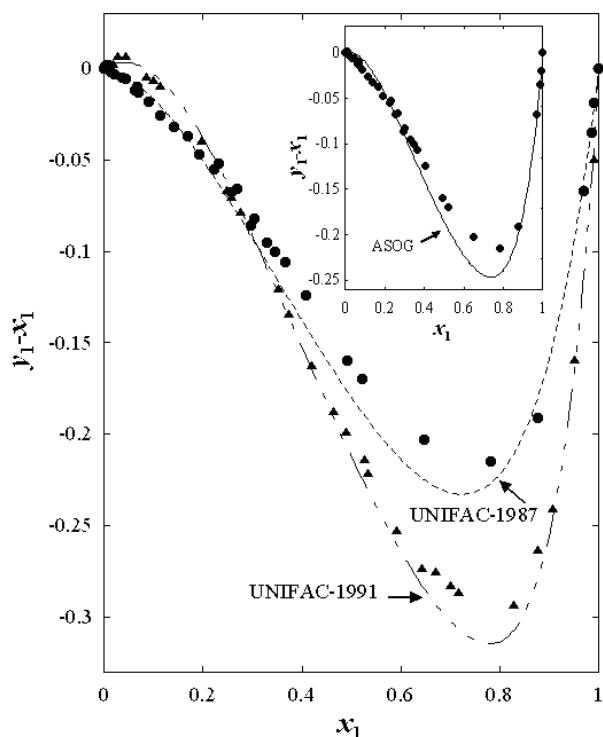
Fig. 4. Experimental points of $(y_1–x_1)$ *vs.* x_1 for *n*-propyl acetate (1) + ethanol (2) at 0.15 MPa (▲) and *n*-propyl acetate (1) + 2-propanol (2) at 0.15 MPa (●). Fitting curves of data prediction for *n*-propyl acetate (1) + ethanol (2) with UNIFAC-1991[9] and for *n*-propyl acetate (1) + 2-propanol (2) with UNIFAC-1987[8] or ASOG[11] for the inset.
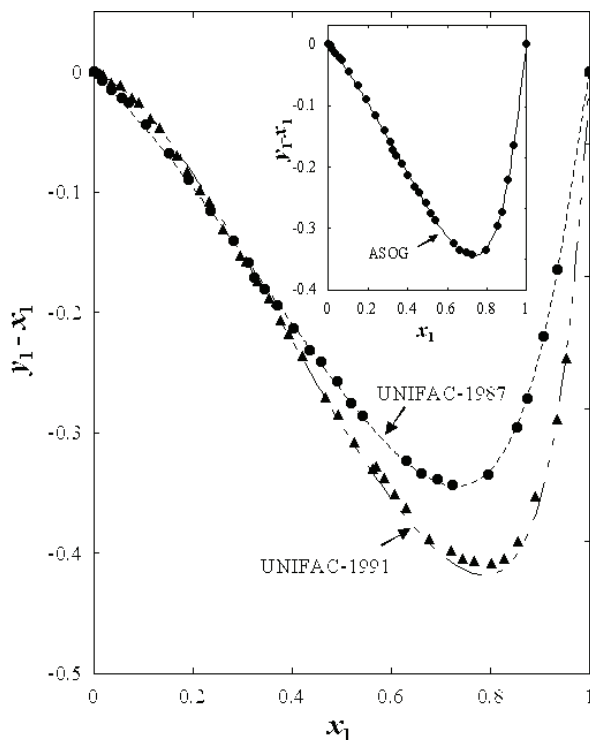
Fig. 5. Experimental points of (y_1–x_1) *vs.* x_1 for *iso*-butyl acetate (1) + ethanol (2) at 0.15 MPa (▲) and isobutyl acetate (1) + 2-propanol (2) at 0.15 MPa (●). Fitting curves of data prediction for isobutyl acetate (1) + ethanol (2) with UNIFAC-1991[9] and for isobutyl acetate (1) + 2-propanol (2) with UNIFAC-1987[8] or ASOG[11] for the inset.

Azeotropic data

The azeotropic points have been described in various works[5] for the PAE system. Ortega *et al.*[3] established that the composition and temperature of the azeotrope at 0.1600 MPa were x_{1az} = 0.041 and T_{az} = 363.14 K. On the other hand, for the system PA2P at 0.10132 MPa, the only azeotropic point was reported by González *et al.*[4] as x_{1az} = 0.037 and T_{az} = 355.2 K. Accordingly, the singular points in both systems, studied in this paper at 0.15 MPa (x_{1az} = 0.051 and T_{az} = 361.93 K for PAE system and x_{1az} = 0.011 and T_{az} = 365.77 K for PA2P system), are plotted in Fig. 6, together with literature data,[3–5] in order to verify, by means of the evolution of the azeotrope, the modifications introduced in the experimental installation. The azeotropic data from the literature[3–5] together with the azeotropic data from this work are presented in Fig. 6. For the PAE system these are indicated by the composition of the ester in x_1–T_r coordinates; and for the PA2P system in $\log_{10}(p_r)$–T_r coordinates. The azeotropic points of this paper are also indicated by pressure in x_1–$\log_{10} p_r$ coordinates.

The azeotropic data from this work present a good agreement with those in the literature.[3–5] The systems PAE and PA2P show a modification in the $T–x_1–y_1$ values with increasing pressure (Figs. 1 and 2); *i.e.*, the azeotrope moves towards lower ester mole fractions with increasing pressure. This produces a change in the $y_1–x_1$ values, which decrease, thus leading to the disappearance of the azeotrope with increasing pressure. This behaviour can be observed from the data presented in Fig. 6.
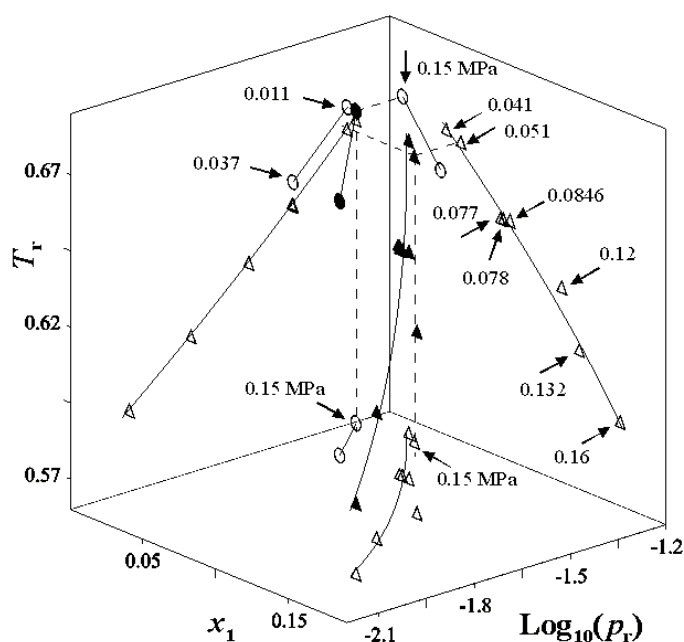
Fig. 6. Azeotropic data in reduced coordinates for the systems *n*-propyl acetate (1) + ethanol (2) (▲,△) and *n*-propyl acetate (1) + 2-propanol (2) (●,○) from literature[3-5] and this work at 0.15 MPa.

On the other hand, Table II shows the predictions made by the thermodynamic models for the azeotropic point for the systems studied in this work. It can be seen that, generally, they all give good predictions. However, when considering the group contribution models (Table IV) the ASOG[11] model is the one that globally best represents the azeotropic data of this work, while the UNIFAC-1991[9] model predicts well the singular point of the PAE system at 0.15 MPa; although the UNIFAC-1987[8] model predicts well the azeotropic data in the PA2P system at 0.15 MPa. In addition, the model UNIFAC-1993[10] does not give a good prediction of the azeotropic point, as shown in Table IV.

CONCLUSIONS

The isobaric VLE data for the binary systems n-propyl acetate + ethanol, n-propyl acetate + 2-propanol, isobutyl acetate + ethanol and isobutyl acetate + 2-propanol at 0.15 MPa have been measured using a stainless steel ebulliometer. The thermodynamic consistencies of the experimental data were checked by the van Ness Test[6] and agree with the Fredenslund validation criterion.[7]

Thermodynamically consistent VLE data and vapour pressures of 2-propanol, n-propyl acetate and isobutyl acetate were obtained and compared to those in the literature. The results showed that the new equipment introduced in the experimental installation enabled reliable data to be obtained.

The singular points of the systems n-propyl acetate + ethanol and n-propyl acetate + 2-propanol at 0.15 MPa were determined. The azeotropic data were correlated and discussed considering literature data and the effect of the system pressure on the elimination of azeotropes.

Several thermodynamic mathematical models, as well as group contribution models, the ASOG, the original UNIFAC, the UNIFAC-Lyngby and the UNIFAC-Dortmund, were applied, and the predictions were verified and discussed with respect to the experimental data obtained in this study.

SUPPLEMENTARY MATERIAL

Tables S-I–S-III (experimental data) are available electronically from http:// //www.shd.org.rs/JSCS/, or from the corresponding author on request.

NOMENCLATURE

A, B, C	Antoine Equation parameters (Eqs. (1) and (3))
A_k	Parameter of Eqs. (6)–(8)
B_{ii}	Second virial coefficient of the pure component, $m^3 \cdot mol^{-1}$
B_{ij}	Cross second virial coefficient, $m^3 \cdot mol^{-1}$
ΔH_{vap}	Enthalpy of vaporization, $J \cdot mol^{-1}$
$\bar{e}$	Average error, %
F	Property ($F = y_1$; $F = (y_1 - x_1)$; $F = \gamma_1$; $F = \gamma_2$; $F = T$; $F = G^E/RT$)
G^E	Excess free energy, $J \cdot mol^{-1}$
m	Number of equation parameters
n	Number of experimental data
n_D	Refractive index
p_i^0	Vapour pressure for pure substance, kPa
p	Total pressure, kPa
R	Universal gas constant, $J \cdot K^{-1} \cdot mol^{-1}$
R_T	Parameter of Eqs. (6)–(8)
T	Temperature, K
v_i^L, v_i^G	Pure substances liquid and gas molar volumes, $m^3 \cdot mol^{-1}$
x	Liquid-phase mole fraction
y	Vapour-phase mole fraction
Z_T	Active fraction of vapour phase or liquid phase.

Greek symbols

γ	Activity coefficient
δ	Mean deviation
ρ	Density, kg·m^{-3}
σ	Standard deviation.

Subscripts

az	Azeotrope
bp	Normal boiling point
cal	Calculated
exp	Experimental
i, j	Chemical substances
Lit	Literature
1	Ester.

И З В О Д

НАПОНИ ПАРА И РАВНОТЕЖА ПАРА–ТЕЧНОСТ ПРОПИЛАЦЕТАТА И ИЗОБУТИЛАЦЕТАТА СА ЕТАНОЛОМ ИЛИ 2-ПРОПАНОЛОМ НА ПРИТИСКУ 0,15 MPa. БИНАРНИ СИСТЕМИ

PEDRO SUSIAL, JOSÉ J. RODRÍGUEZ-HENRÍQUEZ, JOSÉ C. APOLINARIO, VICTOR D. CASTILLO и ESTEBAN J. ESTUPIÑAN

Escuela de Ingenierias Industriales y Civiles, Universidad de Las Palmas de Gran Canaria, Canary Islands, Spain

Одређени су напони пара пропилацетата, изобутилацетата и 2-пропанола, на апсолутном притиску од 0,004 MPa до 1,6 MPa, као и подаци за равнотежу пара-течност бинарних система пропилацетат + етанол, пропилацетат + 2-пропанол, изобутилацетат + етанол и изобутилацетат + 2-пропанол на притиску од 0,15 MPa. Експериментални подаци за равнотежу пара-течност су проверени преко теста van Ness-a и Fredenslud-овог критеријума. Бинарни системи пропилацетат+етанол и пропилацетат+2-пропанол имају тачку азеотропа на притиску 0,15 MPa. Примењене су различите верзије модела коефицијената активности универзалних квази-хемијских фунционалних група и аналитичких решења за групе да би се описали доприноси група.

(Примљено 13. децембра 2011, ревидирано 18. марта 2012)

REFERENCES

1. P. Susial, A. Sosa-Rosario, R. Rios-Santana, *J. Chem. Eng. Data* **55** (2010) 5701
2. P. Susial, A. Sosa-Rosario, J. J. Rodríguez-Henríquez, R. Rios-Santana, *J. Chem. Eng. Jpn.* **44** (2011) 155
3. J. Ortega, C. González, J. Peña, S. Galván, *Fluid Phase Equilib.* **170** (2000) 87
4. C. González, J. Ortega, P. Hernández, S. Galván, *J. Chem. Eng. Data* **44** (1999) 772
5. J. Gmehling, J. Menke, J. Krafczyk, K. Fischer, *Azeotropic Data*, Part 1, Wiley-VCH, Weinheim, Germany, 2004, pp. 326 and 445
6. H. C. Van Ness, S. M. Byer, R. E. Gibbs, *AIChE J.* **19** (1973) 238
7. A. Fredenslund, J. Gmehling, P. Rasmussen, *Vapor–liquid Equilibria Using UNIFAC. A Group Contribution Model*, Elsevier, Amsterdam, Netherlands,1977, pp. 11–15, 73 and 214–219

8. L. B. Larsen, P. Rasmussen, A. Fredenslund, *Ind. Eng. Chem. Res.* **26** (1987) 2274
9. H. K. Hansen, P. Rasmussen, A. Fredenslund, M. Schiller, J. Gmehling, *Ind. Eng. Chem. Res.* **30** (1991) 2355
10. J. Gmehling, J. Li, M. Schiller, *Ind. Chem. Eng. Res.* **32** (1993) 178
11. K. Kojima, K. Tochigi, *Prediction of Vapor–Liquid Equilibria by the ASOG Method*, Kodansha Ltd, Tokyo, Japan, 1979, pp. 11–50
12. J. A. Riddick, W. B. Bunger, T. K. Sakano, *Organic Solvents*, 4th ed., Wiley-Interscience, New York, 1986, pp. 398 and 400
13. J. B. Montón, R. Muñoz, M. C. Burget, J. de la Torre, *Fluid Phase Equilib.* **227** (2005) 19
14. Y. He, R. Jiang, F. Zhu, T. Luan, Z. Huang, G. Ouyang, *J. Chem. Eng. Data* **53** (2008) 1186
15. J. Nelder, R. Mead, *Comput. J.* **7** (1965) 308
16. E. Hála, J. Pick, V. Fried, O. Vilím, *Vapour–Liquid Equilibrium*, 2nd ed., Pergamon Press, Oxford, UK, 1967, pp. 249–251
17. C. L. Yaws, *Yaws' Handbook of Thermodynamic and Physical Properties of Chemical Compounds*, Knovel, Norwich, New York, 2003, pp. 456, 480, 1156 and 1180
18. J. G. Hayden, J. P. O'Connell, *Ind. Eng. Chem. Process Des. Dev.* **14** (1975) 209
19. L. C. Yen, S. S. Woods, *AIChE J.* **12** (1966) 95
20. M. J. Holmes, M. Vanwinkle, *Ind. Eng. Chem.* **62** (1970) 21.

SUPPLEMENTARY MATERIAL TO

Vapour pressures and vapour–liquid equilibria of binary systems of *n*-propyl acetate and isobutyl acetate with ethanol or 2-propanol at 0.15 MPa

PEDRO SUSIAL*, JOSÉ J. RODRÍGUEZ-HENRÍQUEZ, JOSÉ C. APOLINARIO, VICTOR D. CASTILLO and ESTEBAN J. ESTUPIÑAN

Escuela de Ingenierias Industriales y Civiles, Universidad de Las Palmas de Gran Canaria, Canary Islands, Spain

TABLE S-I. Experimental vapour pressures

T / K	p_i^0 / kPa	T / K	p_i^0 / kPa	T / K	p_i^0 / kPa	T / K	p_i^0 / kPa	T / K	p_i^0 / kPa	T / K	p_i^0 / kPa
2-Propanol											
303.56	8	345.30	66	366.07	152	377.07	224	411.57	630	439.61	1250
311.44	12	345.81	68	367.12	158	377.87	230	412.83	652	440.50	1275
316.51	16	346.48	70	367.90	162	378.39	234	414.36	677	441.23	1297
319.19	20	348.01	74	368.48	166	378.89	238	417.34	732	442.03	1320
324.18	24	349.26	78	369.51	172	379.95	246	418.21	750	442.81	1342
326.53	28	350.40	82	370.52	178	383.66	275	419.23	767	443.61	1367
328.03	30	351.73	86	371.16	182	387.08	307	421.88	822	444.31	1390
329.48	32	352.79	90	372.14	188	391.67	355	423.21	850	445.31	1420
332.50	36	353.80	94	372.66	192	396.12	407	424.69	882	446.15	1447
334.25	40	358.44	116	373.24	196	398.35	432	427.68	947	447.02	1475
336.38	44	359.92	124	374.35	204	399.85	452	428.98	977	447.68	1497
338.14	48	362.66	134	374.95	208	401.41	475	432.25	1055	448.59	1527
339.77	52	363.46	138	375.51	212	405.52	532	435.33	1132	450.13	1577
341.35	56	364.65	142	376.12	216	406.85	555	437.20	1182	450.86	1602
342.89	60	365.31	148	376.65	220	408.62	582	438.84	1227	451.83	1635
343.75	62	–	–	–	–	–	–	–	–	–	–
n-Propyl acetate											
302.38	6	357.81	58	394.33	170	423.22	357	448.73	627	487.55	1282
309.27	8	359.20	62	397.74	187	424.18	365	451.04	657	488.95	1315
315.38	10	362.40	68	399.26	195	425.46	375	455.14	712	490.05	1337
320.58	14	364.27	72	401.24	205	426.57	385	460.59	792	491.35	1365
325.60	18	365.48	74	402.83	215	427.66	395	465.04	862	492.75	1397
328.41	20	367.16	78	406.50	235	429.93	415	467.92	907	493.35	1412
332.40	24	368.08	82	408.00	245	431.15	427	469.84	942	494.65	1442

* Corresponding author. E-mail: psusial@dip.ulpgc.es

TABLE S-I. Continued

T / K	p_i^0 / kPa	T / K	p_i^0 / kPa	T / K	p_i^0 / kPa	T / K	p_i^0 / kPa	T / K	p_i^0 / kPa	T / K	p_i^0 / kPa
					n-Propyl acetate						
335.68	26	369.09	84	409.60	255	432.20	437	472.33	985	495.35	1462
339.33	30	370.28	86	411.25	267	433.50	450	475.65	1045	496.85	1495
342.21	34	371.66	90	412.54	275	434.35	460	476.95	1067	498.15	1527
343.81	36	373.30	94	413.53	282	435.48	470	479.55	1117	499.05	1547
346.06	38	373.38	96	415.32	295	436.50	480	481.45	1155	500.05	1572
348.04	42	379.45	110	418.10	315	437.21	490	482.55	1180	500.75	1592
350.03	44	382.17	120	419.28	325	438.90	507	483.95	1205	501.95	1622
352.94	50	385.15	130	420.60	335	440.50	525	486.75	1265	502.85	1645
354.50	52	392.84	165	422.07	347	444.26	572	–	–	–	–
					Isobutyl acetate						
300.37	4	362.48	44	382.54	83	437.17	360	479.05	860	500.05	1250
309.69	6	364.22	47	383.57	86	439.16	380	480.25	880	501.65	1285
314.21	7	365.73	49	384.87	89	444.08	420	482.55	920	502.85	1312
324.01	10	366.75	51	385.95	91	446.83	450	483.85	940	503.95	1335
328.95	13	368.21	54	387.33	95	451.64	497	485.25	965	504.85	1355
333.57	15	369.67	57	387.82	96	454.17	527	486.45	985	505.65	1375
338.71	19	370.70	58	388.48	98	456.23	550	487.55	1005	506.85	1402
343.41	23	372.46	61	395.75	122	458.84	580	488.95	1030	507.75	1422
345.40	24	374.00	64	401.04	142	462.15	620	490.55	1060	508.55	1442
348.39	27	375.80	68	406.50	167	463.55	637	491.55	1080	509.45	1462
351.91	31	376.72	70	414.56	205	465.14	657	493.75	1122	510.25	1482
354.14	34	378.20	74	416.65	217	466.87	680	494.95	1145	511.85	1520
356.77	37	379.85	77	420.55	242	469.53	717	496.95	1185	512.65	1540
358.25	39	380.56	79	423.76	260	471.14	740	497.95	1205	513.45	1560
360.63	42	381.80	82	434.94	170	472.34	760	498.85	1225	515.15	1602

TABLE. S-II. Experimental T–x_1–y_1 data and calculated values for the activity coefficients of the liquid phase for the *n*-propyl acetate systems

T / K	x_1	y_1	γ_1	γ_2	T / K	x_1	y_1	γ_1	γ_2
				n-Propyl acetate (1) + ethanol (2) at 0.15 MPa					
362.13	0.000	0.000	–	1.000	365.31	0.464	0.276	1.238	1.190
361.97	0.008	0.009	2.619	0.989	365.79	0.489	0.290	1.215	1.204
361.95	0.018	0.020	2.588	0.989	366.22	0.525	0.311	1.196	1.238
361.93	0.028	0.034	2.830	0.985	366.82	0.532	0.310	1.154	1.233
361.93	0.044	0.050	2.648	0.985	367.60	0.592	0.339	1.106	1.319
361.96	0.086	0.081	2.192	0.996	368.47	0.641	0.367	1.075	1.393
362.01	0.098	0.091	2.157	0.996	369.38	0.669	0.393	1.071	1.405
362.07	0.113	0.103	2.113	0.998	370.05	0.700	0.417	1.063	1.456
362.56	0.196	0.156	1.815	1.018	370.39	0.716	0.429	1.058	1.489
362.99	0.247	0.180	1.638	1.040	374.57	0.828	0.534	0.999	1.747
363.17	0.256	0.185	1.614	1.040	377.27	0.876	0.612	0.996	1.848
363.44	0.275	0.196	1.578	1.043	379.26	0.907	0.666	0.986	1.991
364.32	0.352	0.231	1.411	1.082	383.06	0.951	0.791	0.997	2.098
364.58	0.373	0.238	1.360	1.098	387.53	0.989	0.939	1.001	2.379

TABLE S-II. Continued

T / K	x_1	y_1	γ_1	γ_2	T / K	x_1	y_1	γ_1	γ_2
				n-Propyl acetate (1) + ethanol (2) at 0.15 MPa					
365.01	0.419	0.256	1.284	1.140	389.26	1.000	1.000	1.000	–
				n-Propyl acetate (1) + 2-propanol (2) at 0.15 MPa					
365.88	0.000	0.000	–	1.000	366.65	0.232	0.180	1.539	1.034
365.79	0.002	0.003	3.058	0.998	366.77	0.256	0.188	1.452	1.052
365.79	0.005	0.007	2.854	0.997	366.81	0.268	0.202	1.488	1.050
365.78	0.006	0.007	2.379	0.998	366.94	0.297	0.211	1.397	1.075
365.77	0.008	0.010	2.550	0.998	367.02	0.303	0.221	1.430	1.068
365.77	0.014	0.012	1.749	1.002	367.16	0.330	0.235	1.390	1.085
365.77	0.021	0.018	1.749	1.003	367.19	0.345	0.245	1.385	1.095
365.80	0.036	0.031	1.755	1.004	367.44	0.365	0.259	1.373	1.098
365.83	0.043	0.037	1.752	1.004	367.92	0.408	0.284	1.326	1.119
365.85	0.063	0.051	1.647	1.010	368.91	0.492	0.332	1.246	1.174
365.85	0.066	0.056	1.727	1.008	369.34	0.521	0.351	1.227	1.191
365.89	0.070	0.057	1.655	1.009	371.78	0.648	0.445	1.158	1.272
365.95	0.089	0.071	1.618	1.013	375.92	0.781	0.566	1.075	1.388
365.99	0.114	0.088	1.564	1.021	379.26	0.877	0.686	1.049	1.599
366.04	0.140	0.108	1.561	1.027	386.11	0.969	0.902	1.022	1.589
366.11	0.168	0.131	1.574	1.031	387.46	0.985	0.950	1.019	1.607
366.31	0.193	0.146	1.517	1.037	387.98	0.991	0.972	1.021	1.476
366.58	0.223	0.168	1.498	1.040	389.26	1.000	1.000	1.000	–

TABLE. S-III. Experimental T–x_1–y_1 data and calculated values for the activity coefficients of the liquid phase for the isobutyl acetate systems

T / K	x_1	y_1	γ_1	γ_2	T / K	x_1	y_1	γ_1	γ_2
				Isobutyl acetate (1) + ethanol (2) at 0.15 MPa					
362.13	0.000	0.000		1.000	366.49	0.467	0.196	1.275	1.276
362.17	0.020	0.017	3.010	0.986	367.15	0.494	0.209	1.256	1.292
362.22	0.036	0.027	2.651	0.990	367.80	0.527	0.219	1.206	1.335
362.30	0.054	0.043	2.806	0.990	368.45	0.563	0.233	1.175	1.388
362.36	0.077	0.055	2.511	1.000	368.65	0.571	0.243	1.200	1.386
362.40	0.091	0.065	2.507	1.003	369.13	0.586	0.248	1.174	1.404
362.50	0.116	0.077	2.321	1.015	369.70	0.608	0.257	1.150	1.437
362.61	0.133	0.086	2.252	1.020	370.25	0.631	0.269	1.138	1.474
362.91	0.168	0.098	2.010	1.038	371.70	0.677	0.289	1.086	1.560
363.05	0.190	0.107	1.930	1.051	373.40	0.720	0.322	1.075	1.622
363.23	0.215	0.117	1.853	1.065	374.30	0.743	0.338	1.061	1.675
363.40	0.233	0.125	1.816	1.074	375.50	0.767	0.361	1.056	1.715
363.66	0.261	0.130	1.670	1.098	377.15	0.801	0.393	1.043	1.808
364.02	0.297	0.144	1.605	1.122	378.70	0.827	0.422	1.032	1.885
364.15	0.307	0.149	1.600	1.126	381.29	0.856	0.466	1.014	1.927
364.60	0.330	0.156	1.534	1.137	383.95	0.891	0.538	1.035	2.027
364.97	0.355	0.167	1.506	1.151	389.15	0.935	0.646	1.011	2.224
365.40	0.378	0.172	1.435	1.169	391.86	0.952	0.714	1.012	2.245
365.50	0.393	0.175	1.400	1.189	403.32	1.000	1.000	1.000	–

TABLE S-III. Continued

T / K	x_1	y_1	γ_1	γ_2	T / K	x_1	y_1	γ_1	γ_2
Isobutyl acetate (1) + ethanol (2) at 0.15 MPa									
365.80	0.422	0.186	1.371	1.220	–	–	–	–	–
Isobutyl acetate (1) + 2-propanol (2) at 0.15 MPa									
365.88	0.000	0.000		1.000	371.00	0.435	0.204	1.217	1.169
365.98	0.009	0.007	2.393	0.994	371.50	0.459	0.218	1.212	1.178
366.07	0.017	0.010	1.804	0.996	372.18	0.490	0.233	1.186	1.197
366.14	0.036	0.021	1.785	1.002	372.90	0.518	0.243	1.143	1.220
366.28	0.057	0.035	1.870	1.004	373.50	0.541	0.255	1.126	1.235
366.46	0.071	0.045	1.918	1.002	375.83	0.631	0.308	1.080	1.318
366.75	0.105	0.061	1.741	1.012	376.80	0.661	0.327	1.061	1.350
367.06	0.151	0.083	1.629	1.031	378.04	0.693	0.354	1.053	1.373
367.49	0.192	0.102	1.552	1.044	379.15	0.723	0.380	1.046	1.408
367.58	0.235	0.119	1.475	1.079	383.30	0.795	0.460	1.011	1.449
368.29	0.281	0.141	1.426	1.091	387.37	0.853	0.558	1.009	1.455
368.72	0.313	0.154	1.378	1.107	389.58	0.873	0.601	0.994	1.421
368.80	0.323	0.152	1.315	1.123	392.84	0.907	0.687	0.993	1.380
369.20	0.344	0.163	1.306	1.128	395.69	0.935	0.771	0.995	1.328
369.86	0.371	0.177	1.286	1.130	403.32	1.000	1.000	1.000	–
370.36	0.402	0.189	1.246	1.151	–	–	–	–	–

Artificial neural network prediction of aluminum extraction from bauxite in the Bayer process

ISIDORA ĐURIĆ[1], IVAN MIHAJLOVIĆ[1*#], ŽIVAN ŽIVKOVIĆ[1]
and DRAGANA KEŠELJ[2]

[1]*University of Belgrade, Technical Faculty in Bor, Serbia*
[2]*Faculty of Technology Zvornik, Republic of Srpska, Bosnia and Herzegovina*

Abstract: This paper presents the results of statistical modeling of the bauxite leaching process, as part of the Bayer technology for alumina production. Based on the data collected during the period 2008–2009 (659 days) from the industrial production in the Alumina Factory Birač, Zvornik (Bosnia and Herzegovina), the above-mentioned process was statistically modeled. The dependant variable, which was the main target of the modeling procedure, was the degree of Al_2O_3 recovery from boehmite bauxite during the leaching process. The statistical model was developed as an attempt to define the dependence of the degree of Al_2O_3 recovery on the input variables of the leaching process, *i.e.*, the composition of the bauxite, the composition of the sodium aluminate solution and the caustic module of the solution before and after the leaching process. As statistical modeling tools, multiple linear regression analysis (MLRA) and artificial neural networks (ANNs) were used. The fitting level obtained using MLRA, was $R^2 = 0.463$, while the ANN resulted in an R^2 value of 0.723. In this way, the model defined using the ANN methodology could be used for the efficient prediction of the degree of recovery of Al_2O_3 as a function of the process inputs, under the industrial conditions of the Alumina Factory Birač, Zvornik. The proposed model also has a universal character and, as such, is applicable in other factories employing the Bayer technology for alumina production.

Keywords: leaching; bauxite; Bayer process; statistical modeling; neural networks.

INTRODUCTION

The Bayer process of alumina extraction is a basic commercial procedure and more than 90 % of the world alumina production is obtained in this way. Despite the fact that this process has been used for alumina production for a long

---

1259

period, there are still attempts to improve the process further.[1] Bauxite is a complex heterogeneous material used in the Bayer process of alumina production. Aluminum is usually present in bauxite in the form of hydroxide minerals, such as gibbsite (hydrargillite) ($Al(OH)_3$), boehmite ($AlO(OH)$) or diaspore ($HAlO_2$). Besides aluminum minerals, bauxite ore contains various combinations of silica (SiO_2), aluminosilicates, iron oxide (Fe_2O_3), titanium oxide (TiO_2) and other impurities, such as carbonates and sulfides, in trace amounts.[2,3]

The Bayer process includes the leaching of bauxites in a concentrated sodium hydroxide (caustic) solution at temperatures ranging from 373 K (100 °C) to 523 K (250 °C), depending on the mineralogical form of the aluminum hydroxide in the bauxite. The process includes reactions with soluble silica compounds and titan dioxide under certain conditions.[4] Silicon is usually present in bauxite in two potential forms: *i*) soluble, which is usually in the form of kaolinite ($Al_2O_3 \cdot 2SiO_2 \cdot 2H_2O$) or the amorphous form of silicon dioxide (silica) and *ii*) insoluble, in the form of quartz. In a caustic solution, the dissolved kaolinite and amorphous silicon dioxide form a sodalite-type product, with the general formula $3(Na_2O \cdot Al_2O_3 \cdot 2SiO_2 \cdot 2H_2O)$ $2NaX$, where X could be: OH^-, Cl^-, CO_3^{2-} or SO_4^{2-}.[5–8] The rate of the aluminum hydroxide leaching process depends on its mineral form in the bauxite. The trihydrate bauxite type gibbsite can be dissolved in a caustic solution in the temperature range 373–453 K (100–180 °C). Monohydrate bauxite forms (boehmite and diaspore) are dissolved in the temperature ranges 403–453 K (130–180 °C) and 473–523 K (200–250 °C), respectively.[9,10]

Sodium aluminosilicate is precipitated in red mud, which is the source of aluminum and sodium hydroxide losses during the Bayer process. Sedimented red mud also presents an environmental problem.[11] This problem has attracted much attention recently, especially because of global environmental protection problems, which demand the compliance with global principles during local actions.[12]

During the process of bauxite leaching in alkaline sodium aluminate, the aluminum ions in the solution are hydrolyzed in the aqueous environment, forming numerous mononuclear and polynuclear hydroxo complex ions. Finally, in mild-to-strong alkaline solutions, $Al(OH)_4^-$ is predominant at pH values higher than 10.[11] Kinetic parameters indicate that the bauxite leaching process is conducted in the so-called "kinetic area", which suggests that the temperature is the main parameter influencing the overall rate of the process.[10,13] The process parameters influencing the leaching rate and the degree of Al_2O_3 recovery are: the mineralogical and chemical composition of bauxite, grain size distribution, caustic module of the starting solution and its Na_2O (caustic) mass fraction, leaching process temperature, stirring speed and duration of the process.[1,10,11,13]

The process of bauxite leaching, under industrial conditions of Bayer technology for alumina production is highly complex. The ability to predict the reco-

very of Al_2O_3 during leaching as the result of modeling of the input process variables presents a great challenge for the management of the process.[4]

The main objective pursued in this work was to create a mathematical model for the prediction of the degree of Al_2O_3 recovery (output of the process), during bauxite leaching, as the function of the input variables of the process. The obtained model presents a great advantage due to its ability to predict accurately the output of the investigated process.

EXPERIMENTAL

A data set suitable for the calculations and presented in this paper was formed according to the data collected during the industrial production in the Alumina Factory Birač, Zvornik (Bosnia and Herzegovina). This factory has a production capacity of 600 000 tons of alumina per year. The important process parameters included in the obtained data set were the chemical composition of the bauxite (including Al_2O_3, SiO_2, Fe_2O_3, TiO_2, CaO and H_2O, and the mass loss during calcination); the composition of the starting aluminate solution (including Al_2O_3, Na_2O and the starting caustic module); the chemical composition of the residual autoclave mud – red mud (including Al_2O_3, $Na_2O_{(total)}$, SiO_2, TiO_2 and CaO); the composition of the aluminate solution at the end of the leaching process (including Al_2O_3, Na_2O and the final caustic module). The chemical composition of the samples was expressed as the mass fraction of the constituents. All of these process parameters were measured daily during the years 2008 and 2009, and in this way, 659 samples were collected during each day of stabile production in the factory. All the samples were examined for potential outliers before any further modeling procedure. No strong extreme behavior of the variables was detected. Thus, the obtained results could be considered as true representatives of the investigated process.

The output of the investigated process was the "Al_2O_3 leaching recovery", which is presented as Y in the further text, and it refers to the alumina recovery in the digestion process that was calculated using the following equation:

$$Y = 100(1 - Al_2O_{3(rm)} \cdot Fe_2O_{3(b)}/Al_2O_{3(b)} \cdot Fe_2O_{3(rm)}) \tag{1}$$

where $Al_2O_{3(b)}$ and $Fe_2O_{3(b)}$ are the mass fraction in the bauxite (%) and $Al_2O_{3(rm)}$ and $Fe_2O_{3(rm)}$ are the mass fraction in the residual autoclave mud (red mud) (%).

On application of Eq. (1) for calculating the degree of recovery Al_2O_3 during the leaching process, which is based on adopting the "inert" Fe_2O_3, acceptable results (accuracy above 99 %) were obtained.

The following process parameters were selected as the inputs included in the statistical modeling procedure:

X_1 – Na_2O (caustic) concentration in the starting solution (g dm^{-3}),

X_2 – Al_2O_3 concentration in the starting solution (g dm^{-3}),

X_3 – starting caustic ratio of the solution,

X_4 – moisture mass fraction in the bauxite (%),

X_5 – Al_2O_3 mass fraction in the bauxite (%),

X_6 – SiO_2 mass fraction in the bauxite (%),

X_7 – Fe_2O_3 mass fraction in the bauxite (%),

X_8 – TiO_2 mass fraction in the bauxite (%),

X_9 – CaO mass fraction in the bauxite (%),

X_{10} – mass loss during calcinations of the bauxite (%) and

X_{11} – final caustic ratio of the solution at the end of the leaching process.

ĐURIĆ *et al.*

During the period when these parameters were measured and the corresponding data set formed, the operation of the factory was in a stable mode. The bauxite used for alumina production was from the ore body Vlasenica (Bosnia and Herzegovina). This ore body has large reserves of boehmitic bauxites. The temperature of the leaching process was kept constant at 518 K (245 °C). The pressure in the autoclave reactors was 35 bar. The size distribution of the bauxite grains was 100 % –74 µm, obtained after the hydrocyclone classification. The solid to liquid ratio of the autoclave charge was $S:L = 1:5$. The solid phase concentration was 160–200 g dm^{-3}, depending on the Na_2O (caustic) concentration in the returned aluminate solution. The rate of mechanical stirring was 31 rpm.

RESULTS AND DISCUSSION

For modeling the bauxite leaching process, the data were collected by measuring the above-defined input and output process variables. The values of the measured input variables of the technological process as well as the process quality indicators, the output of the process (Y) in the form of descriptive statistics results, are presented in Table I.

TABLE I. Descriptive statistics of the input (X_i) and output (Y) variables of the bauxite leaching process including 659 data sets

Parameter	Range	Minimum	Maximum	Mean		Std. deviation	Variance
				Statistic	Std. error		
X_1	90.19	129.66	219.86	2.040E2	0.4050	10.398	108.131
X_2	48	81	129	109.79	0.329	8.442	71.274
X_3	1.898	2.075	3.972	3.069	0.0080	0.2059	0.042
X_4	7.21	8.11	15.32	11.533	0.056	1.439	2.073
X_5	4.58	50.08	54.66	51.975	0.034	0.866	0.750
X_6	3.54	4.88	8.42	6.3208	0.022	0.562	0.316
X_7	4.39	22.42	26.81	24.833	0.031	0.803	0.645
X_8	0.63	2.22	2.85	2.540	0.003	0.078	0.006
X_9	2.82	0.29	3.11	1.253	0.014	0.370	0.137
X_{10}	3.17	11.40	14.57	12.459	0.023	0.581	0.337
X_{11}	0.524	1.116	1.639	1.414	0.00122	0.0314	0.001
Y	13.077	76.293	89.370	84.427	0.06574	1.687	2.848

It should be noted that X_8 and X_{11} have a small variance (Table I). However, these variables are important for the investigated technological process, especially X_{11}. The variable X_{11} presents the caustic ratio of the solution at the end of the leaching process; it is one of the most important parameters of the Bayer process; thus, it cannot be omitted from the analysis.

Linear regression analysis

For defining the correlation dependence in the form of output of the process $Y = f$ input of the process (X_1–X_{11}), a bivariate correlation analysis was performed. In this analysis, the Pearson correlation coefficients (PCC) with responding statistical significance were calculated (Table II) using statistical software

TABLE II. Correlation matrix for the input (X_1–X_{11}) and output variables (Y) of the investigated process (number of data points for each variable was 659)

Parameter	Correlation	X_1	X_2	X_3	X_4	X_5	X_6	X_7	X_8	X_9	X_{10}	X_{11}	Y
X_1	PC[a]	1											
	S[b]												
X_2	PC	0.534c	1										
	S	0.000											
X_3	PC	0.151c	–0.752c	1									
	S	0.000	0.000										
X_4	PC	–0.368c	–0.561c	0.367c	1								
	S	0.000	0.000	0.000									
X_5	PC	–0.379c	–0.463c	0.238c	0.570c	1							
	S	0.000	0.000	0.000	0.000								
X_6	PC	–0.378c	–0.240c	–0.012	0.107c	–0.105c	1						
	S	0.000	0.000	0.758	0.006	0.007							
X_7	PC	0.223c	0.425c	–0.320c	–0.393c	–0.431c	–0.282c	1					
	S	0.000	0.000	0.000	0.000	0.000	0.000						
X_8	PC	0.251c	0.030	0.164c	0.127c	0.049	–0.353c	–0.026	1				
	S	0.000	0.439	0.000	0.001	0.210	0.000	0.499					
X_9	PC	0.153c	0.055	0.063	–0.127c	–0.380c	–0.108c	–0.247c	–0.011	1			
	S	0.000	0.155	0.108	0.001	0.000	0.005	0.000	0.771				
X_{10}	PC	0.474c	0.205c	0.123c	–0.220c	–0.384c	–0.307c	–0.277c	0.233c	0.346c	1		
	S	0.000	0.000	0.002	0.000	0.000	0.000	0.000	0.000	0.000			
X_{11}	PC	–0.327c	–0.479c	0.312c	0.367c	0.300c	0.163c	–0.237c	–0.082d	–0.022	–0.180c	1	
	S	0.000	0.000	0.000	0.000	0.000	0.000	0.000	0.035	0.573	0.000		
Y	PC	0.233c	–0.069	0.265c	0.169c	0.311c	–0.494c	–0.289c	0.424c	0.126c	0.325c	0.103c	1
	S	0.000	0.076	0.000	0.000	0.000	0.000	0.000	0.000	0.001	0.000	0.008	

[a]Pearson correlation; [b]Sig. (2-tailed); [c]correlation is significant at the 0.01 level (2-tailed); [d]Correlation is significant at the 0.05 level (2-tailed)

SPSS v.18 (PASW Statistics). The results obtained revealed considerable statistical significance of the correlations ($p \leq 0.01$) for most of the coupled variables, Table II. To define the dependence of the output variable as a function of input variables, using the multiple linear regression analysis (MLRA) with acceptable level of fitting, it is necessary that the value of PCC between Y and X_i should be with statistical significance ($p \leq 0.01$).[14,15] The analysis of the data presented in Table II revealed that this constraint was attained in all cases except for Y–X_2: $PCC = -0.069$ ($p = 0.076$).

As most of the variables had an acceptable level of correlation and statistical significance, it was concluded that the MLRA approach should be considered as an adequate tool for modeling the investigated process. For the purpose of MLRA analysis, the assembly of 659 input and output samples was divided into two groups. The first group consisted of 458 (70 %) randomly selected samples. This group was used for the creation of the model, whereas the second group, consisting of the remaining 201 (30 %) samples from the starting data set, was used for testing the model. The selection of the variables for these two stages was performed using a random number generator.

Using multivariable regression, the following equation was developed to describe the relationship between the leaching recovery and the selected input variables:

$$Y = 38.437 - 0.024X_1 + 0.098X_2 + 3.603X_3 - 0.022\,X_4 + 0.478X_5 - 1.101X_6 -$$
$$- 0.562X_7 + 4.892X_8 + 0.203X_9 + 0.270X_{10} + 6.586X_{11}\ (R^2 = 0.555) \tag{2}$$

Equation (2) represents the complete linear model developed during the first phase of the MLRA modeling procedure.

The results of the ANOVA tests of the developed model are presented in Table III. The small value of the F statistics (Table III) indicates that the developed model was below the level for an accurate prediction of the value of dependent variable (Y) based on the values of input variables (X_i). The ratio of the regression to the residual was 55:45 %, advocating that only 55 % of the variance in the dependant variable (Y) values, is explained by the model.

TABLE III. Results of the ANOVA[a] test (predictors (constant): X_{11}, X_8, X_9, X_7, X_3, X_6, X_1, X_4, X_{10}, X_5 and X_2; dependent variable: Y) performed during the training of the model

Parameter	Sum of squares	Degree of freedom (df)	Mean square	F	Sig.
Regression	708.744	11	64.431	50.511	.000[a]
Residuals	568.913	446	1.276	–	–
Total	1277.657	457	–	–	–

The summary results describing the MLRA model in the development phase, are presented in Table IV. The relatively small value of the correlation coefficient ($R = 0.745$), resulting by a low coefficient of determination ($R^2 = 0.555$),

suggests that the model developed according to MLRA seems unacceptable for the prediction of alumina extraction from bauxite in the Bayer process.

TABLE IV. MLRA summary of the model developed during the training phase

Model	R	R^2	Adjusted R^2	Standard error of the estimate
1	0.745	0.555	0.544	1.1294

However, some further validation of the model was performed in the testing stage using the second part of the data set (total 201 vectors). During the testing phase of the MLRA model, the calculated coefficient of determination (R^2), as expected, further decreased in comparison to the testing phase and was now 0.463. A comparative presentation of the measured and the calculated values using the MLRA approach for the investigated process is illustrated in Fig. 1.
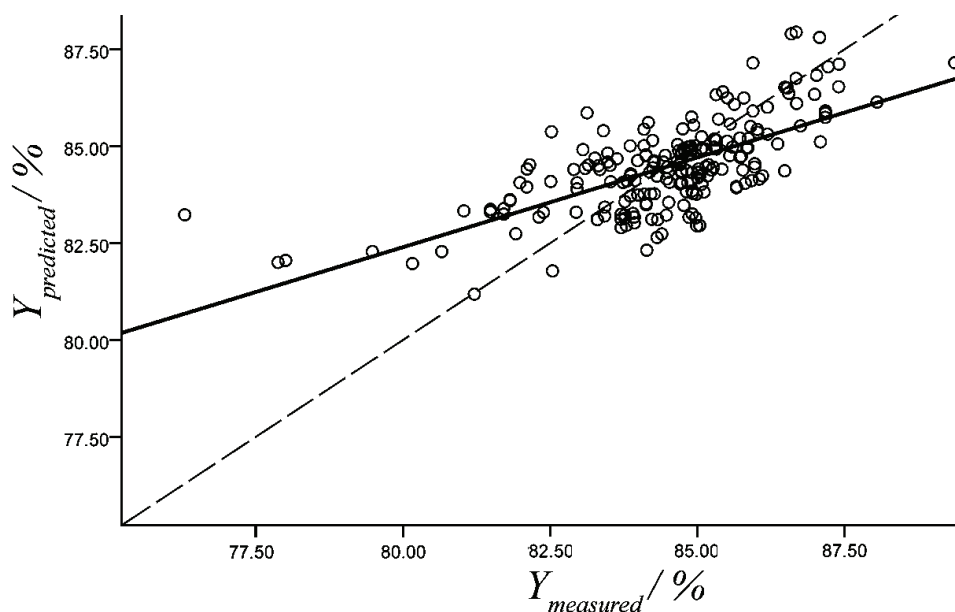
Fig. 1. Dependence between the calculated and measured values of the Al$_2$O$_3$ recovery (Eq. (2)); - - - = ideal position; ▬ = regression lines; ○ = values calculated using the MLRA model in the testing stage).

The difference distribution between the recoveries calculated from Eq. (2) and the actually determined amounts of recovery is shown in Fig. 2. The multivariable regression analysis predicted the alumina leaching recovery with a determination coefficient $R^2 = 0.463$ and differences of – 7.20 to 2.50 from actually determined recoveries in the plant, which does not represent a large significance. Thus, the results showed that the MLRA modeling methodology lead to no acceptable correlation between the selected variables and the Al$_2$O$_3$ recovery.

Artificial neural network

Artificial neural networks can be viewed as nonlinear approaches to multi-variate statistical methods, not bound by assumptions of normality or linearity. Although neural networks originated outside the field of statistics and have even been seen as an alternative to statistical methods in some circles, there are signs that this viewpoint is initiating an appreciation of the manners in which neural networks complement classical statistics.[16,17]

The ANN used in the development of the model described in this paper is depicted in Fig. 3. As shown, this network consists of three layers of nodes. The layers, described as input, hidden and output layers, comprise i, j and k numbers of processing nodes, respectively. Each node in the input (hidden) layer is linked to all the nodes in the hidden (output) layer using weighted connections. In addition to the i and j numbers of input and hidden nodes, the ANN architecture also houses a bias node (with a fixed output +1) in its input and hidden layers and they provide additional adjustable parameters (weights) for model fitting. The number of the nodes (i) in the ANN network input layer is equal to the number of inputs in the process, whereas the number of output nodes (k) equals the number of process outputs. However, the number of hidden nodes (j) is an adjustable parameter the magnitude of which is determined by issues, such as the desired approximation and generalization capabilities of the network model.[18,19]

The employment of an ANN usually comprises three phases. First is the training phase, which is achieved using 70–80 % of randomly selected data from the starting data set. During this phase, the correction of the weighted parameters of the connections is achieved through the necessary number of iterations, until the mean squared error between the calculated and measured outputs of the network is minimal. During the second phase, the remaining 20–30 % of the data are used for testing the "trained" network. In this phase, the network uses the weighted parameters determined during the first phase. These new data, excluded during the network learning stage, are now incorporated as the new input values (X_i) that are then transformed into the new outputs (Y_i). The third phase is a validation of the network on a new data set. This data set usually consists of the data from the new experimental measurements of the same process. The validation phase presents the final level of a successful or unsuccessful prediction obtained by using the network developed in the two previous stages on a new data set.[17,20,21]

In this study, the ANN methodology was applied for modeling the process of bauxite leaching under industrial conditions using the available data, the descriptive statistics of which is presented in Table I. The assembly of 659 input and output samples was divided into two groups. The first group consisted of 458 (70 %) randomly selected samples, which was used for training the network, while the second group consisted of the 201 (30 %) remaining data, which was used for testing the network.
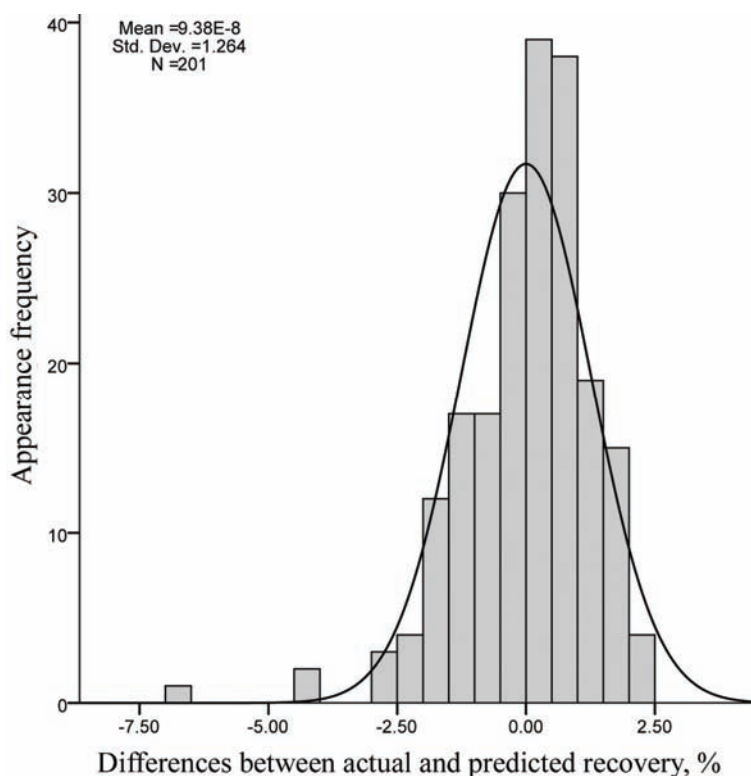
Fig. 2. Distribution of the differences between the actual Al_2O_3 recovery and the Al_2O_3 recovery estimated from Eq. (2) for 659 samples.

For the development of a relational ANN configuration, the previously defined input variables X_1–X_{11} and the output variable Y (described in the previous text), were used as the elements of the network architecture, Fig. 3.

As previously discussed, the ANN presented in Fig. 3 consists of three layers: the input, output and hidden layers. The neurons of the input layer present the information on the process input variables – X_i (independent variables), while the only neuron in the output layer generates the output information – the process quality indicator – Y (dependent variable). The methodology of choosing the appropriate number of neurons in the hidden layer as well as the procedure of the back-propagation learning algorithm is described in detail in the literature.[17]

In the phase of the network training, the necessary number of iterations was performed until the error between the measured output of the bauxite leaching process, Al_2O_3 leaching recovery, Y and the calculated values did not minimize and remained constant. The obtained results from the training stage could be evaluated by comparison of the calculated values Y with the measured ones. The obtained coefficient of the determination ($R^2 = 0.773$) show a large degree of fit-

ting among calculated and measured values, obtained during the training phase and could be used in the subsequent testing and validation.
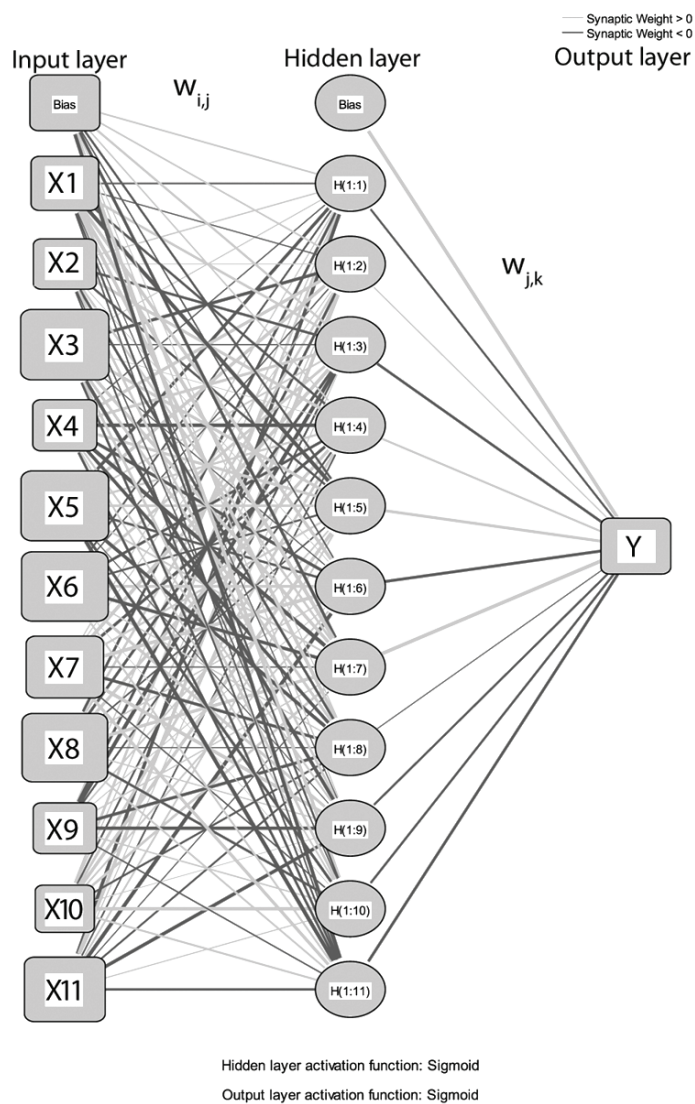
Fig. 3. The ANN architecture for the determination of the Al_2O_3 degree of recovery during bauxite leaching.

The test set (total 201 vectors), which examines the fidelity of the model, showed that the model could be used to estimate the leaching recovery quite satisfactorily. The value of the determination coefficient (R^2) for the test set was to some extent smaller 0.723 (Fig. 4). The differences of –3.20 to 2.25, between

predicted and the actually determined Al_2O_3 recovery (Fig.5), which were calculated by the $(X_1–X_{11})$ input sets in the ANN model, are proof that the listed variables could be considered as reliable inputs for the prediction of the Al_2O_3 recovery in the Birač Alumina Plant.
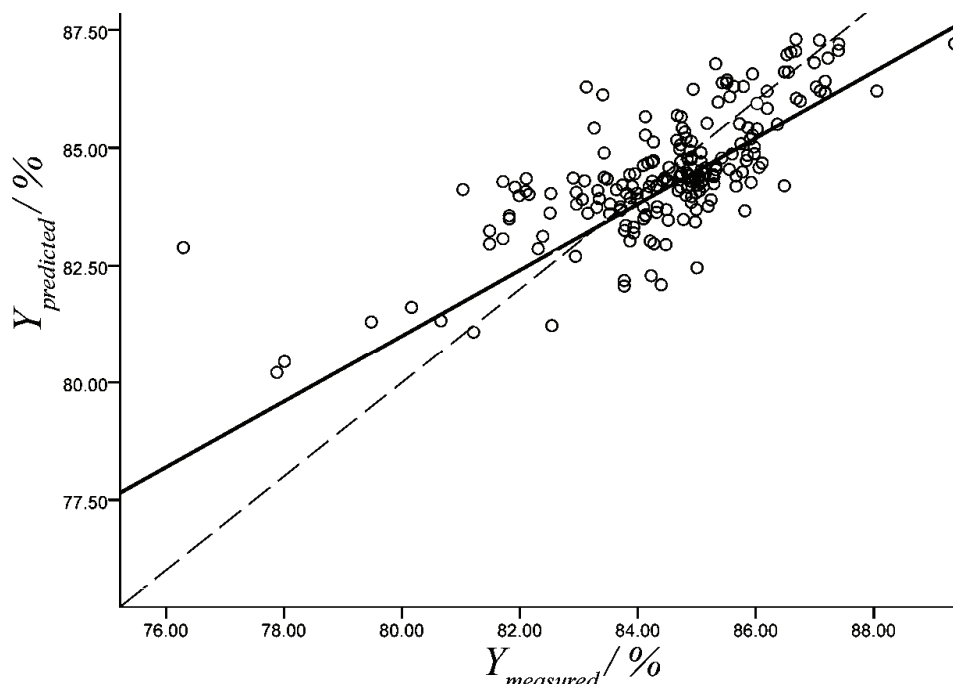
Fig. 4. The recovery predicted by neural network *vs.* the actual measured Al_2O_3 recovery (- - - = ideal position; — = regression lines; o = values calculated using the ANN model in the testing stage).

CONCLUSIONS

Values of the correlation analysis of the degree of Al_2O_3 recovery from the leaching of boehmitic bauxite under industrial conditions in the factory Birač, Zvornik (Bosnia and Herzegovina) were determined using the MLRA and ANN methodologies. The values of the coefficient of determination (R^2) were 0.463 and 0.723, respectively. These results indicated a highly acceptable degree of fitting of the dependence $Y = f(X_1–X_{11})$ obtained using ANN procedure as part of the SPSS software application, version 18 (PASW Statistics).[22]

The ANN procedure predicted the Al_2O_3 leaching recovery with good accuracy; it achieved a determination coefficient of $R^2 = 0.723$ and differences of –3.20 to 2.25 from actual determined recoveries in the plant. The selected ANN structure consisted of 458 (70 %) samples for training and 201 (30 %) for testing.

The defined elements of the ANN structure could be applied generally to conditions in any factory that employs the Bayer technology for alumina production.
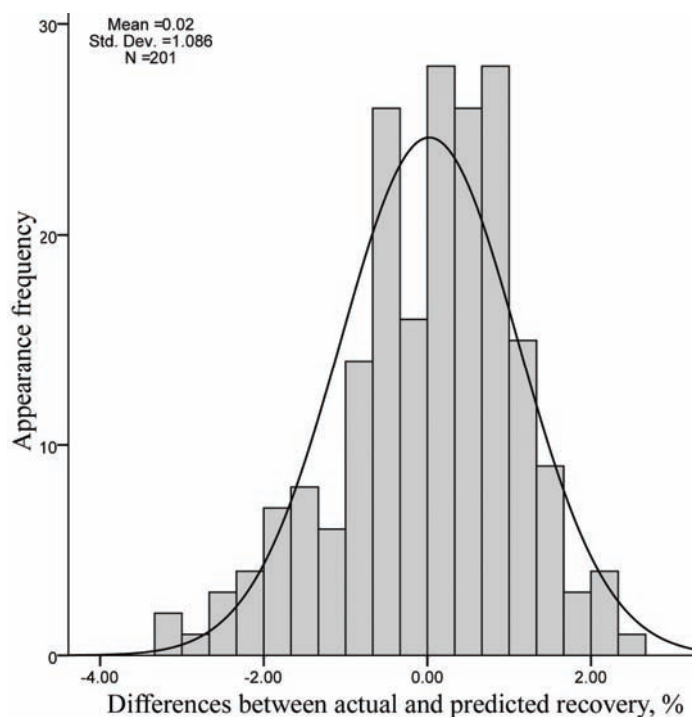
Fig. 5. Distribution of the differences between the actual Al_2O_3 recovery
and that estimated by the neural network.

ИЗВОД

ПРЕДВИЂАЊЕ ЕКСТРАКЦИЈЕ АЛУМИНИЈУМА ИЗ БОКСИТА У БАЈЕРОВОМ
ПРОЦЕСУ ПРИМЕНОМ ВЕШТАЧКИХ НЕУРОНСКИХ МРЕЖА

ИСИДОРА ЂУРИЋ[1], ИВАН МИХАЈЛОВИЋ[1], ЖИВАН ЖИВКОВИЋ[1] и ДРАГАНА КЕШЕЉ[2]

[1]*Универзитет у Београду, Технички факултет у Бору*
[2]*Технолошки факултет Зворник, Република Српска, Босна и Херцеговина*

Овај рад представља резултате статистичког моделовања процеса лужења боксита као дела Бајеровог процеса производње алуминијума. Засновано на подацима, сакупљеним током периода 2008–2009 (659 дана), који потичу из индустријске производње у фабрици алуминијума Бирач – Зворник (Босна и Херцеговина), извршено је статистичко моделовање наведеног процеса. Зависна промењива, чије одређивање је и основни циљ процедуре моделовања, представља степен издвајања Al_2O_3 из бемитног боксита током процеса лужења. Статистички модел је добијен као покушај да се дефинише зависност

степена издвајања Al_2O_3 од улазних промењивих процеса лужења: састав боксита, састав раствора натријум-алумината као и каустичног модула раствора пре и након процеса лужења. Као алати статистичког моделовања коришћени су вишеструка линеарна регресиона анализа (MLRA) и вештачне неуронске мреже (ANN). Ниво фитовања, добијен употребом MLRA, износио је $R^2 = 0,463$, док је ANN резултовала са $R^2 = 0,723$. На овај начин, модел дефинисан употребом ANN методологије, може се користити за ефикасно предвиђање нивоа издвајања Al_2O_3 у функцији процесних промењивих, у условима индустријске производње у фабрици Бирач – Зворник. Предложени модел, такође има и универзални карактер и као такав је примењив у другим фабрикама које примењују Бајерову технологију за производњу алуминијума.

REFERENCES

1. G. S. Gontijo, A. C. Brandao de Araujo, S. Prasad, L. G. S. Vasconcelos, J. N. N. Alves, R.P. Brito, *Miner. Eng*. **22** (2009) 1130
2. F. Habashi, *Handbook of Extractive Metallurgy*, vol. 1, Wiley, New York, USA, 1997, p. 103
3. F. Habashi, *J. Min. Metall.,B* **45** (2009) 1
4. S. C. Chelgani, E. Jorjani, *Hydrometallurgy* **97** (2009) 105
5. B. I. Whittington, B. L. Fletcher, C. Talbot, *Hydrometallurgy* **49** (1998) 1
6. M. Jamialahmadi, H. Muller-Steinhagen, J. Minerals Metals Mater. Soc. **50** (1998) 44
7. D. A. Palmer, P. Benezeth, D. J. Weselowski, S. Hilic, in: Proceeding of the TMS Light Metals, Warrendale, PA, USA, 2003, p. 5
8. B. Xu, C. Wingate, P. Smith, *Hydrometallurgy* **98** (2009) 108
9. G. Songqing, Y. Zhonling, Q. Lijuan, *Light Metals* **1** (2002) 83
10. J. A. M. Pereira, M. Schwaab, E. Dell'Oro, J. C. Pinto, J. L. F. Monteiro, C. A. Henriques, *Hydrometallurgy* **96** (2009) 6
11. D. Panias, P. Asimidis, I. Paspaliaris, *Hydrometallurgy* **59** (2001) 15
12. F. G. Umukoro, O. L. Kuye, A. H. A. Sulaimon, *Serb. J. Manag.* **4** (2009) 259
13. S. Cao, Y. F. Zhang, Y. Zhang, *Hydrometallurgy* **98** (2009) 298
14. Ž., Živković, I. Mihajlović, Dj. Nikolić, *Serb. J. Manag.* **4** (2009a) 143
15. R. N. Moroney, *J. Wind Eng. Ind. Aerodyn*.**77**–**78** (1998) 543
16. H. Demuth, M. Beale, *Neural Network Toolbox for use with MATLAB*, *Handbook*, MathWorks Inc., Natick, MA, USA, 2002, p. 238
17. Ž. Živković, I. Mihajlović, I. Đurić, N. Štrbac, *Metall. Mater. Trans., B* **41** (2010) 1116
18. Y. F. Zhang, Y. H, Li, Y. Zhang, *J. Chem. Eng. Data* **48** (2003) 617
19. G. Dreyfus, *Neural Networks, Methodology and Applications*, Springer, Berlin, Germany, 2004, p. 127.
20. Ž. Živković, N. Mitevska, I, Mihajlović, Dj, Nikolić, *J. Min. Metall., B* **45** (2009b) 23
21. D. Liu, Y. Yuan, S. Liao, *Expert Syst. Appl*. **36** (2009) 10397
22. PASW Statistics, formerly called SPSS Statistics, SPSS Inc., Chicago, IL, 2009.

An aqueous chemistry module for a three-dimensional cloud resolving model: sulfate redistribution

DRAGANA VUJOVIĆ* and VLADAN VUČKOVIĆ**

University of Belgrade, Faculty of Physics, Department of Meteorology, Dobračina 16, Belgrade, Serbia

Abstract: An aqueous chemistry module was created and included into a complex 3D cloud-resolving mesoscale advanced regional prediction system (ARPS) model to examine the characteristics of in-cloud sulfate. The complex orography of Serbia was included in the model. The chemical species included in the module were sulfur dioxide, sulfate ion, ammonium ion, hydrogen peroxide and ozone. Six water categories are considered: water vapor, cloud water, rain, cloud ice, snow and hail. Each chemical species in each microphysical category was represented by a differential equation of mass continuity. This paper gives a detailed description of the chemistry module and demonstrates the utility of an atmospheric model coupled with the chemistry module in forecasting the redistribution of chemical species in all water categories. The main mean microphysical and chemical conversion rates of sulfate averaged over a 2 h simulation period for a base run were for the oxidation of S(IV) in rain water and cloud water, SO_4^{2-} scavenging by Brownian diffusion in cloud droplets and cloud ice as well as the impact scavenging of SO_4^{2-} by rain. The calculated values of sulfates in all water categories and the shape of the sulfate profiles depend on radar reflectivity.

Keywords: oxidation; sulfate transfer; cumulonimbus; microphysics; mass transfer.

INTRODUCTION

Clouds play an important role in environmental redistribution of chemistry species. The average global cloud coverage over the oceans is estimated at 65 % and over land at 52 %,[1] so it is clear that clouds play the role of a "large factory" for the aqueous-phase production of chemistry species. The clouds receive trace gases from their inflow regions, their wind redistributes the gases and the clouds transform the gases through gas and aqueous-phase chemistry. The most important gas that leads to acidification is sulfur dioxide. When clouds are present, the

1273

loss rate of atmospheric SO_2 is faster than can be explained by gas phase chemistry alone. This rate of loss is due to reactions in the liquid water droplets where acids are produced. Acid rain can have harmful effects on the environment and on human health through the process of wet deposition.

The first atmospheric models had simple dynamics and microphysics,[2] but in time, the models become more complex. Taylor[3] used a 1.5-dimensional Eulerian cumulus cloud model to examine the characteristics of the in-cloud chemistry. Studies by Tremblay and Leighton[4] and Niewiadomski[5] used three-dimensional cloud chemistry models, but they focused on warm convective clouds only. Scamarock et al.[6] examined tracer transport in 3D simulations, but only on flat ground. Yin et al.[7] examined trace gas redistribution using a two-dimensional cloud model with detailed microphysics and spectral treatment of gas scavenging. Barth et al.[8] examined the redistribution of trace gases during deep convection. Spiridonov and Ćurić[9] examined the relative importance of scavenging, oxidation and ice-phase chemistry in sulfate production in 2D and 3D model runs. This study takes a step forward by developing a new chemistry module and coupling it with a very comprehensive 3D mesoscale atmospheric model. The real orography is included in the model. This paper describes detailed chemistry parameterization. The aim was to demonstrate the fact that a relatively simple chemical module coupled with a comprehensive cloud-resolving model with detailed microphysics could be used as a diagnostic and prognostic tool for chemical species.

EXPERIMENTAL

Description of atmospheric numerical model

A very comprehensive 3D cloud-resolving mesoscale advanced regional prediction system (ARPS) model developed in the Center for Analysis and Prediction of Storms (CAPS) at the University of Oklahoma[10,11] was used to simulate a Cumulonimbus (Cb) life cycle in conditions of a real orography.[12,13]. This model numerically integrates time-dependent, non-hydrostatic and fully compressible equations. The model uses the Lin[14] bulk-water microphysical scheme and represents six water categories: water vapor, cloud water, cloud ice, rain, snow, hail. Rain, hail and snow are each represented by the Marshall–Palmer distribution.[15] Cloud droplets and non-precipitating cloud ice are supposed to be monodispersing. Turbulence was treated by 1.5 order turbulent kinetic energy formulation. The advection of momentum and scalars were treated with a 4th-order scheme in the horizontal direction and 2nd-order scheme in the vertical direction. Radiating (open) conditions were used for lateral boundaries. Rigid-wall boundary conditions were applied for the top and on the bottom of the domain. The large time step was 6 s and the small step (for acoustic waves) was 1 s.

Description of the chemistry module

This section contains the development of the equations that were used to describe the chemical species incorporated in the cloud model. The chemical module is based on the sulfate chemistry taken from Rutledge et al.,[16] Taylor,[3] and Spiridonov and Ćurić.[17] Five chemical species are carried explicitly into the model: SO_2, O_3, H_2O_2, SO_4^{2-} and NH_4^+ in the

form of mixing ratios. All chemical reactions included in the module with the appropriate coefficients are given in Table I.

TABLE I. Equilibrium reactions and rate constants. The equilibrium constants are of the form $k = k_{298} \times \exp(-\Delta H_{298}/R(1/298-1/T))$, where T is the temperature, K[18]

Reaction	k_{298} / mol dm^{-3} s^{-1}	$(-\Delta H_{298}/R)$ / K
$SO_2(g) \leftrightarrows SO_2(aq)$	1.23	3120
$SO_2(aq) \leftrightarrows HSO_3^- + H^+$	1.3×10^{-2}	-2000
$HSO_3^- \leftrightarrows SO_3^{2-} + H^+$	6.3×10^{-8}	-1495
$O_3(g) \leftrightarrows O_3(aq)$	1.15×10^{-2}	-2560
$H_2O_2(g) \leftrightarrows H_2O_2(aq)$	8.33×10^4	-7379
$H_2O_2(aq) \leftrightarrows HO_2^- + H^+$	2.2×10^{-12}	3700
$NH_3(g) \leftrightarrows NH_3(aq)$	92,7	-4085
$S(IV) + H_2O_2 \rightarrow S(VI) + H_2O$	7.5×10^7	4750

The model was formulated in terms of Continuity equations:

$$\frac{\partial q_{i,j}}{\partial t} + \mathbf{V} \cdot \nabla q_{i,j} - FR_{i,j} = S_{i,j} + CH_{i,j} \qquad (1)$$

where $q_{i,j}$ is the mixing ratio of chemical species i in the water category j (*e.g.*, $q_{SO4,c}$ denotes the cloud water SO_4^{2-} mixing ratio, $q_{SO4,i}$ denotes the cloud ice SO_4^{2-} mixing ratio), $\mathbf{V} \cdot \nabla q_{i,j}$ is the advection of the chemical species i in water category j by the wind $\mathbf{V} = (u, v, w)$, $FR_{i,j}$ denotes the terminal velocity for hydrometeors, $S_{i,j}$ are the subgrid contribution terms (mixing, turbulence) and $CH_{i,j}$ are the source or sink chemical transformation terms that represent either the transfer of the chemical species from one microphysical category to another (*e.g.*, cloud water sulfate to cloud ice sulfate by riming) or a chemical reaction (*e.g.*, oxidation of cloud water SO_2 to cloud water sulfate). Two assumptions were used:[3,16]

a) over the relatively short time scales that characterize cloud interactions, aqueous phase chemistry is dominant. Therefore, gas phase chemistry was neglected.

b) Aqueous-phase photochemistry contributes only in the secondary sense to the sca-venging of sulfur and nitrogen species in clouds, and can therefore be neglected.

The mass transfer between gas and liquid phases

The Henry Law equilibrium does not always exist between water drops and the air.[19] In this study, the Henry Law and a more detailed mass transfer approach that does not assume gas–liquid equilibrium were used. The rate of mass transport between gas species i and a group of aqueous drops with radius r and number concentration of N_r (per mole of air), can be written as:[20]

$$\frac{dM_{i,r}}{dt} = \frac{3\eta D_{g,i} N_{Sh,i}}{R^* T r} \left(V_r N_r p_i - \frac{M_{i,r}}{K_{H,i}^*} \right), \qquad (2)$$

where $M_{i,r}$ is the molar mixing ratio (with respect to air) of gas species i inside drops with radius r; $D_{g,i}$ the diffusivity of gas species i in the air; $N_{Sh,i}$ the Sherwood number; p_i the partial pressure of gas species i in the environment; $K_{H,i}^*$ the effective Henry Law coefficient of species i, R^* the universal gas constant; T the temperature and η a factor to account for the free-molecular effect on the mass transfer rate.[21] Based on previous studies,[17,20,22] a value of $\eta = 0.1$ was used in the simulations for all the species. The effective Henry Law coefficient,

$K^*_{\mathrm{H},i}$, for a species i that undergoes aqueous phase dissociation differs from the Henry Law coefficient $K_{\mathrm{H},i}$ for a molecule, as it accounts for the ionic forms of the dissolved gas.[23]

As dissolved gasses do not normally contribute to the drop size, Eq. (2) becomes a linear first order differential equation that can be solved analytically as:

$$M_{i,\mathrm{r}}(t+\Delta t) = A(t) + [M_{i,\mathrm{r}}(t) - A(t)]\exp(B\Delta t) \tag{3}$$

where t is the time step for gas dissolution and A and B are:

$$A(t) = \frac{4}{3}\pi r^2 N_{\mathrm{r}} p_i(t) K^*_{\mathrm{H},i}; \; B = -\frac{3 D_{\mathrm{g},i} N_{\mathrm{Sh},i}\,\eta}{r^2 R^* T K^*_{\mathrm{H},i}}\,. \tag{4}$$

Sulfate chemistry parameterization terms

Sulfur dioxide is the dominant anthropogenic pollutant in air that contains sulfur. Its presence in the troposphere of the Northern Hemisphere is the result of direct anthropogenic emissions, *i.e.,* combustion of fossil fuels. SO_2 is effectively removed from the atmosphere through processes of dry and moist deposition. However, the dominant mechanism for removing SO_2 from the atmosphere is oxidation, either in the gaseous or liquid phase. The creation of sulfates through the oxidation of SO_2 is an important process with changing aerosol radiation effects. A schematic representation of all the chemical and microphysical processes for SO_2 and SO_4^{2-} that are parameterized in the chemical module is presented in Fig. 1. The left side of Fig. 1 is related to SO_2 and its transport from air to cloud droplets and rain drops (calculated using the exact kinetic mass transport approach), as well as its oxidation in cloud droplets and rain drops by ozone and hydrogen peroxide, whereby sulfate is formed. The rest of the graph shows microphysical processes that transport sulfate from one water category to another.

Ammonium source terms

Ammonium is neither created nor destroyed in the chemical reactions modeled here. Here, it is assumed that the sulfate aerosol is composed of ammonium bisulfate $(NH_4)_2SO_4$. Therefore, ammonium is treated like sulfate. The terms *PS*3–*PS*8, *PS*11–*PS*25 (calculation details are given in Supplementary material) represent the source-sink terms for ammonium (*PN*1–*PN*13, *PN*15–*PN*22), but the mixing ratios for SO_4^{2-} should be replaced by the mixing ratios for NH_4^+. The nucleation scavenging efficiency for ammonium is assumed the same as the nucleation scavenging efficiency for sulfate.

Hydrogen peroxide, ozone and S(IV) source-sink terms

The source-sink terms for H_2O_2 and O_3 include an equilibration between gas and aqueous phases, kinetic mass transport, reduction due to the oxidation of S(IV) in cloud droplets and rain, and a set of microphysical transfer and conversions among the different water categories. As this is a short paper, details of the sources and sinks terms for H_2O_2, O_3 and S(IV) will not be given herein.

Model initialization

A single summer sounding, providing profiles of temperature, humidity, speed and direction of wind, initializes the use of a complex atmospheric model coupled with the chemistry module. The real orography of the Serbian region is used as a very important factor in cumulonimbus formation. The centre of the domain is at 43.8° N, 20° E. It represents the Zapadna Morava Valley (mean height above sea level 300 m), and its surrounding environment. Space resolution in the model is 1000 m in the horizontal and 500 m in the vertical direction.

The domain size is 112 km×112 km×16 km. A two-hour forecast is made. It is assumed that initial concentrations of the chemical fields fall off exponentially from the given values of mixing ratios at the lowest model level[3] for a continental background (CB) and for a polluted background (PB).

Fig. 1. Scheme of sulfur dioxide (SO_2) and sulfate (SO_4^{2-}) reactions.

RESULTS AND DISCUSSION

Several numerical experiments were designed to verify the developed method of using a chemistry module coupled with a 3D atmospheric model. In the base run (fully kinetic calculation of gas dissolution into cloud droplets and rain drops, calculation of nucleation and impact scavenging of aerosols, S(IV) oxidation by O_3 and H_2O_2 in cloud and rain water, ice phase simulation, orography included), the integrated sulfur mass removed by wet deposition was 22.3 kg for CB, and 60.0 kg for PB, which is in agreement with the results of Spiridonov and Ćurić.[9] The total mass of NH_4^+ incorporated in the precipitation was 8.03 kg for PB and 1.55 kg for CB, which is in agreement with the results of Taylor,[3] *i.e.*, 10.5 kg for PB and 2.03 kg for CB. If the oxidation was neglected, the integrated sulfur mass removed by wet deposition was 16.5 (CB) and 32.1 % (PB) of sulfur mass in the base run. Spiridonov and Ćurić[9] obtained values of 24.1 (CB) and 25.7 % (PB). This difference arises from the different parameterization of oxidetion. The omission of scavenging processes gives 82.9 (CB) and 67.8 % (PB) of the total sulfur deposited in the base run (64.6 (CB) and 68.8 % (PB) in Spirido-

nov and Ćurić[9]). Ignoring the ice phase in the chemistry results in an increase by a factor of 1.5 in the sulfur mass deposited for CB (149.6 %), which is in accordance with the conclusion of Taylor[3] (tests of the ice phase impact on in-cloud chemistry and deposition indicated that the total sulfur mass deposited was increased by about a factor of two relative to the base run case). According to Molder *et al.*,[26] including ice phase processes in dynamics modeling leads to lower values of sulfate in the liquid phase when convection is present. Regarding the meteorological part of the model, there was agreement between the calculated and observed radar reflectivity.[12] These results correspond with the published results of other authors; thus, the developed model can be considered valid.

The integration (base run) includes mass transport calculations from gas to liquid phase, oxidation of S(IV) by O_3 and H_2O_2, nucleation and impact scavenging and ice phase simulation. In the 10th minute of integration, a cloud was formed. The cloud developed on the mountaintop and then moved along the Zapadna Morava Valley. The cumulative mass of the sulfate, *i.e.*, the sum of the mass of sulfate in gas phase, cloud water, rainwater, cloud ice, snow and hail in every step is shown in Fig. 2. As it is a source for sulfate in other water categories, the mass of sulfate in the gas phase gradually decreased from the initial va-
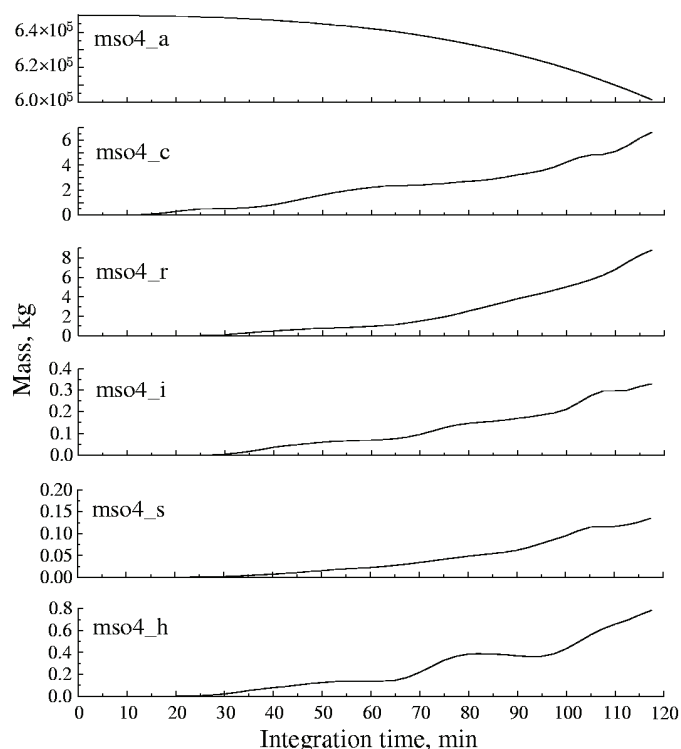
Fig. 2. The cumulative mass of sulfate.

lues. As cloud water formed during the integration, sulfates appear in cloud water at the 10th minute and from the 30th minute in rainwater, snow, hail and cloud ice.

The main mean microphysical and chemical conversion rates of sulfate averaged over a 2-h simulation period for the base run were for the oxidation of S(IV) in rain water and cloud water $PS9 = 4.61\times10^{-11}$, $PS9hp = 2.79\times10^{-12}$, $PS2 == 2.89\times10^{-13}$), SO_2^{4-} scavenging by Brownian diffusion in cloud droplets and cloud ice $PS4cw = 4.91\times10^{-11}$ and $PS4ci = 7.82\times10^{-12}$, the impact scavenging of SO_2^{4-} by rain $PS6 = 2.08\times10^{-11}$, autoconversion of cloud water to form rain, accretion of cloud water by rain, accretion of cloud water by snow $PS11 = = 4.43\times10^{-12}$, and the transfer of SO_2^{4-} from cloud ice to snow as a result of autoconversion of cloud ice to form snow, the accretion of cloud ice by snow and the accretion of cloud ice by rain $PS25 = 1.21\times10^{-12}$). The calculated radar reflectivity (CRR), which is a good indicator of cloud development, is presented in Fig. 3. The figure shows the horizontal plane on the surface in the 85th minute of integration. At this moment, the cloud is in a mature stage of development, with three "separated" cells with a large CRR: point A (59, 73 km), B (70, 85 km) and C (75, 60 km). The CRR at points A and C was approximately 50 dBz, and at point B nearly 55 dBz.

Fig. 3. The radar reflectivity, dBz, in the (x,y) plane on the surface in the 85th minute of integration. The three cells with maximum reflectivity have the coordinates: A (58, 73 km), B (70, 85 km) and C (75, 60 km). Point D (75, 75 km) is at periphery of the cloud.

The vertical profiles of the sulfate following cumulonimbus trajectory could provide considerable information about sulfate redistribution in the troposphere. The vertical profiles of SO_4^{2-} in all categories of water at points A, B and C are shown in Figs. 4–6, respectively. The maximum value of $q_{SO_4^{2-},c}$ in the layer of air above point A was at a height of 5 km and its value was $0.80~\mu g~kg^{-1}$, $q_{SO_4^{2-},r}$
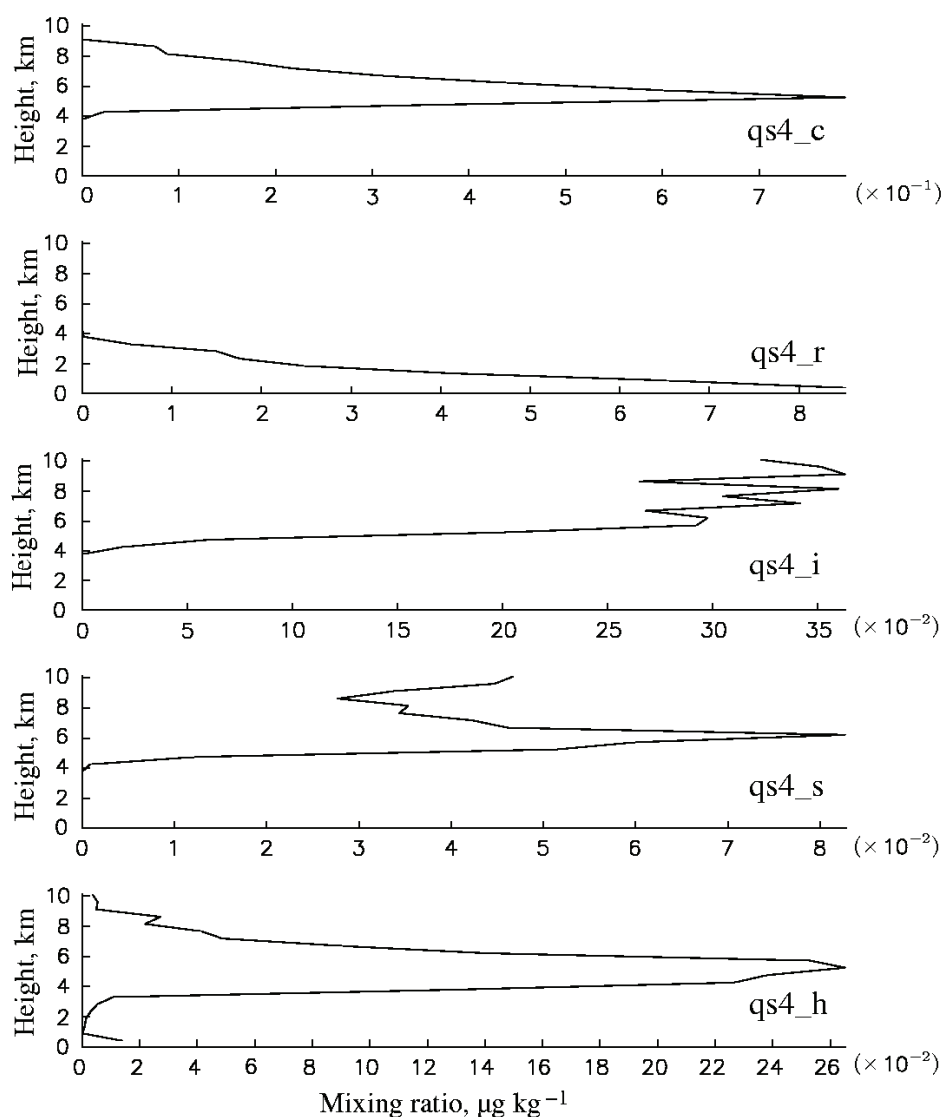
Fig. 4. The vertical profiles of the SO_4^{2-} mixing ratio, $\mu g~kg^{-1}$, in different water categories: in cloud water ($q_{s4,c}$), rain ($q_{s4,r}$), cloud ice ($q_{s4,i}$), snow ($q_{s4,s}$) and hail ($q_{s4,h}$) for the cell A (58, 73 km).

at the surface was 9.0 μg kg^{-1}, $q_{SO_4^{2-},i}$ at a height of nearly 9 km was 0.35 μg kg^{-1}, $q_{SO_4^{2-},s}$ at a height of about 6 km was 0.08 μg kg^{-1}, and $q_{SO_4^{2-},h}$ at a height of 5.5 km was 0.26 μg kg^{-1}. The profiles above the other two vorticities (B and C) could be analyzed similarly. The shapes of the profiles were similar and had similar values of the sulfate mixing ratios.
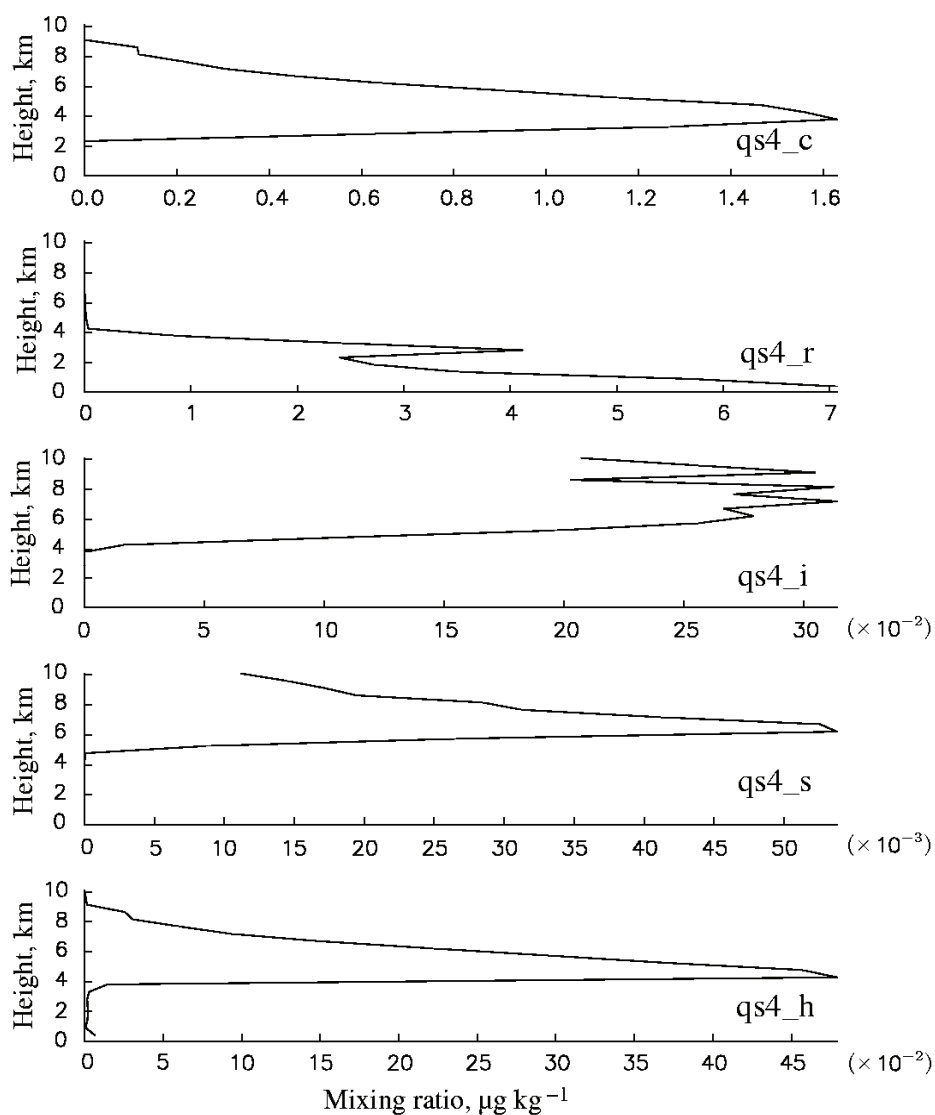
Fig. 5. The vertical profiles of the SO$_4^{2-}$ mixing ratio, μg kg^{-1}, in different water categories: in cloud water ($q_{s4,c}$), rain ($q_{s4,r}$), cloud ice ($q_{s4,i}$), snow ($q_{s4,s}$) and hail ($q_{s4,h}$) for the cell B (70, 85 km).
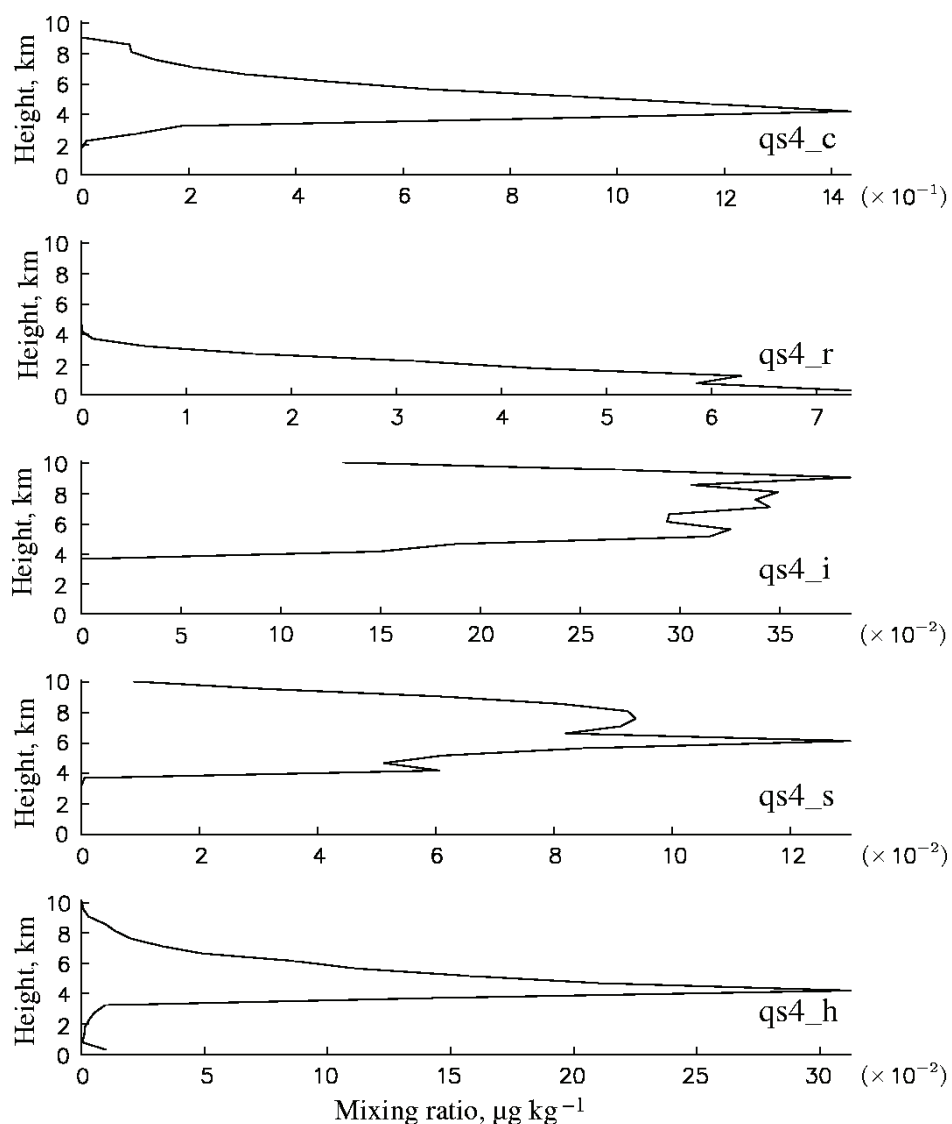
Fig. 6. The vertical profiles of the SO_4^{2-} mixing ratio, µg kg^{-1}, in different water categories: in cloud water ($q_{s4,c}$), rain ($q_{s4,r}$), cloud ice ($q_{s4,i}$), snow ($q_{s4,s}$) and hail ($q_{s4,h}$) for the cell C (75, 60 km).

It is interesting to compare the sulfate profiles in areas with different CRRs. To do this, the sulfate profile at point D (75, 75 km), which is located on the periphery of the cloud and had a CRR of 20 dBz (Fig. 7), is drawn. If this profile is compared with the previous ones, small differences in the shape of the profiles could be seen, especially for sulfate in rainwater. Specifically, at point D the

maximum value of the sulfate-mixing ratio in rainwater was not at the surface but at a height of 2 km. This is because in this part of the cloud, there was no precipitation at the surface. The most considerable differences existed in the values of mixing ratios: all sulfate mixing ratios had smaller values at point D, compared to points A, B and C. This is understandable, given that vortex D has the lowest CRR.
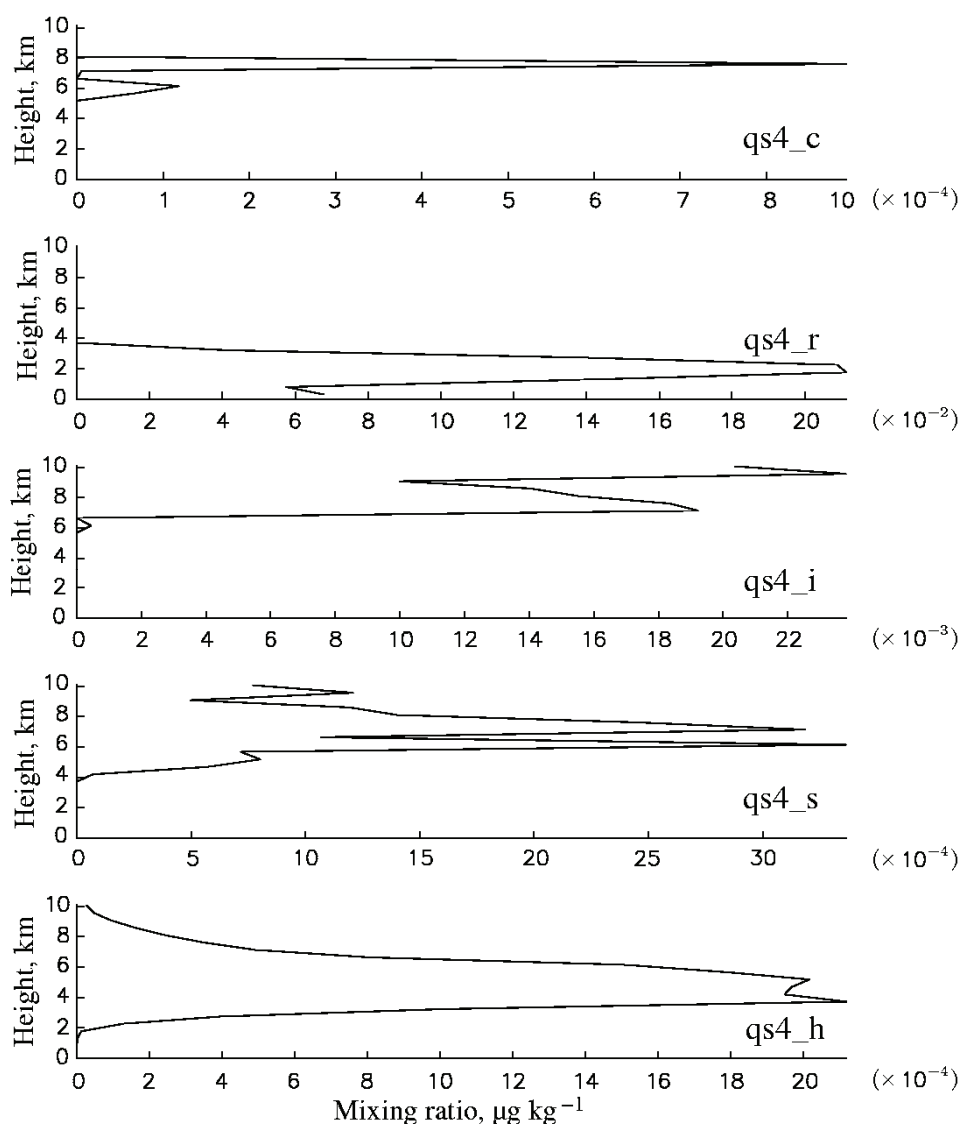
Fig. 7. The vertical profiles of the SO_4^{2-} mixing ratio, µg kg^{-1}, in different water categories: in cloud water ($q_{s4,c}$), rain ($q_{s4,r}$), cloud ice ($q_{s4,i}$), snow ($q_{s4,s}$) and hail ($q_{s4,h}$) at point D (75 km, 75 km) at the cloud periphery.

CONCLUSIONS

This paper described in detail the development of a chemistry module that was incorporated into a very comprehensive, mesoscale cloud-resolving model. The chemistry module contained five chemical species: SO_2, H_2O_2, O_3, SO_4^{2-} and NH_4^+. There were six prognostic continuity equations for mixing ratios of each chemical species, for each of the water categories. Two different approaches were used to express the amount of the chemical species in cloud or rainwater: the Henry Law and a fully kinetic calculation of a gas uptake. After dissolution, the chemical species were transferred from one water category to another by microphysical reactions. Oxidation of S(IV) by H_2O_2 and O_3 in cloud droplets and raindrops were included in the module due to their great importance in sulfate production processes. The pH values for cloud droplets and raindrops were calculated in every time step.

After comparing the mass of wet deposited sulfur with the results of other studies (verification), it was accepted that the model could be used as a good prognostic tool for determining the redistribution of chemical species. In this sense, the results showed that there was no loss of total sulfate mass, that the sulfate values in all water categories depended on the calculated radar reflectivity and that convective clouds provide a suitable environment for sulfate transport from the boundary layer to the upper troposphere.

SUPPLEMENTARY MATERIAL

Calculation details for the parameters *PS*1–*PS*26 are available electronically from http://www.shd.org.rs/JSCS/, or from the corresponding author on request.

ИЗВОД

ХЕМИЈСКИ МОДУЛ ЗА ТРОДИМЕНЗИОНИ МОДЕЛ ОБЛАКА: ПРЕРАСПОДЕЛА СУЛФАТА

ДРАГАНА ВУЈОВИЋ и ВЛАДАН ВУЧКОВИЋ

Универзитет у Београду, Физички факултет, Институт за метеорологију, Добрачина 16, Београд

Дефинисан је хемијски модул и укључен у комплексни тродимензиони модел облака ARPS да би се испитала редистрибуција сулфата у облаку. У модел је укључена комплексна орографија Србије. У модул су укључени сумпор-диоксид, сулфатни јон, амонијумов јон, водоник-пероксид и озон. Разматрано је шест категорија воде: водена пара, облачна вода, киша, облачни лед, снег и град. Свака хемијска врста у свакој категорији воде је представљена диференцијалном једначином континуитета масе. Овај рад даје детаљан опис хемијског модула. Показује се да модел облака са укљученим хемијским модулом може да прогнозира масу сумпора депонованог влажном депозицијом, као и прерасподелу сулфата у свим категоријама воде. Главне микрофизичке и хемијске брзине конверзије сулфата осредњене на 2 h (што је период интеграције) су оксидација S(IV) у облачној и кишној води, испирање сулфата Брауновском дифузијом у облачним кап-

љицама и облачном леду и испирање сулфата кишом. Израчунате вредности сулфата у свим категоријама воде и облик профила сулфата зависе од радарске рефлексивности.

REFERENCES

1. C. G. Warren, C. J. Hahn, J. London, R. M. Chervin, R. L. Jenne, *Global distribution of total cloud cover and cloud type amounts over land*, Tech. Rep. NCAR Technical note TN-273+STR, National Center for Atmospheric Research, Boulder, CO, 1986
2. J. Hales, *Atmos. Environ.* **16** (1982) 1775
3. G. R. Taylor, *J. Atmos. Sci.* **46** (1989) 1991
4. A. Tremblay, H. Leighton, *J. Climate Appl. Meteor.* **25** (1986) 652
5. M. Niewiadomski, *Atmos. Environ.* **23** (1989) 477
6. W. C. Skamarock, J. G. Powers, M. Barth, J. E. Dye, T. Matejka, D. Bartels, K. Baumann, J. Stith, D. D. Parrish, G. Hubler, *J. Geophys. Res.* **105** (2000) 19973
7. Y. Yin, D. J. Parker, K. S. Carslaw, *Atmos. Chem. Phys.* **1** (2001) 19
8. M. C. Barth, A. L. Stuart, W. C. Skamarock, *J. Geophys. Res.* **106** (2001) 12381
9. V. Spiridonov, M. Ćurić, *J. Atmos. Sci.* **62** (2005) 2118
10. M. Xue, K. K. Droegemeier, V. Wong, *Meteor. Atmos. Phys.* **75** (2000) 161
11. M. Xue, K. K. Droegemeier, V. Wong, A. Shapiro, K. Brewster, F. Carr, D. Weber, Y. Liu, D. H. Wang, *Meteor. Atmos. Phys.* **76** (2001) 134
12. M. Ćurić, D. Janc, D. Vujović, V. Vučković, *Meteorol. Atmos. Phys.* **84** (2003) 171
13. M. Ćurić, D. Janc, D. Vujović, V. Vučković, *Atmos. Res.* **66** (2003) 123
14. Y. L. Lin, R. D., Farley, H. D. Orville, *J. Appl. Meteor.* **22** (1983) 1065.
15. J. S. Marshall, W. M. Palmer, *J. Meteor.* **5** (1948) 165
16. S. A. Rutledge, D. A. Hegg, P. V. Hobbs, *J. Geophys. Res.* **91** (1986) 14385
17. V. Spiridonov, M. Ćurić, *Idojaras* **107** (2003) 58
18. M. C. Barth, *Atmos. Res.* **82** (2006) 309
19. C. J. Walcek, H. R. Pruppacher, *J. Atmos. Chem.* **1** (1984) 307
20. S. Pandis, J. H. Seinfeld, *J. Geophys. Res.* **94** (1989) 1105
21. D. J. Jacob, *J. Geophys. Res.* **24** (1996) 113
22. C. Wang, P. J. Crutzen, *J. Geophys. Res.* **100** (1995) 11357
23. J. H. Seinfeld, S. Pandis, *Atmospheric chemistry and physics: From air pollution to climate change*, Wiley, New York, USA, 1998, p. 1225
24. H. R. Pruppacher, J. D., Klett, *Microphysics of Clouds and Precipitation*, Kluwer, Dordrecht, Germany, 2004, p. 954
25. J. Y. Liu and H. D. Orville, *J. Atmos. Sci.* **26** (1969) 1283
26. N. Molder. H. Hass, H. J. Jacobs, R. Laube, A. Ebel, *J. Appl. Meteor.* **33** (1994) 696.

An aqueous chemistry module for a three-dimensional cloud resolving model: sulfate redistribution

DRAGANA VUJOVIĆ* and VLADAN VUČKOVIĆ**

University of Belgrade, Faculty of Physics, Department of Meteorology, Dobračina 16, Belgrade, Serbia

PS*1 – S(IV) solution in cloud water. PS1* is the source term for S(IV) in cloud water and the sink term for SO$_2$ from air. It is calculated using the Henry Law (PS1) or using the mass transport approach (PS1K). The total concentration of four-valence S(IV) species predominantly exists in the form of [HSO$_3^-$] for $2.0 \leq pH \leq 6.0$, which is typical for cloud droplets and raindrops. Thus, the concentration of [HSO$_3^-$] is given by:

$$[HSO_3^-] = K_{Hs}K_{1s}p_{SO_2}/[H^+],$$

where K_{Hs} is the Henry coefficient, K_{1s} is the first ionic dissociation coefficient, p_{SO_2} is the partial pressure of SO$_2$ in the air, and [H$^+$] is the hydrogen ion concentration. The rate for SO$_2$ leaving the atmosphere (or returning in its gaseous phase) is calculated as:

$$PS1 / SUL1 = \frac{K_{Hs}K_{1s}}{[H_c^+]} p_{SO_2} \frac{M_{SO_2}}{M_{HSO_3}} \frac{dq_c}{dt} \qquad (S\text{-}1)$$

where dq_c / dt is the condensation rate during one model time step, and M_{SO_2} and M_{HSO_3} are the molecular masses of SO$_2$ and HSO$_3^-$, respectively.

The other way to calculate this term is according to Eq. (3) (see the native article):

$$PS1K(t + \Delta t) = A_{SO_2} + (PS1K(t) - A_{SO_2})\exp(B_{SO_2}\Delta t) \qquad (S\text{-}2)$$

A_{SO_2} and B_{SO_2} are calculated according to Eq. (4) (native article).

PS*2 and* PS2hp *– S(IV) oxidation by O$_3$ and H$_2$O$_2$ to SO$_4^{2-}$ in cloud water*. The aqueous-phase conversion of dissolved SO$_2$ to sulfate is considered the most important chemical transformation in cloud water. Although ozone reacts very slowly with SO$_2$ in the gas phase, the aqueous-phase reaction:

$$S(IV) + O_3 \rightarrow S(VI) + O_2 \qquad (S\text{-}3)$$

is rapid. The parameterization of this term is performed according to the rate expression:

$$-\frac{d[S(IV)]}{dt} = k_0[SO_2 \cdot H_2O] + k_1[HSO_3^-] + k_2[SO_3^{2-}][O_3] \qquad (S\text{-}4)$$

Correspondence: E-mail; dvujovic@ff.bg.ac.rs (*); vvladan@ff.bg.ac.rs (**)

where $k_0 = (2.4\pm1.1)\times10^4$ M^{-1} s^{-1}, $k_1 = (3.7\pm0.7)\times10^5$ M^{-1} s^{-1} and $k_2 = (1.5\pm0.6)\times10^9$ M^{-1} s^{-1} are oxidation rate coefficients. If the assumption that HSO$_3^-$ is the predominant form of S(IV) is applied, then:

$$PS2 = k_1(K_{Hs}K_{1s}p_{SO_2})^{1/2}q_{O_3,c} \tag{S-5}$$

where p_{SO_2} is the partial pressure of SO$_2$ in the air. This reaction plays an important role as a source of cloud water acidification.

Hydrogen peroxide, H$_2$O$_2$, is one of the most effective oxidants of S(IV) in clouds. The rate expression is:

$$-\frac{d[S(IV)]}{dt} = \frac{k[H^+][H_2O_2][HSO_3^-]}{1+K[H^+]}[H_2O_2] \tag{S-6}$$

As H$_2$O$_2$ is a very weak electrolyte, $\left[H^+\right]\left[HSO_3^-\right] = K_{Hs}K_{1s}p_{SO_2}$, and for pH > 2, $1+K\left[H^+\right]\approx1$, the rate expression can be parameterized by:

$$PS2hp = k_{H_2O_2}K_{Hs}K_{1s}p_{SO_2}q_{H_2O_2,c} \tag{S-7}$$

PS3 – *Nucleation scavenging of SO$_4^{2-}$ aerosol by cloud condensation nuclei (CCN)*. The term for nucleation scavenging of SO$_4^{2-}$ aerosol by CCN simply shows the primary activation of CCN based on numerical integration of the droplet growth equation. Taylor approximated this process with:[3]

$$PS3 = \begin{cases} (\varepsilon_{SO_4^{2-}}q_{SO_4^{2-},a})dq_c/dt, & dq_c/dt > 0 \\ 0, & dq_c/dt \le 0 \end{cases} \tag{S-8}$$

where, dq_c is the condensation of cloud droplets during the current time step in the model and $\varepsilon_{SO_4^{2-}} = 0.55$ is the fractional nucleation efficiency.

PS4cw and PS4ci – *SO$_4^{2-}$ scavenging by Brownian diffusion in cloud droplets and cloud ice*. Scavenging of SO$_4^{2-}$ by Brownian diffusion was computed using the following equation for continuous collection:

$$-\frac{\partial q_{SO_{4,a}}}{\partial t} = q_{SO_4,a}\int_0^\infty K(a,D)n_c(D)dD \tag{S-9}$$

where $K(a,D)$ is the collection kernel for an aerosol with diameter a and a cloud droplet with diameter D. Assuming a monodisperse cloud droplet spectrum, the term PS4cw can be approximated by:

$$PS4cw = 2\pi D_p N_c D_c q_{SO_4,a} \tag{S-10}$$

where $D_p = 1.56\times10^{-8}$ m^2 s^{-1} is the particle diffusivity,[24 (Reference list in native article)] N_c the cloud droplet concentration, and D_c is the mean cloud droplet diameter. The term *PS4ci* is similar to the term *PS4cw*:

$$PS4ci = 2\pi D_p N_i D_i q_{SO_4,a} \tag{S-11}$$

where N_i is the cloud ice concentration and D_i is the mean cloud ice diameter.

PS5 – *Nucleation scavenging of SO$_4^{2-}$ by ice nuclei (IN)*. The term for nucleation scavenging of SO$_4^{2-}$ by IN is computed in an analogous way to the PS3:

$$PS5 = \varepsilon_{SO_4^{2-}} q_{SO_4, a} \frac{dq_i}{dt} \tag{S-12}$$

dq_i is the cloud ice formation during the current time step in the model.

$PS6$ – *Impact scavenging of SO_4^{2-} aerosol by rain*. This term represents the scavenging of sulfate particles by inertial impaction with raindrops. The impact scavenging of SO_4^{2-} by rain is computed for continuous collection processes:

$$-\frac{\partial q_{SO_4, a}}{\partial t} = \int_0^\infty \frac{\pi}{4} D_r^2 V_r(D_r) q_{SO_4, a} \varepsilon_r N(D_r) dD_r \tag{S-13}$$

where D_r is the mean diameter of raindrops, $V_r(D_r)$ is the terminal velocity of rain, $\varepsilon_r = 0.048$[16] is the aerosol–rain collection efficiency and $N(D_r)$ is the size distribution of rain. Assuming a Marshall–Palmer distribution[15] (Reference list in native article) for the rain drops, $n_r(D) = N_{0r} \exp(-\lambda_r D_r)$, where N_{0r} is the intercept parameter, $N_{0r} = 8\times10^6$ m^{-4}, λ_r is the slope parameter of the rain size distribution, and assuming the raindrops terminal velocity:[25] (Reference list in native article)

$$V_r(D_r) = aD_r^b(\frac{\rho_0}{\rho})^{1/2} \tag{S-14}$$

where $a = 842$ m^{1-b} s^{-1}, $b = 0.8$, $\rho_0 = 1.225$ kg m^{-3} (the surface air density), $PS6$ is then calculated as:

$$PS6 = \frac{\pi}{4} \frac{\Gamma(3.8)}{\lambda_r^{3.8}} \varepsilon_r a N_{0r}(\frac{\rho_0}{\rho})^{1/2} q_{SO_4, a} \tag{S-15}$$

$PS7$ – *SO_4^{2-} impact scavenging by hail*. When a hail particle falls through a field of dry sulfate particles, some of the sulfate particles are removed by impaction with the hail. This removal could be calculated, assuming continuous collection, as:

$$PS7 = \frac{3\pi}{7} \varepsilon_h V_h(D_h) N_h D_h^2 q_{SO_4, a} \tag{S-16}$$

Where $\varepsilon_h = 0.048$ is the collection efficiency for hail,[16] $V_h(D_h)$ is the terminal velocity of the hail, N_h is the hail concentration and D_h is the mean hail diameter.

$PS8$ – *SO_4^{2-} impact scavenging by snow*. This term is computed in a similar way to the terms $PS6$ and $PS7$:

$$PS8 = \frac{\pi}{4} \varepsilon_s V_s(D_s) N_s D_s^2 q_{SO_4, a} \tag{S-17}$$

where $\varepsilon_s = 0.008$[16] (Reference list in native article) is the collection efficiency for snow, $V_s(D_h)$ is the terminal velocity of snow, N_s is the snow concentration and D_s is the mean snow diameter.

$PS9$, $PS9hp$ – *S(IV) oxidation by O_3 and H_2O_2 to SO_4^{2-} in rainwater*. These terms are calculated similarly to $PS2$ and $PS2hp$:

$$PS9 = k_{O_3} (K_{Hs} K_{1s} p_{SO_2})^{1/2} q_{O_3, r} \, dt$$
$$PS9hp = k_{H_2O_2} K_{Hs} K_{1s} p_{SO_2} q_{H_2O_2, r} \, dt \tag{S-18}$$

where dt is the current time model step.

$PS10$ – *Rain evaporation*. This term determines the amount of SO_2 that is returned to the atmosphere during the evaporation of rain. The relation could express the conversion from HSO_3^- to SO_2 in the gas phase:

VUJOVIĆ and VUČKOVIĆ

$$PS10 = \frac{K_{Hs}K_{1s}}{[H_r^+]} p_{SO_2} \frac{M_{SO_2}}{M_{HSO_3}} ern \qquad \text{(S-19)}$$

where *ern* is the evaporation of rain. All microphysical processes used in the paper are described in Table S-I.

TABLE S-I. Microphysical reactions used in the chemistry module

Symbol	Meaning
ern	Rain evaporation
dep	Deposition or sublimation of cloud ice
praut	Autoconversion of cloud water to form rain
pracw	Accretion of cloud water by rain
psacw	Accretion of cloud water by snow; product snow (P_{sacw}) if $T < 273.16$ or rain (Q_{sacw}) if $T > 273.16$
dgacw	Accretion of cloud water by hail
psfw	The Bergeron processes (deposition and riming) - cloud water transfer to snow
pidw	Depositional growth of cloud ice at the expense of cloud water
pihom	Homogeneous freezing of cloud water to form cloud ice
psacr	Accretion of rain or snow; product hail if rain or snow exceed limit value; on the contrary, product snow
dgacr	Accretion of rain by hail
pgfr	Rain freezing to form hail
piacr	Accretion of rain by cloud ice; product snow or hail in dependence on the amount of rain
pgmlt	Hail melting to form rain
pgsub	Hail sublimation
psmlt	Snow melting to form rain
pgaut	Autoconversion (aggregation) of snow to form hail
pgacs	Accretion of snow by hail
pracs	Accretion of snow by rain
pssub	Snow sublimation
psdep	Depositional growth of snow
pgaci	Accretion of cloud ice by hail
praci	Accretion of cloud ice by rain; product snow or hail in dependence of the amount of rain
pimlt	Cloud ice melting and formation of cloud water
psaut	Autoconversion (aggregation) of cloud ice to form snow
psaci	Accretion of cloud ice by snow
psfi	Bergeron process – cloud ice transfer to snow

PS11 – SO$_4^{2-}$ transfer from cloud water to rain. This term follows the microphysical transition and transfer of SO$_4^{2-}$ from cloud water to rain:

$$PS11 = \frac{q_{SO_4,c}}{q_c}(praut + pracw + psacw) \qquad \text{(S-20)}$$

Autoconversion is the initial stage of the collision-coalescence process, whereby cloud droplets collide and coalesce to form rain; accretion is the growth of a bigger hydrometeor by collision with super-cooled cloud droplets that freeze wholly or partially upon contact.

PS*12 – SO₄²⁻ transfer from cloud water to hail*. This term represents the action of hail collecting cloud water containing sulfate:

$$PS12 = \frac{q_{SO_4,c}}{q_c} dgacw \tag{S-21}$$

PS*13 – SO₄²⁻ transfer from cloud water to snow*. This term represents the action of snow collecting cloud water that contains sulfate:

$$PS13 = \frac{q_{SO_4,c}}{q_c} (psacw + psfw) \tag{S-22}$$

PS*14 – SO₄²⁻ transfer from cloud water to cloud ice*. Due to the depositional growth of cloud ice at the expense of cloud water and the freezing of cloud water to form cloud ice, there is SO_4^{2-} transfer from cloud water to cloud ice:

$$PS14 = \frac{q_{SO_4,c}}{q_c} (pidw + pihom) \tag{S-23}$$

PS*15 – SO₄²⁻ transfer from cloud water to aerosol*. When cloud water droplets that contain SO_4^{2-} evaporate, some amount of SO_4^{2-} converts to dry sulfate particles. This process is calculated as:

$$PS15 = q_{SO_4,c} \frac{dq_c}{dt} \tag{S-24}$$

PS*16 – SO₄²⁻ transfer from rain to snow*. When raindrops and cloud ice particles collide, initiating snow formation, both the cloud ice sulfate and the rain sulfate must be transferred to the snow sulfate field:

$$PS16 = \frac{q_{SO_4^{2-},r}}{q_r} (piacr + psacr) \tag{S-25}$$

PS*17 – SO₄²⁻ transfer from rain to hail*. Similar to the previous term, *PS*17 follows the microphysical transitions from rain to hail:

$$PS17 = \frac{q_{SO_4^{2-},r}}{q_r} (dgacr + pgfr + piacr + psacr) \tag{S-26}$$

PS*18 – SO₄²⁻ transfer from hail to rain*. When hail melts, the sulfate in hail becomes sulfate in rain at a given proportion:

$$PS18 = \frac{q_{SO_4^{2-},h}}{q_h} pgmlt \tag{S-27}$$

PS19 – SO₄²⁻ transfer from hail to aerosol. Owing to the sublimation of hail, the amount of SO_4^{2-} that transfers from hail to aerosol is:

$$PS19 = \frac{q_{SO_4^{2-},h}}{q_h} \, pgsub \tag{S-28}$$

PS*20 – SO$_4$$^{2-}$ transfer from snow to rain*. Similar to the PS18 term, and owing to snow melt, the sulfate from snow transfers to rain as:

$$PS20 = \frac{q_{SO_4^{2-},s}}{q_s} \, psmlt \tag{S-29}$$

PS*21 – SO$_4$$^{2-}$ transfer from snow to hail*. Due to the autoconversion of snow to hail the accretion of snow by hail and the accretion of snow by rain, the sulfate transfer from snow to hail given by:

$$PS21 = \frac{q_{SO_4^{2-},s}}{q_s} (pgaut + pgacs + pracs) \tag{S-30}$$

PS*22 – SO$_4$$^{2-}$ transfer from snow to aerosol*. This term follows microphysical transitions, thus the transfer of sulfate from snow to aerosol fields is given by:

$$PS22 = \frac{q_{SO_4^{2-},s}}{q_s} (pssub + psdep) \tag{S-31}$$

PS*23 – SO$_4$$^{2-}$ transfer from cloud ice to hail*. Cloud ice sulfate is transferred to hail sulfate when cloud ice and hail collide. This process is represented by:

$$PS23 = \frac{q_{SO_4^{2-},i}}{q_i} (pgaci + praci) \tag{S-32}$$

PS*24 – SO$_4$$^{2-}$ transfer from cloud ice to cloud water*. When cloud ice melts and forms cloud water, cloud ice sulfate is transferred to cloud water sulfate:

$$PS24 = \frac{q_{SO_4^{2-},i}}{q_i} \, pimlt \tag{S-33}$$

PS*25 – SO$_4$$^{2-}$ transfer from cloud ice to snow*. This term follows microphysical processes that transfer cloud ice sulfate to cloud water sulfate:

$$PS25 = \frac{q_{SO_4^{2-},i}}{q_i} (psaut + psaci + psfi + praci) \tag{S-34}$$

PS*26 – SO$_4$$^{2-}$ transfer from cloud ice to aerosol*. This term describes the transfer of cloud ice sulfate to aerosol sulfate during the evaporation of cloud ice:

$$PS26 = \frac{dq_{SO_4^{2-},i}}{dt} \, dep \tag{S-35}$$

Journal of the Serbian Chemical Society

Ultrasound-assisted extraction of matrix elements and heavy metal fractions associated with Fe, Al and Mn oxyhydroxides from soil

SVETLANA M. STANIŠIĆ[1], LJUBIŠA M. IGNJATOVIĆ[1*#], IVAN ANĐELKOVIĆ[2], MILICA C. STEVIĆ[1#], ALEKSANDRA M. TASIĆ[1] and MARJETKA SAVIĆ BISERČIĆ[1]

[1]Faculty of Physical Chemistry, University of Belgrade, Studentski Trg 12–16, Belgrade, Serbia and [2]Faculty of Chemistry, University of Belgrade, Studentski Trg 12–16, Belgrade, Serbia

Abstract: Single agent extractions of major and trace metals from soil samples were conducted by means of a rotary mixer and an ultrasonic bath with sonication times of 10, 20, 30, 40 and 50 min. The sequential extraction was undertaken according to the European Community Bureau of Reference. The obtained soil extracts were analyzed by inductively coupled plasma-optical emission spectrometry and according to the results, the rotary mixer-assisted extraction was more efficient in the case of alkaline earth elements. However, by use of ultrasound, several times higher amounts of matrix elements (Fe, Al and Mn) and heavy metals predominantly associated with Fe, Al and Mn oxyhydroxides were extracted. The increase of the sonication time failed to improve the extraction yields. The changes in the conductivity, pH, redox potential, particle size diameter and zeta potential of colloid particles with increasing sonication time were measured. The extraction mechanism and expressed selectivity of ultrasound is discussed and an explanation is suggested.

Keywords: soil analysis; extraction mechanism; sequential extraction; soil phases.

INTRODUCTION

The measurements of major elements in soil samples are required to expand knowledge of the elemental composition of soil, while the assessment of the soil trace metal content is of major importance nowadays, due to their toxic effects and bio-accumulative nature. An excessive presence of metals in soils and sediments of industrial regions, particularly, and their potential leakage into surface and groundwaters could pose environmental problems. Thus, the determination of the metal amounts that are bound within soil solid phases and knowledge the

---

chemical mechanism of metal binding are important for predicting possible metal transfer to the aquatic systems.

The total metal content in soil is partitioned between the solid phases, *i.e.*, phyllosilicate minerals, carbonates, sulfides, Fe, Al and Mn oxyhydroxides and organic matter.[1] In addition, the different mechanisms of binding of metal ions to the different phases (ion exchange, outer- and inner-sphere surface complexation (adsorption), precipitation or co-precipitation) influence their mobility and bio-availability to a great extent.[2] In order to determine the manner in which the total metal content is subdivided between the soil phases, fractionation of the metal content, either by ion exchange processes or by dissolution of selected soil phase, is required. For this purpose, a sequential extraction (SE) procedure was introduced and widely accepted, and subsequently, numerous extraction schemes, *i.e.*, according to Tessier, The European Community Bureau of Reference (BCR), Gibbs, Ure, Campanella, *etc.*,[3] in which different extraction agents and conditions were suggested, were adopted. Many studies have been conducted in an attempt to define the optimal extraction conditions and to harmonize operational extraction procedure, since the results obtained by application of different extraction schemes are often non-comparable. In addition, SEs often give unreliable results because of the non-selectivity of the extraction agents simultaneously for the selected phase and ions, precipitation of new mineral phases or redistribution of ions between already existing soil phases during extraction.[4] However, a major disadvantage of the SEs is related to the fact that they are time and labor consuming, and according to the Tessier or BCR scheme require an overall operation time of about 18 and 51 h, respectively. Thus, there exists considerable interest in the development of ultrasound-assisted extractions (UAE) or microwave-assisted extractions, which provide the same information as conventional SEs, but are faster to realize.

Initially, ultrasonic energy was used for the dispersion of soil aggregates[5] or the disintegration of sewage sludge,[6] since the ultrasonic cavitation phenomenon together with the turbulent flow of aqueous suspension of soil and acoustic streaming result in friction, stress and dispersion of soil aggregates. In addition, ultrasonic energy has been widely used for accelerating the extraction of metal,[7] aliphatic and polycyclic aromatic hydrocarbons[8] and organochlorine pesticides[9] from soil or other solid samples. Thereby, the ultrasonic energy was applied by the use of an ultrasonic probe,[10] an ultrasonic bath[11] or cup-horn sonoreactors[12] with the conclusion that the probe provides shorter extraction time (up to 100 times), while the ultrasonic bath enables simultaneous replicate extractions. Perez-Cid *et al.*[13] described an ultrasound-assisted BCR SE of Cu, Cr, Ni, Pb and Zn ions from sewage sludge, whereby the duration was only 22 min, while recoveries were similar to those obtained by the conventional BCR extraction. A similar study was conducted by Davidson and Delevoye[14] and as they reported, the

recoveries were similar to those of conventional shaking for all metals (Cu, Mn and Zn) except from the important matrix element Fe. Väisänen and Kiljunen[15] performed a five-step ultrasound assisted SE of As, Cd, Cu, Pb and Zn ions from soil sample, according to the Tessier scheme. With the exception of the As concentrations, which were too high, the results of the UAE procedure were highly comparable with the results obtained by the conventional procedure. Arain *et al*.[16] showed that by the use of optimized sonication conditions, a three-step BCR UAE could be successfully completed in 15–30 min, thus providing considerable time saving, with a high treatment rate and low sample and reagent usage. The acceleration of the first step of the BCR extraction for trace and matrix elements was investigated by Rusnák *et al*.,[17] whereby the experiment included soil, sediment and gravitation dust samples. The results showed that the effect of ultrasound was different for all the studied sample types and each element. According to Filgueiras *et al*.,[18] the ultrasound-assisted versions of the BCR extraction scheme showed a better performance than the Tessier ones in terms of obtaining good agreement with the conventional SE, with the best results being found for metal partitioning in sewage sludge. To summarize, according to some studies, UAEs have proved to be successful for achieving quantitative recoveries from various environmental matrices, such as soil, sewage sludge, marine and lake sediments and reference materials.[19] However, according to others, ultrasonic energy did not affect all the types of solid samples in precisely the same way as conventional shaking. When it comes to soil sample, the difficulty of developing a rapid version of SEs is related to the different fractionation patterns obtained by UAE in comparison to conventional ones, mainly for the matrix elements, such as Fe.[4]

The aim of this study was to investigate the influence of ultrasonic energy on aqueous suspensions of soil, through changes in different physico-chemical parameters, in order to determine whether ultrasound could be used for accelerating the extraction of major and trace elemental from soil samples.

A sample of serpentinite soil type Ranker was used as the substrate in this research. Rotary mixer-assisted extraction (RAE) and UAE were performed as single extractions using deionized water as the only extracting agent. A SE was performed in order to assess the amounts of heavy metals associated with different soil phases. For the determination of the cation concentrations in the soil extracts obtained by RAE, UAE and SE, inductively coupled plasma-optical emission spectrometry (ICP-OES) measurements were performed. For all the soil suspension during the UAEs, conductivity (κ) measurements were continuously performed. Additionally, the UAEs were repeated in order to measure the suspension parameters, *i.e*., the oxido-reduction potential (*ORP*), the particle size diameter (*PSD*), the zeta potential of the colloidal particles (*ZP*) and the pH, during the ultrasonic treatment.

EXPERIMENTAL

The soil sample was taken from a site covered with natural vegetation, at the location Bubanj Potok, near Belgrade, Serbia, which had been exposed to minimal influences of anthropogenic pollution. The geographical coordinates of the location are 44° 44' 4" North, 20° 32' 36" East and the height is 157 m above sea level. The soil sample, weighing 1 kg in total, was obtained by combining samples taken from the surface horizon, rich in humus, from 30 different sites, at a depth of 20 cm. The depth of the total soil profile at this location is 50 cm. The sample was air dried for 72 h. Subsequently, the large fractions were removed, crushed in a mortar and sieved through a 1 mm pore diameter sieve. The basic pedological analysis included: the potentiometric determination of the pH in H_2O and 1.0 mol L^{-1} KCl, the humus content after the Turin method, the adsorptive complex of the soil (H, T, S) after Kappen, determination of the soil texture by the pipette method, determination of the hygroscopic moisture by drying at 105 °C and determination of the mass loss during heating at 700 °C for 30 min.

The extraction suspensions were prepared in 50 mL volumetric flasks by mixing the soil sample with deionized water in a ratio 1:10, *i.e.*, 2 g:20 mL. Two series of three extractions each were performed using an Overhead Mixer Reax 20/8 (Carl Roth, Germany) rotary mixer in which the suspension was processed for 22 h mixing at 10 rpm at room temperature (20 °C). The second technique involved the use of an ultrasonic bath with the suspension positioned at the same place in the bath and at the same initial water temperature, 17 °C. Two extractions were made for each of the following extraction times: 10, 20, 30, 40 and 50 min. A Transsonic T 760 DH (Elma, Germany) ultrasonic bath operated at an ultrasonic frequency of 40 kHz and effective ultrasound power of 170 W was employed for these experiments. Deionized water (18.2 MΩ cm) produced by a Milli-Q Reagent Grade system (Phenomenex, USA) was used for the extractions and preparation of all suspensions. The substances used for the analyses were of high analytical purity. After the extraction processes were completed, each of the extraction suspensions was first centrifuged, then filtered through medium pore size filter paper and finally through 0.2 µm pore size syringe membrane filter (Phenomenex, USA). The thus obtained soil extract was acidified by addition of 1 µl of 70 % concentrated perchloric acid (Merck, Germany) per 1 mL of extract and preserved at 4 °C in a laboratory refrigerator for further analysis.

Furthermore, the soil sample was subjected to SE according the scheme suggested by the Standards, Measurements and Testing Program of the European Commission (BCR, formerly).[3] The last step of the extraction procedure using *aqua regia*, according to EPA 3050B digest extract method was added in order to determine the total metal contents. Additionally, in order to distinguish between the easily reducible fraction bound to Mn oxyhydroxides and the moderately and poorly reducible one bound to amorphous and crystalline Fe and Al oxyhydroxides, the procedure was modified by the inclusion of a third extraction step.[20] Dry soil samples (1 g) were weighed into 50 mL polystyrene flasks and after addition of the extraction agents, the flasks were shaken on a rotary mixer at 15 rpm. The residue was washed with 25 mL of deionized water, and centrifuged at 3000 rpm, prior to the next extraction step. The extraction was performed in triplicate, according to the procedure summary (Table I).

A Thermo Scientific iCAP-6500 DUO ICP (Thermo Fisher Scientific, UK) spectrometer, with continuous wavelength coverage ranging from 166 to 847 nm, equipped with RACID86 charge injector device (CID) detector, pneumatic cross-flow type nebulizer and quartz torch, was used for the ICP-OES measurements. The instrumental conditions were set at: input power, 1150 W; auxiliary gas flow, 0.5 L min^{-1}; coolant gas flow, 12 L min^{-1} and nebulizer

flow, 0.7 L min^{-1}. For ICP-OES calibration, multi-element plasma standard solution 4, Spec-pure (Alfa Aesar, Germany, Cat. No. 42885) was used and two series of standard solutions were prepared: for alkali and alkaline earth metal elements of concentration 0.01, 0.05, 1, 10 and 50 mg L^{-1} and for the transition elements of concentration 0.1, 1, 10, 100 and 500 µg L^{-1}. The relative standard deviation was calculated automatically, $RSD = (SD/\mu) \times 100$, where SD is standard deviation and μ represents the mean value of three measurements. After accuracy evaluation, the relative standard deviations of the ICP-OES measurements were determined to be: Al, 1.06 %; Ca, 0.21 %; Cd, 8.69 %; Co, 6.91 %; Cr, 7.17 %; Cu, 6.21 %; Fe, 0.63 %; K, 2.68 %; Mg, 0.79 %; Mn, 4.86 %; Na, 0.82 %; Ni, 8.42 %; Pb, 7.62 % and Zn, 8.67 %.

TABLE I. A summary of the SE operating conditions

Elements fraction	Extraction time, h	Agitation method	Extractant amount, mL	Extraction reagent
Water-exchangeable, weakly adsorbed	16	Shaking, room temp.	40	0.11 mol L^{-1} acetic acid (HOAc)
Easily reducible (Mn oxyhydroxide phase bound)	16	Shaking, room temp.	40	0.1 mol L^{-1} NH$_2$OH·HCl/HNO$_3$ pH 2
Moderately reducible (Fe, Al oxyhydroxide phase bound)	10	Shaking, room temp.	40	0.2 mol L^{-1} ammonium oxalate/ 0.2 mol L^{-1} oxalic acid
Oxidizable (organically bound)	3	Occasional agitation, 85 °C	2x10	30 % (8.8 mol L^{-1}) H$_2$O$_2$/HNO$_3$ pH 2
	16	Shaking, room temp.	40	1 mol L^{-1} NH$_4$OAc, pH 5
Residual	0.5	Water bath, 95 °C	10	*Aqua regia*, HNO$_3$/HCl (1:3)

With the exception of κ, for the determination of each suspension parameter, additional UAEs were performed in five replicates with an aqueous soil suspension. In order to adjust ionic strength for the κ measurement, the extraction solutions were prepared with an ionic strength buffer (1 mol L^{-1} KCl) instead of deionized water. The conductivity, *ORP* and pH measurements were performed using a 3540 Conductivity/pH meter (Jenway, UK). The *PSD* and *ZP* measurements were performed by dynamic light scattering spectroscopy using a Zeta-sizer Nano Red ZS, with a 633 nm He–Ne laser (Malvern, UK). The instrumental conditions were set at: run duration, 10 s; temperature, 25 °C; refractive index of material, 1.600 and absorption index, 0.01. The measurements were conducted during the extraction process every 10 min for the colloid *PSD* and *ZP*, every 5 min for *ORP* and pH, while the value of κ was measured continuously. For the duration of the pH and *ORP* measurements, the ultrasonic bath was turned off.

RESULTS AND DISCUSSION

The measured pH value in 1 mol L^{-1} KCl was 6.0 and in deionized water, the pH value was (5 g soil:10 mL water) 6.9. The results of the other pedological analyses are given in Table II.

TABLE II. The results of the basic pedological analysis

Soil parameter	No. 1	No. 2	No. 3	Mean value
Humus, %	5.15	5.23	5.12	5.16
Total C, %	2.99	3.03	2.97	2.99
The sum of base cations, mEq 100 g^{-1}	34.6	33.5	39.6	35.9
Large sand particles, %	4.87	6.22	6.83	5.97
Small sand particles, %	30.10	30.8	31.58	30.85
Colloid clay, %	45.75	43.61	40.99	43.45
Silt, %	19.28	19.28	20.60	19.72
Hygroscopic moisture, %	3.1	3.1	3.1	3.1
Heating loss, %	14.2	14.6	14.4	14.4

According to the results, the investigated soil sample contained low levels of some elements; thus, the extracted amounts of Li were in range from 0.003 to 0.024 mg 100 g^{-1} soil, the extracted amounts of Cd were in the range of 0.386 to 0.963 µg 100 g^{-1} soil and for Co the values ranged from 0.101 to 0.969 µg 100 g^{-1} soil. Since the amounts of these elements extracted by both extraction techniques were too small for conclusions to be drawn, these elements were not taken into further consideration.

A comparison of the amounts of the elements extracted by UAE and RAE is shown in Fig. 1, from which it can be seen that significantly higher amounts of the matrix elements (Fe, Al and Mn) were extracted in the UAE than in the RAE. Compared to the amounts extracted using the rotary mixer, the average amounts of Fe and Al ions extracted during the UAE were 7.5 and 8.2 times higher, respectively. However, in the case of the alkaline earth elements (Ca and Mg), higher amounts were extracted in the RAE than in the UAE. Considering the concentrations of Mg ion, the high amounts extracted using both techniques could be explained by the properties of the soil itself, since Ranker over serpentinite type of soil has a ratio Ca:Mg<1, unlike other soil types.[21] The lower amounts of the alkaline earth elements were obtained using UAE compared to those extracted by RAE could be explained either by the significantly longer agitation time of the RAE (22 h) and subsequent dissolution, or by the re-adsorption of extracted cations onto the sorption sites newly exposed by the influence of ultrasound.

The amounts of all elements extracted in the UAE as a function of sonication time are shown in Fig. 2, from which it can be seen that the extracted amounts of all elements changed, which was most noticeable in the case of the matrix elements (Fe, Al and Mn) and some trace elements (Cr, Cu and Zn).

During the UAE, the pH also changed in the range of 5.60 to 8.12 (Fig. 3). As it can be seen in Fig. 3, the largest increase in pH to 8.12 was registered after 20 min of sonication, at the same time a decrease of the acid (Al and Fe) and the increase of the base cation (Mg and Ca) concentrations were observed in the extract. At an extraction time of 40 min, the extracted amounts of both base and

acid cations were the largest observed, but the pH fell simultaneously to 7.58, indicating that the total content of acid cations (Al, Fe and Mn) exceeded the total content of base cations (Ca and Mg). With further increase in the sonication time, the extracted amounts of Fe, Al and Mn decreased and a subsequent increase in the pH of the soil suspension was observed. It is assumed that the changes in the pH value were caused by adsorption and desorption processes, but were not the cause of these processes. Large amounts of various cations were released into the solution, influencing the pH change. This pH change can influence the adsorption and desorption processes to some extent, but these processes are mainly related to competitive cation interactions for the sorbing phase and the exchange of sorbed cations with those from solution is influenced by ultrasound.
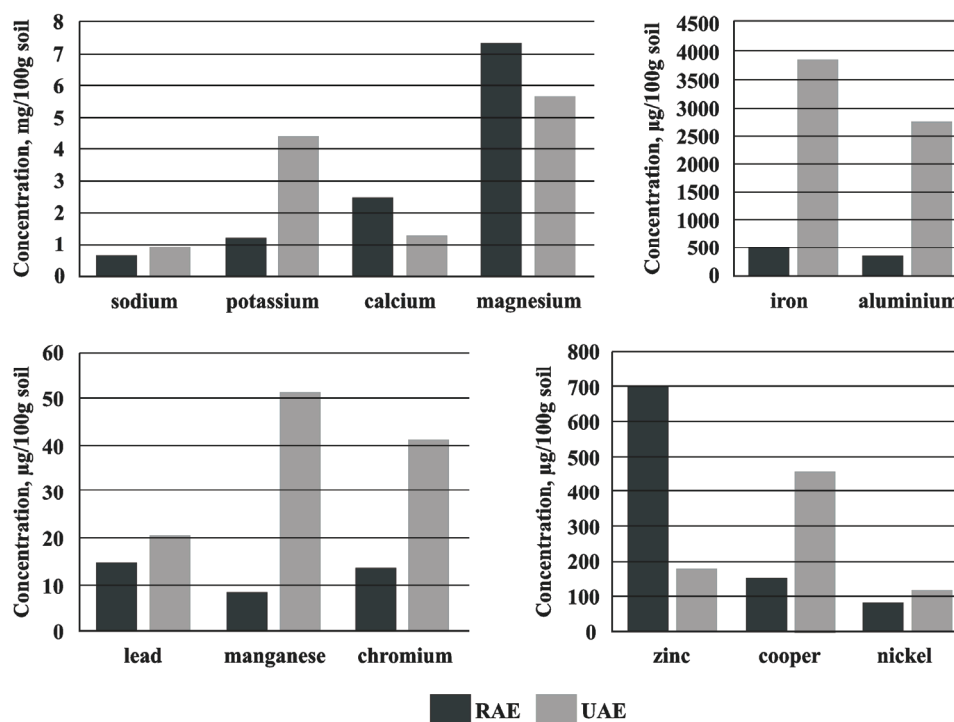
Fig. 1. Comparison of the average amounts extracted using a rotary mixer and ultrasound.

The results of the SE procedure, obtained for Cd, Co, Cr, Cu, Ni, Pb, Zn, Fe, Al and Mn, are shown in Table III. Considering that deionized water was used as the extraction agent in the UAE and RAE processes, the extracted amounts are significantly lower compared to the amounts extracted by means of the chemical agents proposed in the SE procedure. Thus, the results present the percentage of the total content of elements contained in the water-exchangeable, easily and

moderately reducible, oxidizable and residual fraction. Although not the most abundant in the soil, the oxyhydroxides of Fe, Al and Mn have a large surface area, which makes them important reactive phases with respect to metal sorption. Concerning the other fractions, the largest amounts of Cr and Cu ions were contained within the moderately reducible fraction and hence associated with the amorphous and crystalline Fe, Al oxyhydroxides.
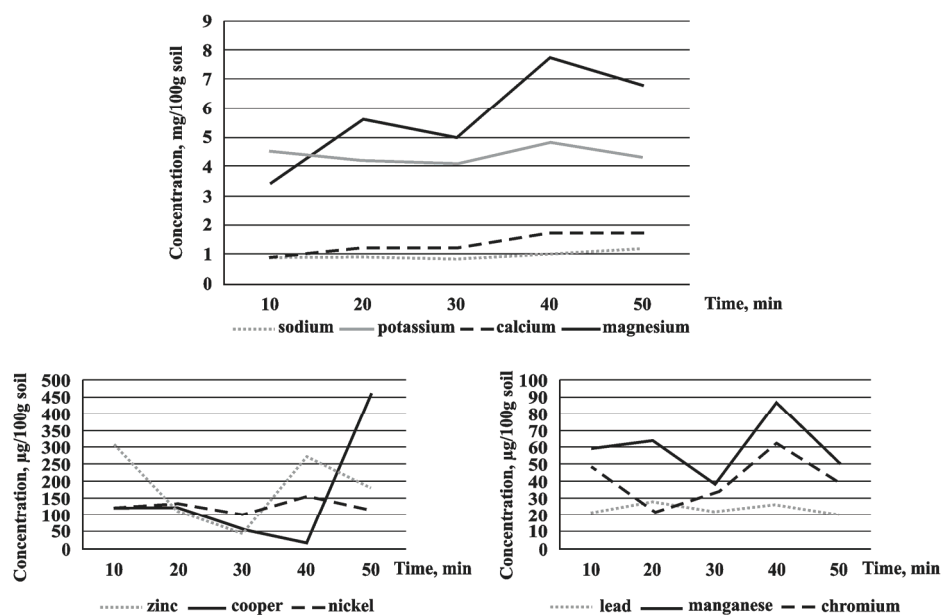
Fig. 2. The effectiveness of the UAE for the extraction of Na, K, Ca, Mg, Pb, Mn, Cr, Zn, Cu and Ni ions as a function of sonication time.
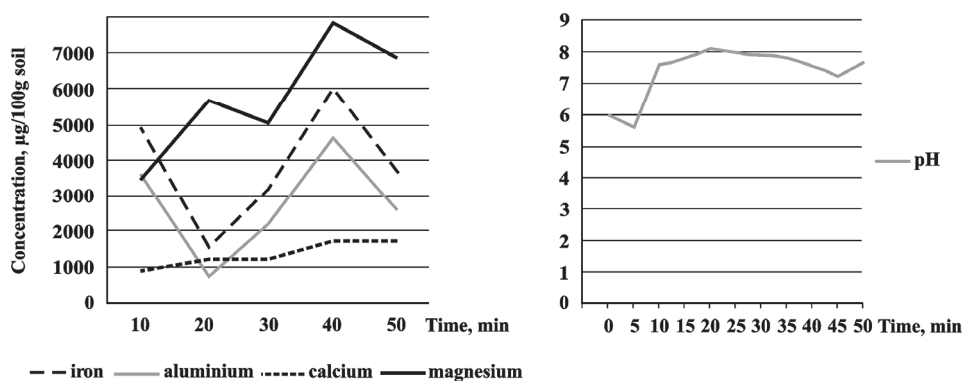
Fig. 3. The effectiveness of the UAE for the extraction of Fe and Al ions (left) and changes in pH value (right) as a function of sonication time.

Furthermore, the largest amounts of Cd, Co, Ni, Pb and Zn ions were contained within the easily reducible fraction of elements, which are associated with Mn oxyhydroxides. The manner in which metals are retained in the soil refers to the type of surface sorption complex, which is influenced by surface loading, as well as by pH, ionic strength and type of sorbing phase. Hence, outer-sphere complexation is a rapid and reversible process that involves electrostatic interactions and occurs on surfaces of opposite charge. On the contrary, inner-sphere complexation can increase or reduce the surface sorptive charge regardless of the original charge.[22] Since sorption includes adsorption, precipitation and polymerization, the sorption mechanisms can be determined only through molecular investigations by use of spectroscopic techniques.

TABLE III. The results obtained by the SE procedure. Participations of different metal fractions in total metal content, %. Bold values present the largest non-residual fraction for each element

Fraction	Cd	Co	Cr	Cu	Ni	Pb	Zn	Fe	Al	Mn
Water-exchangeable	–	0.05	–	–	1.4	0.01	–	–	–	1.4
Easily reducible (Mn oxyhydroxides)	90.3	49.9	0.9	1.2	17.1	18.9	15.4	1.2	1.6	73.5
Moderately reducible (Fe and Al oxyhydroxides)	9.7	14.7	17.8	22.7	7.1	1.3	6.5	13.2	6.2	10.3
Oxidizable	–	3.9	16.3	0.05	15.8	5.9	5.1	0.1	0.3	1.6
Residual	–	31.5	65.0	76.0	58.6	73.9	72.9	85.5	92.0	13.2

The changes in extracted amounts of some trace elements (Cr, Cu and Zn) as a function of sonication time are dependant on the cation sorption mechanism, as well as on the type of mineral or organic matter with which they are associated. According to Charlet and Manceau,[23] Cr (III) can be found on goethite (iron oxyhydroxide) surfaces, either adsorbed as an inner-sphere complex or in the form of Cr hydroxide surface precipitates. The results of the SE showed that 17.8 % of the total Cr content (50.8 % of the non-residual content) was associated with Fe and Al oxyhydroxides. In keeping with this, as shown in Figs. 2 and 3, the increases in the extracted amounts of Fe and Cr with the extraction time follow the same change pattern. The same pattern of change was observed in the case of Mn and Zn. Scheinost et al.[24] demonstrated that Zn(II) can form both inner-sphere surface complexes and a Zn hydrotalcite-hydroxide phase upon sorption to Al-bearing minerals, inner-sphere surface complexes on goethite and both inner-sphere and multinuclear hydroxo-complexes on manganite surfaces. In the studied soil sample, Zn had predominantly formed complexes on manganite surfaces since, according to the SE results, 70.3 % of the non-residual content of Zn was associated with Mn oxyhydroxides within the easily reducible fraction. According to Weesner and Bleam,[25] Cu(II) can form outer- and inner-sphere surface complexes upon sorption to boehmite (Al oxyhydroxide). This observation was

confirmed by the results of the SE, which showed that 94.8 % of non-residual content of Cu was found within the moderately reducible fraction. However, the variations in the changes of pattern of the extracted amounts of Cu and Al were not the same, which implies that certain portions of the metal released by ultrasonic treatment were re-adsorbed onto the other remaining soil phases.

An explanation could be suggested for the high amounts of extracted matrix elements (Fe, Al and Mn), as well as to the variations of the amounts of extracted cations with increasing sonication time. First, the influence of the ultrasound on the aqueous soil solution could be attributed to the cavitation effect. The cavitation is caused by interaction of the ultrasound with soil solution, by implosion of cavitation bubbles, subsequent increases in the local pressure and the formation of elastic shock waves. This leads to the production of localized high temperatures in the solution and thus creates extreme conditions for chemical reactions to occur. At the beginning of the ultrasonic extraction, the temperature of the water was 17 °C and the increase in temperature was 11 degrees, which makes 28 °C at the end of the extraction process. This rise in the temperature influences on the amounts extracted, however it is hard to measure to what extent. The maximum temperature T_{max} and maximum pressure P_{max} in the cavitation bubble before collapse is defined as:

$$T_{max} = T_{in} \left[P_a (\gamma - 1)/P_{in} \right] \tag{1}$$

$$P_{max} = P_{in} \left[P_a (\gamma - 1)/P_{in} \right]^{\gamma/(\gamma - 1)} \tag{2}$$

where T_{in} and P_{in} are the initial temperature and pressure in the bubbles, respectively, P_a is the acoustic pressure at the beginning of collapse and γ is the average specific heat ratio at constant volume of the gas in the bubble.[26] Furthermore, the temperature and pressure rise inside cavitation bubbles leads to the formation of free radicals. Related to this, the application of ultrasound for decomposition of different organic contaminants in water has been widely researched. In these reactions, the production of highly reactive oxygen species by sonolysis of water molecules, *i.e.*, hydroxyl-, peroxy- and superoxide- radicals, is considered to play an important role. Their generation is supposed to occur on the inside/interface of the adiabatic cavitation bubbles that are formed in aqueous suspensions during sonication.[27] In the present case, the effectiveness of the sonochemical decomposition of water was also highly dependent on the presence of soil particles, which could facilitate the cavity formation process and thereby intensify the generation of radical species. According to Tuziuti *et al.*,[28] the presence of soil particles can also influence the scattering of the ultrasound waves followed by subsequent attenuation of the cavitation effect and decrease in formation of reactive species. Once generated, highly reactive species influence changes in the redox status in the soil suspension. The changes in the redox status have a large influence on the mobility of certain metal species, such as Fe, Mn

and Cr. Under reductive conditions, oxyhydroxides of Fe and Mn are subjected to reductive dissolution and hence metal species, associated with these phases can have changes in solubility. Related to this, the conducted measurements showed that the *ORP* of the extraction suspension increased within 5 min after stopping sonication from 30 to 130 mV *vs.* Ag/AgCl, 3 mol L^{-1} KCl reference electrode, probably due to the generation of multiple redox couples.

In addition to this, ultrasound has an influence on desorption processes and the ability of ultrasonic energy to intensify desorption processes and to release metals from soil, activated carbon or other materials with high sorption capacity is well documented. Hwang *et al.*[29] showed that the efficiency of leaching solutions (both citrate and EDTA) for heavy metal removal from soil was increased with sonication compared to those of soil washing. Hamdaoui *et al.*[30] explored the effects of ultrasound on the desorption of metal ions from activated carbon, and the results of the conducted study indicated that the desorption rates of Cu(II), Mn(II), Hg(II) and Cr(VI) were significantly improved by ultrasonic irradiation.

Beside desorption, re-adsorption processes are also intensified under the influence of ultrasound. The re-adsorption process and subsequent decrease of the extracted amount after 40 min of sonication occurred in the cases of all other mentioned elements, also of Fe, Al, Mn, Cr and Zn. The rate of adsorption and re-adsorption in soils is dependent on the type and quantity of inorganic and organic components and the charge and radius of the ion being considered.[31] Surface reactive sites of the soil phases comprise permanent and variable charge sites, depending on their origin. For example, various functional groups, such as phenolic, carboxyl and alcoholic, are found on organic molecules. The major inorganic surface functional groups are the siloxane, associated with the silica tetrahedral layer of phyllosilicates and hydroxyl groups, such as silanol and aluminol, originating from broken mineral lattice of clay minerals or associated with the edges of metal oxyhydroxides. However, besides the mentioned reactive groups, ultrasonic energy can cause fragmentation of the soil particle and dispersion of soil aggregate, thus increasing the surface area available for reaction with the extraction agent. Sonication produces a significant increase of the specific surface area due to particle size reduction; hence, the number of sites available for adsorption is increased. Factors affecting soil aggregate dispersion during ultrasound application are the soil–water ratio, the total applied energy and the power output per volume of the extracting suspension. This was explained by enhanced surface diffusivity, which is related to the phenomena induced by acoustic cavitation, such as acoustic vortex micro-streaming, high-speed microjets, high-pressure shock waves and intense localized heating. In the aqueous soil suspension, ultrasonic treatment modifies the particle size, morphology and structural order of clay minerals. The elongated crystals are broken up into smaller units

that retain the typical lamellar morphology of the starting crystals.[32] The results of *PSD* analysis of the sonicated suspensions are given in Table IV, from which it could be seen that the mean particle size decreased with increasing sonication time.

Thereby, the *ZP* of colloid particles ranged from –49.54 to –11.08 mV with the largest change being observed between 40 and 50 min of sonication. *ZP* values more negative than –30 mV are considered to represent sufficient mutual repulsion to ensure the stability of a suspension.[33] It could be assumed that due to Fe, Al and Mn sorption processes in the last 10 min of sonication, the surface charge of colloidal particles decreased, and simultaneously the *PSD* showed a slight increase. As the results showed (Table IV), the suspension κ increased during sonication, partly due to the heating of the suspension and partly due to an increase in the number of total charged particles in the suspension.

TABLE IV. Changes in the colloid *PSD*, *ZP* and conductivity of extraction suspension as a function of sonication time

Extraction time, min	Detected particle size fraction, nm	Fraction participation, %	Average particle size, nm	Zeta potential mV	Conductivity μS cm^{-1}
10	4843	14.2	1258	–25.42	18
	1127	39.8			
	265	46.0			
20	4853	12.7	1090	–35.82	20
	860	47.8			
	158	39.5			
30	4886	10.2	1074	–28.04	23
	690	81.4			
	163	8.4			
40	4294	9.3	966	–49.54	28
	653	85.7			
	141	5.0			
50	4731	7.7	970	–11.08	38
	691	86.3			
	156	6.0			

CONCLUSIONS

As indicated above, the influence of ultrasonic energy on the soil sample preparation was found to be significant. However, not only due to a possible decrease in the extraction time, but mainly due to the expressed selectivity for the matrix elements (Fe, Al and Mn) and heavy metal portions associated with Fe, Al and Mn oxyhydroxides. As shown, the interaction of ultrasonic energy with the aqueous soil suspensions, alternately, influenced the processes of cation adsorption and desorption, thereby leading to a change in the extracted amounts of cations as function of sonication time. In addition to the aforementioned, the interaction of ultrasonic energy with the soil suspension created extreme conditions for chemical reactions to occur, some of them resulting in the generation of

highly reactive species. Therefore, it could be concluded that ultrasound cannot simply replace conventional treatments, such as conductive heating, in each extraction step of the sequential procedure. The introduction of ultrasound requires further investigation, first, to determine whether it has the same effect on different soil samples. Further investigations are required in order to explore whether ultrasound can be used to assess the heavy metal fraction associated with the easily reducible Mn oxyhydroxides and moderately reducible Fe and Al oxyhydroxides. For this purpose, ultrasound could be combined with deionized water only in particular SE steps for the efficient enhancement of the SEs, since compared to salt and acid solutions, deionized water is a preferable extractant, leading to avoidance of sample contamination.

И З В О Д

ЕКСТРАКЦИЈА ГЛАВНИХ ЕЛЕМЕНАТА И ФРАКЦИЈЕ ТЕШКИХ МЕТАЛА ВЕЗАНИХ У СКЛОПУ Fe, Al И Mn ОКСИДНИХ ФАЗА ЗЕМЉИШТА ПОТПОМОГНУТА УЛТРАЗВУКОМ

СВЕТЛАНА М. СТАНИШИЋ[1], ЉУБИША М. ИГЊАТОВИЋ[1], ИВАН АНЂЕЛКОВИЋ[2], МИЛИЦА Ц. СТЕВИЋ[1] и АЛЕКСАНДРА М. ТАСИЋ[1]

[1]*Факулш за физичку хемију, Универзишеш у Беоїраду, Сшуденшски Трї 12–16, Беоїрад и* [2]*Хемијски факулш, Универзишеш у Беоїраду, Сшуденшски Трї 12–16, Беоїрад*

Вршена је екстракција главних катјона и катјона елемената у траговима из узорка земљишта помоћу дејонизоване воде употребом ротационе мућкалице и ултразвучне каде са екстракционим временом од 10, 20, 30, 40 и 50 min. Узорак земљишта је подвргнут секвенционалној екстракцији према BCR процедури. Садржај добијених екстракта земљишта је одређен оптичке емисионе спектрометрије са индуктивно спрегнутом плазмом, и према резултатима екстракција изведена помоћу ротационе мућкалице се показала ефикасном у случају земноалкалних елемената. Употребом ултразвука екстраховане су неколико пута веће количине матрикс елемената (Fe, Al и Mn) и тешких метала који се у земљишту претежно налазе у склопу Fe, Al и Mn оксидне фазе. Продужење екстракционог времена није резултирало повећањем екстраховане количине. Током ултразвучне екстракције вршена су мерења проводљивости, pH, оксидоредукционог потенцијала суспензије земљишта, величине и зета потенцијала колоидних честица. Предложено је објашњење механизма екстракције и утицаја ултразвука на екстракцију главних елемената и тешких метала из оксидних фаза земљишта.

(Примљено 29. септембра, ревидирано 17. новембра 2011)

REFERENCES

1. M. B. Arain, T. G. Kazi, M. K. Jamali, N. Jalbani, H. I. Afridi, J. A. Baig, *J. Hazard. Mater.* **154** *(*2008) 998
2. G. S. P. Ritchie, G. Sposito, in *Chemical Speciation in the Environment,* 2nd ed., A. M. Ure, C. M. Davidson, Eds., Blackie, Glasgow, UK, 1995, p. 462

3. G. Rauret, *Talanta* **46** (1998) 449
4. J. R. Bacon, C. M. Davidson, *Analyst* **133** *(*2008) 25
5. A. Mentler, H. Mayer, P. Strauß, W. E. H. Blum, *Intern. Agrophys.* **18** (2004) 39
6. P. Sorys, E. Zielewicz-Madej, *Mol. Quant. Acoust.* **28** (2007) 247
7. C. Bendicho, I. Lavilla, in *Encyclopedia of Separation Science*, I. D. Wilson, E. R. Adlard, M. Cooke, C. F. Poole, Eds., Academic Press, London, UK, 2000, p. 391
8. P. Richter, M. Jimenez, R. Salazar, A. Marican, *J. Chromatogr., A* **1132** (2006) 15
9. A. Tor, M. E. Aydin, S. Özcan, *Anal. Chim. Acta* **559** (2006) 173
10. I. López-García, N. Campillo, I. Arnau-Jerez, M. Hernández-Córdoba, *Anal. Chim. Acta* **531** (2005) 125
11. D. Remeteiová, S. Ruzciková, R. Rusnák, *Microchim. Acta* **163** (2008) 257
12. H. Güngör, A. Elik, *Microchem. J.* **86** (2007) 65
13. I. de la Calle, N. Cabaleiro, M. Costas, F. Pena, S. Gil, I. Lavilla, C. Bendicho, *Microchem. J.* **97** (2011) 93
14. B. Perez-Cid, I. Lavilla, C. Bendicho, *Anal. Chim. Acta* **360** (1998) 35
15. C. M. Davidson, G. Delevoye, *J. Environ. Monit.* **3** (2001) 398
16. A. Väisänen, A. Kiljunen, *Int. J. Environ. Anal. Chem.* **85** (2005) 1037
17. M. B. Arain, T. G. Kazi, M. K. Jamali, J. A. Baig, H. I. Afridi, N. Jalbani, R. A. Sarfraz, *Pedosphere* **19** (2009) 476
18. R. Rusnák, G. Halász, M. Horváth, D. Remeteiová, *Toxic. Environ. Chem.* **92** (2010) 443
19. A. V. Filgueiras, I. Lavilla, C. Bendicho, *J. Environ. Monit.* **4** (2002) 823
20. A. V. Filgueiras, I. Lavilla, C. Bendicho, *Fresenius J. Anal. Chem.* **369** (2001) 451
21. W. Salomons, U. Förstner, *Metals in the Hydrocycle,* Springer-Verlag, Berlin, Germany, 1984, p. 218
22. A. Chiarucci, A. J. M. Baker, *Plant Soil* **293** (2007) 1
23. H. L. Bohn, B. L. Mc Neal, G. A. O'Connor, *Soil Chemistry*, 3rd ed., Wiley, New York, USA, 2001, p. 119
24. L. Charlet, A. A. Manceau, *J. Colloid Interface Sci.* **148** (1992) 443
25. A. C. Scheinost, R. Kretzschmar, S. Pfister, *Environ. Sci. Technol.* **36** (2002) 5021
26. F. J. Weesner, W. F. Bleam, *J. Colloid Interface Sci.* **196** (1997) 79
27. T. J. Mason, *Sonochemistry: The Uses of Ultrasound in Chemistry*, Royal Society of Chemistry, Cambridge, UK, 1990, p. 94
28. S.-I. Ueno, T. Fujita, D. Kuchar, M. Kubota, H. Matsuda, *Ultrason. Sonochem.* **16** (2009) 169
29. T. Tuziuti, K. Yasui, Y. Ilda, H. Taoda, S. Koda, *Ultrason. Sonochem.* **42** (2004) 597
30. S.-S. Hwang, J.-S. Park, W. Namkoong, *J. Ind. Eng. Chem.* **13** (2007) 650
31. O. Hamdaoui, E. Naffrechoux, *AIChE J.* **53** (2007) 363
32. D. L. Sparks, *Environmental Soil Chemistry*, 2nd ed., Academic Press, London, UK, 2003, p. 86
33. F. Franco, J. A. Cecila, L. A. Perez-Maqueda, J. L. Perez-Rodriguez, C. S. F. Gomes, *Appl. Clay Sci.* **35** (2007) 119
34. D. Li, M. B. Muller, S. Gilje, R. B. Kaner, G. G. Wallace, *Nat. Nanotech.* **3** (2008) 101.

Epiphytic lichen *Flavoparmelia caperata* as a sentinel for trace metal pollution

TATJANA MITROVIĆ[1]*, SLAVIŠA STAMENKOVIĆ[1], VLADIMIR CVETKOVIĆ[1], MILOŠ NIKOLIĆ[1], RADA BAOŠIĆ[2#], JELENA MUTIĆ[2], TATJANA ANĐELKOVIĆ[3#] and ALEKSANDAR BOJIĆ[3#]

[1]*Department of Biology and Ecology, Faculty of Sciences and Mathematics, University of Niš, Višegradska 33, 18000 Niš, Serbia,* [2]*Faculty of Chemistry, University of Belgrade, Studentski trg 12, P. O. Box 51, 11158 Belgrade, Serbia and* [3]*Department of Chemistry, Faculty of Sciences and Mathematics, University of Niš, Višegradska 33, 18000 Niš, Serbia*

Abstract: The widely spread lichen specie *Flavoparmelia caperata* was used in a biomonitoring study for atmospheric trace metal pollution in natural eco-systems in south-eastern Serbia. The concentration and distribution pattern of 21 metals in lichens were determined by inductively coupled plasma atomic emission spectrometry. The difference observed between metal deposition in the peripheral and central parts of lichen thalli reflected air quality changes in the last and previous years. These findings were confirmed with principal component analysis. The study demonstrated the accumulation of Ba, K, Mg, Na, Tl and Zn in the peripheral parts of thalli, while As, B, Cd, Cr, Cu, Fe, Ga, In, Li, Ni, Pb and Se were concentrated in the central parts of thalli.

Keywords: lichen; *Flavoparmelia caperata*; trace metals; sentinel; biomonitoring.

INTRODUCTION

Biological monitoring is an effective way of detecting early changes of the environment.[1] Species capable of accumulating pollutants are considered as sentinels. Accumulation of trace metals causes chronic changes to ecosystems and permanent damage to the health of biota and thus must be carefully monitored. Urban, industrial and traffic heavy metal pollution has had a serious impact on distance natural oasis, such as National Parks and Special Nature Reserves.

Lichens represent unique life forms – symbioses between fungi (mycobionts) and algae and/or cyanobacteria (photobionts). The lack of a waxy cuticle and

---

1301

long life span result in the absorption of pollutants across the entire thalli surface. Epyphitic lichens as rootless plants show no substantial metal uptake from substrates and thus their metal content is obtained from aerial supplies only (*i.e.*. wet and dry atmospheric deposition).[2] Metal accumulation in lichens is in correlation with their environmental levels[3–5] and spatial- and/or temporal-deposition patterns were demonstrated.[6] Additionally, intra- and inter-specific variability in metal accumulation in lichens and a relationship between the metal content and the age of the thalli was observed.[7,8]

In this study, the potential of a widely distributed lichen species, *Flavoparmelia caperata* (L.) Hale, as a bioindicator and bioaccumulator of trace metal pollutants was investigated. The study was performed at 3 different natural ecosystems: north-western (near the village Cerje), south-eastern (near the village Vlase) and north-eastern (Jelašnička Gorge) from the biggest urban and industrial centre of south-eastern Serbia Niš (approximately 350.000 inhabitants). The importance of the last location, Jelašnička Gorge, which has the status of a Special Nature Reserve, should be emphasized. This study is the first attempt to evaluate the anthropogenic impact on this protected area. Lichen samples were analyzed for their trace metal contents. The composition data were submitted to principal component analysis and interpreted.

EXPERIMENTAL

Sampling and sample preparation

The study was performed in natural ecosystems of south-eastern Serbia. The collection sites were: Jelašnička Gorge (330 m altitude), Vlase (350 m altitude) and Cerje (600 m altitude) in the vicinity of a road (2, 500 and 2000 m, respectively, Fig. 1).

The nearest urban and industrial area is the city of Niš (approximately 350000 inhabitants). The climate is a moderate continental with a mean annual rainfall of 543.3 mm, a mean annual temperature of 11.5 °C, and a mean annual relative humidity of approximately 69 %. The prevailing winds are north-westerly in winter and north-easterly and easterly in summer. The wind rose is shown in Fig. 1.

Foliose lichen *Flavoparmelia caperata* (L.) Hale (syn. *Parmelia caperata* (L.) Ach.; common name: greenshield lichen) was collected in April 2009. Determination of lichen was performed using several standard method.[9-11] The lichen material was sorted into two samples: peripheral and central, corresponding to peripheral and central parts of the thalli. The peripheral samples contained the outermost 3–4 mm of the thalli, distinguishable by a paler colour, absence of rhizinae and easy separation from the bark. These parts of the thalli are the most active physiologically and have a known age of approximately 1 year.[5] The central samples included the inner, older parts of thalli. The samples were air-dried, homogenized and further analyzed.

Analysis of trace metals

Lichen samples (0.5 g) were digested with a mixture of 7 mL of concentrated HNO_3 and 1 mL of 30 % H_2O_2 in an Advanced Microwave Digestion System (Ethos 1, Milestone, Italy) under the following programme: heated up to 200 °C in 10 min and held for 10 min at that temperature. The digested samples were transferred into a volumetric flask (25 mL).
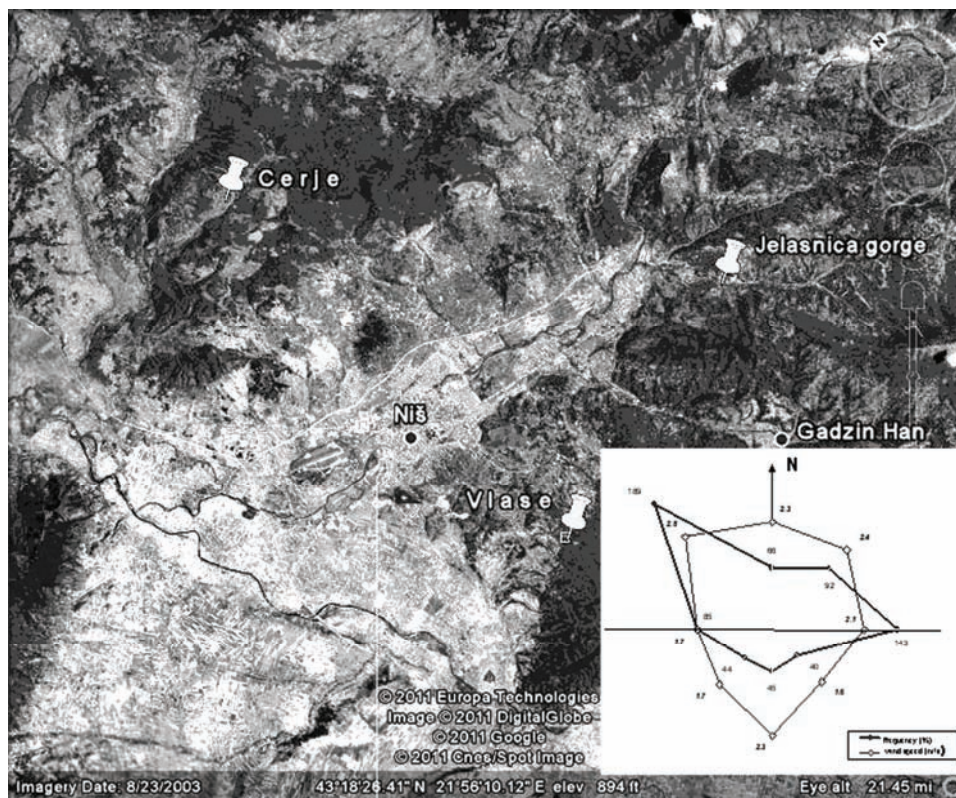
Fig. 1. Study area (Jelašnica Gorge, Vlase and Cerje with respect to the city of Niš) with the wind rose for the area of Niš (data from the Republic Hydrometeorological Service of Serbia).

The contents of the metals in the samples were determined using an inductively coupled atomic emission spectrometer model 6500 Duo (Thermo Scientific, United Kingdom) equipped with a CID86 chip detector. The system was equipped with an integrated unit for hydride generation. This instrument operates sequentially with both radial and axial torch configuretions. The entire system was controlled with Iteva software. The instrument operating conditions for the determination of the heavy metals in the lichen samples and selected emission lines are shown in Tables I and II, respectively.

To identify the relationship among the metals in samples and their possible sources, Pearson's correlation coefficient analysis and principal component analysis (PCA) were performed using PLS Toolbox, version 5.2.2 (Eigenvector Research), for MATLAB version 7.4.0.287 (R2007a) (MathWorks, Natick, MA, USA). The principal component analysis was performed using Varimax Normalized rotation.

RESULTS AND DISCUSSION

The bioaccumulation capacity for trace metals of lichen species *F. caperata* was determined by inductively coupled atomic emission spectrometry, Pearson's

correlation coefficient analysis and principal component analysis. The analyses of 21 metals in the three different ecosystems are given in Table III.

TABLE I. Instrument operating conditions for the determination of the concentration of heavy metals in the lichen samples

Spectrometer	ICAP 6500 (Thermo Scientific)
Nebulizer	Concentric
Spray chamber	Cyclonic
Radio frequency power, W	1150
Principal argon flow rate, L min^{-1}	12
Auxiliary argon flow rate, L min^{-1}	0.5
Nebulizer flow rate, L min^{-1}	0.5
Sample flow rate, mL min^{-1}	1.0
Detector	CID86

TABLE II. Selected emission lines

Element	λ / nm
Ag	328.0
As	193.7
B	249.6
Ba	455.4
Cd	228.8
Co	228.6
Cr	283.5
Cu	324.7
Fe	259.9
Ga	294.3
In	230.6
K	766.4
Li	670.7
Mg	280.2
Mn	257.8
Na	588.9
Ni	231.6
Pb	220.3
Sr	215.0
Tl	276.7
Zn	213.8
Hg	253.6
Se	196.0

Two types of lichen samples were used in this study: central and peripheral. The central samples represented the inner, older parts of the thalli that had been exposed longer to pollutants. The peripheral samples consisted of the outermost 3–4 mm of the thalli, with a maximum age of 1 year.[12,13] Thus, the peripheral

samples reflected recent changes of the environment. The obtained data indicated differences in metal content of the central and peripheral samples of lichens.

TABLE III. Concentration of metals in central and peripheral parts of the thalli of *F. caperata* (μg g^{-1} dry weight)

| Element | Location | | | | | |
| | Jelašnička Gorge | | Cerje | | Vlase | |
	Centre (sample 1)	Periphery (sample 2)	Centre (sample 3)	Periphery (sample 4)	Centre (sample 5)	Periphery (sample 6)
As	0.0037	0.0038	0.0036	0.0033	0.0031	0.0027
B	19.4303	9.5051	6.1341	6.9682	5.8576	6.7637
Ba	27.2333	21.5575	9.5615	24.5084	13.8145	15.2969
Cd	0.2558	0.1942	0.1681	0.1864	0.1310	0.1546
Co	0.1512	0.0822	1.0894	2.1865	0.0970	0.0856
Cr	1.9119	1.4572	3.7140	1.4670	1.7550	1.4879
Cu	8.3806	5.9573	15.3721	5.7307	6.1412	6.5179
Fe	476.6209	374.5863	645.2168	397.9597	493.2096	399.2086
Ga	0.1069	0.0000	0.0413	0.0000	0.0346	0.0177
In	0.0000	0.0000	0.0802	0.0341	0.0810	0.0000
K	2608.8040	2852.2720	2300.1670	2706.2540	2506.7160	3156.7050
Li	0.6932	0.5035	0.7566	0.4607	0.5617	0.4582
Mg	251.8673	315.6654	274.1127	313.7536	287.8818	373.2304
Mn	14.1271	13.5242	13.6761	12.4049	13.9091	15.6287
Na	71.1085	98.1346	89.5684	103.6953	78.8976	110.4994
Ni	1.2703	1.0977	1.5682	1.1916	1.4227	1.3011
Pb	22.3011	10.0742	12.0318	7.3955	9.8771	7.4223
Se	0.0043	0.0045	0.0042	0.0039	0.0036	0.0031
Sr	31.4610	23.8918	16.8445	11.3996	40.6104	32.6951
Tl	0.0000	0.6093	0.0000	0.9164	0.0000	1.5415
Zn	17.6053	17.0019	18.0832	19.5534	20.7641	24.2578

Furthermore, the trace metal content data were submitted to Pearson's correlation coefficients analysis (Table IV).

The correlation matrix was created from the values of the variables for all 21 metals in 6 samples. The Pair-Wise method was employed for the missing values. The results showed that these metals were strongly interrelated ($p < 0.01$), with correction coefficients ranging from –0.790 to 0.990 at the 99 % confidence level. B, Cd, Ga and Pb evidently displayed significant positive correlations with each other (Table IV), which indicated their association in the analyzed samples. Other metals, such as Cr, Cu, Fe, Li and Ni, also showed significant correlations. The exceptions were the element pairs As–Zn and Se–Zn, with significant negative correlations and As, Mn and Zn without any observed correlations.

In order to better describe the relationship among the metals and/or samples, principal component analysis (PCA) was performed. The analytical data were represented in a multidimensional space with variables defining the axes, and

TABLE IV. Pearson correlations coefficient matrix for the metals concentrations

	B	Ba	Cd	Co	Cr	Cu	Fe	Ga	In	K	Li	Mg	Mn	Na	Ni	Pb	Sr	Tl	Zn	As
Ba	0.717																			
Cd	0.921	0.792																		
Co	-0.303	0.123	0.002																	
Cr	-0.135	-0.605	-0.068	0.186																
Cu	-0.046	-0.542	0.033	0.161	0.988															
Fe	-0.094	-0.615	-0.125	0.099	0.953	0.916														
Ga	0.795	0.232	0.603	-0.329	0.293	0.340	0.432													
In	-0.558	-0.684	-0.596	0.290	0.614	0.489	0.734	-0.048												
K	-0.019	0.271	-0.031	-0.282	-0.735	-0.658	-0.828	-0.390	-0.776											
Li	0.371	-0.246	0.324	-0.076	0.841	0.849	0.881	0.728	0.408	-0.786										
Mg	-0.523	-0.166	-0.479	-0.050	-0.487	-0.457	-0.601	-0.708	-0.376	0.854	-0.809									
Mn	0.073	-0.328	-0.175	-0.726	-0.064	0.001	-0.032	0.233	-0.310	0.511	-0.028	0.432								
Na	-0.591	-0.135	-0.379	0.317	-0.276	-0.243	-0.478	-0.824	-0.288	0.669	-0.706	0.896	0.100							
Ni	-0.311	-0.789	-0.423	0.020	0.819	0.767	0.916	0.313	0.789	-0.641	0.670	-0.332	0.201	-0.328						
Pb	0.915	0.427	0.796	-0.309	0.222	0.282	0.303	0.943	-0.211	-0.363	0.698	-0.760	0.067	-0.807	0.075					
Sr	0.179	-0.147	-0.210	-0.848	-0.299	-0.322	-0.082	0.366	-0.036	0.187	-0.025	0.022	0.663	-0.420	0.130	0.218				
Tl	-0.322	0.089	-0.219	0.109	-0.540	-0.478	-0.678	-0.600	-0.547	0.892	-0.802	0.945	0.341	0.900	-0.465	-0.620	-0.139			
Zn	-0.453	-0.353	-0.600	-0.134	-0.312	-0.311	-0.246	-0.273	-0.034	0.577	-0.522	0.745	0.640	0.494	0.149	-0.526	0.394	0.671		
As	0.504	0.359	0.651	0.062	0.315	0.333	0.227	0.298	-0.063	-0.504	0.533	-0.702	-0.547	-0.461	-0.175	0.561	-0.380	-0.621	-0.990	
Se	0.47	0.373	0.633	0.097	0.284	0.299	0.188	0.240	-0.066	-0.485	0.484	-0.672	-0.587	-0.419	-0.213	0.513	-0.414	-0.591	-0.992	0.998

projected into a few principal components (PCs) that were linear combinations of the original variables and described the maximum variation within the data.[14] The obtained results clearly showed that Co, Mn and Sr had no impact. This was in accordance with the results of the determinations of the metals (Table III) as small differences in their values in different samples were found. Therefore, the PC analysis was realised without these metals, which resulted in a three-component model explaining 91.78 % of the data variation. The first PC comprised 49.75 % of the total data variability, and the cumulative variance explained by the first two components was 81.09 %. The addition of more PCs did not significantly change the classification of the analates described below. The score values for the samples, *i.e.*, their mutual projections, for the first two PCs are shown in Fig. 2.
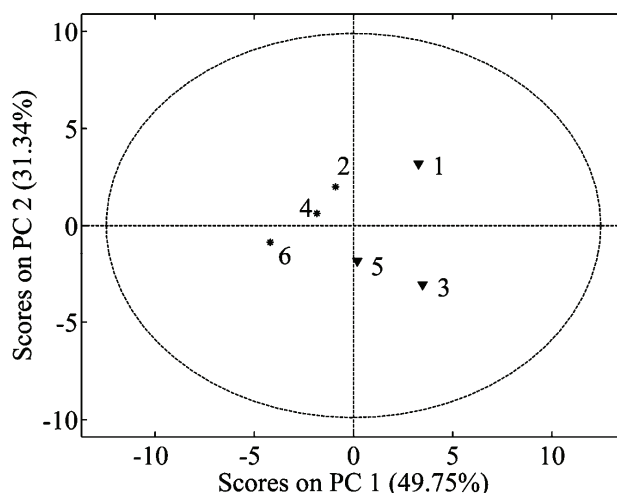

Fig. 2. Score values of the first and the second PC for the samples.

Additionally, the score values for the samples and metals for the first two PCs are shown in Fig. 3.

The first PC distinguished two separate groups of samples according to metals content and the age of the sampled lichen thalli. The first group was formed from samples 2, 4 and 6, obtained from the peripheral (younger) thalli parts, with a characteristic accumulation of Ba, K, Mg, Na, Tl and Zn. The second group contained samples 1, 3 and 5, and belonged to the central (older) thalli parts with higher concentrations of As, B, Cd, Cr, Cu, Fe, Ga, In, Li, Ni, Pb and Se. These findings revealed differences in the air quality in the last and previous years.

Compared to the location of sampling, it is obvious that the Special Nature Reserve, Jelašnička Gorge, from which sample 1 and 2 originated, is becoming polluted. The deposition of As, B, Ba, Cd, Ga, Pb and Se in sample 1 reflected
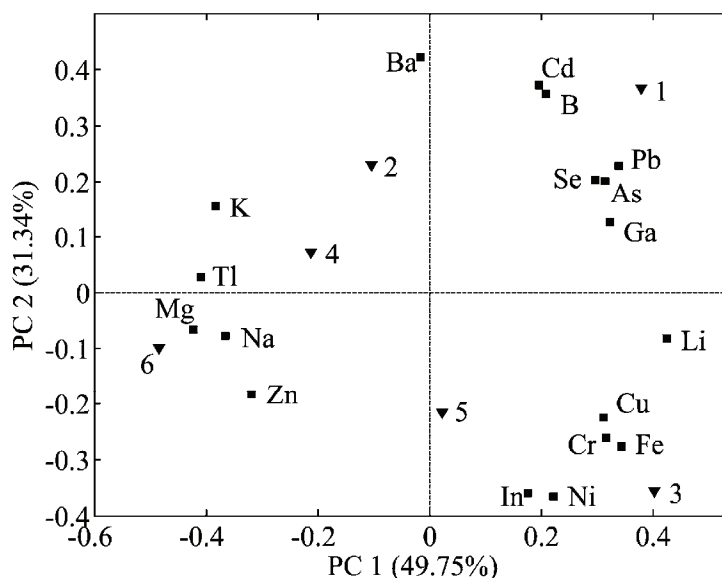
Fig. 3. Biplot of the first and the second PC for the samples and metals.

the vicinity of the road (2 m) and the towns Niš and Niška Spa at 15 and 3 km, respectively. The values of Pb in this sample were higher than the values reported for *F. caperata* near a motorway in Turkey in the study of Mendil *et al.* (2009).[15] The high concentration of Ba, K and Tl in sample 2 could be considered as being due to a probable contribution of particles from roadway dust to the soil material, as previously suggested in some studies. The other two locations, Cerje and Vlase, with samples 3–6, showed presence of trace metals of crustal and anthropogenic origin. An accumulation of Cr, Cu, Fe, In, Li and Ni was noticed in samples 3 and 5. Higher concentrations of Ba, K and Tl were determined in sample 4, as in sample 2. Finally, increased concentrations of Mg, Na and Zn were observed in sample 6. The deposition of trace metals of crustal origin, such as Cr, Cu, Fe, In, K, Li, Mg and Na, implied a specific composition of the geological substrate, as well as the influence of vegetation, *i.e.*, the substrate from which the lichen samples were collected. Anthropogenic emission of trace metals (Ni, Cd, Cr, Cu, Pb, Zn) from motor vehicles is mainly from the combustion of the fossil fuels or abrasion of vehicle parts (tyres, paint, greases and catalysts).[17,18] Although vehicles using unleaded petrol prevail, a high density of old vehicles using leaded petrol or diesel oil is still present on the Serbian roads. Diesel soot is the main source of emission of Zn and Cu in urban areas.[16] Besides its utilization as an oil additive, Zn is well-known, together with Cd, as a rubber additive.[16] Both Zn and Cd are atmophile elements subjected to a long-distance transport.[19] Moreover, a part of Zn could be obtained from a supporting tree since higher

plants are known to release 20 % of the total Zn from natural sources.[20] Among lichen species, *F. caperata* is famous for its higher capacity for Zn and Cd uptake.[7]

Bearing in mind the low frequency of traffic on the road in close range of the location of lichen sampling, the high concentrations of Cu, Pb and B detected are surprising. This is probably due the specific wind rose (see Fig. 1) which put this area under indirect impact of huge metal complexes, situated 10–15 km north-westerly (at the periphery of the city of Niš). Further research and monitoring should be performed in order to obtain the correct conclusions.

CONCLUSION

This study is the first biomonitoring study of atmospheric trace metal pollution in natural ecosystems in Serbia. The lichen species *Flavoparmelia caperata* was chosen because of its wide distribution and proven sentinel functions. Its peripheral parts were used as sensors of annual changes in the environment, while the central, older parts of the thalli were treasurers of the pollutants from the past. The deposition pattern of trace metals in the studied samples probably reflected the volume of traffic and the types of engines on the nearby roads, the activity of industrial complexes, soil and substrate compositions and the prevailing wind directions. This study is evidence that there is a need for continuous biomonitoring surveys of the studied areas, especially, the Special Nature Reserve Jelašnička Gorge.

И З В О Д

ЕПИФИТНИ ЛИШАЈ *Flavoparmelia caperata* КАО ИНДИКАТОР ЗАГАЂЕЊА МЕТАЛИМА У ТРАГОВИМА

ТАТЈАНА МИТРОВИЋ[1], СЛАВИША СТАМЕНКОВИЋ[1], ВЛАДИМИР ЦВЕТКОВИЋ[1], МИЛОШ НИКОЛИЋ[1], РАДА БАОШИЋ[2], ЈЕЛЕНА МУТИЋ[2], ТАТЈАНА АНЂЕЛКОВИЋ[3] и АЛЕКСАНДАР БОЈИЋ[3]

[1]*Департман за биологију и екологију, Природно–математички факултет, Универзитет у Нишу, Вишеградска 33, 18000 Ниш,* [2]*Хемијски факултет, Универзитет у Београду, Студентски трг 12, п. пр. 51, 11158 Београд и* [3]*Департман за хемију, Природно–математички факултет, Универзитет у Нишу, Вишеградска 33, 18000 Ниш*

Широко распрострањена врста лишајева *Flavoparmelia caperata* је коришћена у биомониторингу атмосферског загађења металима у траговима у природним екосистемима на југоистоку Србије. Концентрација и дистрибуција 21 метала у лишајевима је одређена атомско-емисионом спектрометријом са индуктивно спрегнутом плазмом. Примећена разлика у нагомилавању метала између периферних и централних делова талуса лишајева је приписана разликама у квалитету ваздуха последње и претходних година. Ови налази су потврђени анализом главних компоненти (PCA). Истраживање је пока-

зало акумулирање Ba, K, Mg, Na, Tl и Zn у периферним деловима талуса, односно As, B, Cd, Cr, Cu, Fe, Ga, In, Li, Ni, Pb и Se у централним деловима талуса.

REFERENCES

1. B. Wolterbeek, *Environ. Poll.* **120** (2002) 11
2. M. E. Conti, G. Cecchetti, *Environ. Poll.* **114** (2001) 471
3. A. Bari, A. Rosso, M. R. Minciardi, F. Troiani, R. Piervittori, *Environ. Monit. Assess.* **69** (2001) 205
4. R. Bargagli, F. Monaci, F. Borghini, F. Bravi, C. Agnorelli, *Environ. Poll.* **116** (2002) 279
5. S. Loppi, L. Fratia, L. Paolia, V. Bigagli, C. Rossetti, C. Bruscoli, A. Corsini, *Sci. Total Environ.* **326** (2004) 113
6. T. Zschau, S. Getty, C. Gries, Y. Ameron, A. Zambrano, T. H. III Nash, *Environ. Poll.* **125** (2003) 21
7. P. L. Nimis, S. A. Pittao, *Sci. Total Environ.* **275** (2001) 43
8. M. Blasco, C. Domeno, P. Lopez, C. Nerin, *Environ. Poll.* **13** (2011) 2588
9. V. Wirth, *Die Flechten Baden-Würtembergs, Teil 1 und 2*, Eugen Ulmer, Stuttgart, Germany, 1995, p. 1006
10. M. Boqueras, *Líquens Epífits i Fongs Liquenícoles del Sud de Catalunya: Flora i Comunitats,* Institut d'Estudis Catalans, Barcelona, Spain, 2000, p. 556
11. F. S. Dobson, *Lichens: An Illustrated Guide to the British and Irish Species*, Richmond Publ., Slough, UK, 2005, p. 480
12. P. J. Fisher, M. C. F. Proctor, *Lichenologist* **10** (1978) 81
13. S. Loppi, L. Nelli, S. Ancora, R. Bargagli, *Bryologist* **100** (1997) 251
14. R. G. Brereton, *Chemometrics data analysis for the laboratory and chemical plant,* Wiley, Chichester, UK, 2003, p. 503
15. D. Mendil, F. Celik, M. Tuzen, M. Soylak*, J. Hazard. Mater.* **166** (2009) 1344
16. G. Dongarra, G. Sabatino, M. Triscari, D. Varrica, *J. Environ. Monitor.* **5** (2003) 766
17. A. Aslan, A. Cicek, K. Yazici, M. Karagoz, F. Turan, O. S. Yildirim, *Afr. J. Agr. Res.* **6** (2011) 1698
18. C. Pecheyran, B. Lalere, O. F. X. Donard, *Environ. Technol.* **34** (2000) 27
19. S. Loppi, S. A. Pirintsos, *Environ. Poll.* **121** (2003) 327
20. J. O. Nriagu, *Nature* **279** (1979) 409.